NASA CONTRACTOR
REPORT

Report No. 61307

EXPERIMENTAL MATERIAL HANDLING DEVICE

By W. H. Tobey, R. T. French, and D. M. Adams

Martin Marietta Corporation
Denver Division
Denver, Colorado 80201

September 1969

Final Report

Prepared for

NASA-GEORGE C. MARSHALL SPACE FLIGHT CENTER
Marshall Space Flight Center, Alabama 35812

TECHNICAL REPORT STANDARD TITLE PAGE

1. REPORT NO.	2. GOVERNMENT ACCESSION NO.	3. RECIPIENT'S CATALOG NO.
NASA CR-61307		

4. TITLE AND SUBTITLE	5. REPORT DATE
EXPERIMENTAL MATERIAL HANDLING DIVICE Final Report	September 1969 6. PERFORMING ORGANIZATION CODE
7. AUTHOR(S) W. H. Tobey, R. T. French, and D. M. Adams	8. PERFORMING ORGANIZATION REPORT # MCR-69-414
9. PERFORMING ORGANIZATION NAME AND ADDRESS Martin Marietta Corporation Denver Division Denver, Colorado 80201	10. WORK UNIT NO. 11. CONTRACT OR GRANT NO. NAS 8-30069
12. SPONSORING AGENCY NAME AND ADDRESS George C. Marshall Space Flight Center Marshall Space Flight Center, Alabama 35812 Manufacturing Engineering Laboratory	13. TYPE OF REPORT & PERIOD COVERED NASA Contractor Report Final 14. SPONSORING AGENCY CODE

15. SUPPLEMENTARY NOTES

Distribution of this report is provided in the interest of information exchange. Responsibility for the contents resides in the author or organization that prepared it.

16. ABSTRACT

This report, submitted in two volumes; Final Report and Summary Report, describes a study of an Experimental Material Handling Device (EMHD). The study was divided into two basic phases. In the first, the feasibility of a Man Rated Flight Material Handling Device (MRFMHD) was examined. This analysis indicated it was feasible to build and use a MRFMHD that would be mounted on an Apollo Command/Service Module (CSM). The device would aid space manufacturing operations by attaching to, stabilizing, transporting, positioning, and releasing a wide variety of objects.

In the second phase, an EMHD was designed, fabricated, and tested to evaluate MRFMHD concepts. The tests utilized the Martin Marietta Corporation's Space Operations Simulation facility. Two test subjects, seated in a fixed base CSM mockup, controlled the CSM dynamics and the EMHD operations. A target was mounted on the simulator's six-degree-of-freedom moving base. Tests involved approaching and positioning relative to the target, attaching to it, and stabilizing it after attachment. Three attachment modes were used; 1) clamping on the target exterior, 2) hooking flanges on the target, and 3) attaching with a simulated adhesive head.

(Continued on back of this page)

17. KEY WORDS	18. DISTRIBUTION STATEMENT
	STAR Announcement (See DRF)

19. SECURITY CLASSIF. (of this report)	20. SECURITY CLASSIF. (of this page)	21. NO. OF PAGES	22. PRICE
U	U	190	

MSFC - Form 3292 (May 1969)

ABSTRACT (Concluded)

The simulation technique involves computation of the problem dynamics on an analog computer which determines the commands for the moving base.

The tests obtained the desired data on pre-attachment alignment errors and dynamic functioning and control of the EMHD under dynamic conditions similar to those found in space. The data provide dynamic and subjective information that will make possible the design of a more advanced Material Handling Device.

FOREWORD

The research described in this report (Experimental Material Handling Device, National Aeronautics and Space Administration Contract NAS8-30069) was performed by Martin Marietta Corporation, Denver Division, P. O. Box 179, Denver, Colorado for the NASA Marshall Space Flight Center, Huntsville, Alabama. Mr. Dan Dane was the NASA Contracting Officer's Representative. Alternate Contracting Officer Representatives were Mr. Vaughn H. Yost and Mr. Walter H. Stafford.

Mr. George W. Smith was Martin Marietta's Program Manager and Mr. William H. Tobey was the Technical Director for the program. William H. Tobey, Richard T. French, Dennis M. Adams, Fredrick J. Greeb, Donald F. Widerspan, Dale H. Wine, Arlen W. Schlaht, Walter F. Thiemet, and Ellis R. Brown performed the effort described in this report. Mr. Peter F. Kuenzinger assisted these personnel in preparing this report. The authors submitted the report, in final form, in September 1969.

TABLE OF CONTENTS

TABLE OF CONTENTS (Concluded)

LIST OF ILLUSTRATIONS

LIST OF ILLUSTRATIONS (Cont'd)

LIST OF ILLUSTRATIONS (Concluded)

LIST OF TABLES

LIST OF TABLES Cont'd

LIST OF ABBREVIATIONS AND SYMBOLS

EMHD	-	Experimental Material Handling Device
AMHD	-	Advanced Material Handling Device
CSM	-	Command/Service Module
ACS	-	CSM Attitude Control System
RCS	-	CSM Reaction Control System
AH	-	Attachment Head
X_c	-	Carriage longitudinal position command
Y_c	-	Carriage lateral position command
Z_c	-	Carriage vertical position command
ψ_c	-	Gimbal yaw position command
θ_c	-	Gimbal pitch position command
$\dot{\phi}_c$	-	Gimbal roll rate command
X_I	-	Carriage longitudinal position readout
Y_I	-	Carriage lateral position readout
Z_I	-	Carriage vertical position readout
ψ_I	-	Gimbal yaw position readout
θ_I	-	Gimbal pitch position readout
$\dot{\phi}_I$	-	Gimbal roll rate readout
X_v	-	CSM c.g. longitudinal position in room
Y_v	-	CSM c.g. lateral position in room
Z_v	-	CSM c.g. vertical position in room
$X_T = X_I$	-	Target c.g. longitudinal position in room
$Y_T = Y_I$	-	Target c.g. lateral position in room
$Z_T = Z_I$	-	Target c.g. vertical position in room
X_{LC}	-	Load cell center longitudinal position in room

Y_{LC} - Load cell center lateral position in room

Z_{LC} - Load cell center vertical position in room

M_{XL} - Moment about load cell array X axis

M_{YL} - Moment about load cell array Y axis

M_{ZL} - Moment about load cell array Z axis

F_{XL} - Force along load cell array X axis

F_{YL} - Force along load cell array Y axis

F_{ZL} - Force along load cell array Z axis

M_{XT} - Moment on target c.g. parallel to room X axis

M_{YT} - Moment on target c.g. parallel to room Y axis

M_{ZT} - Moment on target c.g. parallel to room Z axis

$F_{XT} = -F_{XL}$ - Force on target parallel to room X

$F_{YT} = -F_{YL}$ - Force on target parallel to room Y

$F_{ZT} = -F_{ZL}$ - Force on target parallel to room Z

I_T - Moment of inertia of inertially symmetric target

M_T - Target mass

I_{xx} - CSM roll moment of inertia

I_{yy} - CSM pitch moment of inertia

I_{zz} - CSM yaw moment of inertia

M_c - CSM mass

$\dot{X}_v$ - Thrusted acceleration along CSM X axis

$\ddot{Y}_v$ - Thrusted acceleration along CSM Y axis

$\ddot{Z}_v$ - Thrusted acceleration along CSM Z axis

$\ddot{\psi}_v$ - Thrusted CSM yaw acceleration

$\ddot{\theta}_v$	-	Thrusted CSM pitch acceleration
$\ddot{\phi}_v$	-	Thrusted CSM roll acceleration
TX	-	CSM X thrust hand controller command
TY	-	CSM Y thrust hand controller command
TZ	-	CSM Z thrust hand controller command
$T\psi$	-	CSM yaw thrust hand controller command
$T\theta$	-	CSM pitch thrust hand controller command
$T\phi$	-	CSM roll thrust hand controller command
MS:	-	Thrust mode select signal (pulse, rate, accel.)
X_o	-	Target initial longitudinal position
Y_o	-	Target initial lateral position
Z_o	-	Target initial vertical position
ψ_o	-	Target initial yaw position
θ_o	-	Target initial pitch position
$\dot{\phi}_o$	-	Target initial roll rate
a	-	EMHD arm open angle
ω	-	EMHD spin rate

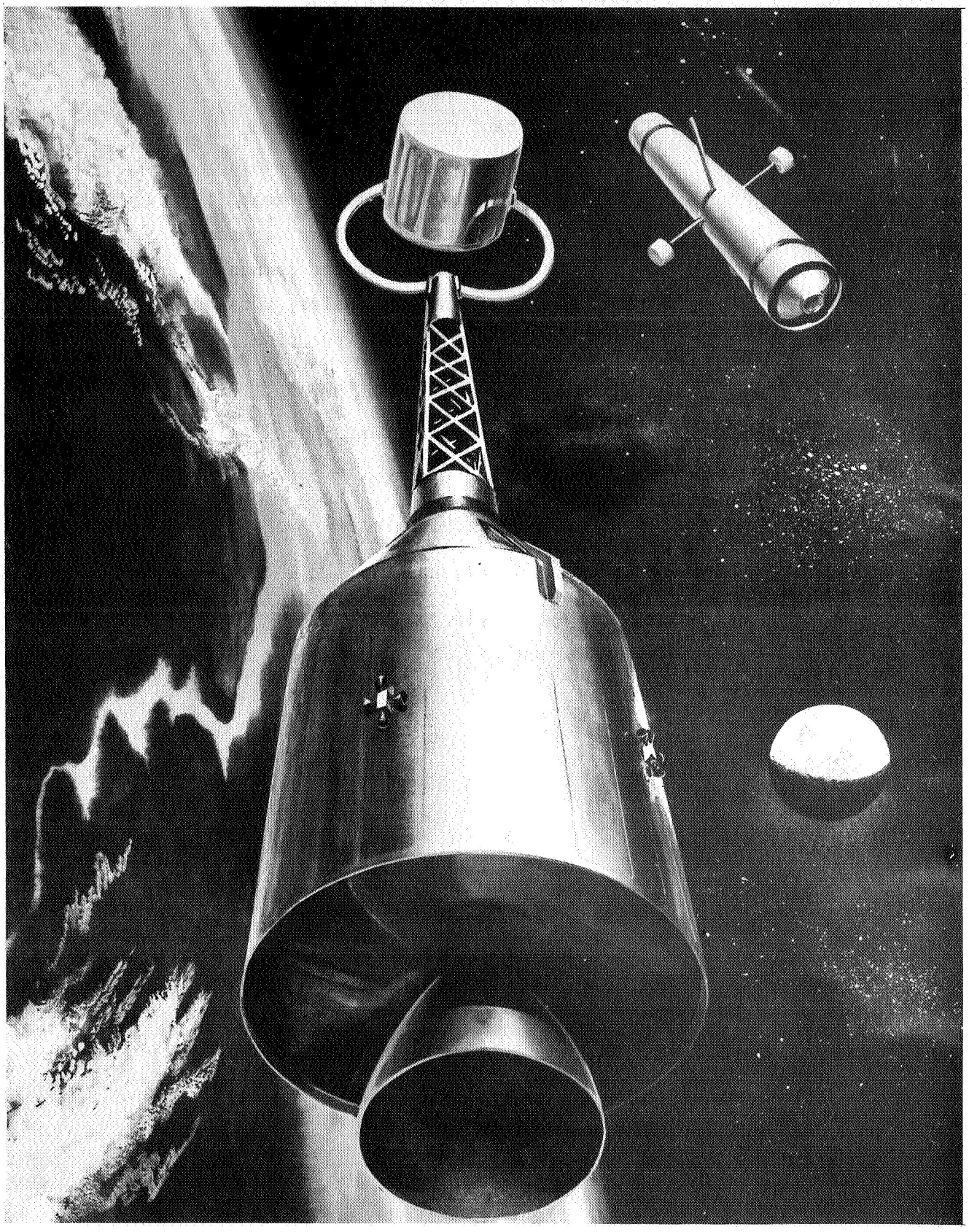

SECTION I

INTRODUCTION

A need exists to develop material handling capability for use in orbital assembly operations. This document is the result of a NASA contract (NAS8-30069) with the Denver Division of the Martin Marietta Corporation. The primary objective of this contract was the development of an Experimental Material Handling Device (EMHD) having capabilities of: 1) attaching to an object; 2) stabilizing the relative linear and rotational motion of the object; 3) moving the object from one site into position at a second site; 4) inducing the original relative rotational motion to the object; 5) releasing the object; and 6) performing 1 thru 5 repeatedly.

The contract was divided into five (5) segments designated Tasks A through E. In brief they were as follows: Task A-Conduct a feasibility study concerning development of a Man Rated Flight Material Handling Device (MRFMHD); Task B-Design an Experimental Material Handling Device (EMHD) and Target(s); Task C-Devise a simulation test plan for evaluating the EMHD concept; Task D-Devise an EMHD Proof Test Procedure; and Task E-Fabricate, assemble, proof test and evaluate the EMHD.

Many types and configurations of Material Handling Devices were considered in the feasibility study. The results of that study led to a decision to proceed with a mechanical grappling arm system with provision to utilize a simulated adhesive attachment interface (normal adhesive process or electro-adhesive) resulting in three (3) possible grappling modes. EMHD and target design drawings, the Simulation Test Plan and the proposed Proof Test Procedure were submitted to and approved by the Marshall Space Flight Center, Huntsville, Alabama. The EMHD and associated hardware were fabricated, proof tested and evaluated at Martin Marietta Corporation's six-degree-of-freedom Space Operations Simulator (SOS).

The body of this report presents the major parts of the program in the following order: Feasibility Study, EMHD and Target Design, Proof Test Procedure and Results, Experiment Design for EMHD Evaluation, EMHD Test Results, Analysis of Test Results, Conclusions and Recommendations for Future Studies.

SECTION II

FEASIBILITY STUDY RESULTS

1. Introduction

The basic purpose of this portion of the program was to examine the fabrication and use of a material handling device mounted on the Apollo Command/Service Module (CSM) to determine whether such a system is feasible. To be feasible, the MRFMHD/CSM must be capable of the following:

a. Fabrication within the current or near-term expected state-of-the-art.

b. Attachment to a significant number of current and future in-orbit objects without damaging these objects.

c. Despinning and stabilizing appropriate target objects in preparation for maintenance, repair, or material transport operations.

d. Support for target objects during maintenance, repair, and transport.

e. Accurate positioning, spin-up, and release of payloads having specific orientation and spin requirements.

Within the framework of the contract's assumptions, guidelines, and overall objectives, the MRFMHD was divided into seven basic hardware problem areas;

a. attachment devices

b. spinning interface

c. impact attenuation

d. deployment structure

e. CSM interface

f. CSM/MRFMHD control

g. launch location

These areas are paralleled by three non-hardware problem areas that determine the functional requirements for the MRFMHD;

a. system dynamics

b. safety

c. operational timelines

In addition, an analysis was made of existing and expected targets to determine the range of physical and dynamic characteristics that the CSM/MRFMHD will be required to handle.

The following sections present the results of the feasibility study that encompassed the eleven areas specified above. Since a change in any one area feeds into and influences virtually all other areas, the study was accomplished largely in an iterative manner as illustrated in Figure 1. However, it is felt that system dynamics is the one area that must be understood as a foundation for all others. Therefore, the technical discussion starts with this subject, proceeds to attachment heads, follows through other areas, and terminates with an analysis of system safety.

2. System Dynamics

a. Dynamics During Attachment - In its simplest form, the MRFMHD consists of the three elements shown in Figure 2. These elements provide (1) attachment to the targets, (2) a controllable spinning interface, and (3) structural attachment to the CSM.

Many references are available that present mathematical approaches to the problem of connecting two objects in an inertial environment (zero-g) where the objects have different masses, inertias, and spin characteristics and their analysis leads to the forces and torques at the interface between the objects and their dynamics following attachment.

During the course of the feasibility study, a dynamic analysis technique was used that permits simplified calculation and visualization of the attachment forces and torques and system dynamics without resorting to the gyroscopic interaction equations for each individual set of target characteristics and attachment errors. The technique, though of a first order approximation nature, was found to be very satisfactory in the iterative analysis described previously.

In using this technique, the CSM/MRFMHD is regarded as a fixed mass and inertia object having zero position and attitude rates relative to the target prior to target attachment. This hypothesis is based on the CSM control analysis, Section II-9. The attachment head (AH) is treated initially as a point that can be attached at will to the target. The MRFMHD has a minimum of one-degree-of-freedom (the spin interface axis) and can have more if required due to attachment errors and target sensitivities.

STUDY AREA RELATIONSHIPS

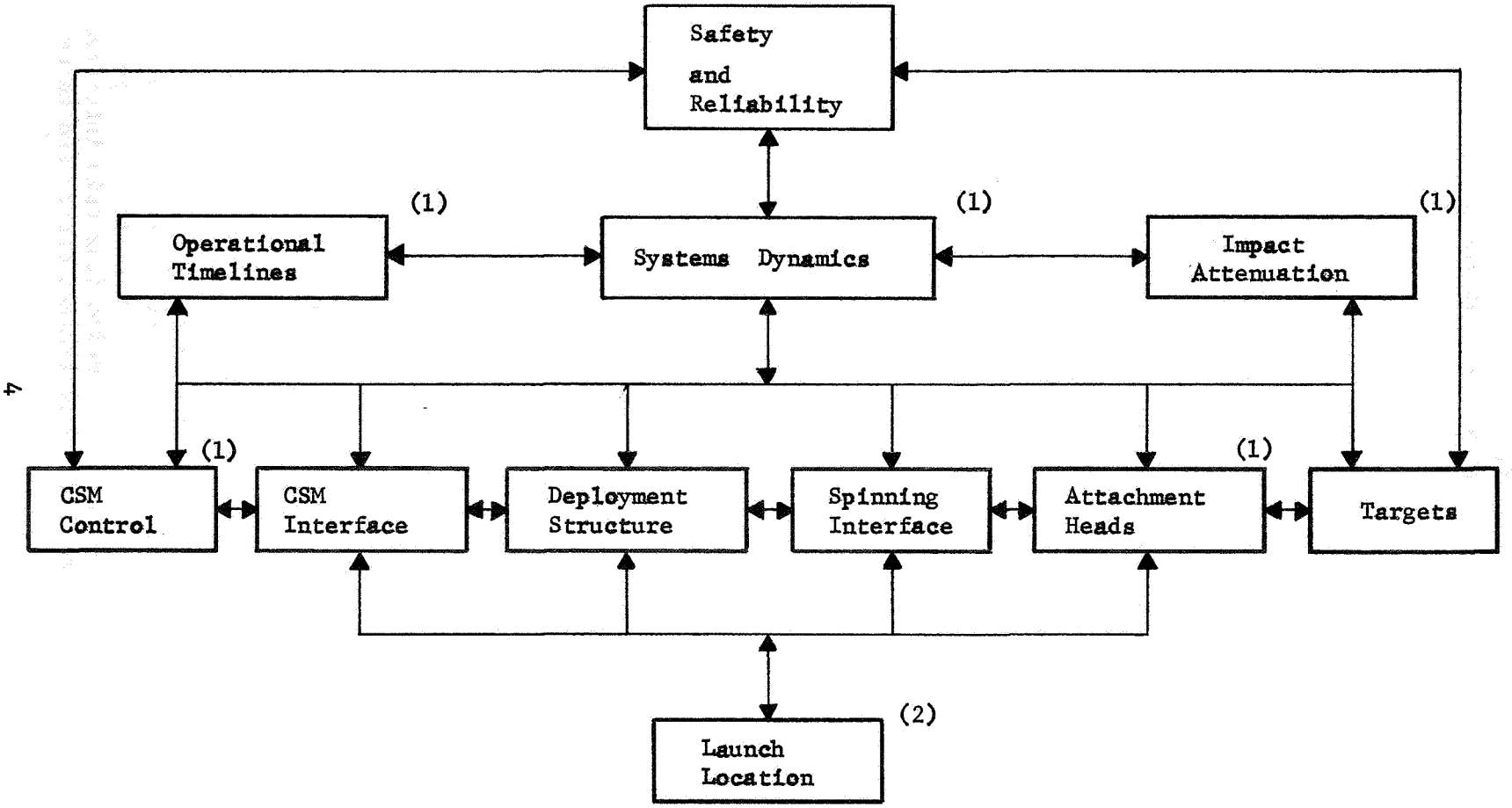

(1) Require Simulation Data (Task E) for Analysis

(2) Dependent on Undefined Future Mission Constraints

Figure 1 Iterative Design Flow Chart

MRFMHD:

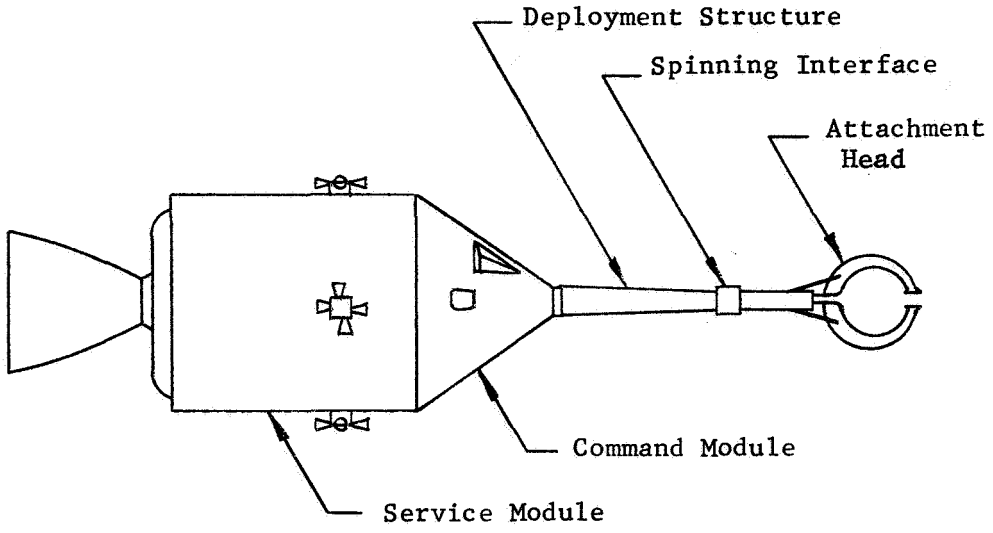

Figure 2 CSM with MRFMHD

The target is treated as a mass (variable in size, distribution, and spin characteristics over the appropriate range) that has one predominant characteristic; the center-of-gravity (c.g.) is inaccessible to the AH.

The next assumption made in developing the technique is that the total angular momentum of the combined system is conserved during the attachment operation. This will be the case if no CSM or target thrusters are fired during attachment.

With these assumptions, the target contains all of the angular momentum prior to attachment. After attachment, the target will rotate with respect to the CSM about the available degrees of freedom in the MRFMHD. The vector sum of the target's angular momentum about each of these axes could add up, ideally, to the angular momentum before attachment. However, unless the MRFMHD is a completely free gimballed system, some differential will exist between the target's pre-attachment and post-attachment angular momentum. This differential will be manifested as a nutation of the total system (CSM, MRFMHD, target) about its combined c.g. If there is no nutation, the MRFMHD's AH is tracking the target's motions perfectly, i.e., no net forces or torques are being transmitted to the target by the CSM/MRFMHD. This

is the desired case for extremely delicate satellite targets. If the MRFMHD axis can be aligned and attached to a non-nutating target's spin axis, only one-degree-of-freedom (MRFMHD spin) is required. If the target is nutating, the MRFMHD spin axis should be aligned to the target's angular momentum axis (axis of nutation cone) and the AH axis should be aligned and attached to the target's principal spin axis. In this case, the AH should be driven to match the principal spin rate and the support (main MRFMHD axis) for the offset AH should be driven at the nutation rate as shown in Figure 3.

To stop the target after attachment, the nutation rate should be nulled first, then the spin rate, and finally the AH should be driven to align with the main MRFMHD axis.

The discussion above assumes that the driven axes in the MRFMHD can be aligned perfectly to the target's principal spin and angular momentum (P) axes. In practice, this will not be possible and the following approach was used to determine the MRFMHD/Target interface forces and torques developed during attachment as a function of alignment errors.

For practical purposes, the problem is examined from a standpoint analogous to attaching to a non-nutating target. Forces and torques on the interface are determined as functions of target inertia, spin characteristics and attachment misalignments. Note that the results will be similar to the case where the target is nutating and the attachment errors are regarded as the sum of the errors in aligning to the nutation and body spin axes.

Starting with an angular misalignment case as illustrated in Figure 4, the AH axis is pointed at the target's c.g., but is misaligned with the target's spin axis and will attach at a point off this axis. At attachment, assuming a rigid attachment is achieved, the target is forced to rotate about the AH axis. The component of P parallel to the AH axis remains on that axis. The remainder of P (component perpendicular to the AH axis) is delivered impulsively during attachment to the combined CSM/MRFMHD/Target through forces and torques at the attachment point. If the target mass is small compared to the mass of the CSM/MRFMHD, the target will see this effect as an impulsive torque about a transverse axis that changes its angular momentum by the off-AH axis increment, ΔP. If T is the duration of the impulsive moment, then, by fundamental rules, the average moment required, N, is given by

$$N = \frac{\Delta P}{T} .$$

Note: Separation between attachment head and target is exaggerated.

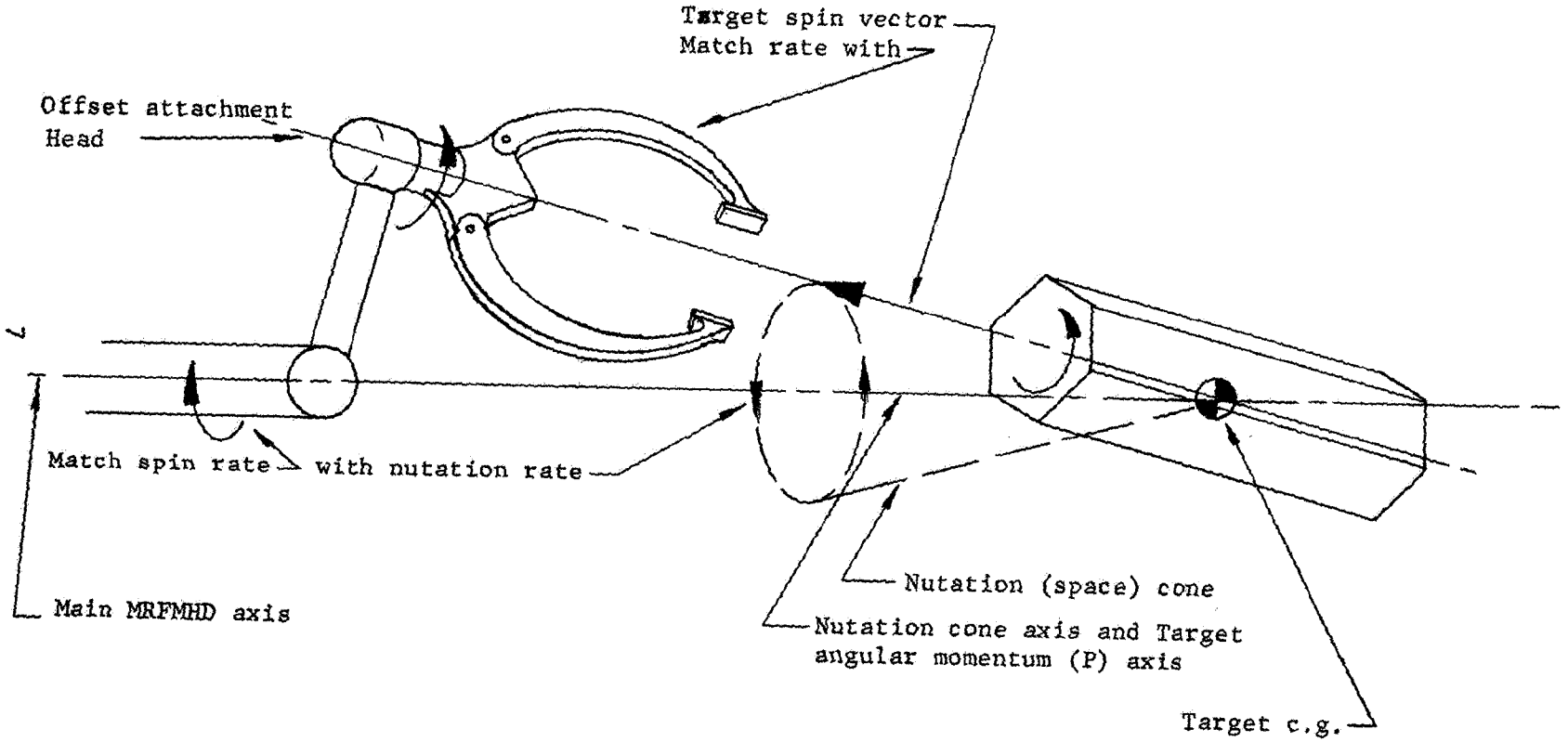

Figure 3 MRFMHD Alignment to Nutating Target

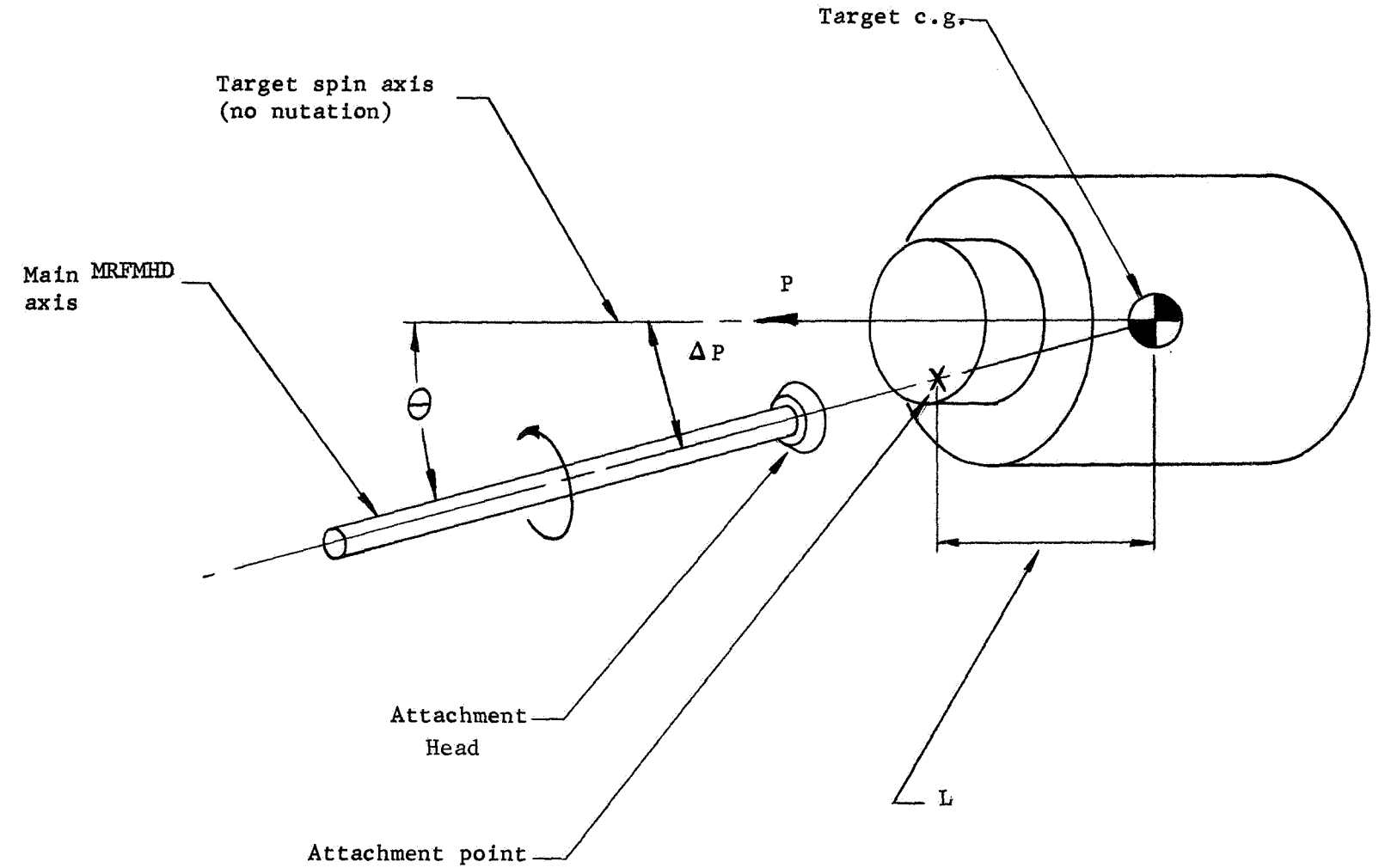

Figure 4 MRFMHD Angular Misalignment with Target

At this point, it is worthwhile to examine a numerical example of this relationship to understand its importance. The example, chosen from what might be described as the mid-range of values specified in the contract's Assumptions and Guidelines, is as follows:

I_T = 50 slug ft.^{2} - - - (moment of inertia about target's spin axis)

ω = 28.6 revolutions/min ≈ 3 radians/sec (target spin rate)

θ = 5.7° = 0.1 radian (angular misalignment).

These give:

$$P = I\omega = 150 \text{ ft. lb. sec.}$$

$$\Delta P = P \sin\theta = 15 \text{ ft. lb. sec.}$$

Using this value for ΔP, Figure 5 depicts the moment, N, as a function of N's duration, T. Note that the example is easily modified to put in other target and angular misalignment characteristics. For a given T, N is a linear function of I_T, ω, and $\sin\theta$.

From this example, it can be seen that the attachment torques can reach large values if the time to achieve rigid attachment is short. This says that for delicate satellites, T must be long if essentially perfect angular alignment cannot be achieved. During this time, the intersection of the axis of the AH with the target surface will describe a path along the target's surface since the attachment point (X in Figure 4) is not located on the spin axis. The length of the AH's slippage path along the target's surface is determined by θ, the distance to the target's c.g., the initial spin rate, and the time required to reach rigid attachment. In the example used, assume that the attachment point is one foot from the target's c.g. This places X at 1.2 inches off the spin axis. With ω = 3 radians/sec, X's locus is traveling at 3.6 inches per second relative to the tip of the AH. If N is applied uniformly for one second to achieve rigid attachment, X will slip 1.8 inches in the AH's grasp. According to Figure 5, the AH must be applying a torque of 15 lb-ft about the target's transverse axis during this one second interval.

If the AH is not a point but consists of, for example, a four-pronged attachment head, and this head is rotating at the same ω as the target, then each point on the attachment head will describe a circle on the target. These circles will be the same size and will be covered at the same rate as the circle that the AH axis intersection describes on the target's surface. For the angular misalignment case under discussion, the first order approximations of interface torques

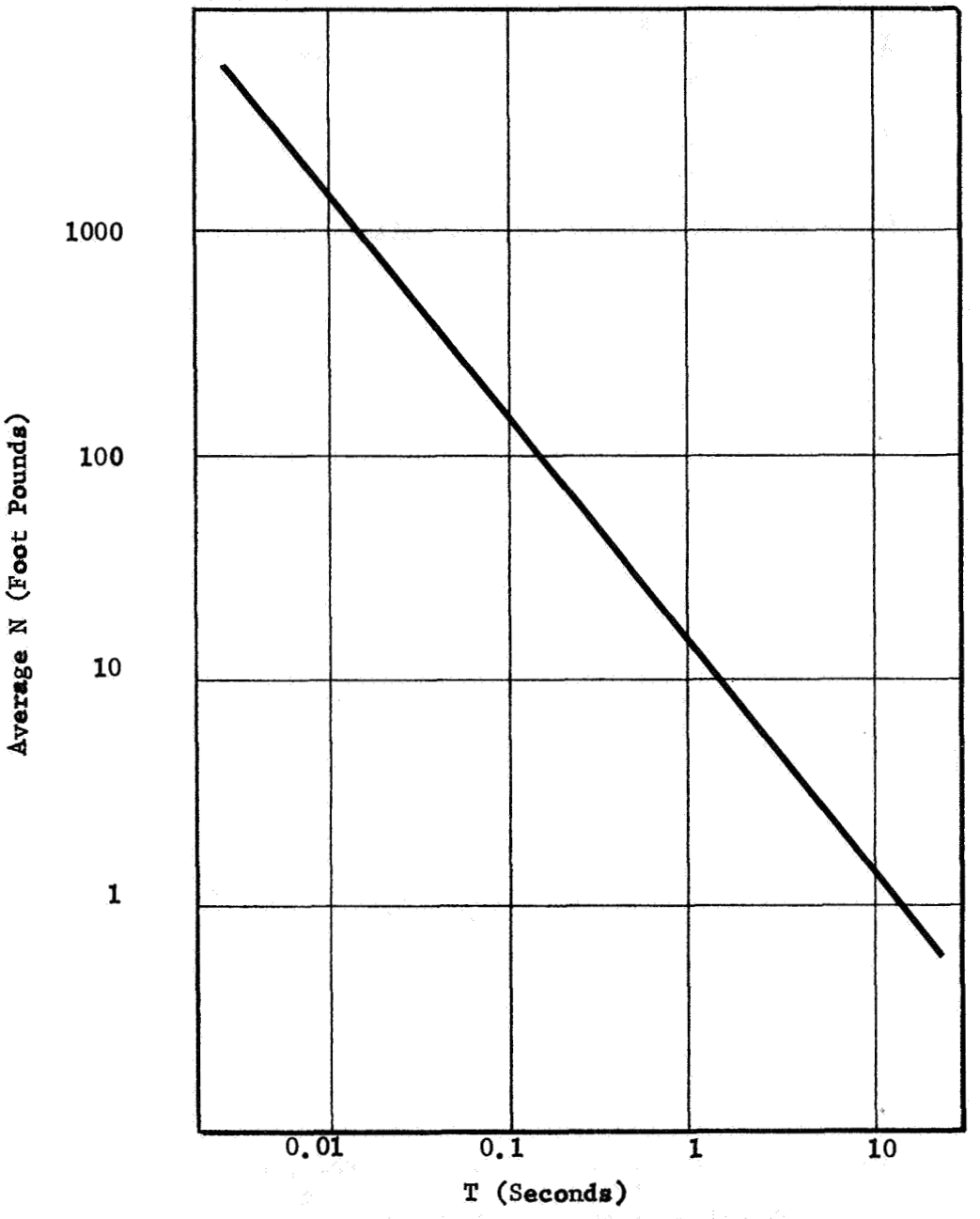

Figure 5 Average N versus T for
ΔP = 15 Foot Pound Seconds

and slippage as functions of the various variables may be computed from the graphs in Figures 6, 7, and 8. Starting with Figure 6, take the target's spin angular momentum, and anticipated angular attachment error and determine ΔP. Going to Figure 7 and working on or between the constant ΔP lines, the average torque may be determined for a given attachment time or a given maximum average torque will lead to the minimum allowable attachment time. After the attachment time is determined, Figure 8 is used to determine the AH slippage based on uniform application of the attachment torque. The slippage distances are based on a one-foot distance from the attachment point to the target's c.g. If the distance is larger or smaller than this, the slippage distance should be changed proportionately.

The next type of attachment error to be considered is the axial misalignment as depicted in Figure 9. In this case, the AH spin axis and the target angular momentum vector are parallel. However, the attachment point is displaced off the spin axis by the perpendicular distance R_e. Again assuming that the target's mass and inertias are not a large fraction of the CSM's mass and inertias, the target will start rotating about a new axis through X and parallel to its original spin axis. If I_T is the target's moment of inertia about its original spin axis, ω_1 the original spin rate, ω_2 the spin rate after attachment, and M the target's mass, then basic rules of angular momentum of an object rotating about an axis not passing through the object's c.g. give:

$$P = I_T\omega_1$$

$$= I_T\omega_2 + MR_e^2\omega_2$$

or

$$\omega_1 = \omega_2 + \frac{MR_e^2}{I}\omega_2$$

assuming angular momentum is conserved.

Therefore, the approximate net effect of the attachment process is a reduction in the spin rate ($\omega_1 > \omega_2$) and the imposition of a torque on the AH due to the off-center rotation of the target. The latter torque, that tends to peel the target off the AH, is given by the product of the centripetal force (due to off-center target rotation)

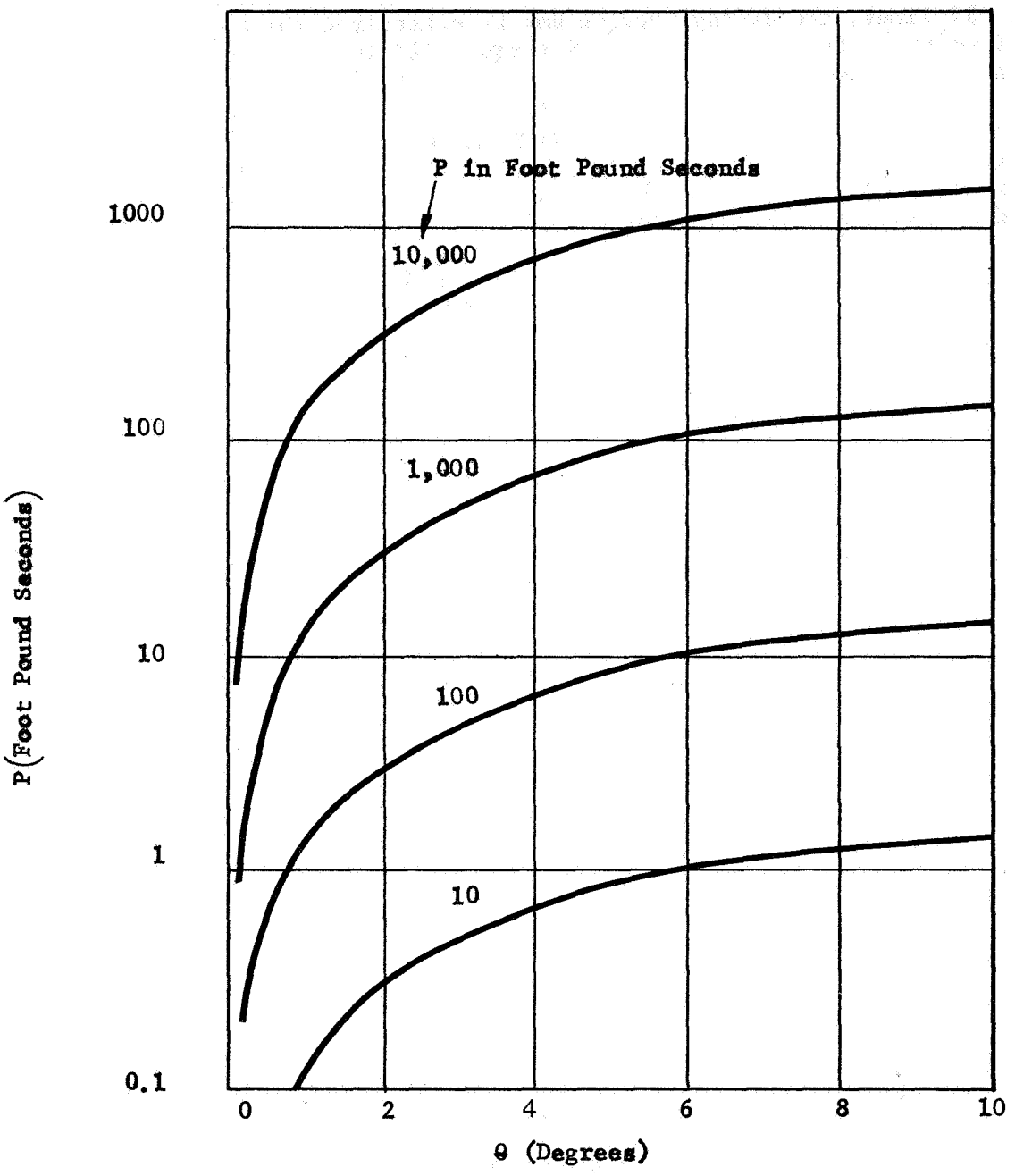

Figure 6 ΔP versus θ for Constant Values of P

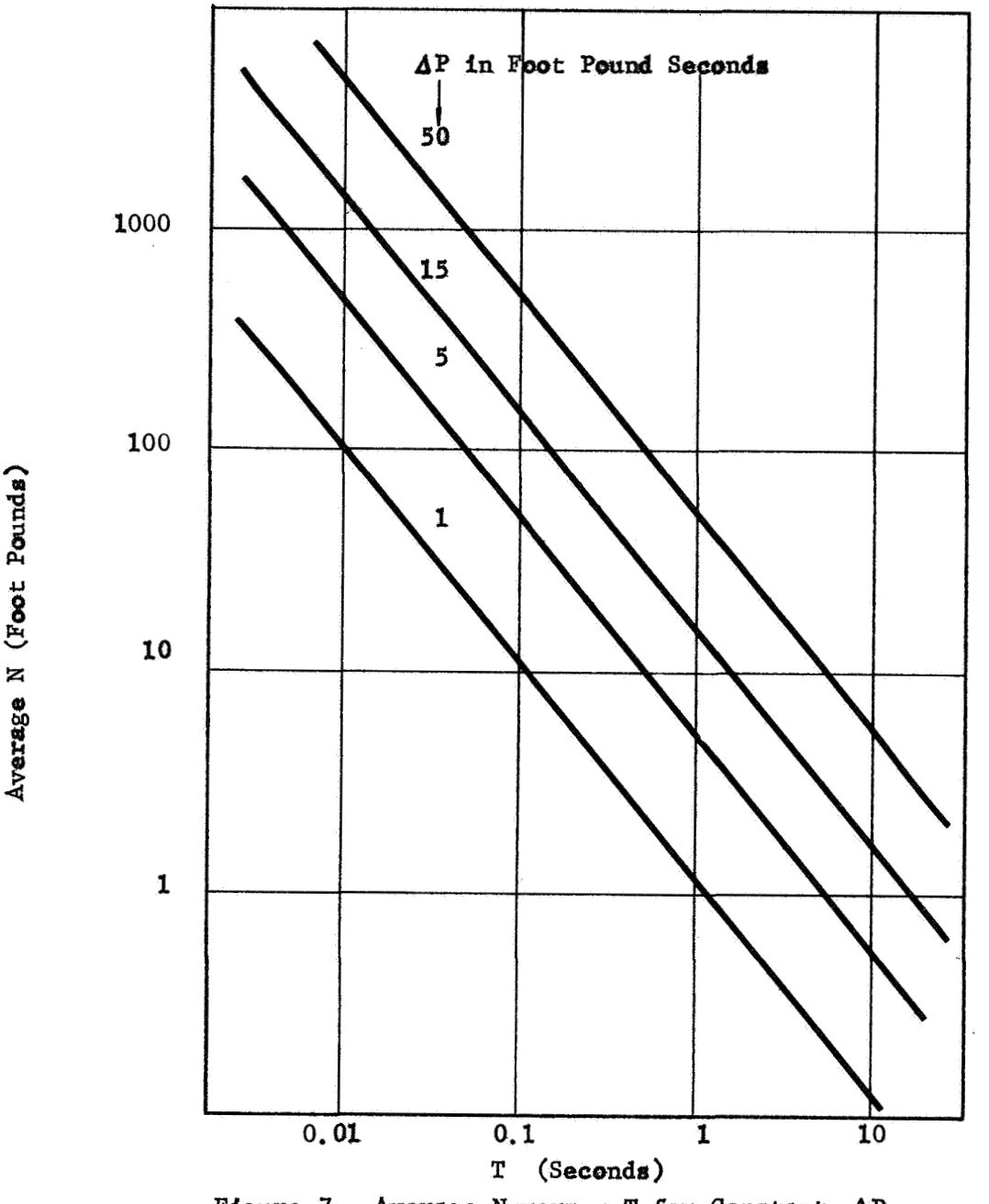

Figure 7 Average N versus T for Constant ΔP

Note:
Slippage rate based on one-foot distance from attachment point to Target's c.g.

Slippage distance ≈ 1/2 rate shown times attachment time.

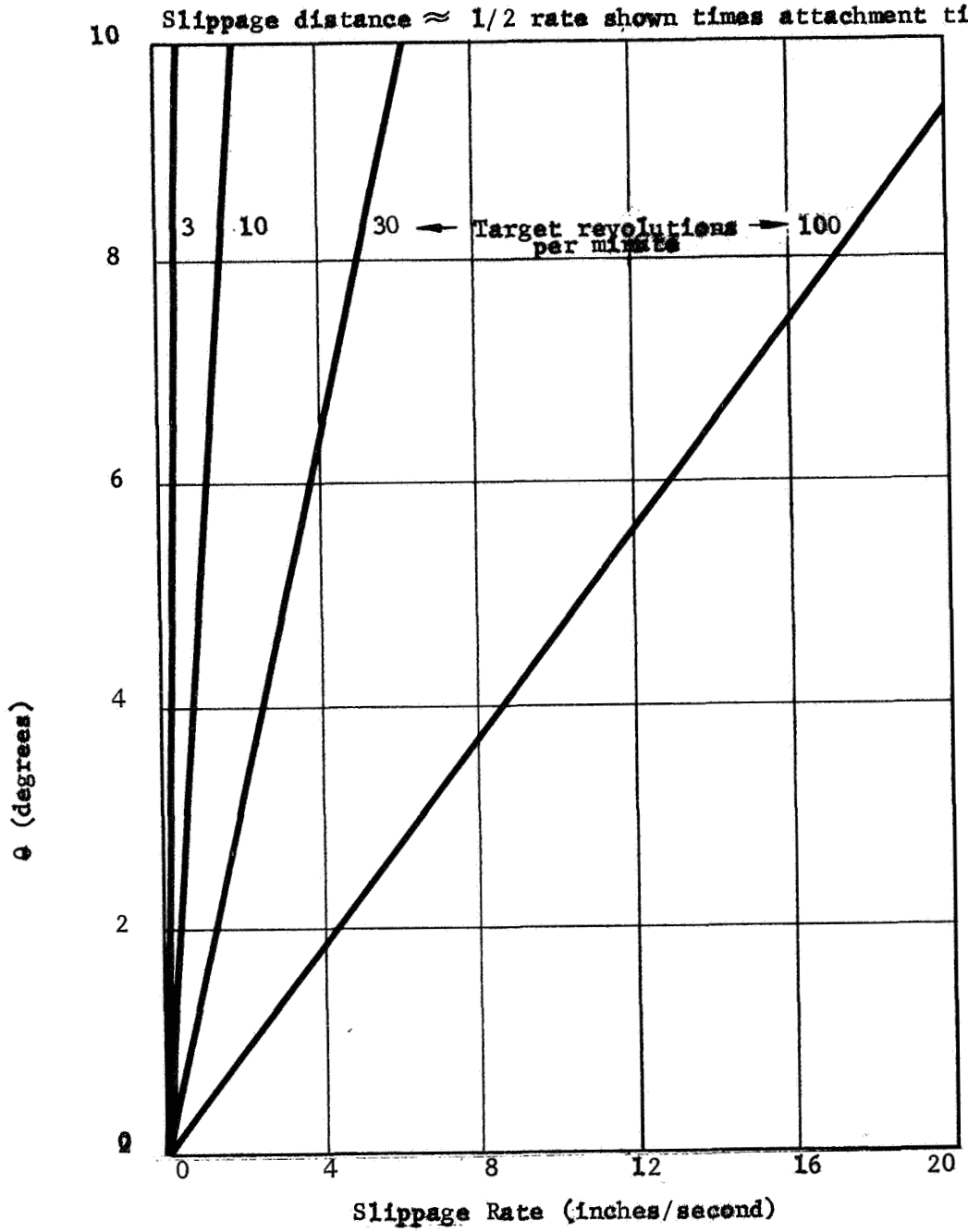

Figure 8 Attachment Head Slippage Rates versus Φ for Constant Target Spin Rates

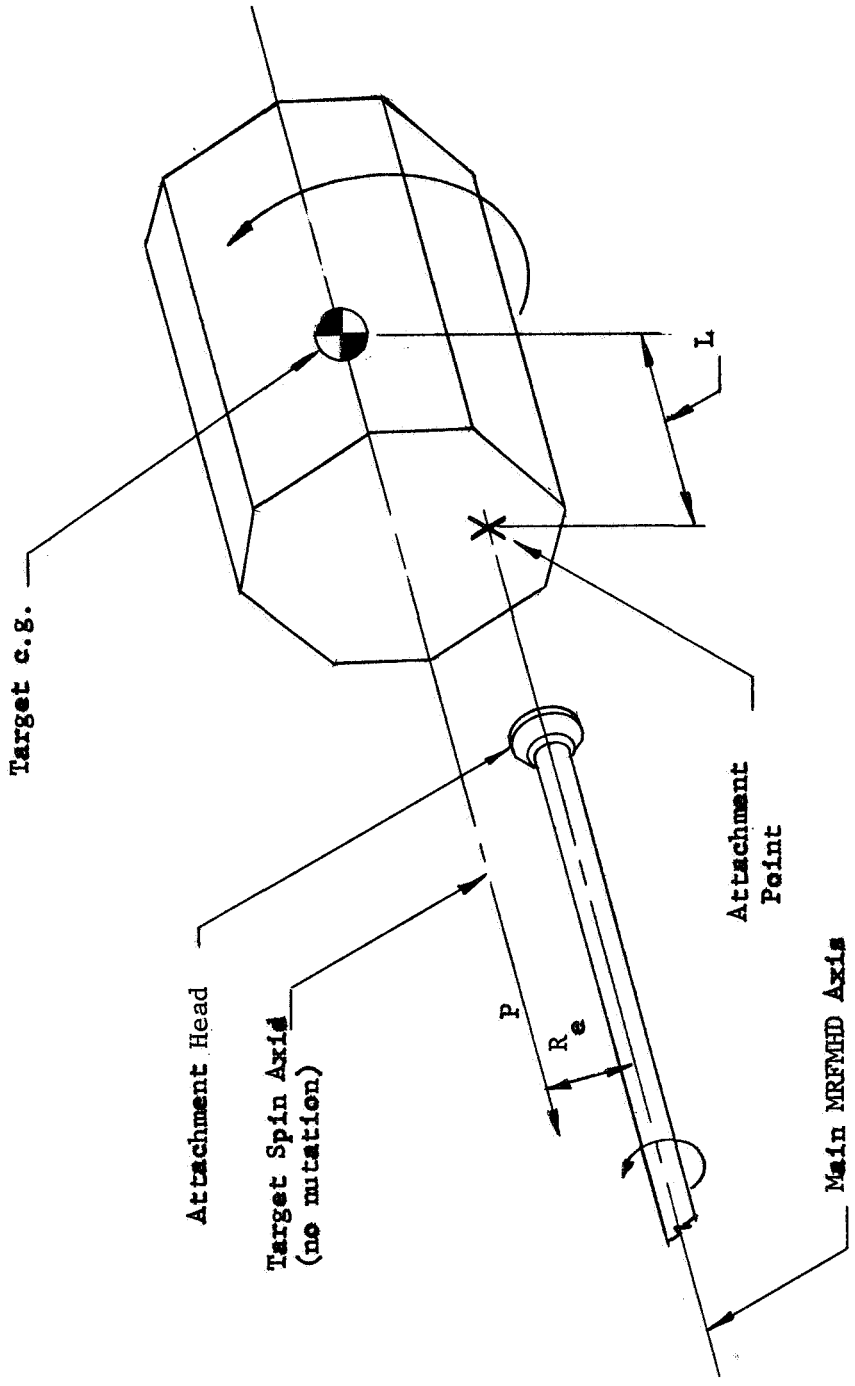

Figure 9 MRFMHD Axial Misalignment with Target

times its moment arm, L, about the AH. This torque, N_c, is, therefore,

$$N_c = M\omega_2^2 R_e L.$$

Using the same mid-range example used previously and adding (1) a target mass of twenty slugs (this being consistent with the other parameters), (2) $\omega_2 = 3$ radians/sec, and (3) $R_e = 0.1$ foot, N_c is found to be

$$N_c = (20)(3)^2(0.1)(1)$$

or

$$N_c = 18 \text{ ft-lb.}$$

Note that, as in the angular misalignment case, slippage will occur at the attachment point during build-up of the rigid attachment. During rigidizing, the attachment must support a progressively larger torque until N_c is fully developed.

In some satellite attachment tasks, it will not be possible to effect an off-axis attachment of the type just described. This is due to the probable axial symmetry of both the AH and the target's attachment interface. In these cases, the attachment operation will convert axis offsets into angular misalignments similar to the angular misalignments discussed earlier in this section.

Although the examples treated in this section are simplified, they serve to point up three significant factors. First, torques on the attachment interface (and, therefore, the target) can reach very large values if a rigid attachment is made rapidly. Second, the size and type of attachment errors will have direct influence on the degrees-of-freedom and structural characteristics that must be designed into the MRFMHD system and its interface to the CSM. Third, the AH must be capable of supporting torques perpendicular to its axis during the time required to develop rigid attachment between the AH and target.

b. Dynamics During Maintenance, Repair, and Transport - After the target is firmly attached to the CSM/MRFMHD, the attachment interface must have sufficient strength to withstand the fifteen foot-pound despinning torque (from Assumptions and Guidelines) and to support the target during maintenance, repair, and transport operations.

Consider first the effect of firing the CSM reaction control system (RCS) quads to generate translation. The forces available along the three principal axes of the CSM are:

$$F_x = 400 \text{ lb.}$$

$$F_y = 200 \text{ lb.}$$

$$F_z = 200 \text{ lb.}$$

If the target mass is M_T and the CSM mass is M_{CSM}, then, for a force applied through the c.g. of the system, the target will be subjected to a force F_T where

$$F_T = F \frac{M_T}{M_T + M_{CSM}}$$

From the contract's Assumptions and Guidelines, the maximum value of M_T is one-hundred and forty-one (141) slugs. With M_{CSM} equal to one-thousand (1,000) slugs, the maximum value of F_T is

$$F_T = F \frac{141}{1141} = 0.124F.$$

Therefore, quad firings on the CSM produce the following forces on a maximum mass target.

$$F_{TX} = 49.6 \text{ lb.}$$

$$F_{TY} = 24.8 \text{ lb.}$$

$$F_{TZ} = 24.8 \text{ lb.}$$

where F_{TX} is the force felt by the target parallel to the CSM's X axis, etc. For smaller targets, the forces are reduced proportionately.

These forces are those that would be exerted on the target during transport operations utilizing the CSM RCS quads. If a major translation maneuver or significant orbit change is required, the Service Module's main engine (20,500 lb. thrust) may be fired. The force would be along the CSM's X axis and would place the MRFMHD in compression. For a maximum mass target, F_{TX} would be twenty-five hundred and forty (2,540) pounds.

If attitude changes are required, the CSM quads will be fired, producing their normal couples on the combined MRFMHD/CSM/Target. The CSM's inertia characteristics are[1]:

$$I_{XX} = 18{,}800 \text{ slug ft}^2 \text{ (roll axis)}$$

$$I_{YY} = 50{,}300 \text{ slug ft}^2 \text{ (pitch axis)}$$

$$I_{ZZ} = 45{,}800 \text{ slug ft}^2 \text{ (yaw axis)}$$

Two one-hundred (100) pound thrusters are fired to produce the attitude control couples, giving a moment of thirteen hundred (1,300) foot-pounds (moment arm for each thruster is six and one-half feet).

The maximum anticipated target moment of inertia is on the order of 3,000 slug feet^2 with a mass of approximately 140 slugs. If this target is attached to the MRFMHD so that the target's c.g. is twenty (20) feet from the combined c.g., the target will add approximately 140×20^2 or 56,000 slug-feet^2 to the CSM's moments of inertia in pitch and yaw. For simplicity, assume that this gives the combined system an I_{YY} and I_{ZZ} of 100,000 slug feet^2. Also, assume that the target's 3,000 slug feet^2 is added to the CSM's I_{XX}, giving a combined I_{XX} of 21,800 slug feet^2. Firing the CSM quads for attitude change will produce the following acceleration levels:

$$\text{roll acceleration} = \dot{p}^{\circ} = \frac{1300 \text{ ft lb}}{21{,}800 \text{ slug ft}^2} = 0.06 \text{ rad/sec}^2$$

$$\text{pitch acceleration} = \ddot{\theta} = \frac{1300 \text{ ft lb}}{100{,}000 \text{ slug ft}^2} = 0.013 \text{ rad/sec}^2$$

$$\text{yaw acceleration} = \ddot{\psi} = \frac{1300 \text{ ft lb}}{100{,}000 \text{ slug ft}^2} = 0.013 \text{ rad/sec}^2$$

(1) North American-Rockwell data on CSM mass properties, not fully fueled, February 1968.

The torque on the target about the roll axis would be 3,000 slug feet^2 x 0.06 rad/sec^2 = 180 ft lb. The attachment head must transmit this torque. In pitch and yaw, one effect is a tangential acceleration of the target at the end of the MRFMHD boom. The attitude acceleration rates of 0.013 rad/sec^2 are equivalent to 0.26 ft/sec^2 under the given conditions. With a 141 slug target, the AH must, therefore, transmit a tangential force of 141 x 0.26 or 36.7 pounds to the target during a pitch or yaw maneuver. If the target's I_{YY} and I_{ZZ} are on the order of 3,000 slug feet^2, the AH must also exert a torque of 3,000 slug ft^2 x 0.013 radian/sec^2 or 39 foot pounds on the target during these maneuvers.

Note that the forces and torques transmitted by the AH to the target during CSM attitude maneuvers are approximately proportional to the target mass and inertia characteristics.

Table 1 presents attachment head interface loads for four target configurations as a function of CSM RCS quad firings and Service Module main engine firing. The mass and inertia characteristics are for the target alone. A twenty foot separation between the target's c.g. and the combined (CSM/MRFMHD/Target) c.g. is assumed. The X axis is the longitudinal axis of the system (passes through CSM c.g. and target c.g.).

With regard to forces and torques generated during maintenance and repair operations, an attachment interface should be capable of supporting these if the interface supports the Target No. 4 interface loads given in Table I. The only restriction might be that an astronaut should not push-off from the target with large forces if he is several feet from the attachment interface. Such push-offs can create extremely large torques at the attachment interface.

c. Dynamics During Spin-up and Release - The third stage of target handling is spin-up, if required, and release. For targets not requiring spin-up, precise maneuvering may be required to place the targets in position relative to other objects. As an example, the MRFMHD could be used to transport and position large antenna or space station segments for assembly. It is imperative that the MRFMHD release these objects without delivering impulses that would disturb the assembly.

A potentially more difficult task is presented if the target requires precise spin characteristics at, and following, release. For a target of this type, a predetermined spin rate must be developed by the main MRFMHD spin axis. Note that the desired target spin axis should be aligned to this axis before spin-up is initiated if post-release nutation is to be avoided. This also allows the CSM's roll thrusters to counteract the CSM's reaction to the spin-up torque. When the spinning target is released, any transverse moments exerted

Table I Attachment Interface Loads During CSM Engine Firing

	Target Characteristics														
					Interface Loads *										
					** Roll	** Pitch		** Yaw		** X	** Y		** Z		*** X
Target	Mass	I_{xx}	I_{yy}	I_{zz}	M_x	M_y	F_z	M_z	F_y	M_x	F_y	M_y	F_z	M_z	F_x
1	5	4	4	4	0.24	.052	1.04	.052	1.04	1.9	.99	0	.99	0	100
2	14	30	30	30	2.1	.700	6.50	.759	7.06	5.5	2.8	0	2.8	0	283
3	40	300	300	300	18	3.90	10.40	3.90	10.40	15.4	7.6	0	7.6	0	788
4	140	3000	3000	3000	180	39.0	36.4	39.0	36.4	49.1	24.3	0	24.3	0	2517

* Forces in Pounds, Torques in Foot-Pounds
** From CSM RGS Quads
*** From SM Main Engine

on the target by non-uniform release will produce nutation in the target. The time integral of these release moments, therefore, must be small enough that the target nutation is within the control range of the target's nutation dampers.

3. Attachment Heads

This portion of the MRFMHD feasibility study covered the methods available to make and break a mechanical link between the CSM/MRFMHD and the target. The approach used in the study was to examine each potential AH to establish its capabilities and limitations. This was followed by selection of the best head that could also be improved easily with advances in the state-of-the-art.

The heads may be divided into two basic categories; adhesive and non-adhesive. Included in the former are thermoplastics, contact adhesives, two-component "epoxy" type systems, and electro-adhesors. The non-adhesive category includes all types of mechanical hands, nets, encircling arms, penetrating probes, etc. Of these, nets, penetrating probes, and momentum-propelled enwrapping arms can be discarded immediately due to their ability to damage external structures (antennas, solar panels) and/or internal parts. The following material covers the remaining potential devices.

a. Adhesive Attachment Heads - Intuitively, one of the most appealing AH concepts is a head with a sticky interface that would bond to a selected target point on contact. The attachment point could be located at any convenient point on the target and the attachment would not rely on cooperative interfaces such as those used for docking. With this thought in mind, a number of studies have been conducted to develop an adhesive attachment system for use in space (Refs. 1,2,3,4,5,6,7). Before discussing these studies and other references that relate to the adhesive problem, it is worthwhile to examine various categories of adhesives and define the terminology associated with them.

The adhesive attachment systems examined during this study fall into the following basic categories:

i. Thermoplastic - Substances that soften and become tacky (capable of wetting and sticking to a target surface) when heated to their working temperature.

ii. Two-component systems - Two chemical substances that, when mixed, generate chemical reactions that cause, or increase the speed of, the setting of the mixture.

iii. Pressure sensitive and contact - Substances possessing tack throughout their working temperature range without the addition of heat or chemicals.

iv. Thermosetting - Fluids, or solids that become fluid when heated initially, that solidify with the application of heat.

v. Electro-adhesive - Devices that develop sufficient electrostatic field across an interface to hold the interface together.

With the exception of the electro-adhesives, the categories above are not mutually exclusive. For example, ordinary rubber cement is thought of as a contact adhesive since surfaces coated with this material will bond together if brought into contact at room temperature. However, if the room temperature was -100°F, the rubber cement would have to be heated to liquify it prior to use, the surfaces to be bonded would have to be heated, and, in that context, we would describe the cement as a thermoplastic.

Similarly, some of the two-component systems are basically thermosetting resins (e.g. urea, epoxy, phenolic) to which a catalyst is added to initiate the curing process at reduced temperatures. The catalytic reaction is frequently exothermic, hastening the cure cycle.

In the material that follows, the adherend is the target surface to which the adhesive must attach and the working temperature of an adhesive is that temperature or temperature range in which the adhesive is capable of wetting the adherend.

All of the adhesives that are discussed have the potential to form a satisfactory bond (i.e., capable of supporting the system dynamic loads) if they are applied properly to the adherend. Such a bond will remain intact if the adhesive support is properly designed. The most critical factor in this support is designing to minimize peel loads (torques on the bond about an axis in the plane of the bond) since adhesives are considerably weaker in peel than in tensile or shear strength.

Emerson Electric Company, while performing a study under Air Force sponsorship (Ref. 1), examined twenty-four adhesives in combination with eight typical aerospace (satellite) adherends under a variety of temperature and vacuum conditions. Their results indicated that cyanoacrylate adhesives[2] (Eastman 910 and Locktite 404) could be used in space if a suitable application method can be developed. The application problem develops because these adhesives develop an inhibiting "skin" when exposed to vacuum. Therefore, the fluid must be released and exposed to vacuum at the instant the AH contacts the target.

Another significant result of Emerson's study was that none of the adhesives tested were capable of forming a bond over the complete target temperature range expected (-250°F to +250°F). Therefore, if current adhesives are used in the AH, means must be provided to preheat the

(2) Cyanoacrylate adhesives are contact-type fluid adhesives that polymerize and set when subjected to pressure on the bond line. (Ref. 7 pp. 409-414).

adherend to a suitable temperature. Generally speaking, this temperature would be on the order of 0°F for pressure sensitive adhesives, 70°F for two-component systems, and 300°F or higher for thermoplastic adhesives.

The National Cash Register Co., under Air Force contract, developed an adhesive pad to provide astronaut attachment points on vehicles while the astronaut performs extravehicular activities (EVA). This study (Ref. 8) examined several adhesives in the pressure sensitive and two-component categories. After screening to find the best adhesive for use in space, Eastman 910 was selected. Dimethyl p-toluidine was found to be beneficial as a catalyst to speed the curing process. National Cash Register has successfully encapsulated these compounds (using their microencapsulation processes) to make them suitable for use in space in pad form. The dry capsules are mixed together in the pads. On contact with the target, the capsules rupture when compressed with a force of two to four pounds per square inch, the compounds mix, and a suitable bond is achieved on the target in less than thirty seconds. The target temperature must be maintained above 0°F during the curing interval.

The combination of the Emerson and National Cash Register studies therefore indicates that Eastman 910, furnished by Eastman Chemical Products, a subsidiary of Eastman Kodak, could become the basis for a successful space adhesive system. The basic problems to be solved for the system are (1) preheating cold targets, (2) replenishing the adhesive pads to provide a sufficient number of attach/detach cycles, and (3) holding the adhesive in position during the cure interval.

Another group of contact adhesives that have potential, but lack sufficient testing and documentation at this time, are the Alloprene chlorinated rubber adhesives produced by I.C. I. Organics/Incorporated, a subsidiary of I.C.I. America Incorporated. These materials, described in reference 9, might be handled in a manner similar to the cyanoacrylates. The chlorinated rubber base material would require preheating of cold targets and extended use on targets above 200°F could result in bond weakening.

With all of the contact adhesives described, preheating of cold targets is required. Equally important, the adhesive must be heated to above 0°F to achieve satisfactory bonds. However, preheating the adhesive on the MRFMHD can be accomplished relatively easily with resistance heaters (Ref. 6) and is not considered a technical problem of the same magnitude as target preheating.

Martin Marietta, under contract to the National Aeronautics and Space Administration, developed an adhesive attachment button for use in space (Ref. 5). A thermosetting epoxy film, FM-98 (70% aluminum filled) supplied by the Bloomingdale Department of American Cyanamid Corporation, was used in the adhesive interface. The one square inch

pad was heated with ninety-six watts for 15-20 seconds to produce bond-line temperatures of 400°F that cured the epoxy. A one pound second impulse delivered to the button during heating was sufficient to seat the softened epoxy film on the aluminum adherend. The bond-line temperature must be monitored with a thermocouple to insure sufficient heating while preventing excess heating.

Bonds made on adherends at room temperature were cooled to -250°F and tensile tested to failure. The failure loads ranged from thirteen to eighty pounds on the one square inch pad. A swivel joint as shown in Figure 10 was placed on the back of the pads to prevent development of peel loads on the bond-line.

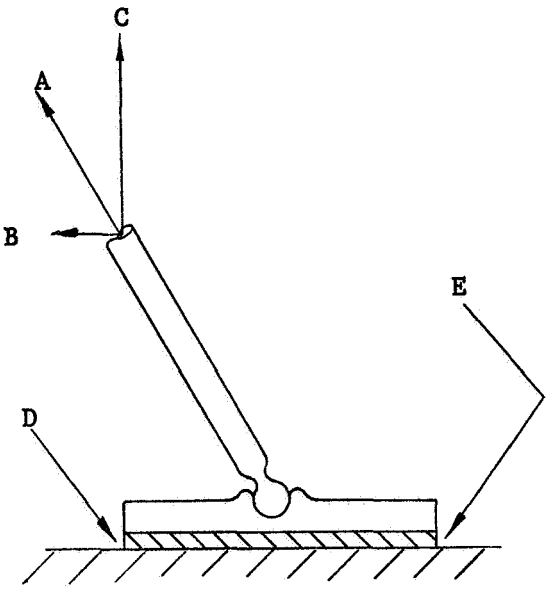

With swivelled pad, support arm aligns with force A, resolving A into shear, B, and tensile, C, forces on the pad. This prevents development of torques about D that would open the adhesive joint at E.

Figure 10 Adhesive Pad with Swivel to Prevent Peel Loads

As in the case of adhesives discussed previously, the adherend temperature must be higher than 0°F for this system to work properly. At this adherend temperature, the adhesive and heater can supply sufficient heat to the adherend to permit adhesive wetting of the adherend. Since this is a thermosetting system, the adhesive button must be replaced for each attach/detach cycle. This system, or any other thermosetting system, has the particular requirement for significant heating to activate and cure the adhesive.

The need to refurbish the thermosetting adhesive led to examination of thermoplastic adhesives. These have the advantage that the adhesive can be used for several attach/detach cycles. A single

pad would be useful until the cumulative adhesive loss to the targets degraded the pad significantly.

One of the most suitable adhesives examined in this class is the phenoxy thermoplastic resin developed by Union Carbide Plastics Company (Ref. 10). These are high molecular weight compounds that exhibit characteristics that indicate they could satisfy the AH requirements. They are thermally stable to 600°F but require heating to only 300°F or above to become fluid. From 210°F to 300°F, phenoxy behaves like a thermoplastic rubber. It transforms to a rigid material (goes through its glass transition) when cooled to 210°F. Tests (Ref. 10) indicate that the material remains highly impact resistant at temperatures down to -40°F. Although no test data were found down to -250°F, the literature indicates satisfactory material properties at least to -80°F. The adhesive heater should be capable of maintaining the adhesive at temperatures above this level once the bond is achieved.

With phenoxy resin, the bond-line must reach a temperature above 300°F in order for the adhesive to wet the adherend. Therefore, unless the target is a poor heat sink that does not draw heat away from the bond-line, the adherend must be heated to the adhesive working temperature. Several methods are available to perform this operation but none has been developed and proven for use in space. Radiant heaters may be used prior to target contact and conduction heaters after contact. D. J. Kolb (Ref. 11) has described a method for heating thermoplastic bond-lines with ultrasonic energy. The high frequency vibrations are transmitted through the plastic to the mechanically-loose bond-line. Here, the vibratory energy is converted to heat as the thermoplastic vibrates against the adherend. This system appears desirable from the standpoint that heat is generated at, and only at, the desired location. However, once the bond is achieved, the ultrasonic method cannot be used to heat the interface for disengagement since the ultrasonic energy will pass through the bond-line and dissipate in the target structure without significant heating at the bond-line. This factor, plus the possible requirement for low-level, steady-state heater operation to maintain the adhesive above some detrimental temperature range, leads to a recommendation of conductive or combined radiant/conductive heaters if thermoplastics are used. Since the bond will not set until its temperature drops below the working temperature, excess heating must be avoided.

When the AH is separated from the adherend, a thermoplastic will tend to separate where the temperature is highest. Therefore, resistance heaters cannot be used in a thermoplastic pad during detachment if the pad is intended for re-use since the adhesive would separate at the heater. To separate satisfactorily, heat must be applied to the adherend and conduction must carry it through the adherend body to the bond-line. Maximum adhesive will be retained on the pad using this

procedure.

Another adhesive concept examined during the study is the electrostatic adhesion system developed and studied by Chrysler Corporation Space Division under NASA contracts (Refs. 3,4). These heads develop attractive forces with electrostatic charges on the AH and adherend. A potential of several thousand volts is applied between the AH and the adherend. They are separated by a thin dielectric film on the AH. The dielectric polarizes and opposite electrostatic charges develop on the target surface. The product of the field strength (voltage differential divided by film thickness or AH/Target separation) times the accumulated electrostatic charge determines the "adhesive" force. Reported results (Refs. 3,4) indicate that "adhesive" forces of several pounds per square inch can be developed on aluminum adherends under laboratory test conditions. However, the dielectric must remain intact, insulating, and capable of being polarized over the -250°F to +250°F range to use this head on the MRFMHD. No state-of-the-art dielectric has been found that will satisfy this requirement. However, temperature control of the interface could make the head practical. If this is done, problems will remain, namely (1) test data indicates several seconds are required for force decay after power is removed, thereby complicating the separation problem, (2) surfaces that are rough, dirty, extremely conductive, or highly insulated are more difficult to attach to, (3) the heads are very susceptible to peel forces, and (4) the heads require use of high voltages at the attachment interface.

The adhesive attachment systems discussed in this section, including the electrostatic heads, represent those systems that appear promising for an adhesive interface on the AH. Table II summarizes the pertinent information for these systems. The problems associated with providing a suitable, dynamic, mechanical support for any of these systems are discussed in Section II.3.c.

b. Non-adhesive Attachment Devices - The apparent thermal control and refurbishing requirements for adhesive heads point up the need to consider non-adhesive attachment heads. One of the prime criteria for such a head is that it must take the form of a controlled manipulator. Any uncontrolled enwrapping arms or snares would almost certainly damage or destroy exposed structures and equipment on certain targets.

In view of the physical variations in satellites (Section II.4), the non-adhesive, or mechanical, AH must have the capability to grapple the targets in a variety of ways. This assumes that the targets are not intentionally equipped with cooperative attachment interfaces. This is the case with current satellites. However, a number of existing satellites (Explorer, Echo, Tiros, Relay, Syncom, Discover, Transit, etc.) have been orbited by Scout, Delta, and Thor-Agena launch vehicles in configurations such that the satellites have payload separation flanges or structures remaining on their surfaces (Ref. 12). These flanges or

Table II. Adhesive Summary

Adhesive	Type	Supplier	Applicable Target Temperatures (without supplementary heating) -250°F 0°F 250°F	To Extend Thermal Range	Other Problems	Reusable
"Eastman 910" (encapsulated) (catalyzed)	Contact and pressure setting	Eastman Chem. Products, National Cash Register		Heat targets to 0°F		No
"Alloprene"	Contact	1C1 Organics		Heat targets to 0°F		No
"FM-98"	Thermo-setting epoxy	American Cyanamid (Bloomingdale)	(1)	Heat targets to 0-70°F	High adhesive setting temp. (400°F)	No
"Phenoxy"	Thermo-plastic	Union Carbide Plastics Co.		Heat targets to 250-300°F	Heat target to separate bond line	Yes
"Electroadhesor"	Electro-static	Chrysler	(2)	Heat or cool targets to proper range	Lower attachment forces on good conductors, good insulators, and rough and/or dirty surfaces. High voltage at interface.	Yes

(1) - adhesive heats target to 70°F
(2) - Buna-N dielectric

structures range from eight to twenty-five inches in diameter and are generally placed symetrically with respect to the spin axis of the spin-stabilized satellites. Therefore, these flanges or structures can be regarded as semi-cooperative attachment interfaces that are available for non-adhesive grappling.

In order to handle those satellites not equipped with semi-cooperative interfaces and the variety of targets that can be classified as bulk material packages in space manufacturing or structural assembly operations, the mechanical AH must have a "hand" that can adjust to a wide range of target sizes and shapes. Figure 11 illustrates a summary of the basic anticipated volume configurations that must be handled. The head must be rugged enough to handle the large objects. Given sufficient structural strength, the head could also be used as a prod or bumper, if required, to alter target dynamics to aid in subsequent assembly or attachment operations.

Taking these factors into consideration, the basic, two-armed, mechanical AH shown in elementary form in Figure 12 was designed. In a trade-off against a three-armed configuration which is inherently more stable after attachment, the two-arm system was chosen because; (1) clamping forces lie in the plane of the arms, (2) the arms occupy a plane, rather than a volume, thereby simplifying the approach to and grappling of targets having delicate appendages, (3) two arms are ideal for clamping on boxes and octagonal sided objects since the arms approach the object surfaces perpendiculary, (4) with given arm size, two arms can grapple a larger target than a three-arm system, (5) when grappling long cylinders or box sections at their centers (approach perpendicular to long axis), the two-arm grappling center coincides with the MRFMHD axis while a three-arm AH would offset the target center from the MRFMHD axis as shown in Figure 13, and (6) the moment of inertia of the two arms is smaller than the moment of inertia of three arms, thereby reducing loads on the MRFMHD structure and spin drive.

Consideration was also given to a four-armed head consisting of two sets of independently controllable arms as illustrated in Figure 14. This head would have the capabilities of the two-armed head plus the option to utilize all four arms to: (1) enhance post-contact stability, (2) reduce any angular misalignment tendency, and (3) eliminate any possibility of axial misalignment when grappling symmetric targets. The main problem associated with this system would be the necessary hardware and control complications. At the present time the four-armed head is not felt necessary to enable definition of MRFMHD problem areas.

Remote manipulators satisfy the controllability requirements for a mechanical AH by using force feedback and the operator's sensory system. Developed for radioactive materials handling, underwater work and

Sizes limited only by launch or assembly constraints

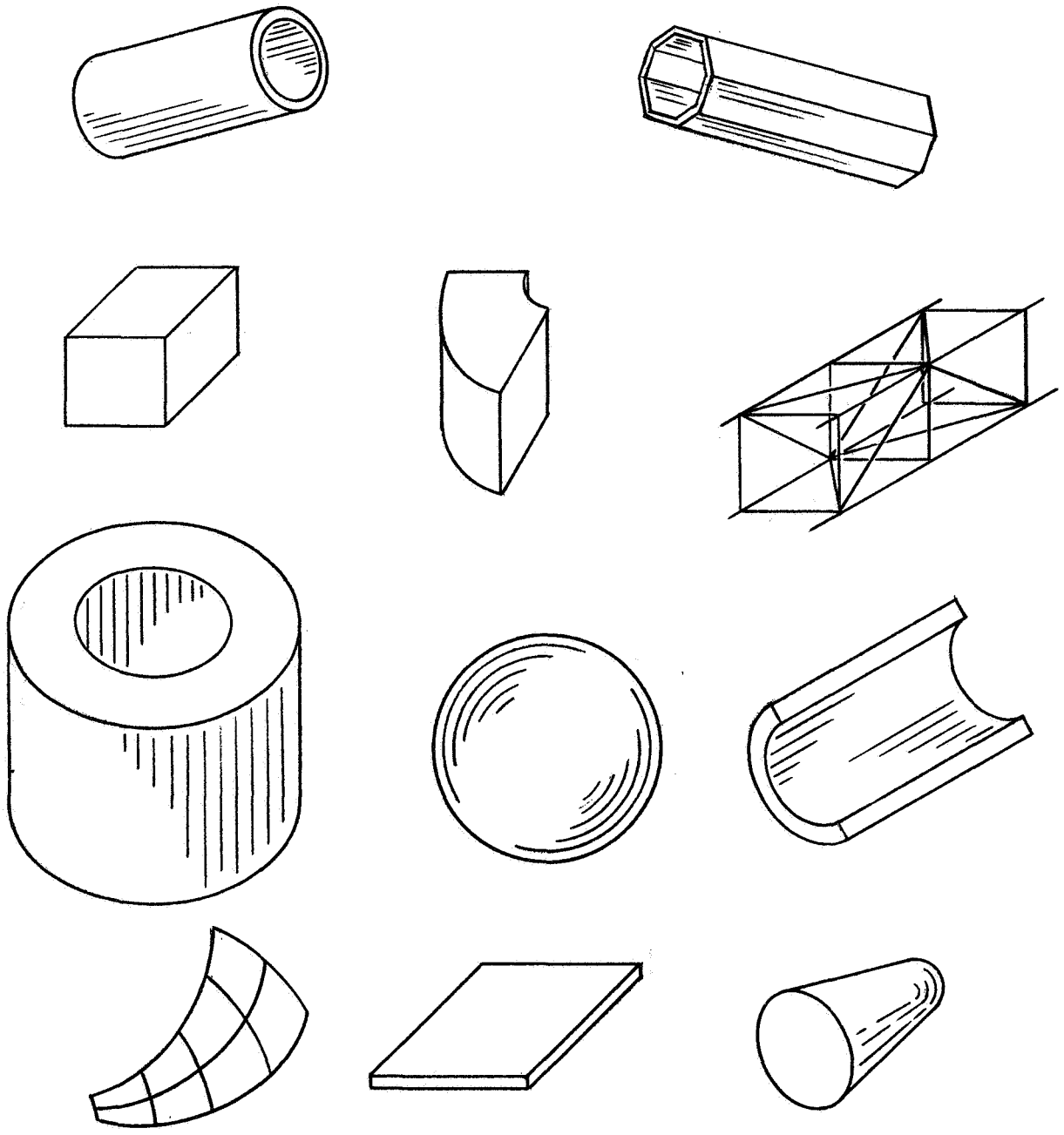

Figure 11 Bulk Material Configurations

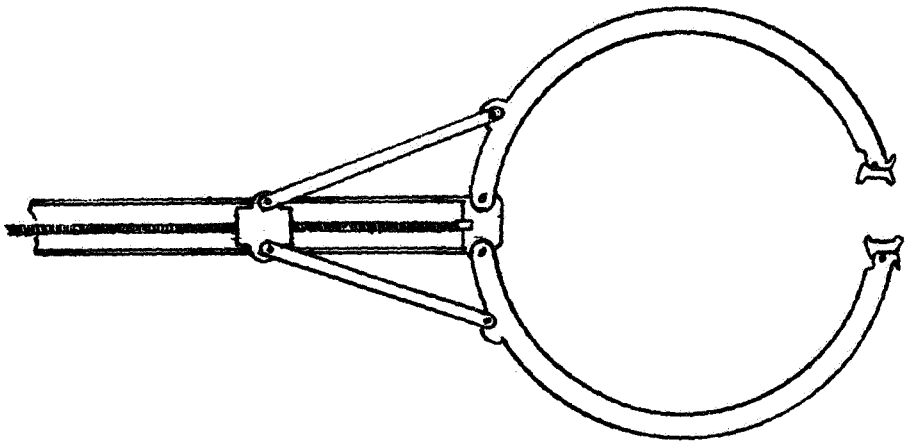

Figure 12 Basic Two-Armed MRFMHD Attachment Head

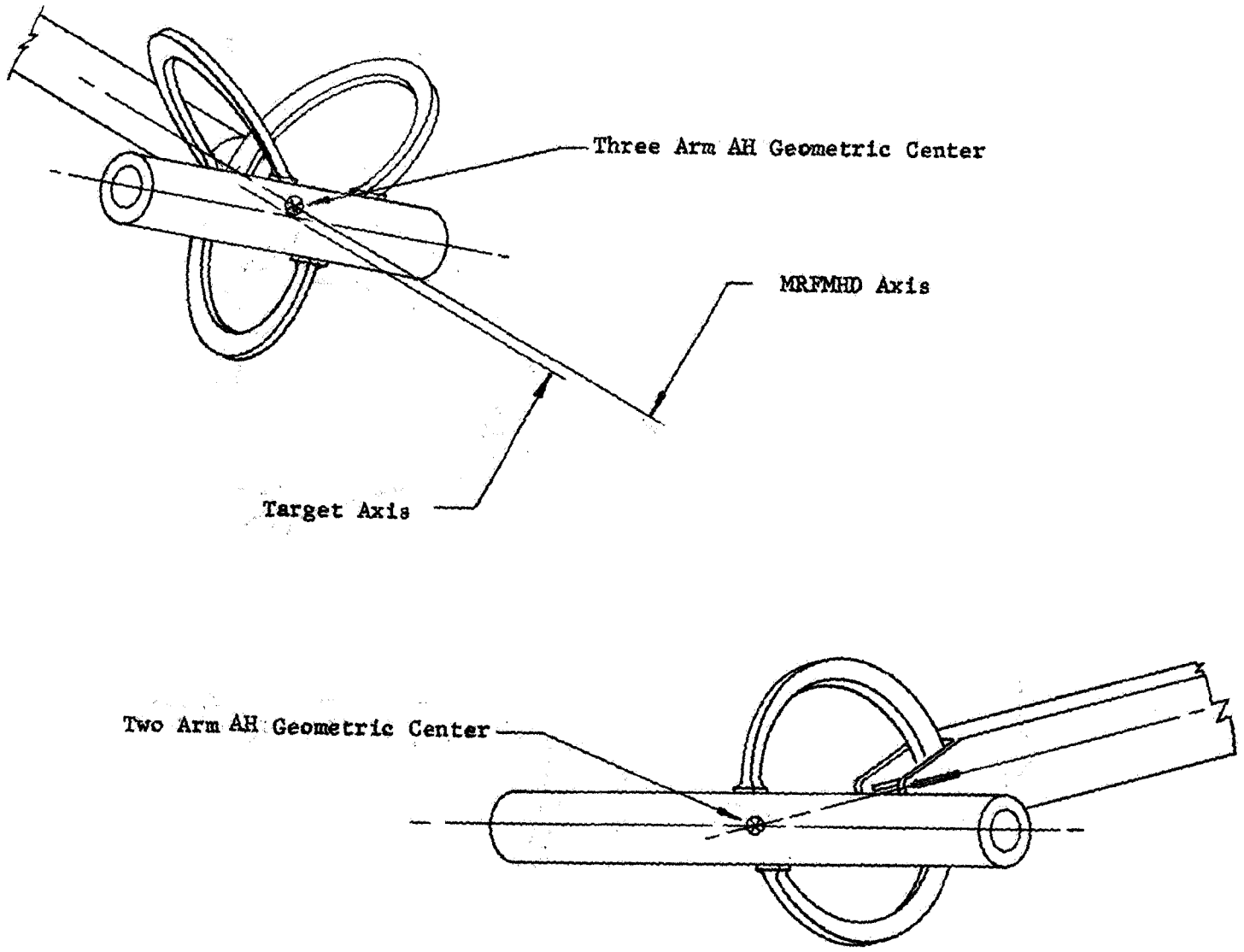

Figure 13 Two-Versus Three Arms Grappling Long Cylinder

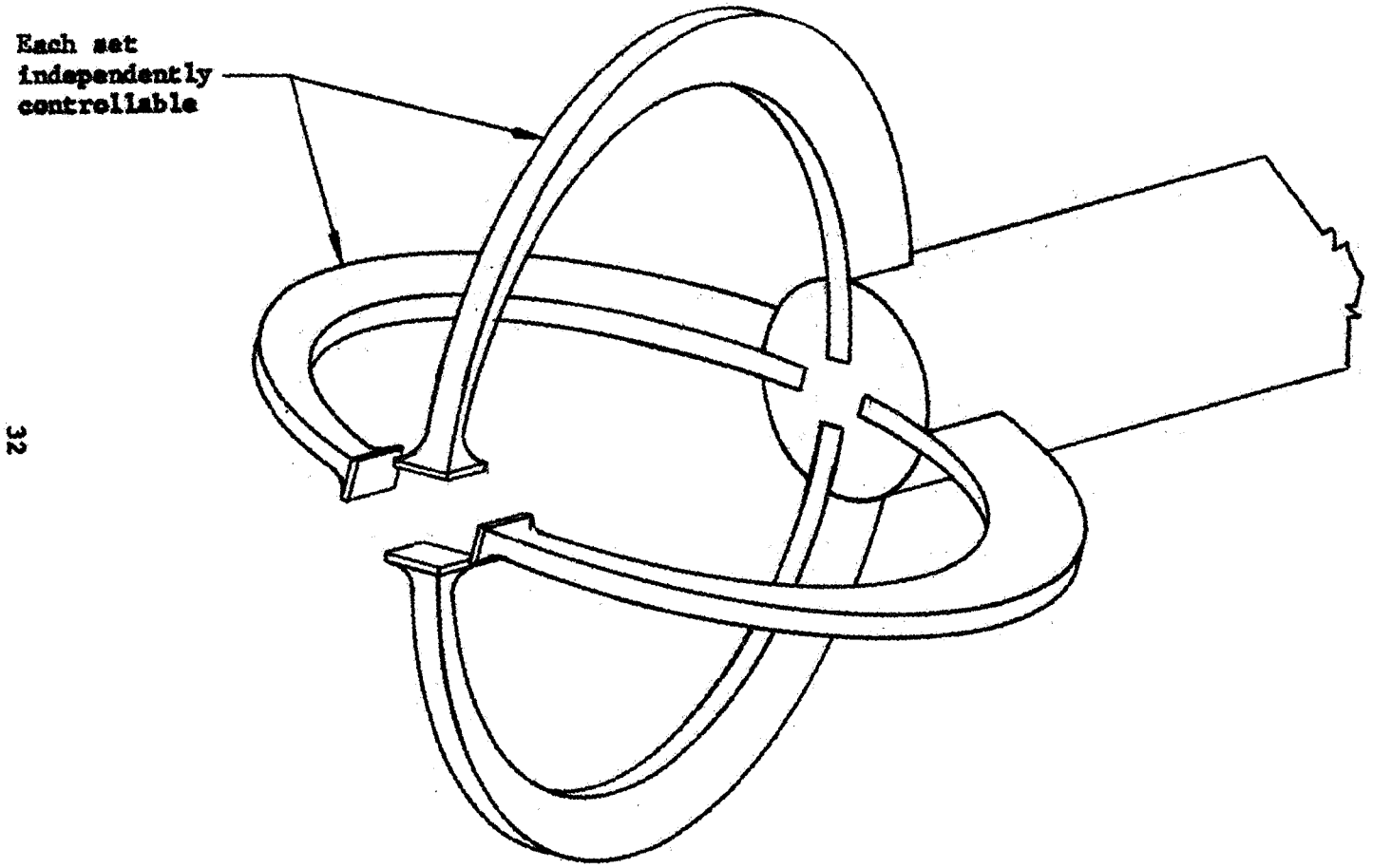

Figure 14 Basic Four-armed MRFMHD Attachment Head

similar tasks, this type of manipulator consists essentially of anthropomorphic mechanical arms and hands connected through a bilateral servo-control system to a master station manned by the human operator. In performing tasks, the servo-mechanical system moves to duplicate the motion of the operator.

However, the remote manipulators represent an overly complex system to satisfy the material handling problem. It is assumed that remote manipulators could be designed to support the dynamic loads, but due to their weight and basic complexity, remote manipulators were ruled out for MRFMHD applications.

c. Selected Attachment Device - Based on the considerations presented in the preceding sections, an integrated adhesive/mechanical AH concept was developed. The prime AH is the two-armed grappler with the following additions that make it more versatile.

The grappling pads at the outer ends of the arms should have a configuration similar to the one shown in Figure 15. The single-axis swivelled pads can pivot in one direction to make the grappling surfaces parallel across a wide range of arm openings. At the same time, the pads are mechanically restricted so that a target projection can be grasped without having the pads pivot outward and lose their grip. In addition, a hook projection is incorporated in each arm adjacent to the pads. These can be used to grapple targets by opening the arms after the ends are inserted into a suitable target cavity or open-center flange. Finally, pads are incorporated on the arm inner surfaces to cushion objects that are encircled by the arms. These pads should be composed of suitably bound packets of material such as steel wool that will remain resilient over the expected range of temperatures.

The next item to be considered is the adhesive AH. Two criteria were developed concerning its configuration and location. First, the head should be physically protected during material handling operations using the two mechanical arms. Second, the head should be easily deployable. The attachment operations described in the system dynamics section require that (1) the head be symmetrically located about the MRFMHD's main spin axis and (2) the pads must incorporate degrees of freedom to allow the pads to follow the target during adhesive setup. The latter requirement is based on the AH slippage. The size of the allowable motion within these degrees of freedom will depend on the simulation results from Task E (position and angular offsets at attachment).

The adhesive AH must be composed of several pads, as opposed to one central pad, in order to develop sufficient strength to support the AH torque loads and to provide attachment stability. During the study, three-pad and four-pad AH's were considered. A three-pad AH would automatically conform to the target in the same way a tripod seats on

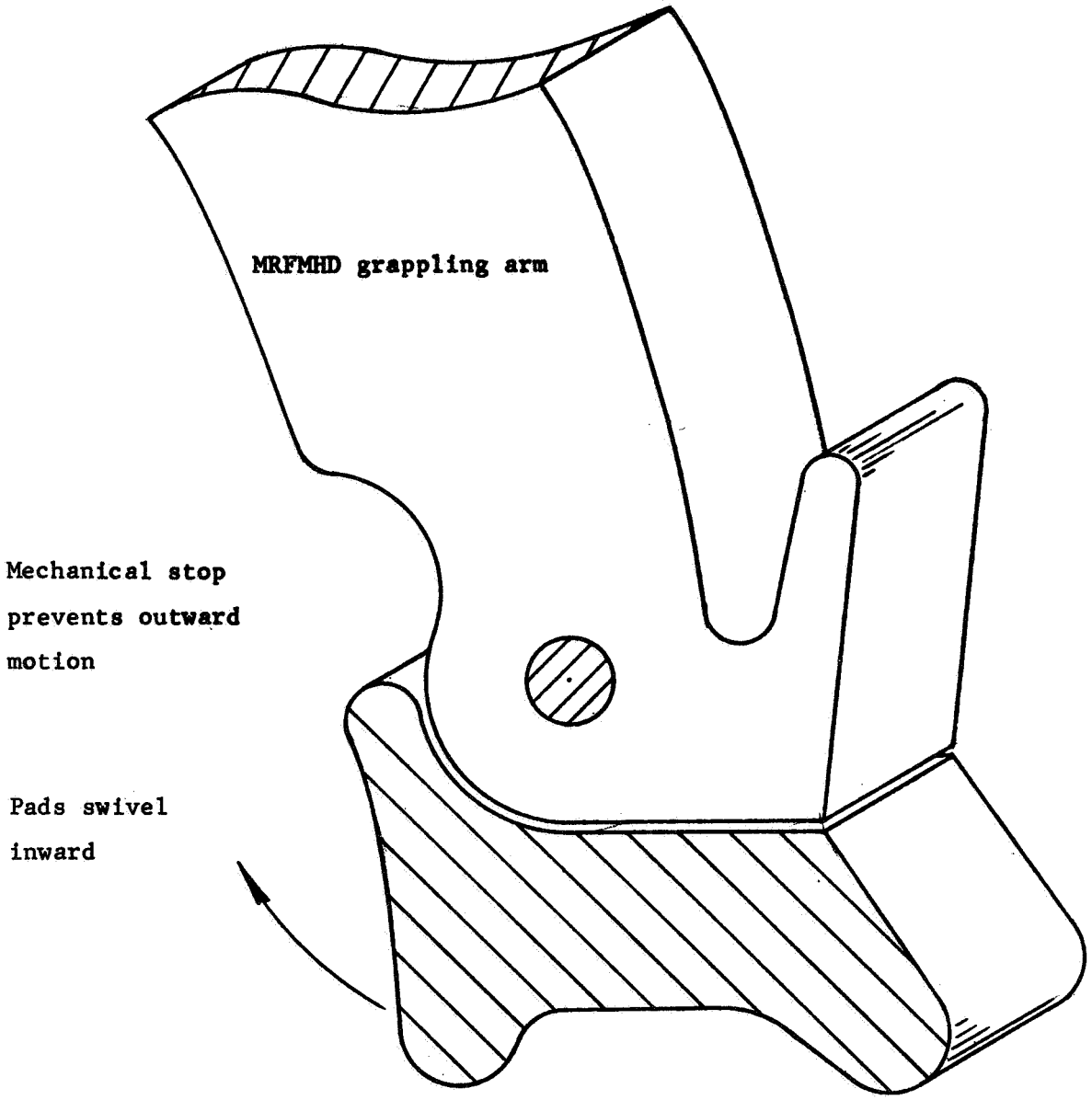

Figure 15 **Pad Configuration for Use on Two AH arms**

an irregular surface. However, in order for a target to be grappled in a stable manner, the line connecting the c.g.'s of the target and CSM must pass through the area whose periphery is defined by a series of lines connecting the pads. With a given spacing between adjacent pads, a four-pad AH provides twice as much stable area as a three-pad AH. The four-pad AH also provides an axially symmetric array of pads which should give better visual cues to the operator who will attempt to place the target's c.g. in line with the MRFMHD axis. In addition, the four pads may be placed in pairs on either side of the plane defined by the two mechanical arms. Another consideration is that four pads will seat on a cylinder with the plane of the pads parallel to the axis of the cyliner. With three pads, the MRFMHD axis would not be perpendicular to the axis of such a cylinder.

With these factors in mind, a four-pad adhesive AH, as shown in Figure 16 was selected. The pads can undergo independent longitudinal motion to seat on an irregular target. In order to provide the protection described previously, the pads are outside the circle of the two mechanical arms. The pivot points of the two arms are placed inward along the MRFMHD so that when the arms are rotated to their full open position, they expose the adhesive AH and do not obstruct its operation.

An additional grappling mode can be provided if the adhesive AH can be extended and retracted. If this feature is incorporated in the design, targets of varying sizes may be grasped simultaneously by the four adhesive pads and the ends of the two mechanical arms.

Going back to the basic adhesive head, the adhesive attachment head must be able to follow the relative circular motion between the target and the MRFMHD boom caused by alignment errors. The motion of the adhesive attachment head must not be allowed to couple with the MRFMHD compressive motion. This would allow the head to peel off from the targets surface. To prevent the coupling and resulting peel from the targets, two concepts were devised as illustrated in Figures 17a and b. The former "Closet Door" concept allows the head to move only in the plane perpendicular to the MRFMHD boom. In the latter illustration, the two pivot points are attached to the boom but rotate allowing the two rods to move the head above and below the pivot points. At the same time the rods can move through the pivot points, thus a circular motion is achieved in the plane perpendicular to the boom. The radius of the adhesive head circular motion perpendicular to the boom will depend on the alignment errors as determined in the simulation (Task E). Note that all of these degrees of freedom, with the exception of the head ball joints, must be subject to controlled damping to stop relative motions between the CSM/MRFMHD and the target after the adhesive sets.

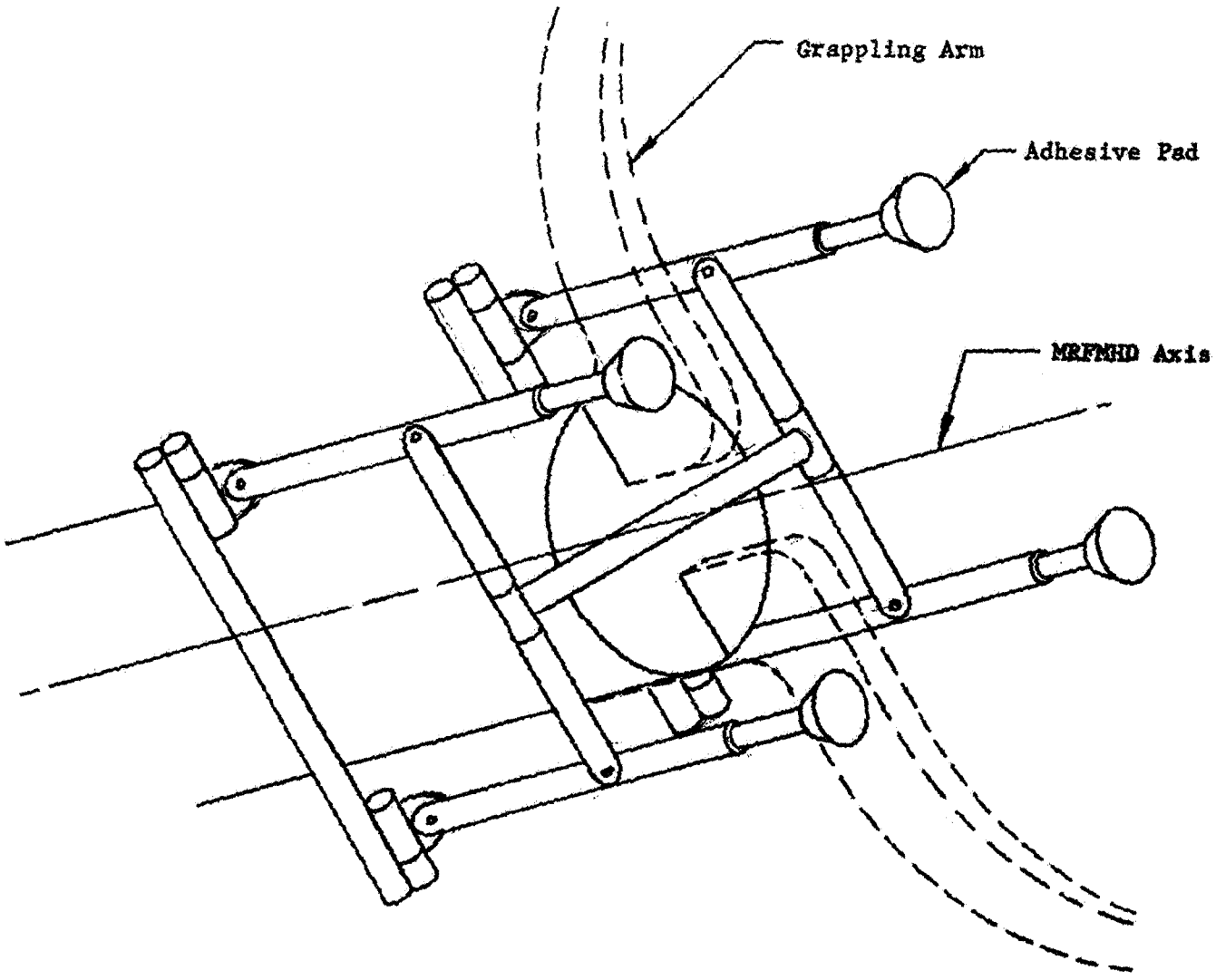

Figure 16 Four-pad Adhesive Attachment Head

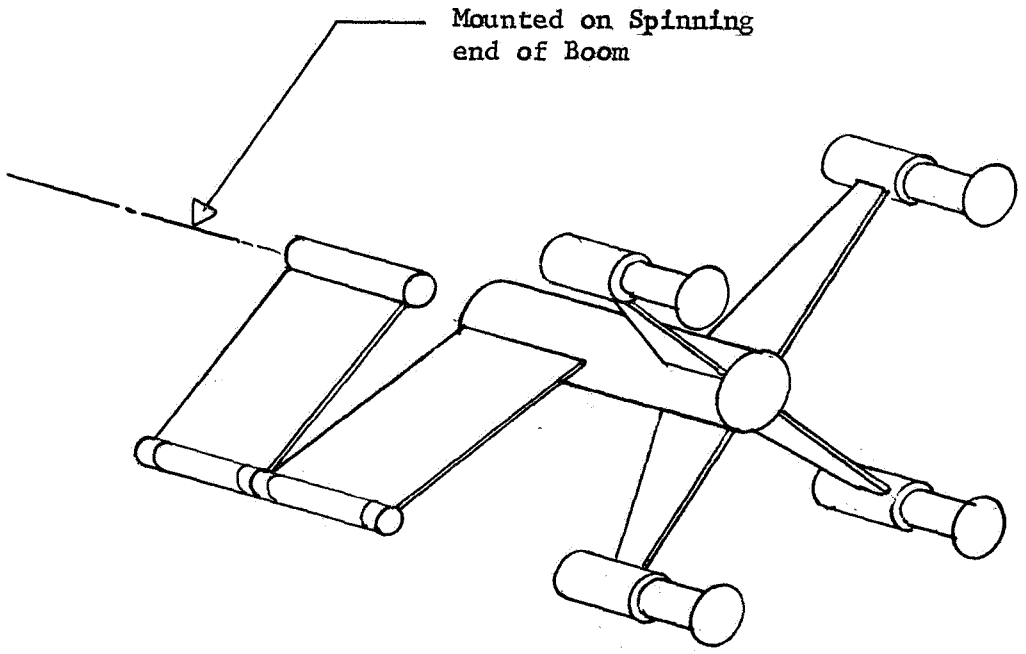

Figure 17a Adhesive AH/Target Relative Circular Motion Tracking System

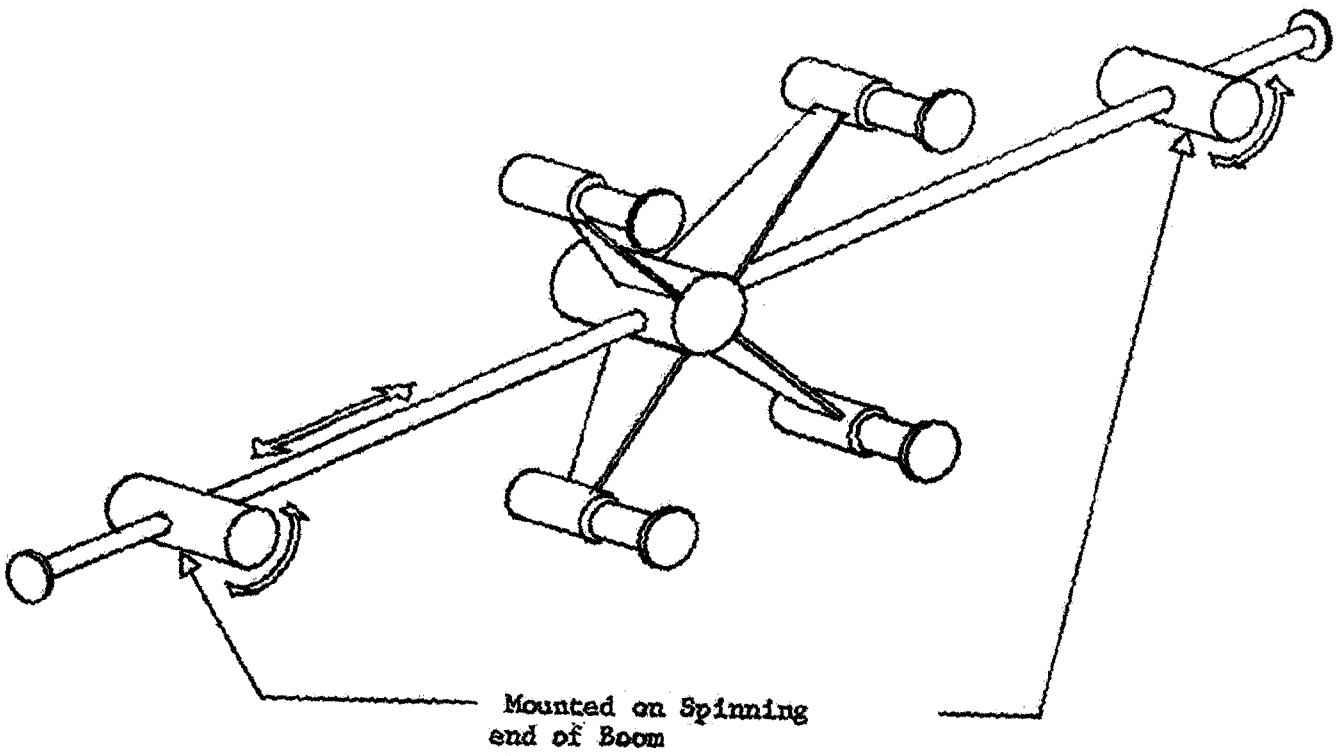

Figure 17b Adhesive AR/Target Relative Circular Motion Tracking System

With regard to the actuation of the mechanical elements in this combined mechanical/adhesive attachment system, the principal problem is the controlled, reliable opening and closing of the two half-circle arms. This problem can be handled effectively using the concept shown in cutaway form in Figure 18. The DC motor is hermetically sealed in a harmonic drive unit that provides high torque at low rpm on the output shaft. This unit is an extrapolation of USM Corporation's model HDUH-10-72-2 that is used to drive the video data storage head in CBS Laboratories' high vacuum "Recorditron" (Ref. 13). The ball-screw drive is of the type furnished by Walter Kidde and Company (Ref. 14) and it should be lubricated using Ball Brothers Vac Kote process (Ref. 15) or an equivalent. In order to monitor forces between the pads on the two arms, it may be advisable to incorporate a strain measuring system into the arms. Connecting the output of this system into a CSM cockpit display audible warning system or a force-feedback controller would reduce the probability of crushing a delicate target.

The AH described to this point would be capable of attaching to a wide variety of targets using the following modes:

i. grip between the pads on the ends of the two arms,

ii. encircle non-spinning objects and grip with the two arms,

iii. expansion grappling in target cavities using the hooks on the outer ends of the two arms,

iv. adhesively attach with the four-pad adhesive AH,

v. grip between the adhesive pads and the ends of the two arms (if the adhesive AH can be extended and retracted).

Mode iv., above, can be used on nutating satellites if the nutation cone motion is within the limits of the degrees of freedom of the pads. If, however, the target's nutation exceeds these limits, the MRFMHD as described will not be able to make a low force and torque attachment. Although this is not expected to be the typical situation on satellite targets in view of the passive nutation dampers incorporated in many satellites, the problem could arise on an important target. Therefore, methods were examined to expand the MRFMHD's capability to handle delicate nutating targets.

Two basic options are feasible for solving this problem. First, the MRFMHD boom can be made flexible or pivoted so that it can follow the target's nutation. The capability would be built into the boom between the CSM and the main MRFMHD spinning interface. Note that, in general, the target's nutation rate (rate at which the principal spin vector traverses the nutation cone or space cone) differs from the principal target spin rate. Therefore, the MRFMHD motion that follows the nutation

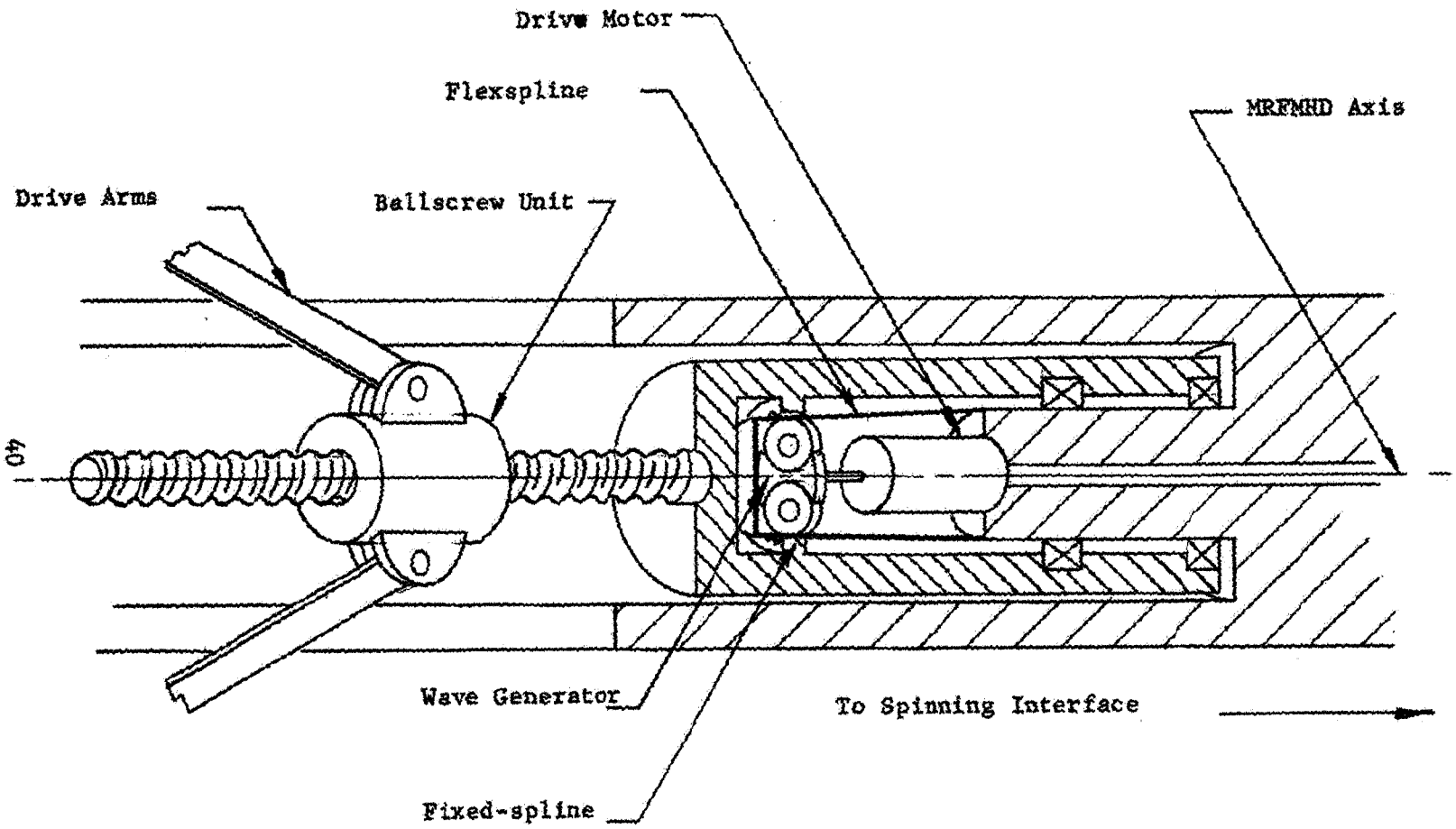

Figure 18 Drive Concept for the Two AH Arms

must be driven at a different rate than the main MRFMHD spin. If the entire outer end of the boom is driven to follow the nutation, significant power will be required and the CSM will react in a noticeable manner to this motion. Because of these effects, a second method was investigated. In it, a supplementary AH is provided to attach to targets with relatively large nutation motions. Shown in Figure 19, the supplementary AH is grasped between the pads on the two arms (this would also be the power and control interface) and utilized in the following manner. First, the MRFMHD axis would be aligned with the target's principal spin axis. The arm would then be extended until the attachment head is displaced off the MRFMHD axis by the same amount the target attachment point (on the target's principal spin axis) is displaced off the nutation cone axis. The supplementary AH arm would then be pitched until the attachment head is in angular alignment with the target spin axis. The attachment head would be driven at the target's spin rate and the main MRFMHD axis would be driven at the target's nutation rate. Final closure and attachment would then be carried out.

As a minimum, either the pivoted MRFMHD or the supplementary AH will present a difficult control problem to the operators. Judgement on the potential acceptability of either of these methods or some other method will depend on the simulation results concerning the operator's ability to align and attach with the basic MRFMHD described previously. It is expected that the simulation will include a test in which a variable off-axis point on the MRFMHD, such as one of the pads on the two arms, must be aligned with a rotating, off-axis point on the target. Data from this test should indicate the degree of accuracy attainable in aligning to a nutating target's principal spin axis.

4. Targets

As stated previously, the expected targets fall into two categories. First are the bulk material packages and structural elements that were illustrated in Figure 11. These may vary in size over a wide range. Note that as the target size increases, the CSM becomes more efficient as a prime mover because its mass becomes a smaller fraction of the combined system mass. However, unless additional viewing aids are provided, large packages will obscure the view out the CSM windows and transport operations, with other objects in the vicinity, may not be practical. In these cases, the MRFMHD will still be useful since it will provide a docking interface to the targets.

With regard to smaller material objects, the CSM/MRFMHD can be useful in retrieving objects ranging from film cassettes and tools to astronauts with disabled maneuvering units.

Satellites of all types are contained in the second target category. The following pages present thecharacteristics of twelve representative satellites that fall within the limits established by the contract's Assumptions and Guidelines. In addition, they provide a variety of

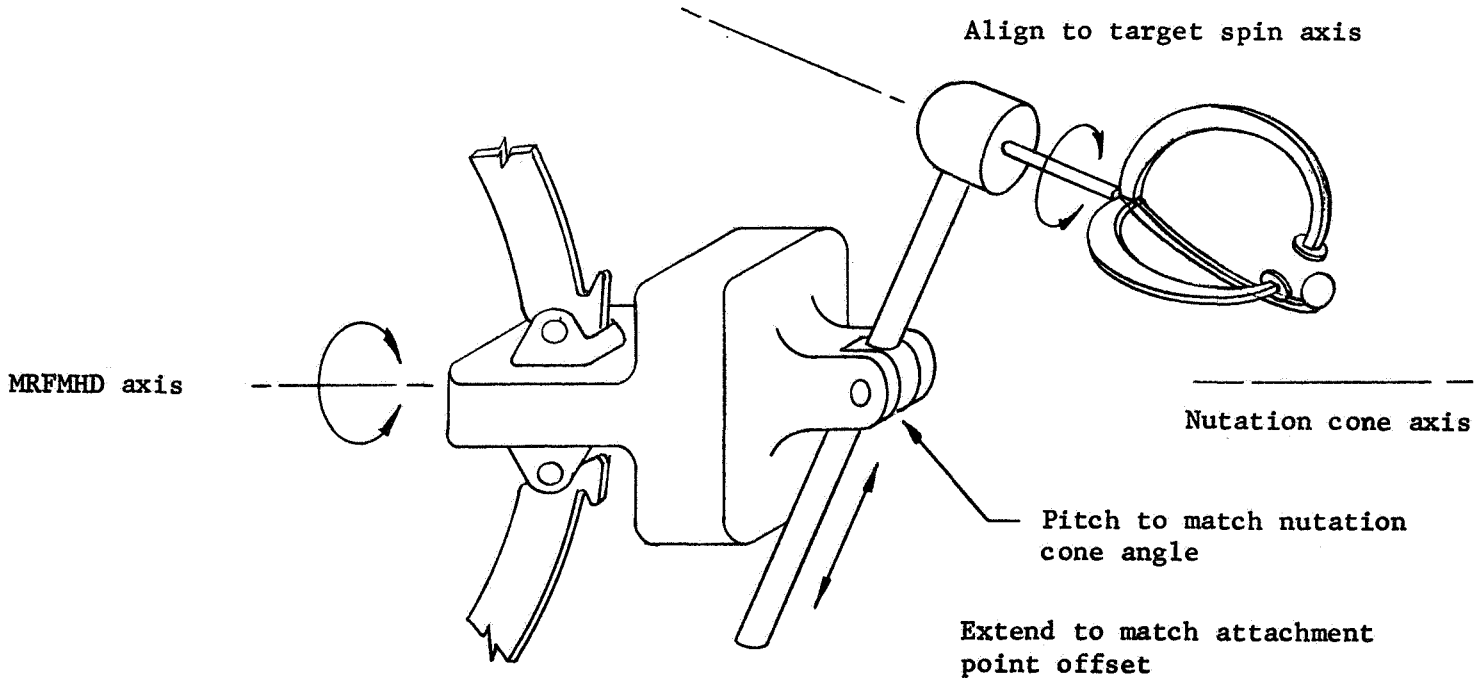

Figure 19 Supplementary AH for Nutating Targets

configurations that can be examined in conjunction with the selected attachment system. Discussion of this subject follows the detailed satellite characteristics.

Energetic Particle Explorer - D

(Explorer XXVI)

Weight: 101 lbs, approximately (Subsystems - 70 lbs. Miscellaneous - 31 lbs).

Spin Rate: (final - 25 rpm.)

Center of Gravity: (from separation plane)
Paddle Extended - 11.41 in above plane
Paddle Folded - 8.45 in above plane

Moments of Inertia: Roll - Paddles Extended - 5.41 slug ft^2
Paddles Folded - 2.14 slug ft^2
Pitch - Paddles Extended - 3.95 slug ft^2
Paddles Folded - 4.90 slug ft^2

Date of Launch: December 21, 1964

Launch Vehicle: Delta (X-258 third stage)

Operational Status: Not transmitting

Mission: To study the injection, trapping, and loss mechanisms of the trapped radiation belts (natural and artificial); the energy spectrum and the pitch - angle distribution of particles as a function of the distance from the surface of the earth at the geomagnetic equator are to be monitored for a period of one year.

Stability: Explorer XXVI has two nutation dampers.

Dimensions: Overall Measurements (with paddles extended)
-74.125 in. x 60.875 in.
Across the flats - 26-3/4 in.
Paddle (each) - 20-1/8 in. x 13-1/8 in.
Length of antennas (each) - 24 in.

Perigee: 310 km

Apogee: 26, 200 km (Current Orbital Elements not maintained)

Inclination: 20^{o}

Period: 456 minutes

Illustration: Figure 20a

Beacon Explorer (22 and 27)

(S-66)

Weight: 124 lbs (132 lbs, including separation mechanism)

Moments of Inertia: (Thrust Axis)

Launch (antennas folded) - $2.05 \pm .3$ slug ft^2

Orbital (antennas extended) - 19.41 ± 2.0 slug ft^2

Date of Launch: Explorer 22 - Oct. 9, 1964

Explorer 27 - April 30, 1965

Launch Vehicle: Scout

Operational Status: Explorer 22 - Transmitting on command only

Explorer 27 - Transmitting on command only

Mission: Conduct worldwide ionospheric measurements which are to serve as a basis for plotting the structure of the ionosphere and for describing its behavior under varying conditions of solar radiation.

Apogee: Explorer 22 - 1080 km.

Explorer 27 - 1310 km.

Perigee: Explorer 22 - 886 km.

Explorer 27 - 940 km.

Orbital Inclination: Explorer 22 - 79.6^{o}

Explorer 27 - 41.1^{o}

Configuration: Right octagonal prism approximately 18 inches across flats by 12 inches high; Overall length - 88 inches (Blades extended).

Solar Blades: Quantity - 4; Dimensions - 10 in. x 70 in. (approx.); Total Solar Area - 16 sq. ft. (approx.)

Illustration: Figure 20b

Direct Measurements Explorer -A

(DME-A) Explorer XXXI

Weight: 218.4 lbs.

Moments of Inertia: Roll - 6.07 slug ft^2
Pitch - 5.81 slug ft^2
Yaw - 5.71 slug ft^2

Date of Launch: November 29, 1965

Launch Vehicle: Thor-Agena

Operational Status: Transmitting on command only

Mission: To obtain direct measurements of the ionosphere including electron temperature, ion temperature, ion mass, temperature equilibrium determination, and simultaneous measurements in conjunction with Alouetti - B.

Apogee: 2877 km.

Perigee: 514 km.

Orbital Inclination: 79.8^{o}

Dimensions: Right octagonal prism 30 inches across the flats by 25 inches high.

Illustration: Figure 20c

Ariel

Formerly United Kingdom International Satellite

No. in Orbit: 2 - Ariel I and Ariel III

Weight Ariel I - 132 lbs.
Ariel III - 198 lbs.

Spin Characteristics: Spin Stabilized

Moment of Inertia: Ariel III - 60 slug ft^2 (approximately)

Date of Launch: Ariel I - April 26, 1962
Ariel III - May 5, 1967

Launch Vehicle: Ariel I - Thor-Delta
Ariel III - Scout

Operational Status: Ariel I - Not transmitting
Ariel II - Not in orbit
Ariel III - Transmitting

Mission: Ariel III - A global atmospheric noise measurement survey is expected to be completed in the first 60 days in orbit. Other experiments will study galactic radio noise, electron density and temperature, molecular oxygen distribution and VLF radiation.

Apogee: Ariel I - 1,045 km.
Ariel III - 577 km

Perigee: Ariel I - 384 km
Ariel III - 479 km.

Orbital Inclination: Ariel I - 53.8°
Ariel III - 80.1°

Dimensions: Diameter - 29.5 inches
Length - 43 inches, exclusive of appendages
Appendages extended - 52 inches from hinges

Illustration: Figure 20d

ESRO

European Space Research Organization

No. in Orbit: 1 - ERSO - 2B
ERSO - 2A failed to orbit

Weight: 185 lbs, including separation mechanism

Spin Characteristics: Spin-stabilized at 30-40 rpm by a cold gas spinup system, after being despun from separation spin of 160-180 rpm by a yo-yo system consisting of two equal weights attached to the satellite by tapes.

Damper System: Ball-in-tube nutation damper used to reduce or eliminate spacecraft coning angle.

Date of Launch: May 16, 1968

Launch Vehicle: Solid-propellant Scout

Operational Status: Six of the seven experiments are operating as planned.

Mission: The study of solar and cosmic radiation in lower layer of Van Allen belt.

Apogee: 1090 km.

Perigee: 330 km.

Orbital Inclination: 97.2^{o}

Dimensions: 30" across the points of the polygon
29.2" high
20.3" command antennas (extended from bottom)

Illustration: Figure 20e

Tiros Operational Satellite and ESSA

No. in Orbit: Tiros 1-10
ESSA 1-6

Weight: Tiros 6 - 281 lbs.
Tiros 7 - 300 lbs.
Tiros 8 - 260 lbs.
Tiros 9 - 300 lbs.
Tiros 10 - 288 lbs.
ESSA I - 304 lbs.
ESSA II - 283 lbs.
ESSA VI - 290 lbs.

Spin Rate: Spin - Stabilized at 10 rpm (ESSA VI)

Moment of Inertia: Thrust (ESSA II) - 165.44 lbs-in-sec^2
Transverse (ESSA II) - 115.69 lbs-in-sec^2

Launch Vehicle: Thor-Delta (Tiros series)
Thrust Augmented Improved Delta (ESSA Series)

Date of Launch: Tiros 1 - April 1, 1960
Tiros 2 - Nov. 23, 1960
Tiros 3 - July 12, 1961
Tiros 4 - Feb. 8, 1962
Tiros 5 - June 19, 1962
Tiros 6 - Sept. 18, 1962
Tiros 7 - June 19, 1963
Tiros 8 - Dec. 21, 1963
Tiros 10 - July 2, 1965
ESSA I - Feb. 2, 1966
ESSA II - Feb. 28, 1966
ESSA III - Oct. 2, 1966
ESSA IV - Jan. 26, 1967
ESSA V - April 20, 1967
ESSA VI - Nov. 10, 1967

Operational Status: The following are operational:

ESSA II - Transmitting on command only
ESSA III - Transmitting on command only
ESSA IV - Transmitting on command only
ESSA V - Transmitting on command only
ESSA VI - Transmitting on command only

Mission: Provide meteorological data

Tiros 6: Apogee - 442 miles
Perigee - 425 miles
Inclination - 58.3°
Period - 98.7 minutes
Design Life - 5 months

Tiros 7: Apogee - 350.8 miles
Perigee - 330.5 miles

Inclination - 58.5°
Period - 97.4 minutes
Design Life - 5 months

Tiros 8: Apogee - 412 miles
Perigee - 374 miles
Period - 99.3 minutes
Inclination - 58.5°

Tiros 9: Apogee - 1392 miles
Perigee - 386 miles
Period - 119.1 minutes
Inclination - 94.4°

Tiros 10: Apogee - 458 n miles
Perigee - 400 n miles
Inclination - 98.63°

ESSA I: Apogee - 463 n miles
Perigee - 379 n miles
Inclination - 97.893°
Period - 100.22 minutes

ESSA II: Apogee - 763 n miles
Perigee - 731 n miles
Period - 113.42 minutes
Inclination - 101.003°

Illustration: Figure 20f

Orbiting Solar Observatory (OSO)

Weight: (OSO II) 547 lbs.

Center of Gravity: (OSO II) 12.08 inches above attach fitting (arms down)
12.90 inches above attach fitting (arms up)

Spin Rate: Approximately 30 rpm

Spin moment of Inertia: 19.31 slug ft^2 (wheel only, arms down)
26.5 slug ft^2 (wheel only, arms up bottles full)
3.8 slug ft^2 (sail)

Attitude Control: Spin stabilized (wheel spins, spin rate maintained by gas jets), sail is maintained normal to sun during daylight, by gas jets in pitch, axis and servomotor in azimuth; pointed experiments aimed at sun in elevation by servomotor.

Launch Date: OSO I - March 7, 1961
OSO II - Feb. 3, 1965
OSO III - March 8, 1967
OSO IV - Oct. 18, 1967

Orbital Status: OSO I through IV are in orbit.

Operational Status: OSO I - not transmitting
OSO II - not transmitting
OSO III - Transmitting on command only
OSO IV - transmitting on command only

Launch Vehicle: Delta Launch Vehicle

Mission: OSO provides a spin stabilized platform for solar experiments.

Apogee: OSO I - 576 km.
OSO II - 617 km.
OSO III - 555 km.
OSO IV - 567 km.

Perigee: OSO I - 538 km.
OSO II - 548 km.
OSO III - 531 km.
OSO IV - 533 km.

Orbital Inclination: (OSO Series) 33°

Dimensions: Diameter - Wheel - 44 inches
Overall - 96 inches
Height - 38.3 inches

Illustration: Figure 20g

Radio Astronomy Explorer

(RAE)

Weight: 601 lbs. maximum including Apogee Kick motor (175 lbs)

Moment of Inertia: fully loaded, launch configuration

X-X axis - 96789 lb-in^2

X-Y axis - 99225 lb-in^2

Z-Z axis - 107180 lb-in^2

Stabilization: Gravity gradient stabilized. Also nutation damper, and libration damper boom.

Date of Launch: April 1968 (planned)

Launch Vehicle: Improved Delta

Mission: Primarily to investigate radio emissions with particular emphasis on phenomena which are not observable from the earth because of ionospheric absorption and man-made radio interference.

Apogee: 6000 km.

Perigee: 6000 km.

Orbital Inclination: 59° retrograde

Period: 288 minutes

Configuration: Central body 36 inches across by 31 inches high having four permanently mounted canted solar blades 63 inches by approximately 9.5 inches wide attached normally to periphery of the structure. Overall dimensions: 63 inches high by 56-1/2 inches in diameter using an 18-inch Delta adapter.

Antennas: Four 750-foot antennas forming a "V" on top and bottom of spacecraft. One 120-foot (tip to tip) dipole antenna. (Revised, August 1967)

Illustration: Figure 20h

Applications Technology Satellite

No. in Orbit: 3, ATS I, ATS II, ATS III

Weight: 725 lbs - ATS I

1500 lbs - prior to firing of apogee motor ATS II, III

750 lbs - after apogee firing - ATS II,III

Spin Rate: 90 rpm - ATS III (Rate at separation from spacecraft)

100 rpm - ATS III (used for longitudinal positioning, orbit inclination, and eccentricity adjustments)

Date of Launch: ATS I - Dec. 7, 1966

ATS II - April 6, 1967

ATS III - Nov. 5, 1967

Launch Vehicle: ATS I - III, Atlas-Agena D

Operational Status: All of the ATS series in orbit are transmitting on command only.

Spin Characteristics: ATS I - Spin-Stabilized and has a nutation damper.

ATS II - Gravity - Gradient and has a Libration Damper.

ATS III - Spin-Stabilized.

Mission: The program is to test advanced components and techniques for future communication, meteorological, and navigation satellites.

Apogee: ATS I - 35,793 km.

ATS II - 7,188 km.

ATS III - 35,792 km.

Perigee: ATS I - 35,783 km.

ATS II - 168 km.

ATS III - 35,778 km.

Orbital Inclination: ATS I - 0.3°
ATS II - 28.4°
ATS III - 0.1°

Dimensions: Spacecraft Minus Booms
Diameter - 58 inches (approximately)
Length - 78 inches (approximately)
Spacecraft Plus Extended Booms
Length - 200 ft.
Width - 40 ft.

Illustration: Figure 20i

Nimbus

Weight: Nimbus I - 832 lbs.
Nimbus II - 1062 lbs.

Spin Characteristics: 3 axis stabilized
earth - oriented

Launch Date: Nimbus I - August 28, 1964
Nimbus II - May 15, 1966

Launch Vehicle: Nimbus I - Thor-Agena
Nimbus II - TAT - Agena B

Orbital Status: Nimbus I and Nimbus II are in Orbit

Operational Status: Nimbus I - Not transmitting
Nimbus II - Transmitting on command only

Mission: Nimbus satellites serve as a testbed for research and development of new meteorological sensors, subsystems and system configurations.

Apogee: Nimbus I - 833 km.
Nimbus II - 1148 km.

Perigee: Nimbus I - 420 km.
Nimbus II - 1095 km.

Orbital Inclination: 98.7° - Nimbus I
100.3° - Nimbus II

Dimensions: Overall - 10 ft x 10 ft
Sensory Ring - 54 in x 13 in
Control Housing - 17.25 in x 33.38 in
Truss Separator - 48 in
Solar Paddles (each) - 3 ft x 8 ft

Illustration: Figure 20j

Eccentric Orbiting Geophysical Observatories
(EGO or OGO)

No. in Orbit: 5 - OGO I, OGO II, OGO III, OGO IV, OGO V

Weight: 1344 lbs. (OGO V)

Spin Characteristics: OGO I - V
Three axis stabilized

Moments of Inertia: (OGO V)
Roll - 665 slug ft^2
Thrust - 340 slug ft^2
Yaw - 910 slug ft^2

Date of Launch: OGO I - Sept. 5, 1964
OGO II - Oct. 14, 1965
OGO III - June 7, 1966
OGO IV - July 28, 1967
OGO V - March 4, 1968

Launch Vehicle: Atlas-Agena B (OGO I and III)
Atlas-Agena D (OGO V)

Operational Status: OGO II was turned off in November 1967, the others are still operating.

Mission: Carries a large number of experiments to study such phenomena of the earth-sun-interplanetary space relationship as polar wind, solar flares, tenestrial magnetic field disturbances,

sudden ionospheric disturbances, radiation belt particle populations, aurora events, polar cap events, ionization, and variations in atmospheric density

Apogee: 124, 204 km. (OGO I)
1,477 km. (OGO II)
117,593 km (OGO III)
851 km. (OGO IV)
148,187 km. (OGO V)

Perigee: 25,593 km. (OGO I)
415 km (OGO II)
4,808 km (OGO III)
410 km. (OGO IV)
272 km (OGO V)

Orbital Inclination: 55.4° (OGO I)
87.3° (OGO II)
60.6° (OGO III)
86.0° (OGO IV)
31.1° (OGO V)

Illustration: Figure 20k

Orbiting Astronomical Observatory
(OAO)

No. in Orbit: 1 - OAO I

Weight: 3,900 lbs - OAO I
4,271 lbs - OAO A2 (To be launched)

Spin Characteristics: Two axis stabilized, roll axis was not stabilized, and designed to point OAO I with an accuracy of one minute of arc $\pm$ 15 arc seconds for 50 minutes. Due to a malfunction in the primary battery and logic circuits, the OAO I could be nutating.

Moment of Inertia: Maximum - 1471 slug ft^2
Minimum - 1453 slug ft^2

Date of Launch: April 8, 1966

Launch Vehicle: Atlas-Agena D

Operational Status: Initial stabilization was achieved but on its second day in orbit the satellite's primary battery began to overheat and soon malfunctioned, rendering OAO I inoperative.

Mission: OAO I carried four experiments to study the UV, X-ray and gamma ray regions from above the obscuring and distorting effects of the earth's atmosphere.

Apogee: 801 km.

Perigee: 793 km.

Orbital Inclination: 35.0°

Dimensions: (OAO II)

Length - 118 in.

Width (across flats) - 80 in.

Diameter (central tube) - 48 in.

Area (solar paddles) - 111.5 sq. ft.

Overall width (solar paddles extended) - 194 in.

Illustration: Figure 20 1

In attaching to these targets, consideration must be given to their tolerance to attachment forces and torques. The magnitude of these cannot be predicted until the attachment errors and rates from the simulation (Task E) are correlated with individual target characteristics. However, it is possible to establish the best approach and attachment plan to be used with the selected attachment head. All of the examples given utilize the two pads on the ends of the two half-circle arms. This is due to the types of surfaces and symmetries present on the satellite targets. The interior of the arms and the adhesive AH will be useful primarily for grappling objects that do not have the delicate external surfaces and appendages that are routine features of scientific and communication satellites.

The selected satellites and the appropriate attachment modes are as follows:

Weight: 101 Lb.
Spin: 25 rpm

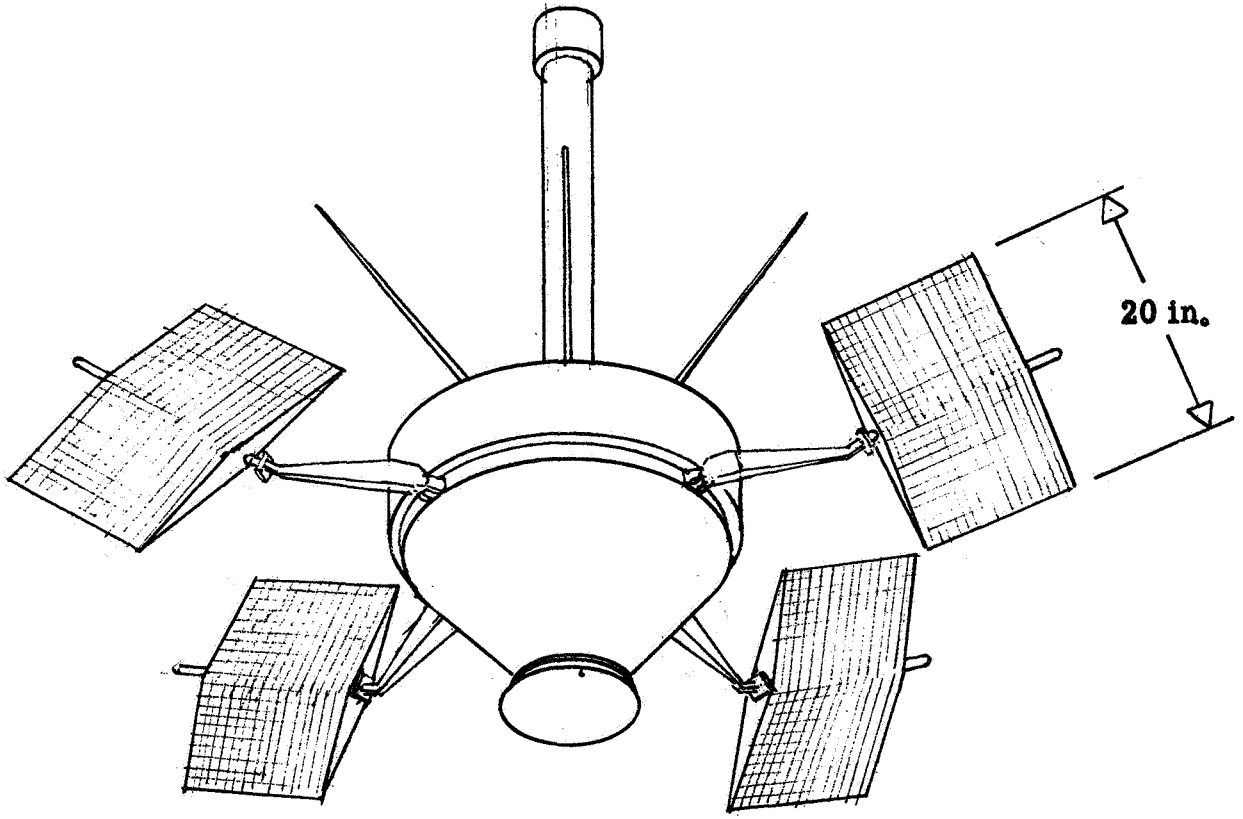

a. Energetic Particles Explorer D

Figure 20 Satellite Geometry

Weight: 132 Lb.

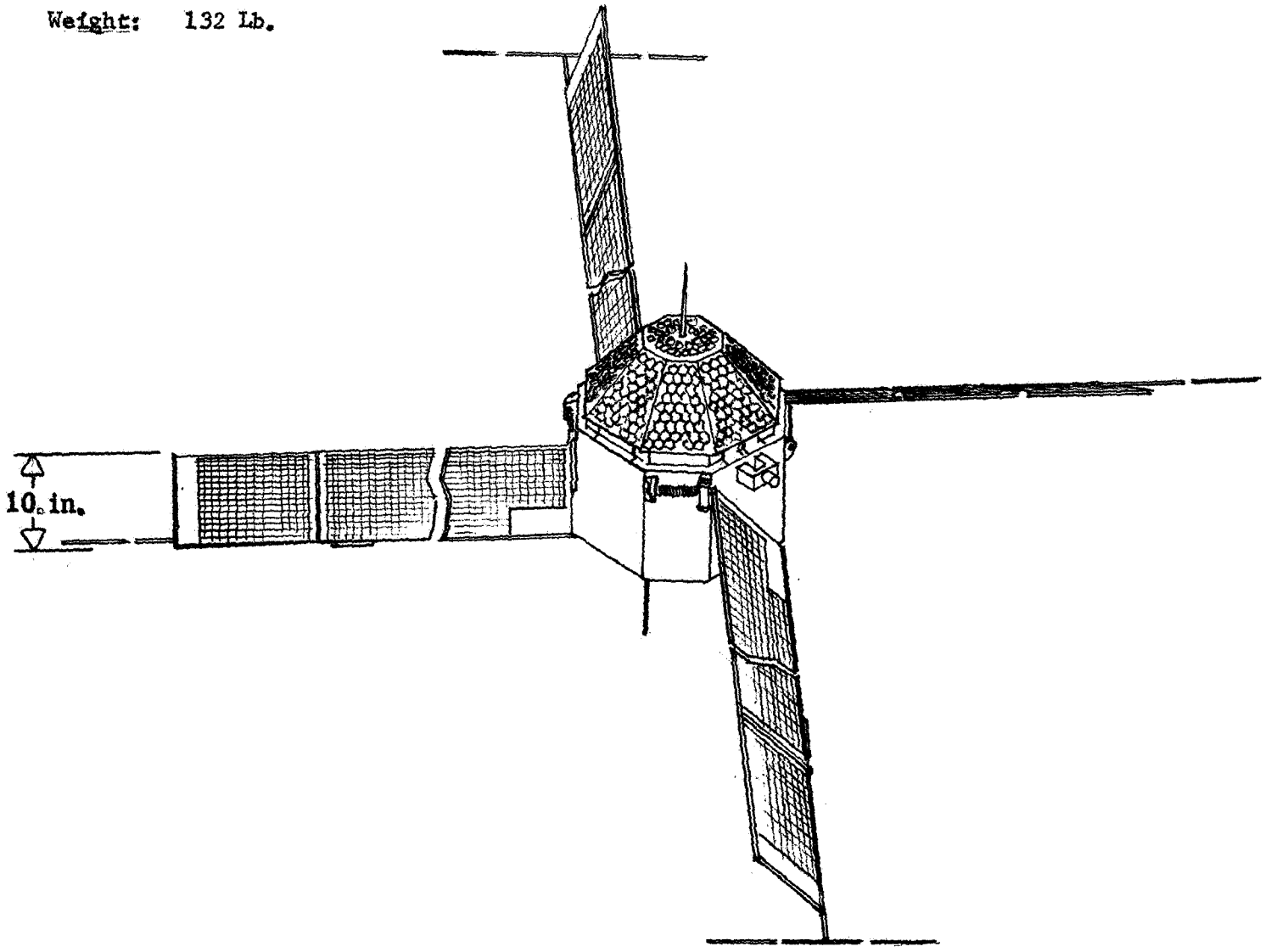

b. Polar Ionosphere Beacon

Figure 20 Satellite Geometry

Weight: 218 Lb.

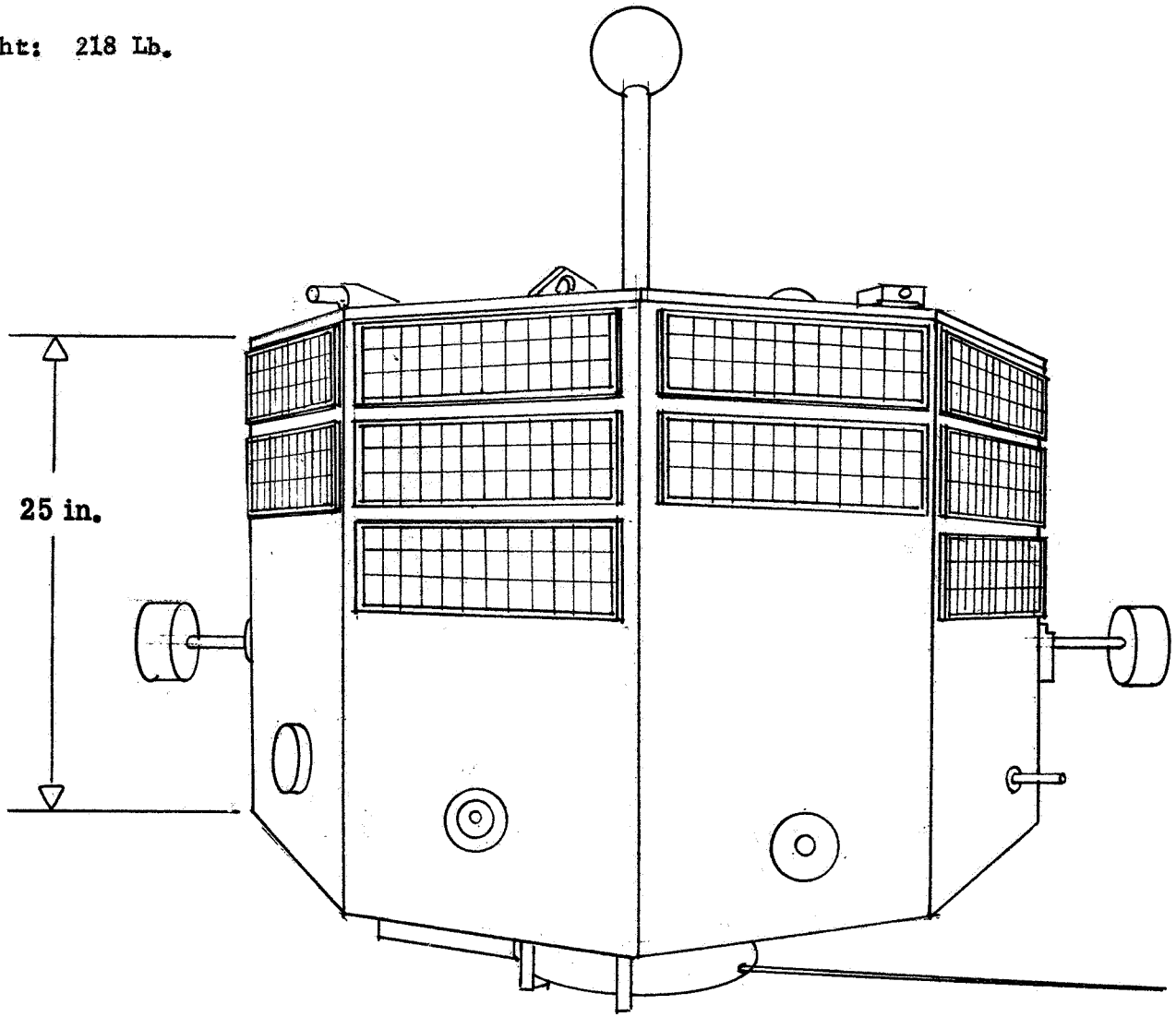

a. Direct Measurements Explorer - A

Figure 20 Satellite Geometry

Weight: 198 Lb.

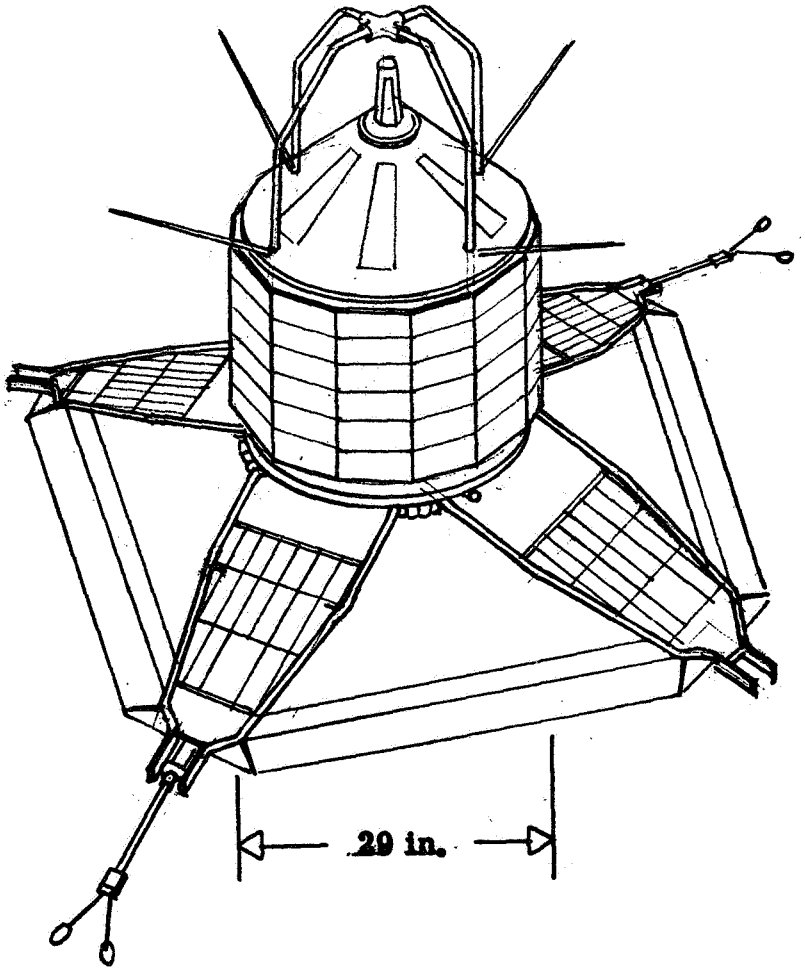

d. Ariel

Figure 20 Satellite Geometry

Weight: 185 Lb.
Spin: 30-40 rpm

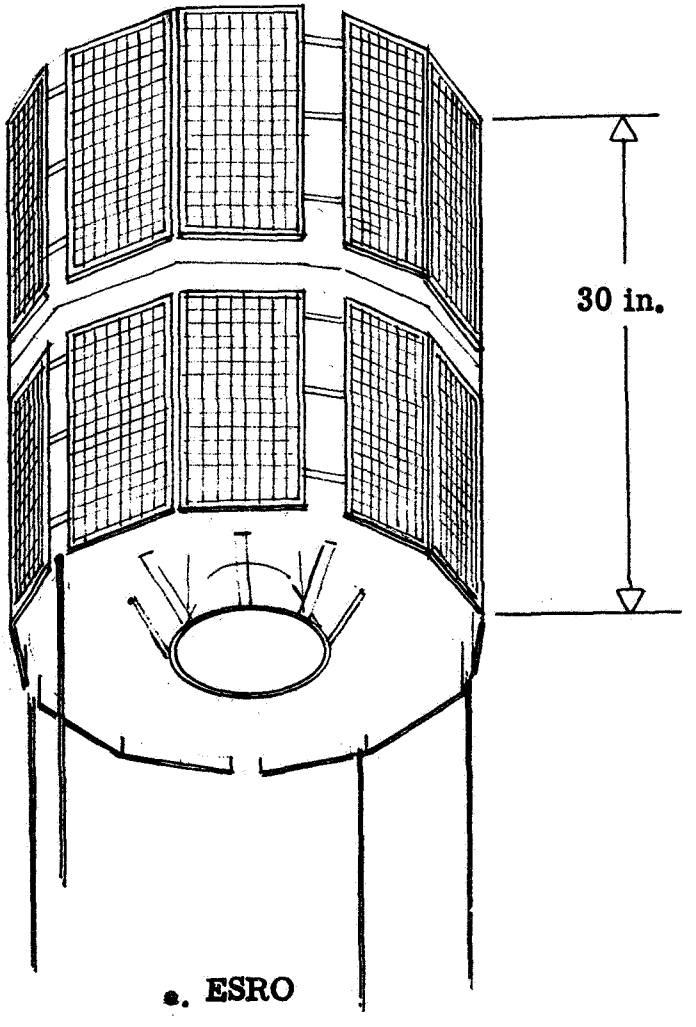

e. ESRO

Figure 20 Satellite Geometry

Weight: 300 Lb.

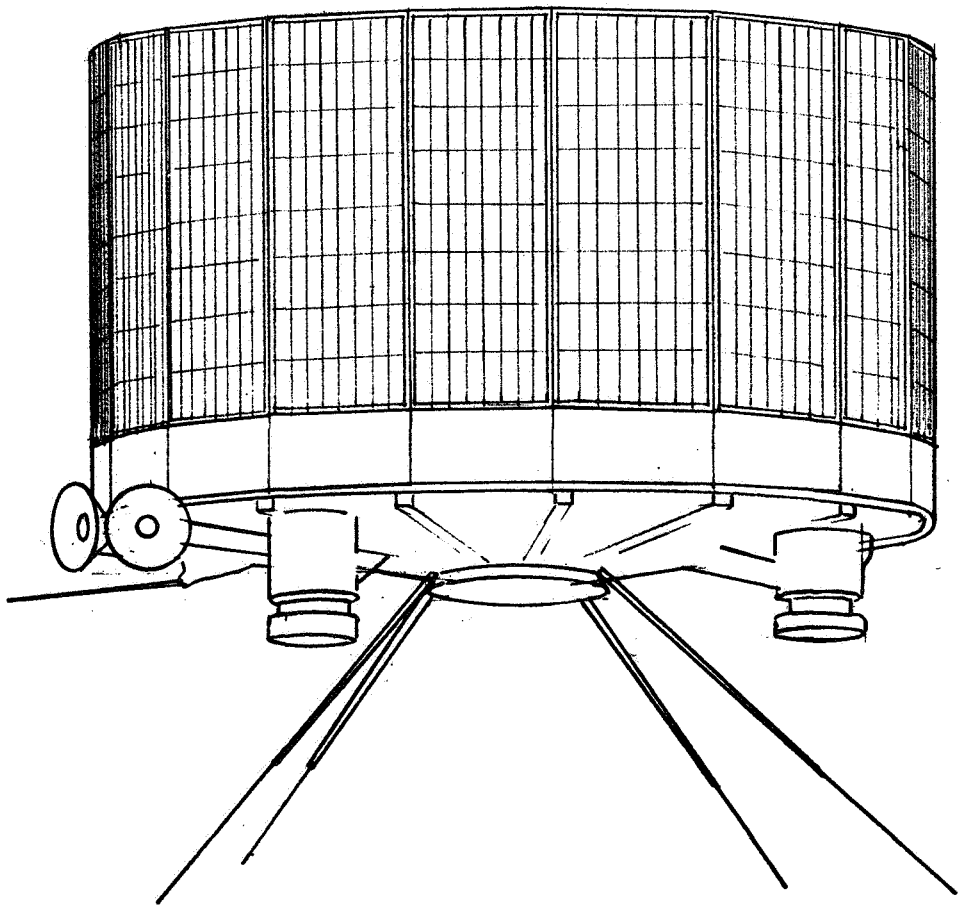

f. TIROS

Figure 20 Satellite Geometry

Weight: 547 Lb.
Spin: 30 rpm (Base)

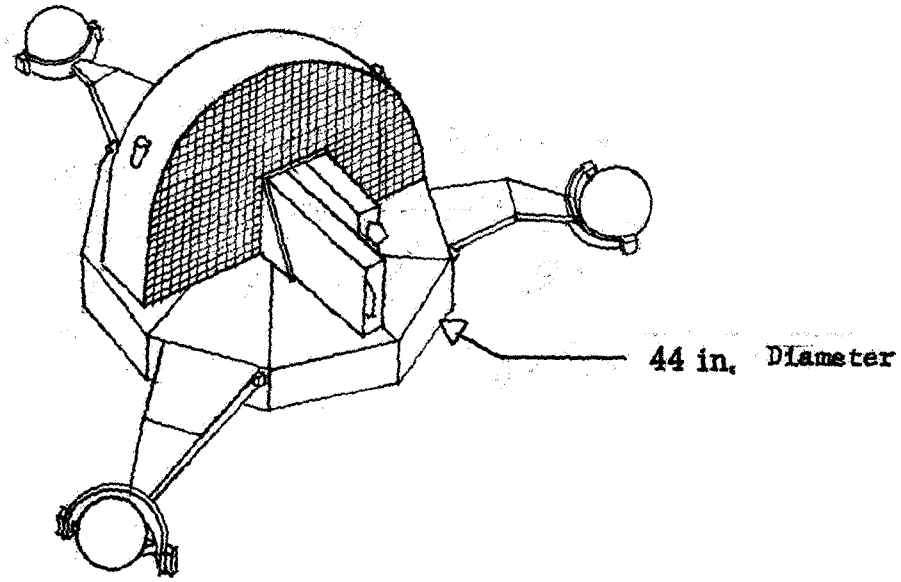

g. Orbiting Solar Observatory

Figure 20 Satellite Geometry

Weight: 601 Lb.
Spin: 0 rpm

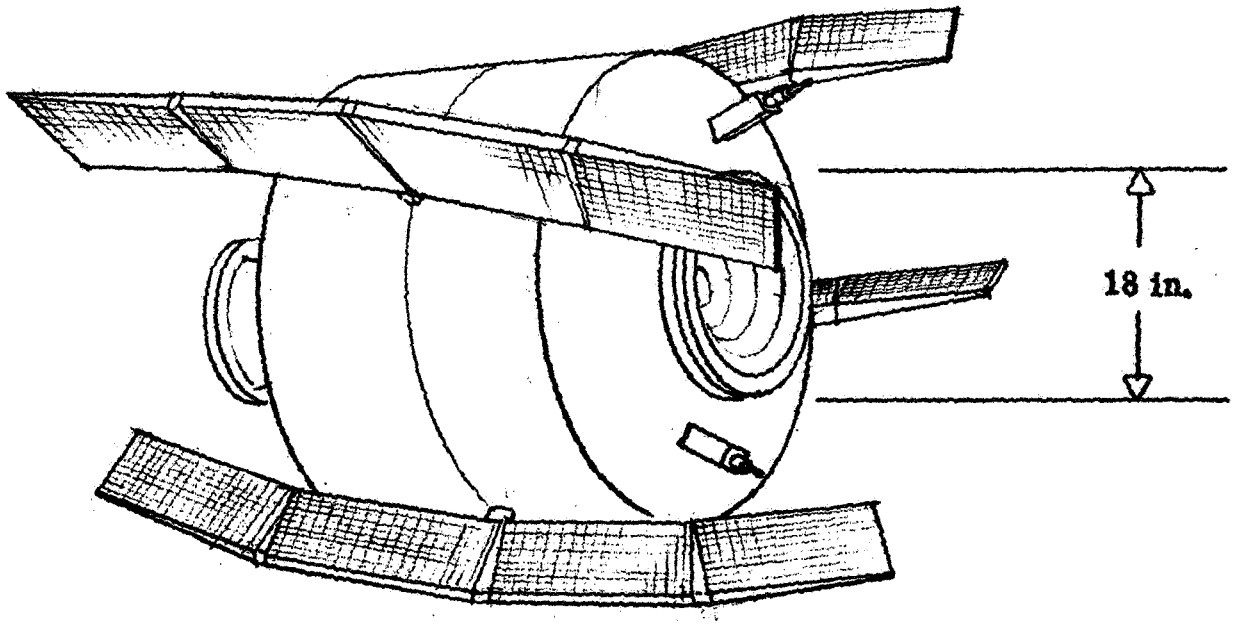

h. Radio Astronomy Explorer

Figure 20 Satellite Geometry

Weight: 750 Lb.
Spin: 90 rpm

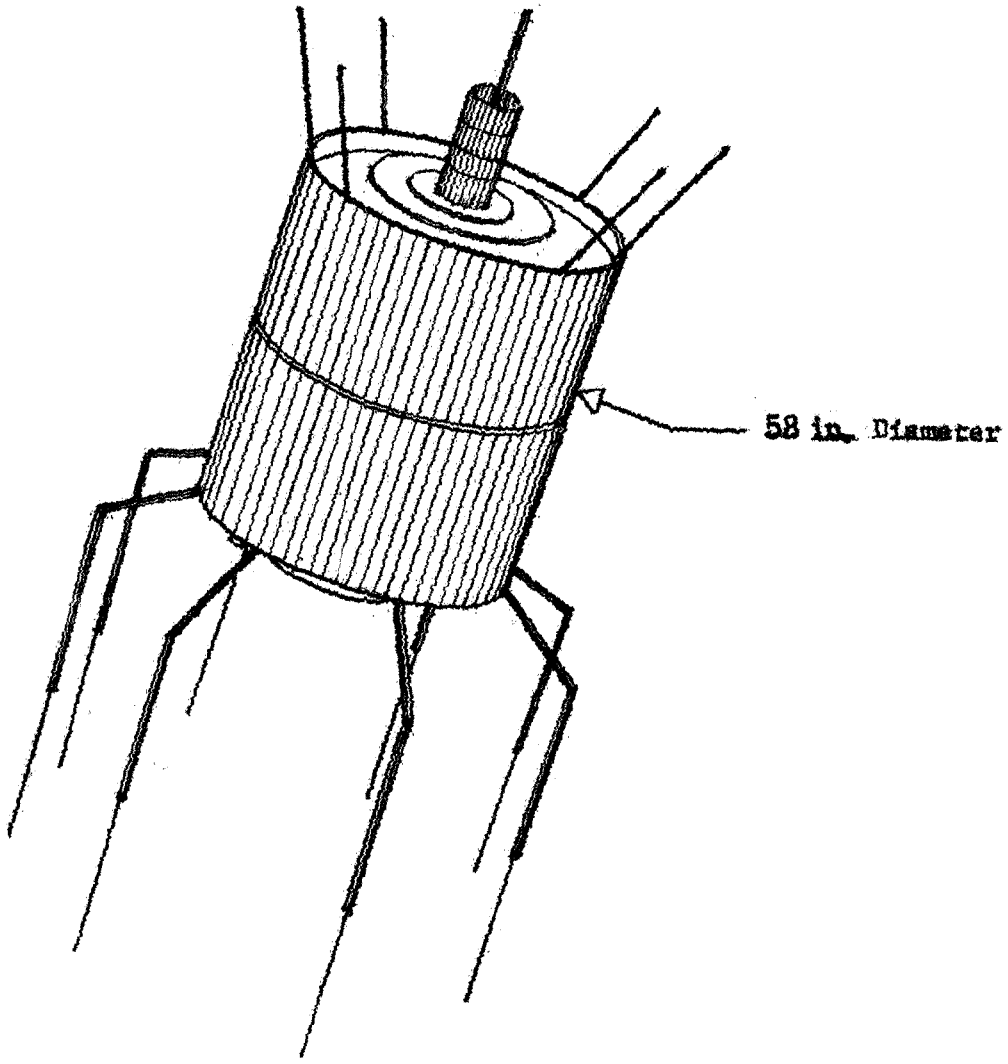

1. Applications Technology Satellite

Figure 20 Satellite Geometry

Weight: 1000 Lb.
Spin: 0 rpm

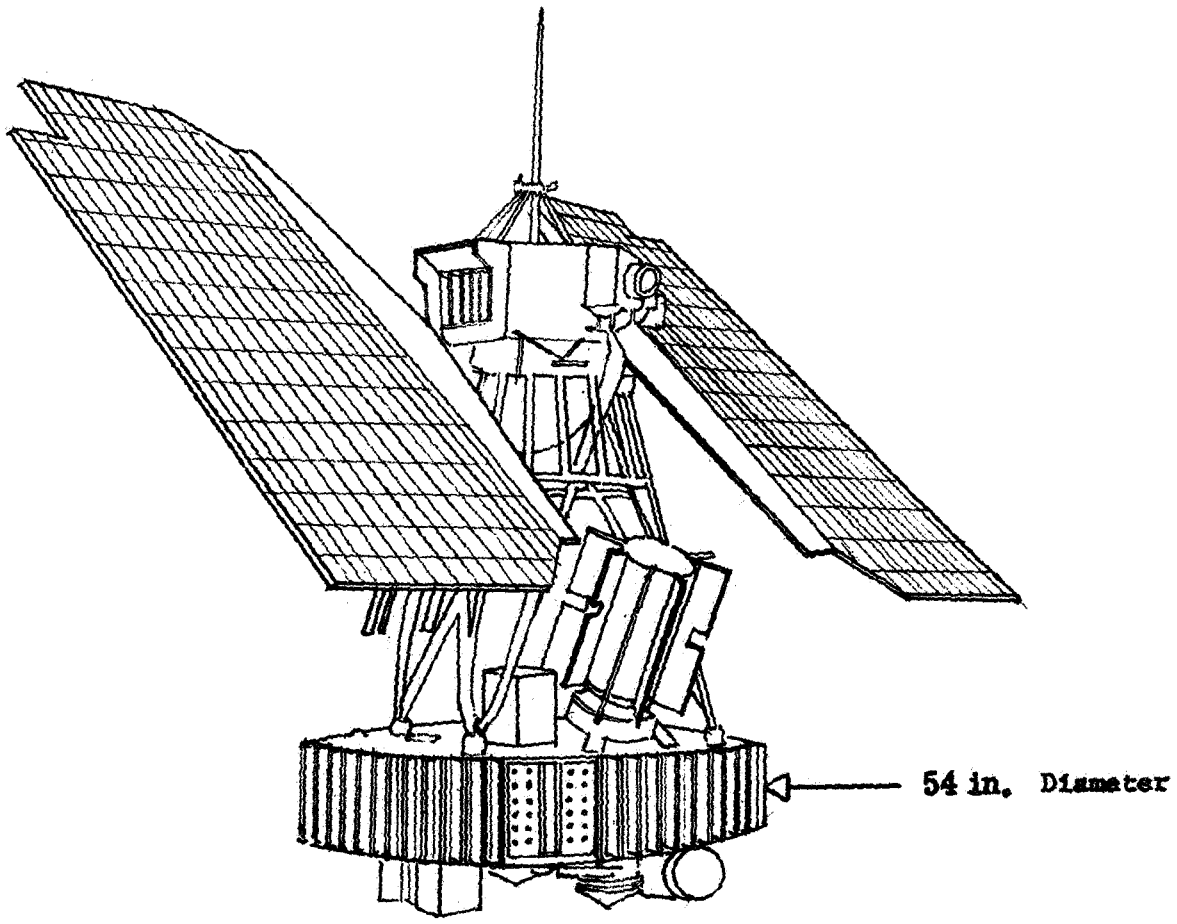

j. Nimbus

Figure 20 Satellite Geometry

Weight: 1344 Lb.
Spin: 0 rpm

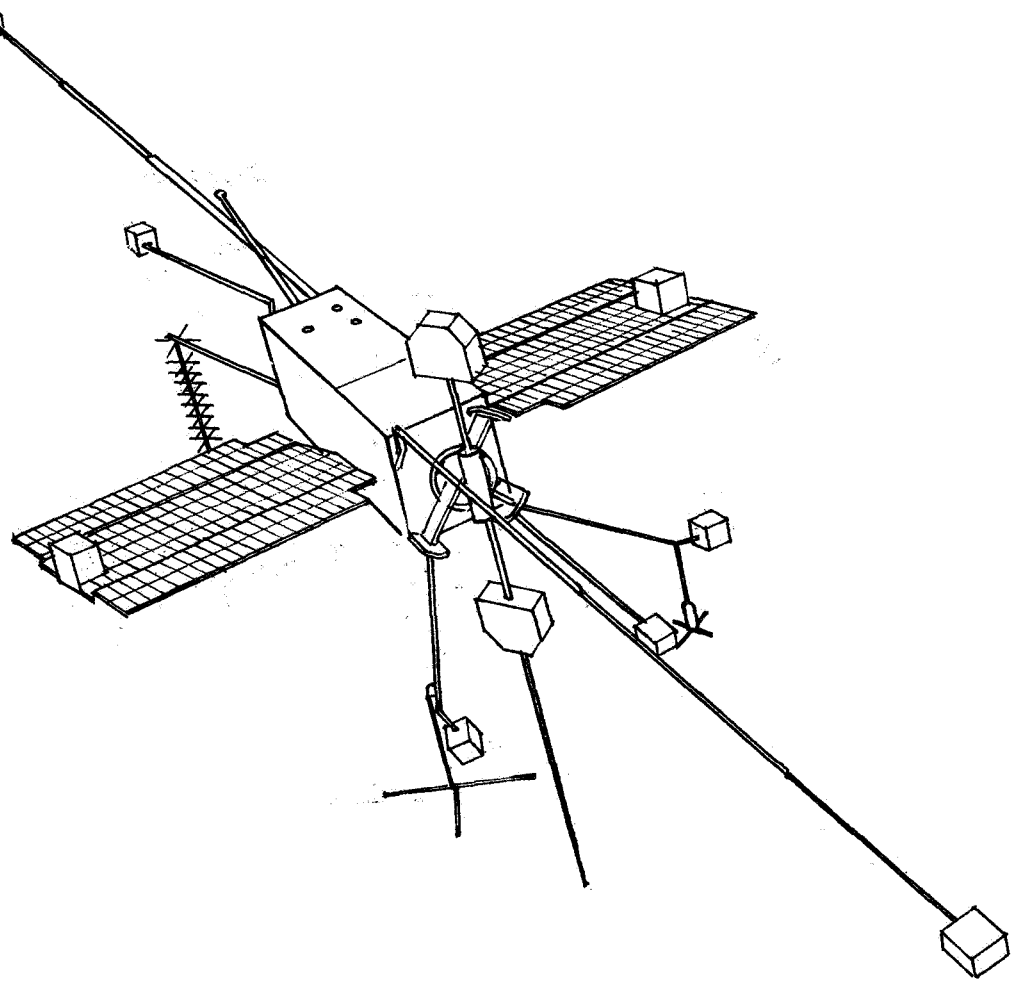

k. Orbiting Geophysical Observatory

Figure 20 Satellite Geometry

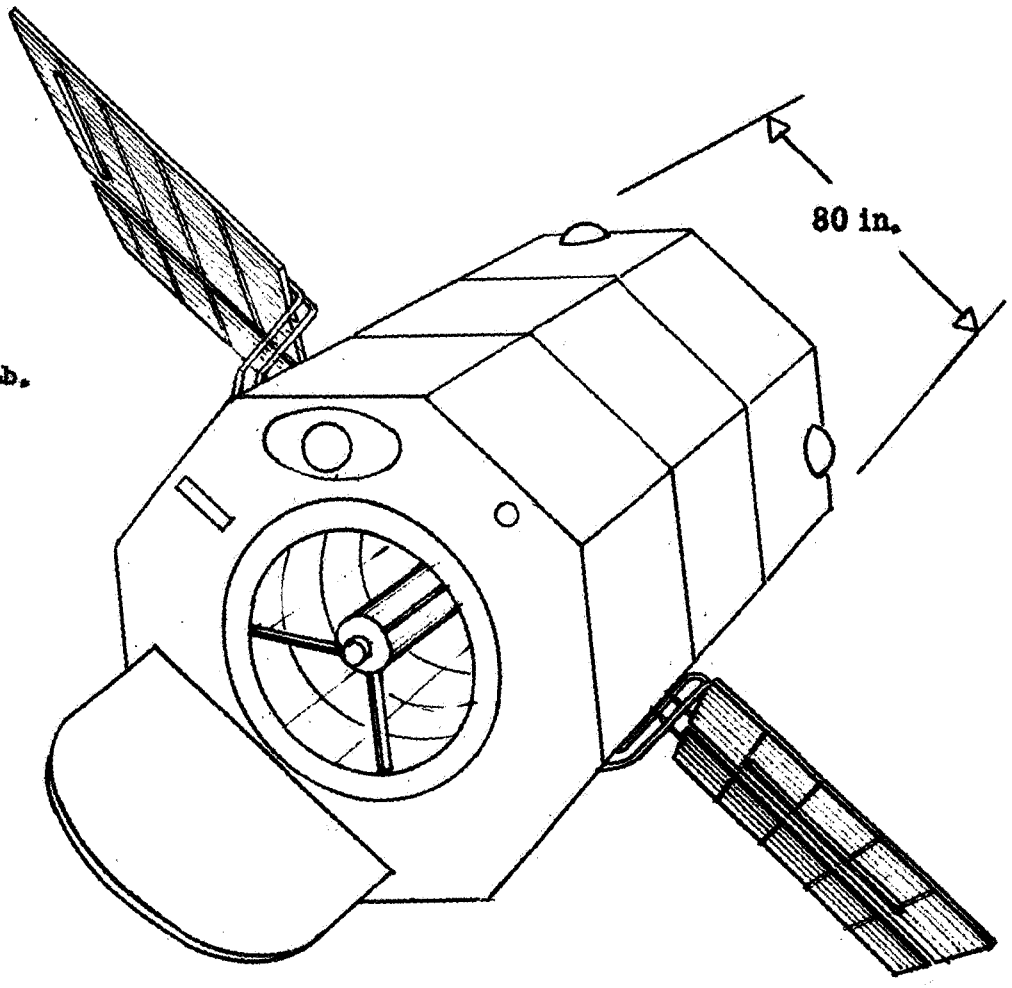

Weight: 4000 Lb.
Spin: 0 rpm

1. Orbiting Astronomical Observatory

Figure 20 Satellite Geometry

a. Energetic Particle Explorer - D (Figure 20a) - This satellite is spinning at 25 rpm and must be approached along the spin axis. A payload separation flange eight inches in diameter is located on the spin axis on the base of the satellite (opposite end from the flux gate magnetometer). The flange can be grasped by the outer edges of the arm end pads. Care must be taken to keep the two arms from contacting the solar paddles.

b. Beacon Explorer (Figure 20b) - The main body of this satellite is a smooth octagonal metal box. It should be approached along the axis perpendicular to the plane of the solar panels. It should be grasped on the two opposing surfaces that do not contain solar paddle supports or the umbilical connector. Care should be taken to avoid closing the arms early or overshooting the desired attachment area. These errors would damage the laser reflector or the solar cell panels.

c. Direct Measurements Explorer - A (Figure 20c) - This satellite is basically an octagonal box (30 inches between flats, 25 inches high) with an experiment probe extending approximately one and one-half feet out on the upper end of the main body axis. A suitable payload separation flange may be available for grappling or two of the side panels may be grasped at the lower end. This would prevent damage to the solar cells mounted on the upper end of the side panels.

d. Ariel (Figure 20d) - This spin-stabilized satellite should be approached along the forward spin axis (opposite end from boom - mounted solar cells). The satellite will be difficult to attach to due to the forward antennas and cone and the solar cells on the main body. It should be grasped at the top of the main cylindrical body.

e. ESRO-2B (Figure 20e) - This satellite must be approached along the spin axis and grasped on the payload separation flange on the base. This flange is ten inches in diameter with an eight inch diameter center hole. This is too small for expansion grappling so the outer edge must be used. Four twenty inch antennas extend from the base and must be avoided with the AH arms.

f. TIROS and ESSA (Figure 20f) - The standard configuration TIROS is orbited with a payload separation flange of approximately nine-inch outside diameter on the base. The forty-two inch diameter drum surfaces and the forward end are covered with solar cells. Approaching along the spin axis perpendicular to the base, the MRFMHD must be maneuvered carefully to avoid the four transmitting antennas before grasping the flange.

g. Orbiting Solar Observatory (OSO) (Figure 20g) - The OSO can be grasped by either the outer octagon panels or the payload separation flange. It should be approached from the base end along the main body spin axis. The sail rotates about an axis perpendicular to the main body axis and should not be grasped since it is covered with solar cells and scientific sensors.

h. Radio Astronomy Explorer (RAE) (Figure 20h) - This satellite is equipped with an eighteen-inch diameter launch adapter ring centered about the main body axis. In approaching the ring, care must be exercised to avoid two seven hundred and fifty foot antennas that form a V-shape centered along the main satellite axis. The sixty degree angular separation between these antennas provides ample maneuvering room for approach and attachment without contacting the antennas.

i. Applications Technology Satellite (ATS) (Figure 20i) - These satellites, spinning at up to one hundred rpm, exceed the spin rates in the contract's Assumptions and Guidelines. However, if the MRFMHD is designed to handle these rates, the spin-stabilized ATS's may be grasped on the apogee motor bell. The approach problem would be complicated by the eight VHF whip antennas that must be avoided during approach along the aft spin axis.

j. Nimbus (Figure 20j) - The Nimbus satellites present a difficult attachment problem even though they are earth-oriented stabilized (essentially no spin). The main circular body may be grasped if this can be done without damaging the thermal control shutters on its surface. If this is not practical, it may be possible to grasp the interconnecting truss structure on the upper body. In this case, the solar paddles must be avoided.

k. Orbiting Geophysical Observatory (OGO) (Figure 20k) - These satellites are stabilized on all three axes but are characterized by a complex array of external booms, panels, sensors, and antennas. With care, the central body (32 x 32 x 72 inches) can be approached and grasped on the side opposite the VHF omnidirectional antenna.

l. Orbiting Astronomical Observatory (OAO)(Figure 20l) - The OAO is the largest of the satellites examined and is stabilized in pitch and yaw but not in roll. The first OAO was rendered inoperative when its primary power system failed during its second day in orbit making it an attractive target for MRFMHD operations. Its precise attitude motion is not known but the large, hexagonal main body may be grasped safely if the solar panels are avoided.

5. Spinning Interface

The spinning interface is required to match the AH spin motion to the target's spin. Therefore, it is located between the AH and the main MRFMHD boom. Only the AH should be outboard from the spinning interface in order to minimize spin-up and de-spin masses and inertias.

The contract's Assumptions and Guidelines specified that the MRFMHD be able to exert fifteen foot pounds of spin-up or de-spin torque. No data werefound during the study to alter this selection. Figure 21 may be used to calculate the approximate time required to de-spin targets having various inertia and spin characteristics if the full fifteen foot pound torque is applied.

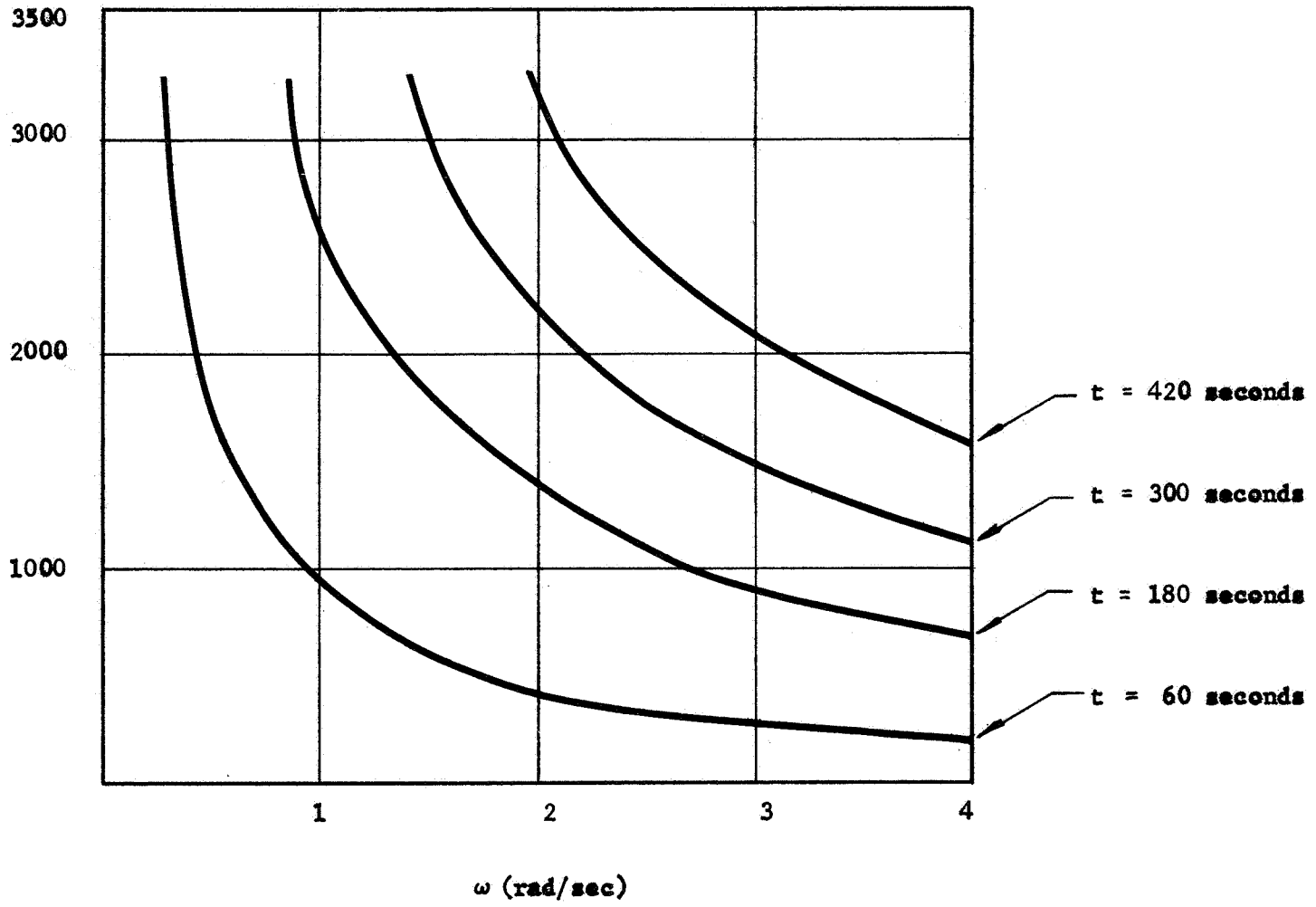

Figure 21 De-Spin/Spin-Up Time as a Function of Target Spin Rate and Inertia Using Fifteen Foot-Pounds of Torque

A variety of methods are available to provide the de-spin/spinup torque and to store or remove the target's angular momentum from the combined system.

The despinning torque may be applied in the following three ways: (1) a direct current (DC) motor, operating with controlled reverse current, (2) thrusters on the AH, mounted to apply pure torque, and (3) a slip clutch or DC motor on the AH can be engaged to a flywheel on the boom, despinning the target as the flywheel spin rate increases. Each of these three modes is reversible to spin-up the target. The DC motor provides the ability to apply precisely controlled torques by varying the reverse or forward current through the motor. In addition, up to approximately seventy percent of the target's rotational kinetic energy can be stored in the MRFMHD drive battery during de-spin since the motor will be operating as a generator. Approximately twenty-five percent of the energy will be dissipated in the motor. In order to remove the target's angular momentum from the CSM/MRFMHD/Target, the CSM roll thrusters must be fired.

In the second method, thrusters would be mounted on the AH to provide roll torque during de-spin and spin-up. Neglecting friction in the spinning interface, no roll moments would be imposed on the CSM during the thruster firings. However, the amount of angular momentum to be removed with these thrusters is the same with either the DC motor or the thrusters so no efficiency is gained by thrusting on the AH only. In addition, the thruster plumbing and controls would have to be relatively sophisticated to duplicate the DC motor's variable dynamic characteristics. However, essentially no heat would be dissipated at the spinning interface with the thrusters.

The third system, in effect, would use a flywheel, rather than the CSM, as the reaction mass to the target torquing. Again neglecting frictional torques, the CSM thrusters need not be fired to remove the target's angular momentum from the system since it is stored in the flywheel. This system only becomes practical if the number and magnitude of MRFMHD de-spin/spin-up cycles is large enough that the flywheel mass becomes smaller than the mass of the CSM RCS roll fuel that would otherwise be required for the cycles. The two roll thrusters on the CSM consume 0.72 pounds of fuel and oxidizer per second while producing 1300 foot-pounds of torque. From the contract's Assumptions and Guidelines, the largest target spin inertia (3000 slug feet^2) with the highest spin rate (36 revolutions/minute or 3.77 radians/second) gives a target angular momentum of 11,300 ft. lb. sec. The roll thrusters would have to be fired for 8.7 seconds to remove this angular momentum from the system. This would consume 6.26 pounds of fuel and oxidizer. Note that with the DC motor or AH thrusters, the target angular momentum must be removed from or added to the CSM during or at the end of both de-spin and spin-up cycles.

With regard to safety, only the DC motor system can be designed to remove all major energy sources from the AH/Target area prior to crew EVA

work on the target. Unless rotating fuel connections are used, the thrusted-AH fuel tanks must be mounted on the AH, thereby creating a potential hazard. With the flywheel, a failure of its bearings or supports could lead to a major structural breakup in the MRFMHD boom.

Based primarily on the controllability and safety considerations, the DC motor was selected as the best MRFMHD spin drive system. A DC motor/generator such as Globe Industries' type GRL wound field motor with three hundred to one gear reduction would provide sufficient torque for this application. The stall torque on the AH, with the gearing described, would be more than eighty (80) foot pounds. The maximum AH spin rate would be approximately forty rpm. Heat dissipation in the motor would be less than two hundred watts throughout the operating range.

The particular problems faced with this system are providing reduction gearing and sealing for motor operation in the space environment. Data indicate that it is feasible to handle both of these problems with a hermetically sealed, harmonic drive unit of the type being built currently by USM Corporation (Ref. 13). Figure 22 illustrates such a head, an extrapolation of USM's model HDUH-10-72-2, in the MRFMHD. The motor is hermetically sealed in the pressurized flexspline chamber and incorporates a three to one gear reducer between the motor and the one hundred to one harmonic drive.

Current flexspline materials require that the drive be mounted such that little or no off-axis torques are exerted on the drive. For this reason, the bearings on the AH/boom interface must be preloaded and rugged enough to keep loads such as AH/Target contact impulses from being transmitted to the harmonic drive. Fafnir Bearing Company's angular contact, duplex pair bearings (Ref. 16), possibly used in tandem, can provide such an AH/boom interface. The bearings should be lubricated with Ball Brothers' Vac Kote (Ref. 15) or an equivalent.

The spinning interface must also include electrical power and command channels to the heads mounted outboard from the interface. The Poly-Scientific Division of Litton Precision Products has developed precision sliding contact heads (capsule slip-ring assemblies) for use in space environments (Ref. 17, 18). One such assembly has twenty-four circuits, each rated at thirty amperes in space. The composition brushes are life-time lubricated for compatibility with the vacuum, thermal, and radiation environment. The head, measuring six and one-half inches long and seven inches in diameter, has less than twenty milliohms RMS contact resistance. This assembly establishes feasibility by providing capability in excess of the anticipated MRFMHD requirements. At present, the required channels would include grappling arm drive power, arm strain readouts, adhesive and target heaters and temperature monitoring circuits, adhesive replenishment power and commands, and possibly the power and commands for a supplementary AH. Eleven circuits (including

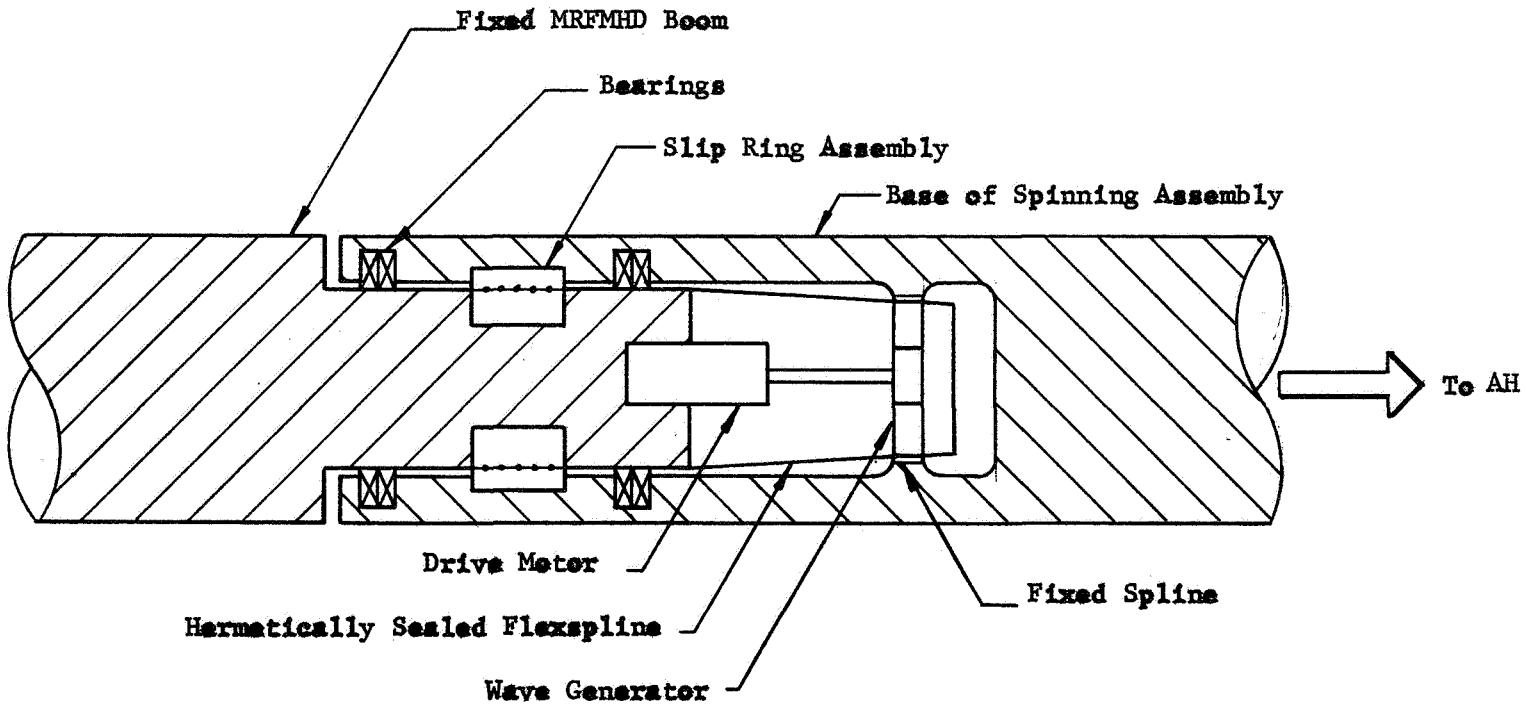

- Components Specified Would Give Up To 80 ft-lb Stall Torque on the AH and 24 Slip Ring Channels at 30 amp/Channel

Figure 22 Spinning Interface Drive Assembly

two for signal and power grounds) plus the circuits required for the supplementary AH would satisfy these requirements.

6. Impact Attenuation

The proposed MRFMHD concept is based on docking the head to the CSM docking interface in place of the Lunar Module. Because of the structural strength of the MRFMHD and the docking interface (Ref. 19) and the minimum seven-to-one ratio between CSM/MRFMHD and target mass, impact attentuators are needed primarily to protect the target and to assist in making adhesive attachments.

The types of dampers in the MRFMHD are almost totally dependent on (1) the target sensitivities to impact and attachment forces and torques, and (2) closure rates and alignment errors at the time the AH contacts the target. The latter are to be determined during Task E. Sufficient longitudinal damped compression capability must be built into the MRFMHD boom to allow the closure velocity differential to be removed without exceeding force limits peculiar to the target. It may also be necessary to build springs and/or dampers into the two MRFMHD arms, their drive mechanism, or the AH pads if the combination of the attachment errors and target angular momentum would produce excessive forces and torques at the AH/Target interface. Detailed simulation data (Task E) and target sensitivity data will be required to analyze this problem.

During target attachment with the four-pad adhesive AH, the pads must be on swivels to follow the relative rotations generated by attachment errors. This motion must be damped after adhesive set-up to rigidize the system. At contact, the pads must have independent longitudinal motion capability to permit seating on the target surface. This motion must be essentially undamped during adhesive set-up so the pads can follow target precessions that may occur due to attachment errors.

7. Deployment Structure

The structure that separates the AH and spinning interface from the CSM docking interface must satisfy three basic requirements; (1) it must be strong enough to withstand the target impact and attachment loads, (2) it must be long enough that the astronauts have a direct view of the AH through the left and right forward viewing (rendezvous) windows, and (3) it must be long enough that target structures capable of damaging the CSM do not reach the CSM during approach and attachment.

Data from previous simulations (Ref. 19), Gemini stationkeeping, and Apollo 7 stationkeeping with the launch vehicle's S-4B stage indicate that closure velocities will be less than one foot per second as opposed to the five foot per second maximum rate specified in the contract's Assumptions and Guidelines. With the lower velocities and the

target masses under consideration, there is no question that a MRFMHD boom can be built with sufficient structural strength.

With respect to AH visibility from the CSM, Martin Marietta has conducted a study under NASA contract NAS8-21004 to determine the field-of-view (FOV) envelopes through the CSM windows (Ref. 20). With the crew couches in the docking position, the crew (helmeted and against the couches) is able to see the area illustrated in Figure 23 at a distance of fifteen feet forward from their eye position. Profiles are shown for the right-hand window. The left-hand window views are mirror images of the views shown. Mirrors providing upright images of the nose of the spacecraft and points forward along the X axis are also available to the crew.

For proper operation of the MRFMHD, the crew must be able to see the spinning interface and the AH arms in all operating positions. Figure 24 gives a top view of the critical dimensions involved if the MRFMHD arms form a three-to-five feet inside diameter circle when closed. If the spinning interface is fifteen feet forward of the crew's eye position, the ball-screw drive structure will place the AH arm pivots twenty feet forward from the eye positions. Under these conditions, the side crew members will be able to see the complete AH arms through their full operating range whenever the arms are above the CSM's XY plane.

With these dimensions, the minimum distance separating a properly-positioned target's main body from the CSM is approximately sixteen feet. This appears to be more than adequate for the third requirement concerning safe vehicle separations. The only satellite in the list given earlier that poses a hazard in this respect is the Radio Astronomy Explorer with its seven hundred and fifty foot tubular antennas.

Several methods are available for fabricating the MRFMHD boom. If a rigid boom is selected, a truss structure of the type shown in Figure 25 could prove to be the most practical. If the boom must deflect to accommodate nutating satellites the boom envelope could be a flexible bellows with articulated members inside to provide the lateral (Y) and vertical (Z) motion of the AH.

Also shown in Figure 25 is the storage concept for a supplementary AH. To deploy the device, the main AH arms are rotated into the CSM's XZ plane and opened. The supplementary AH is extended forward on the end of a tubular structure such as a deHaviland Boom (Ref. 31) or an AMETEK/Hunter Spring Stacer (Ref. 21). The boom is aligned to place the head between the two pads on the main AH arms. These arms are closed, clamping the supplementary AH and engaging power and command plugs recessed in the two pads as illustrated in Figure 19. A spring-catch connecting the tubular boom to the supplementary AH releases as the boom is retracted. The system is now ready for use. The process is reversed for retraction of the supplementary AH into its stored position.

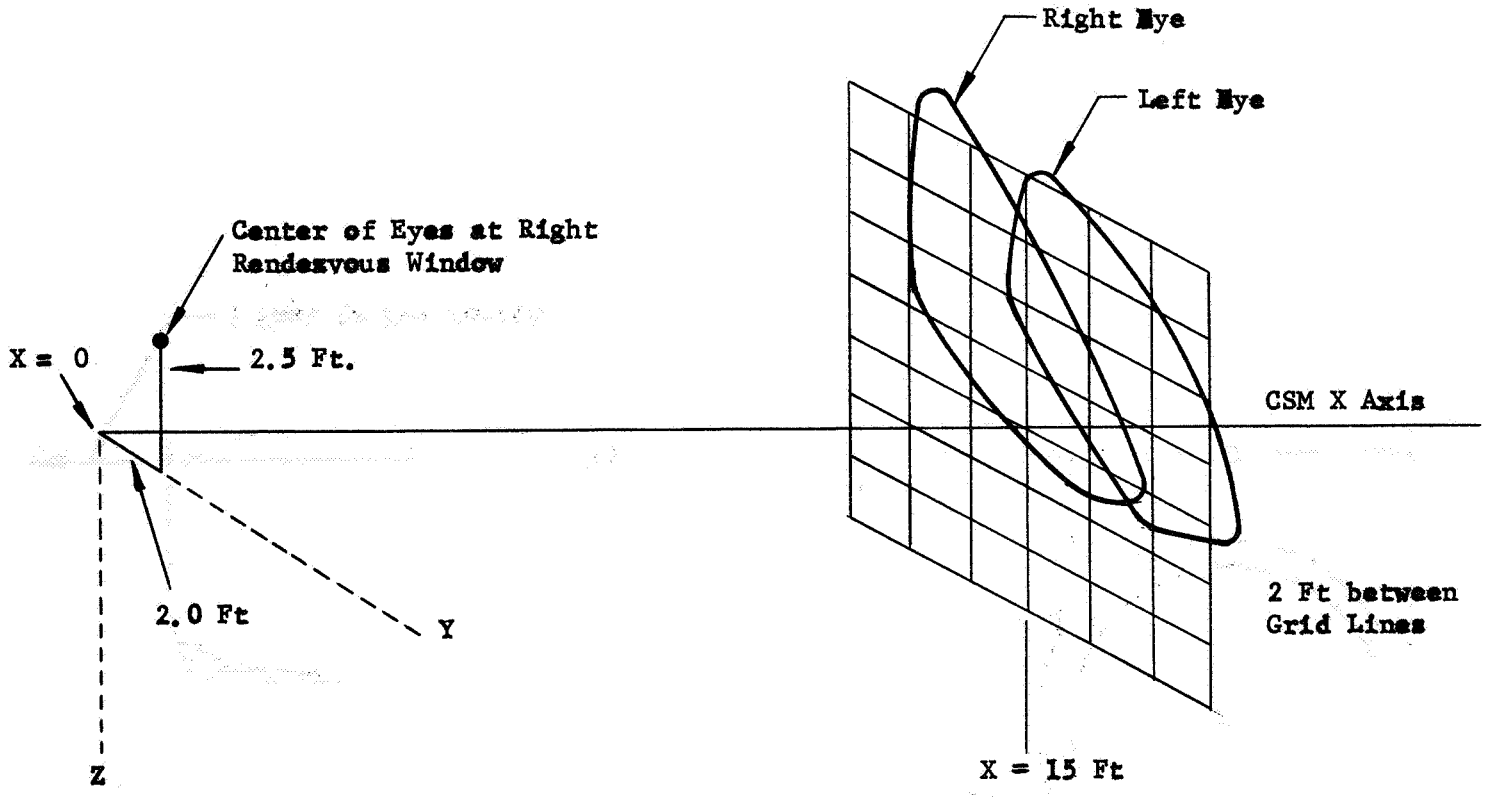

——At approximately 15 ft forward from eye position, X axis comes within FOV (Couch in docking position, helmet against headrest)

Figure 23 Field of View from CSM

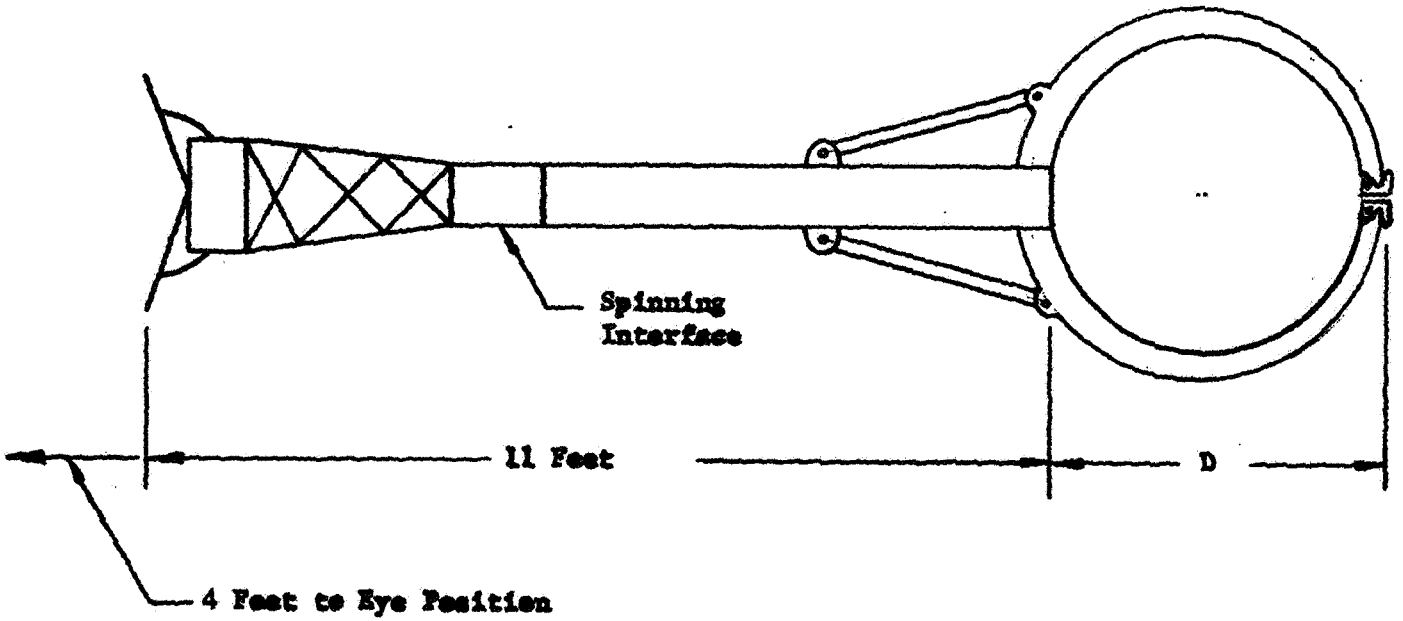

— D Envisioned to be 3 to 5 feet
— Astronauts will be able to see complete arms when they are above the spacecraft's X-Y plane

Figure 24 Recommended MRFMHD Sizing

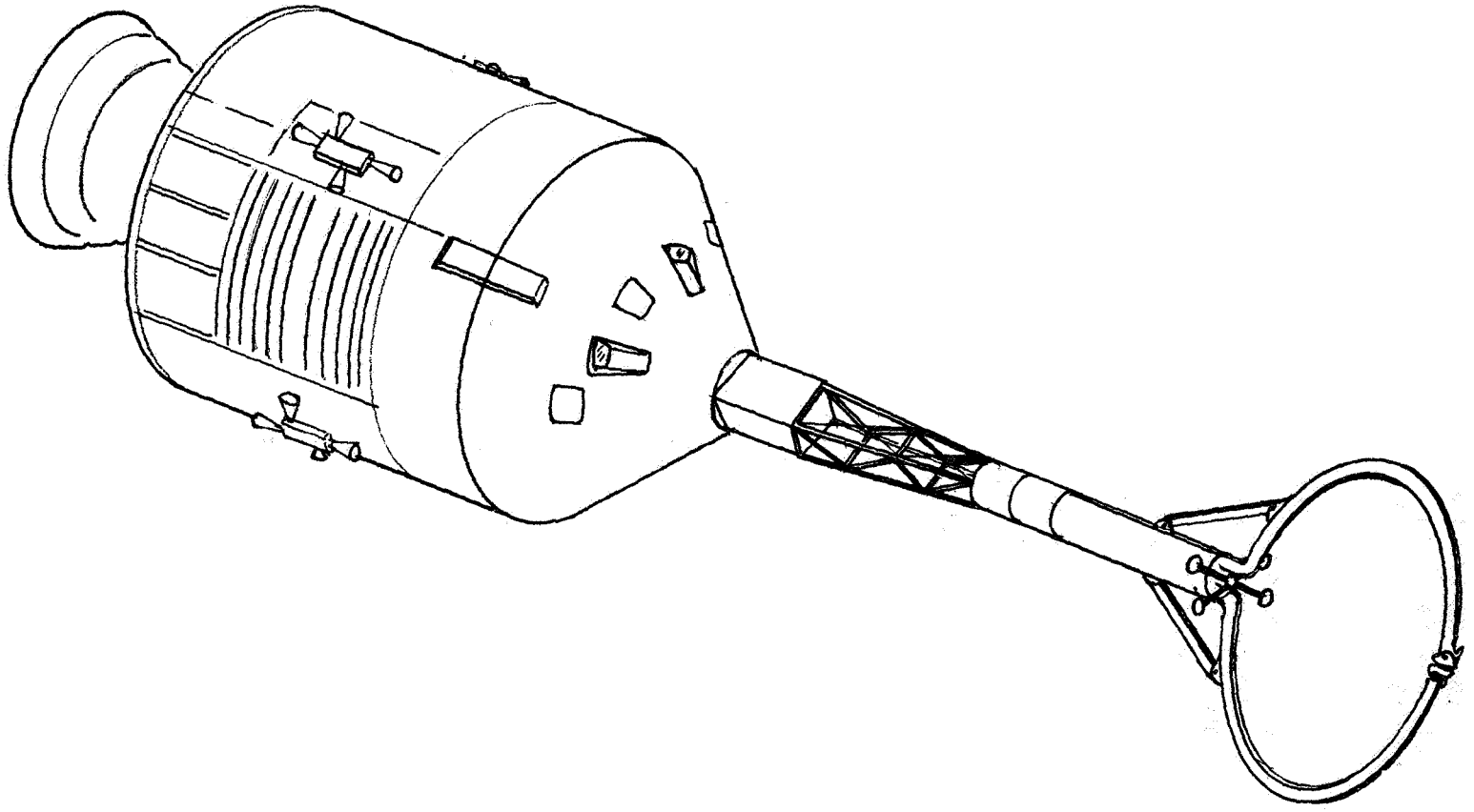

Figure 25 MRFMHD Boom Structure

8. CSM Interface

This section is concerned with the mechanical and electrical link connecting the MRFMHD to the CSM and the control equipment required in the CSM. The mechanical link is illustrated in Figure 25 in the previous section. The end of the MRFMHD duplicates the LM docking cone configuration.

Analysis to determine the feasibility of bringing MRFMHD electrical power and commands across this interface indicated that this would not be practical due to the highly complex configuration of the existing interface. For this reason, the following approach is proposed. The batteries to supply power for all MRFMHD operations should be built into the boom immediately forward of the docking cone. Analysis of the MRFMHD power consumption indicates that one worst-case (highest target inertia and spin rate) de-spin/spin-up cycle will require less than three hundred watt-hours (not including lighting). This would be consumed primarily by the motor in the spinning interface. With respect to battery weight, the Surveyor silver-zinc primary battery's design weight is forty-six pounds and is capable of supplying more than thirty-three hundred (3300) watt-hours when full charged (Ref. 22). This would be enough power for eleven or more maximum MRFMHD cycles. Solar cells, at approximately ten watts per square foot, could be used to recharge the batteries.

An additional benefit of having the batteries in the MRFMHD is their availability for powering tools (Ref. 6) that are used by the astronauts during EVA maintenance, repair, or assembly operations on the target.

One previous study (Ref. 2) proposed that an astronaut work platform should be included in a device related to the MRFMHD. However, the diverse MRFMHD tasks and target configurations do not lend themselves to such a platform. It is possible that a building-block set of handrail elements with attachment points on the MRFMHD could be useful as a MRFMHD accessory.

Approximately twenty MRFMHD command and sensor-readout channels could be required for one of the more complex MRFMHD configurations. It is recommended that these be transmitted over a short-range RF link between the CSM and MRFMHD. This technique, combined with the external batteries, would eliminate any need to modify the CSM's docking adapter.

Normal MRFMHD operations will require installation of the following additional equipment inside the CSM:

a. MRFMHD command receiver/transmitter

b. Spin axis rate control

c. Spin axis torque and rate readouts

d. Main AH arm open/close control

e. Main AH arm interpad force readout

and some of the following depending on MRFMHD configuration:

f. adhesive heater control

g. bondline temperature readout

h. target pre-heater control

i. adhesive replenishment control

j. MRFMHD damper controls

k. Supplementary AH extend/retract control

l. Supplementary AH spin rate control

m. Supplementary AH spin torque readout

n. Supplementary AH arm extend/retract control

o. Supplementary AH arm pitch control

p. Supplementary AH adhesive and target heater controls and readouts

During normal MRFMHD operations, the left-hand pilot would control the CSM maneuvers as described in the next section. The right-hand pilot would control those MRFMHD functions that require direct viewing of the AH and target. The center crew member could monitor and control MRFMHD functions such as adhesive temperature that do not require a window view. The list of CSM equipment given above illustrates the additional workload that arises if a temperature-controlled adhesive or a supplementary AH is used.

9. CSM Control

The MRFMHD concept as presented in this report is dependent on the astronauts' ability to position the AH within a few inches and degrees of perfect alignment to attach to a general class of targets. In addition, closure velocities should be less than one foot per second. Subject to quantitative proof in the simulation (Task E), it is felt that these requirements can be met. The MRFMHD feature that makes precise quantitative analysis of this problem difficult prior to the simulation is the length of the MRFMHD structure. This places the attachment interface fifteen to twenty feet in front of the crew.

The data that makes the requires CSM controllability appear feasible comes from past experience in space and simulations. During the Gemini program, GT-6 and GT-7 were maneuvered safely within one foot of each other and performed prolonged stationkeeping operations. The GT-9 vehicle was maneuvered and stabilized with the malfunctioning Augmented Target Docking Adaptor within a few inches of the spacecraft's windows. The Apollo 7 spacecraft, flown in October of 1968, performed stationkeeping operations within a few feet of the spent S-4B launch vehicle stage for approximately thirty minutes. Martin Marietta, in tests conducted under NASA contract No. NAS9-4410 (Ref. 23), found that the GT-5 crew could align the spacecraft's X (longitudinal) axis to track earth-surface objects with an RMS angular accuracy of less than two-tenths of one degree and pitch and yaw rate errors of less than two-tenths of a degree per second. Due to the approximate four-to-one higher attitude accelerations of the Gemini compared to the Apollo vehicles, the Apollo should be more precisely controllable than the Gemini. This indicates that attitude alignment should not be difficult if the visual cues are adequate.

One of the CSM pilot's main problems could arise due to the cross-coupling between CSM attitude corrections and AH transverse motions. With the AH/Target attachment interface approximately thirty feet forward from the CSM/MRFMHD c.g., one-tenth of a degree per second in pitch or yaw will produce six-tenths of an inch per second $\dot{Z}$ or $\dot{Y}$ motion, respectively, at the outer end of the AH. The pilot may, however, be able to use this cross-coupling to his advantage in positioning the AH.

The pilot's control of CSM translations should not be difficult since, in the direct mode, the Y and Z accelerations are approximately two-tenths (0.2) of a foot per second and, in X, the acceleration level is four-tenths (0.4) of a foot per second. One-fourth second pulses will produce translational rate changes on the order of one inch per second or less on all axes. The MRFMHD mass distribution should shift the system's c.g. less than one-fourth of a foot forward. Therefore, attitude accelerations generated during Y and Z thrusting will be on the order of one milliradian (0.057 degrees) per second^2. This is less than one-twentieth of the direct command attitude acceleration level. A Boeing Study (Ref. 24) rates CSM control levels as satisfactory as illustrated in Figure 26.

These data indicate that the attachment errors will be due more to visibility problems than to control problems. It is felt that the combined left and right-hand pilots should have enough visual information to align to the targets with the required degree of accuracy.

10. Launch Location

There is no question as to the feasibility of launching the MRFMHD. Two potential methods are (1) launch in place of the LM in the Spacecraft Launch Adapter (SLA) and (2) launch with an unmanned booster configured for the MRFMHD by itself. The choice between these two methods or selection

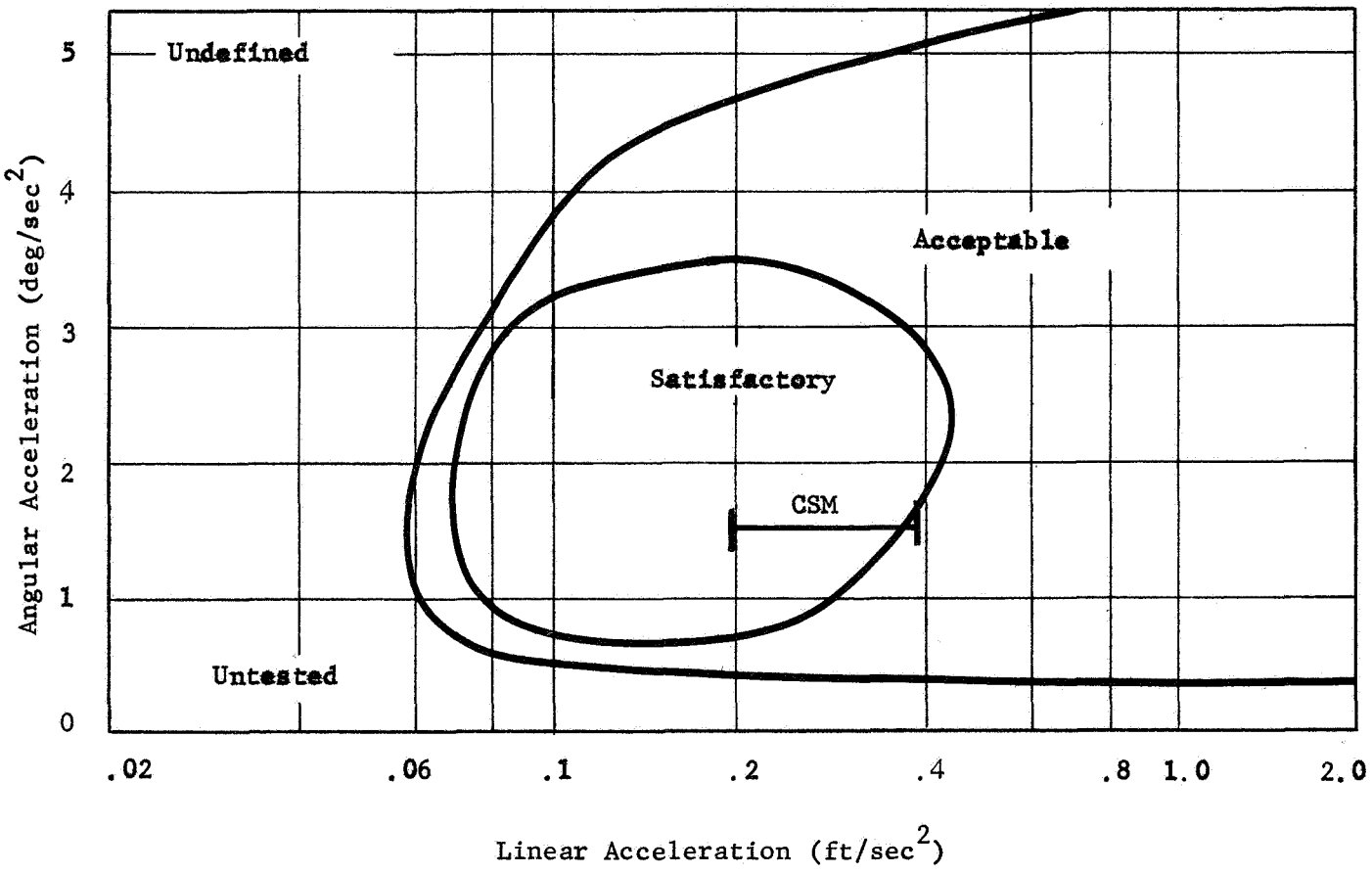

Figure 26 CSM Control Levels

of another method depends on a number of factors beyond the scope of this study. Included in these factors are costs of integrating the MRFMHD into a manned launch, mission timing for particular targets or other material handling operations, and availability of "piggyback" space on other launches.

11. Operational Timelines

Detailed analysis of the MRFMHD operational timelines is difficult at this time due to lack of data on mission profiles. The time required to rendezvous and dock with the MRFMHD depends on the launch mode. If the MRFMHD replaces the LM in the SLA, the transposition docking maneuver will require approximately five minutes (Ref. 19). Transfer time to the target or targets is unknown and the fuel consumption during such maneuvers depends on the mission profiles.

Once target rendezvous is complete, the time required to position the CSM/MRFMHD and attach to the target will depend on the type and configuration of the target and its sensitivity to attachment forces. The time required for the alignment maneuvers is among the data to be determined in the simulation (Task E). The time required for de-spin, work on the target, and spin-up will depend on the target.

12. Safety and Reliability

No major problems are anticipated in being able to design and build a MRFMHD that, of itself, will be safe and reliable. From one viewpoint, the CSM/MRFMHD may be envisioned as a space forklift truck operating without the benefit, and hindrances, of gravity. Therefore, the MRFMHD structure must be relatively rugged compared to typical space vehicle structures that do not have to endure repeated impacts and high force and torque loads. Barring such unlikely occurrences as an accidental SM main engine firing during final maneuvering near a large target, the AH and boom should provide excellent structural separation between the CSM and target.

If possible, active satellite attitude control systems should be disabled prior to attachment. In no case should a target be grasped if its attitude control system cannot be disabled and its dynamics can exceed the control forces and torques imposed by the MRFMHD. If a target enters what appears to be an uncontrollable gyroscopic motion at attachment, it should be released immediately to prevent damage to the MRFMHD.

SECTION III

EMHD AND TARGET DESIGN

1. Design Philosophy

The feasibility study (Section II) resulted in the decision that a combination mechanical/simulated-adhesive device provided the most practical design required to obtain information to support design and development of a more advanced Material Handling Device. Areas of interest were: 1) CSM/EMHD controllability, 2) closure velocities, position and rate errors at target contact, 3) post-contact interface loads and resulting system dynamics and 4) the utility of several grappling modes.

In view of the above areas of interest, the important design considerations were defined to be: 1) proper CSM/EMHD/Target dynamics and control functions, 2) full scale hardware, 3) proper CSM Pilot/EMHD Operator field of view through the CSM docking windows and 4) the ability of the selected design to fulfill contractural requirements.

Both technically and economically speaking, the design was felt to utilize the most efficient building block technique (iterative design/test procedure) leading to eventual MRFMHD hardware. Hence, the EMHD was designed and built to duplicate the functional features of the envisioned space hardware. EMHD materials and packaging were selected to satisfy the needs of the simulation program.

2. EMHD and Target Hardware

The finalized EMHD design consisted of a two-armed mechanical grappling device with provision to utilize a four-pad simulated-adhesive attachment head. Assembly drawings of the EMHD configured as a mechanical grappler and as a simulated adhesive head are presented in Figures 27 and 28, respectively. For clarity, the EMHD sub-assembly designs and resulting hardware will be discussed in the following order: 1) Mechanical grappling head, 2) Six-degree-of-freedom simulated-adhesive head, 3) Spinning Interface, 4) EMHD Drive and Control Systems, 5) Instrumentation Systems and 6) Targets and Associated Grappling Modes.

a. Mechanical Grappling Head - The mechanical arms were fabricated of 0.060-inch, 6061-T6 Aluminum using a box structure to maximize strength while minimizing weight and inertia characteristics. The box structure is illustrated in Figure 29. The fabricated arms were mass and inertia balanced to minimize vibration and drive power requirements. The attachment pads were spring loaded to allow, and

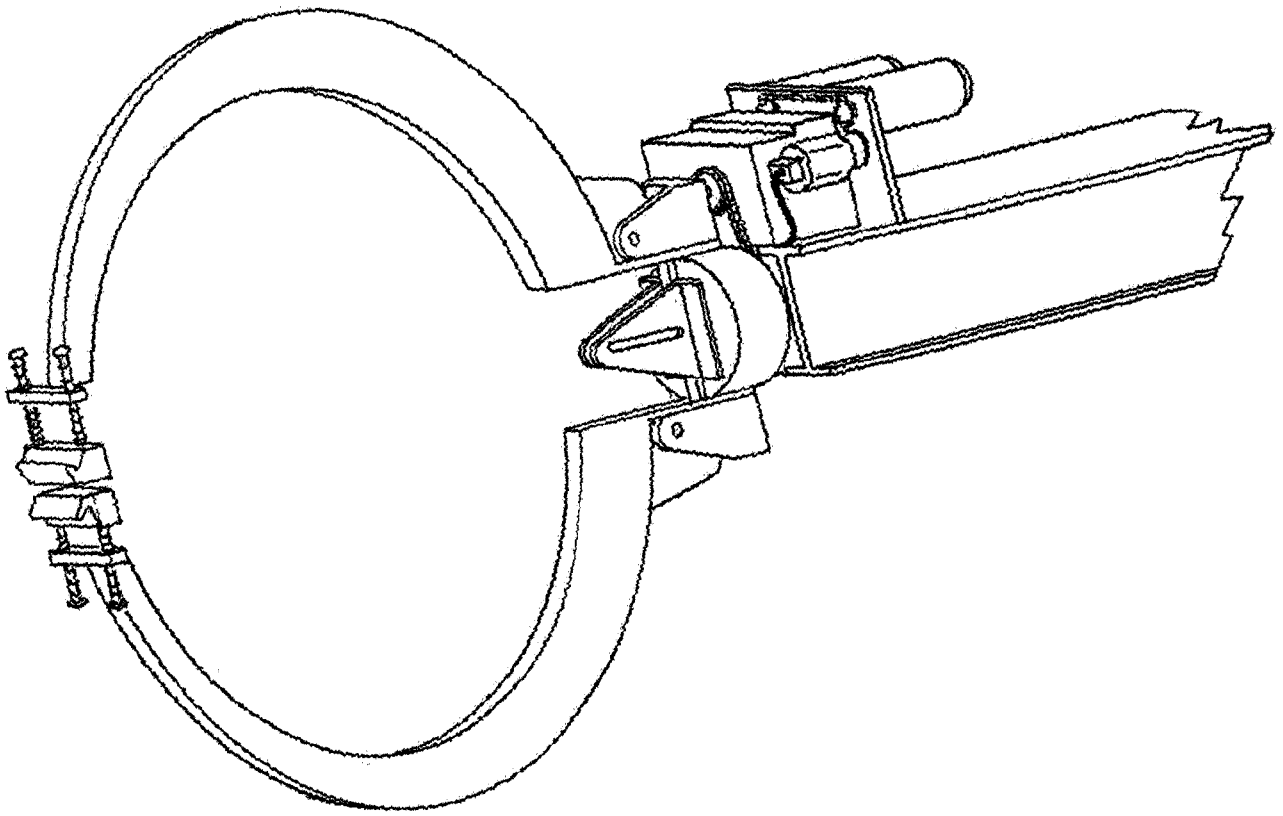

Figure 27 Mechanical Grappling Head Assembly

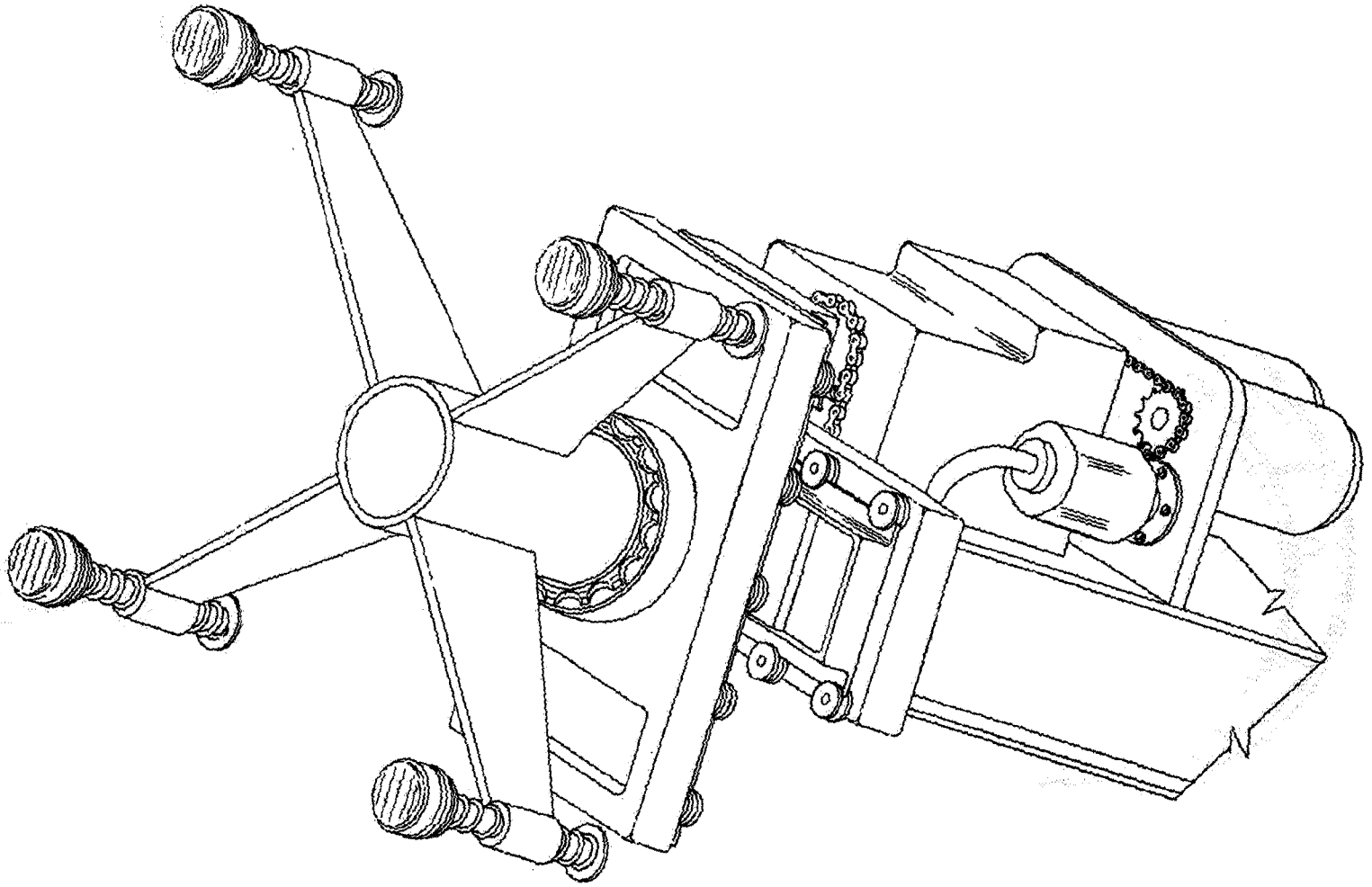

Figure 28 Simulated-Adhesive Grappling Head Assembly

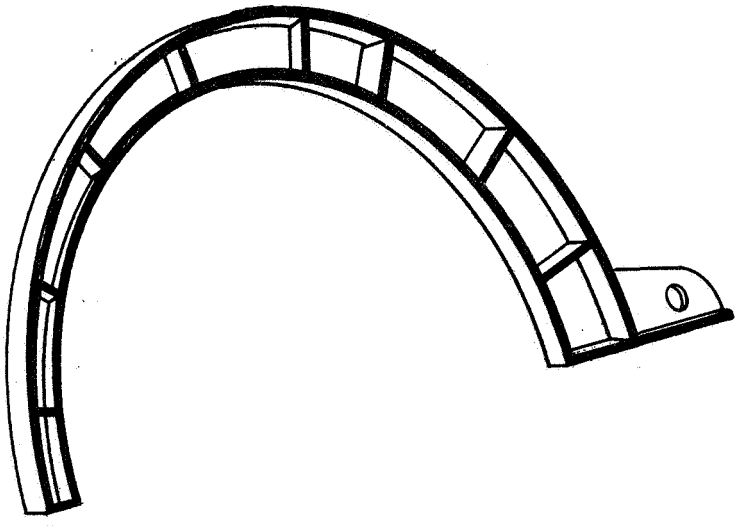

Figure 29 Mechanical Grappling Arms

damp out, target position and attitude errors at contact. Hooks were added to the attachment pads to enable another attachment mode. The two attachment modes available with the Mechanical Grappling Head are: 1) clamping attachment to outer target surface and 2) expansion attachment, using the hooks, to the target adaptor flange. Figure 30 shows the mechanical grappling arms mounted to the spinning interface. The illustrated assembly is referred to as the Mechanical Grappling Head.

b. Six-degree-of-freedom Simulated-adhesive Head - A four-pad head, Figure 28, was chosen to maximize adhesive grappling area thereby minimizing EMHD/Target peel forces and to provide post-contact stability. The pads were swivelled to allow conformation to target geometry and attachment errors. Velcro, made by American Velcro Inc., New York, New York, was chosen to simulate desired adhesive properties. The pads were spring loaded to absorb and damp small translational rate and attitude errors. A roller-track assembly was incorporated into the Adhesive Head to enable the head to track relative target circular motion induced by attachment errors. Provision was made to counter-weight the head since it is free to move on the rollers and tracks except for a low-force detent in the center position. The AH is shown in Figure 31. It is also shown in Figure 32 mounted to the spinning interface and the assembly is referred to as the Six-degree-of-freedom

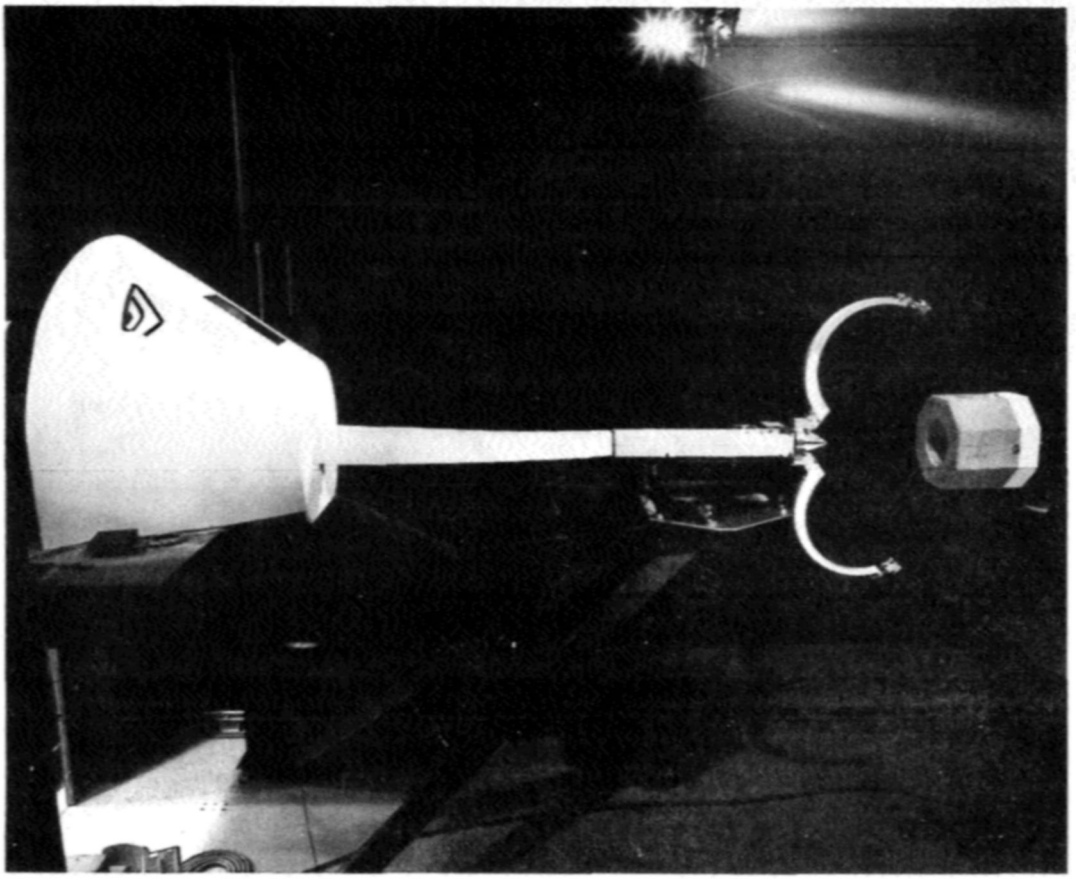

Figure 30 Mechanical Grappling Head, Simulation Assembly

Simulated-adhesive Head.

The attachment mode available is referred to as the simulated-adhesive attachment mode.

c. Spinning Interface - The Spinning Interface was designed and built to ride on a bronze bushing. The bushing is fitted to a stationary steel shaft originating at the forward end of the EMHD boom supporting structure. The interface is chain driven and is capable, by means of a slip-ring assembly, of transmitting six (6) channels of electrical data from the Attachment Head. The Spinning Interface and chain drive are shown in Figure 33.

d. EMHD Drive and Control Systems - EMHD spin rate (ω) was powered by two paralleled D.C. motors. Armature voltage was variable from 0 to 28 volts and the field voltage was maintained at 28 volts.

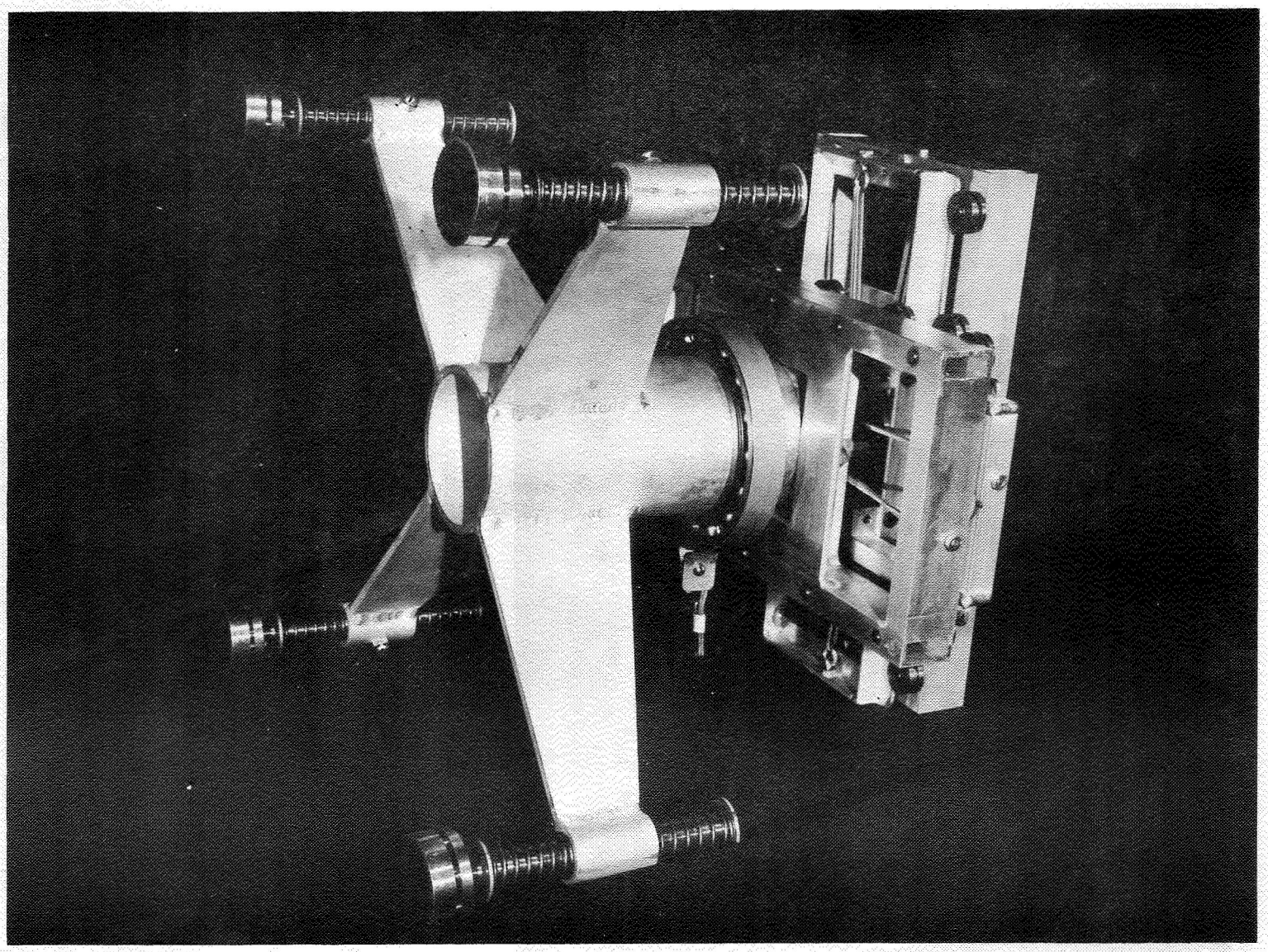

Figure 31 Simulated Adhesive Head

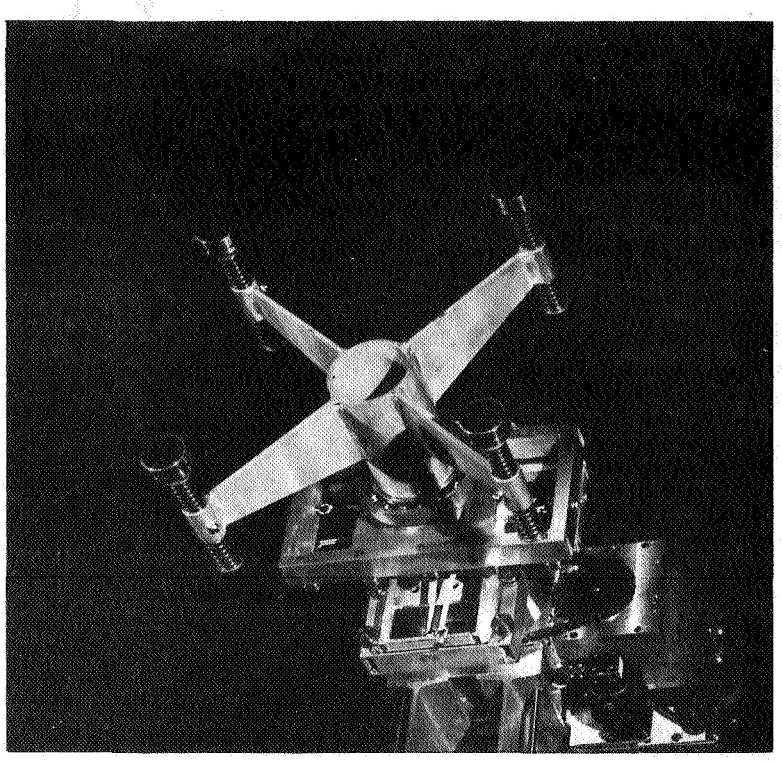

Figure 32 Six-Degree-of-Freedom Simulated-Adhesive Head

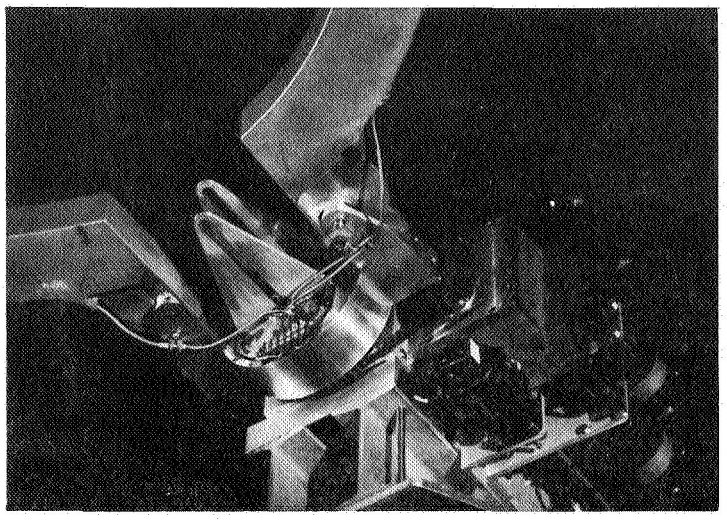

Figure 33 Spinning Interface and Chain Drive Assembly

The arm open angle (α) was controlled by a series-wound D.C. motor driving a linear actuator. Voltage to the motor was variable from 0 to 28 volts and controlled in a variable-amplitude, pulse mode. A schematic of the EMHD power and control system is shown in Figure 34. The EMHD control box was operated from the right seat of the CSM mockup and is shown in Figure 35 in its position below the right-hand docking window.

e. Instrumentation Systems - The parameters displayed to the operator controlling the EMHD were: 1) spin rate (ω), 2) de-spin/spin-up torque (M_{XT}) and 3) attachment clamping force (f_1, f_2). These parameters were transmitted to the EMHD operator, Figure 35, from from the AH via the slip-ring assembly as discussed in Section III.2.c. AH spin-rate was measured with a tachometer on the output of the spin drive motors, f_1 and f_2 were obtained using single turn potentiometers and M_{XT} was obtained from load cell array output.

f. Targets and Associated Attachment Modes - Three target configurations were desired for the simulation (Task E). They were: 1) an octagonal target, twenty-four (24) inches in diameter between the flats, with a twelve (12) inch diameter flange on the forward surface, 2) a cylindrical target twelve (12) inches in diameter with an eight (8) inch diameter flange on the forward surface (this unit attaches to the front surface of the octagonal target) and 3) the octagonal target with an attachment surface composed of Velcro pile to simulate adhesive properties. The octagonal target is shown in Figure 36. Two attachment modes are available with this target. They are: 1) clamping attachment to the outer target surface as shown in Figure 37 and 2) hook attachment to the twelve (12) inch target adapter flange as shown in Figure 38.

The cylindrical Target is shown is Figure 39. The above-mentioned attachment modes are also available with this target. Figure 40 illustrates the outside attachment mode and Figure 41 shows the eight (8) inch flange attachment mode.

Figure 42 illustrates the octagonal target configured with the Velcro attachment surface. The simulated-adhesive attachment mode is shown in Figure 43.

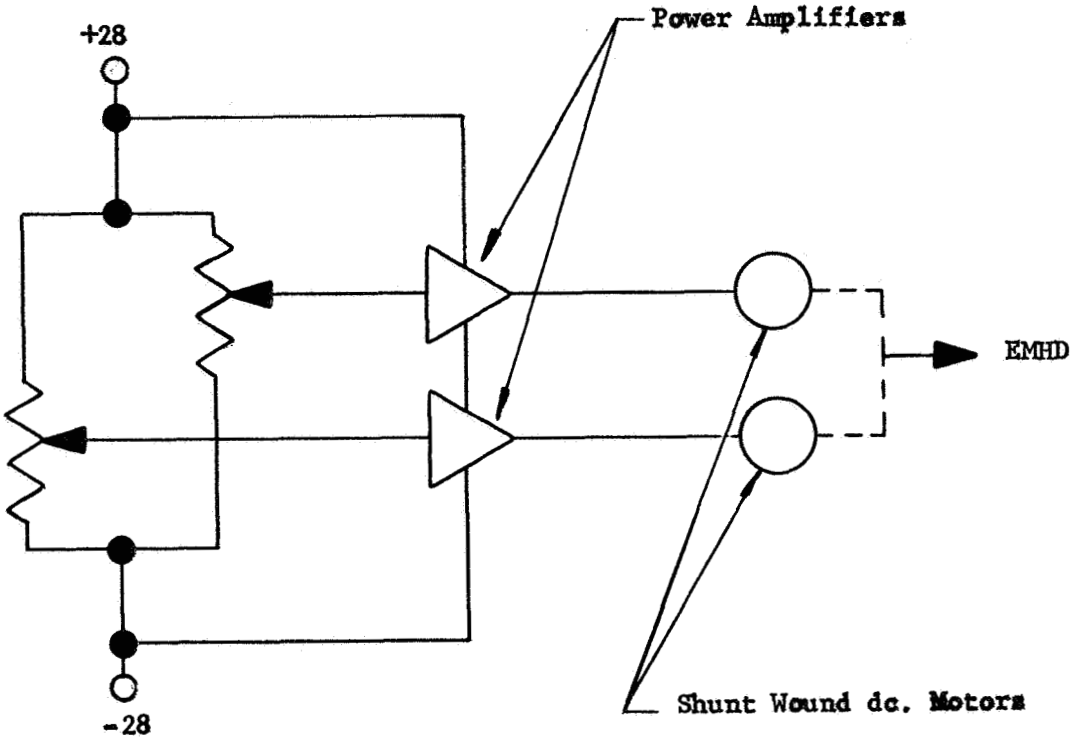

a. Spin Drive Control

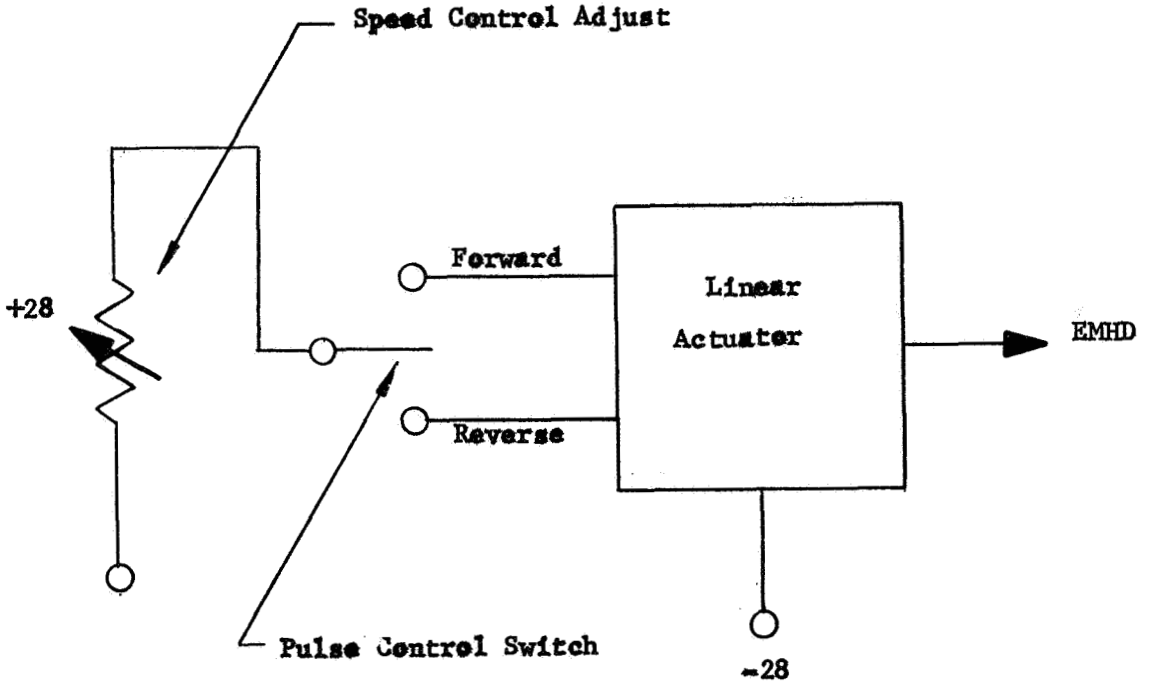

b. Arm Open/Close Control

Figure 34 EMHD Power and Control Schematic

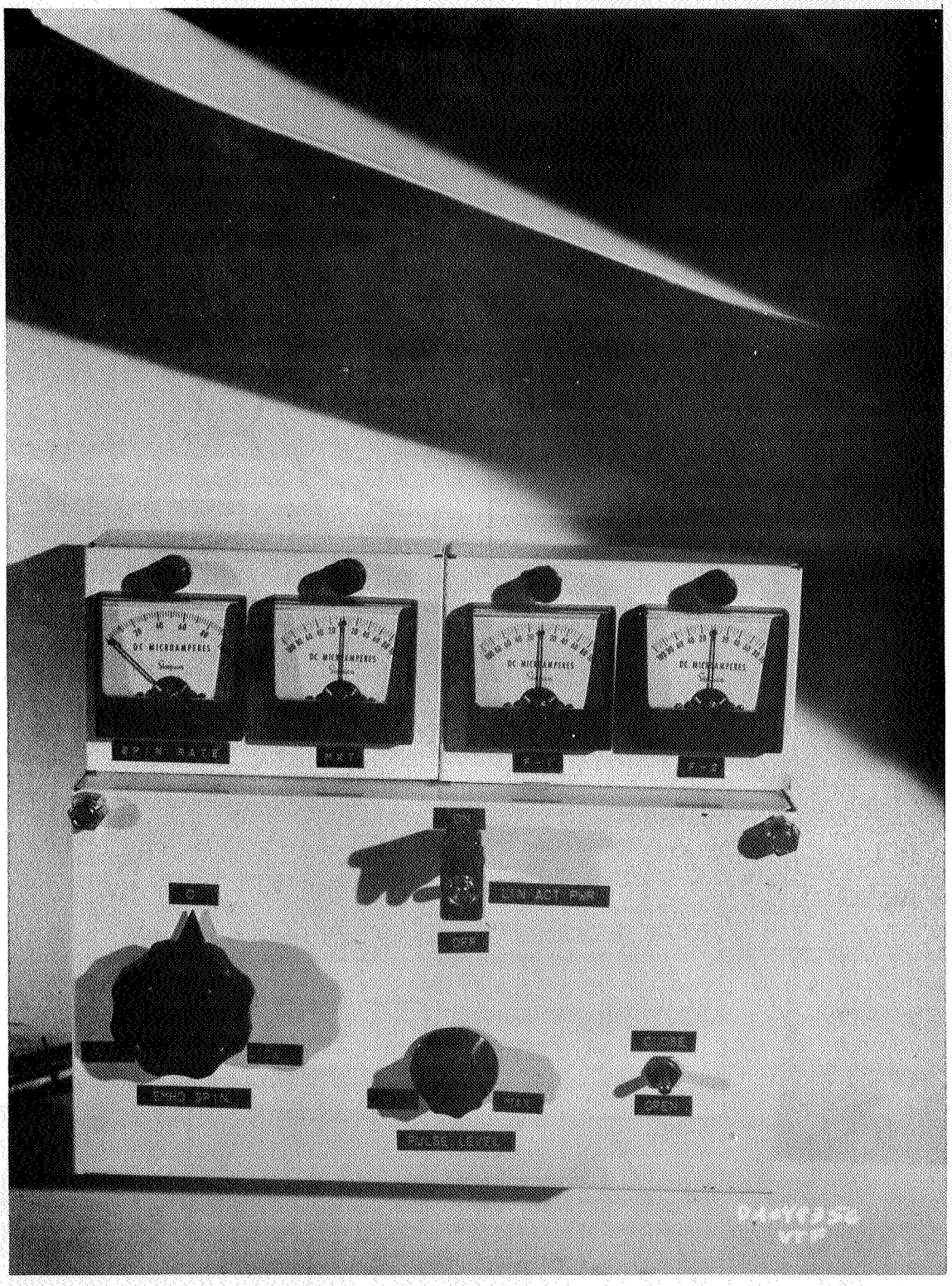

Figure 35 EMHD Control Box

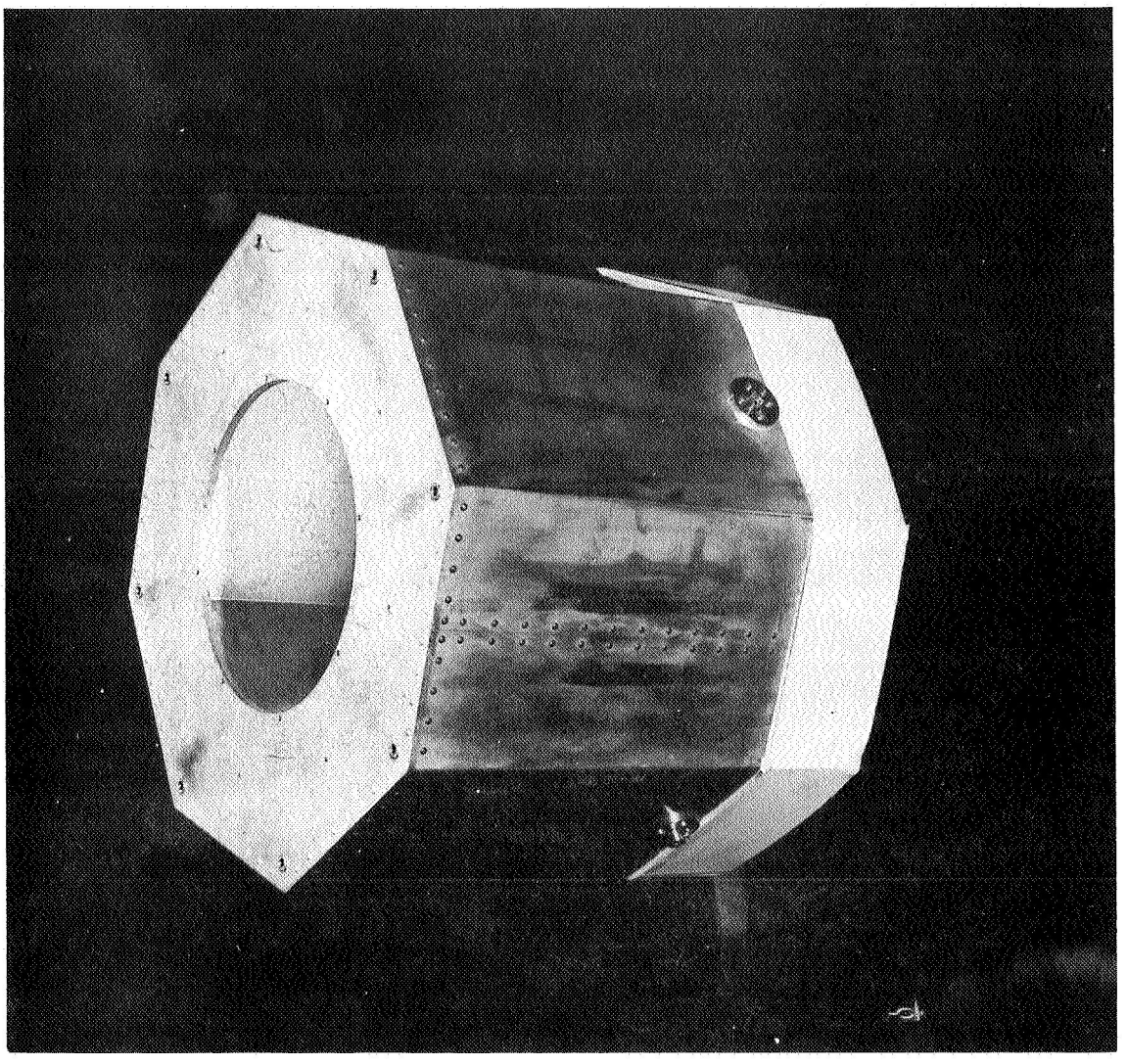

Figure 36 Octagonal Target

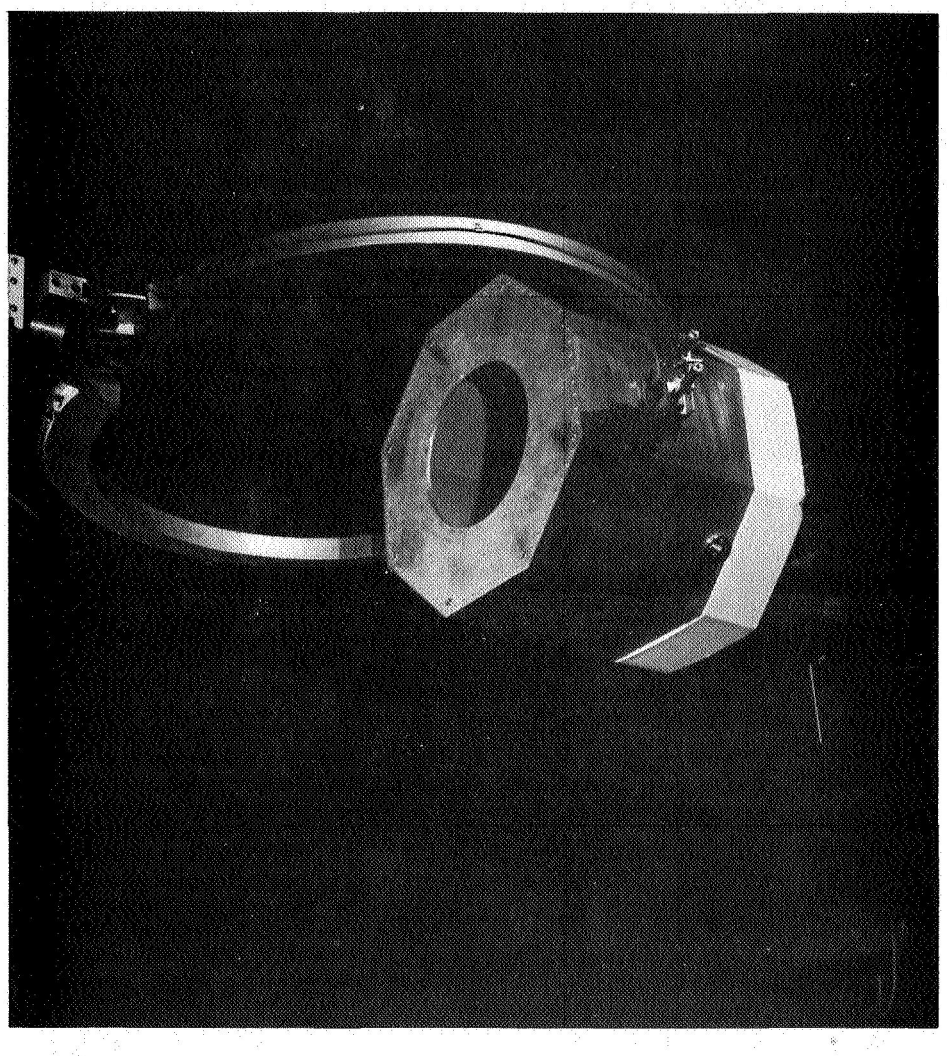

Figure 37 Octagonal Target Surface Attachment Mode

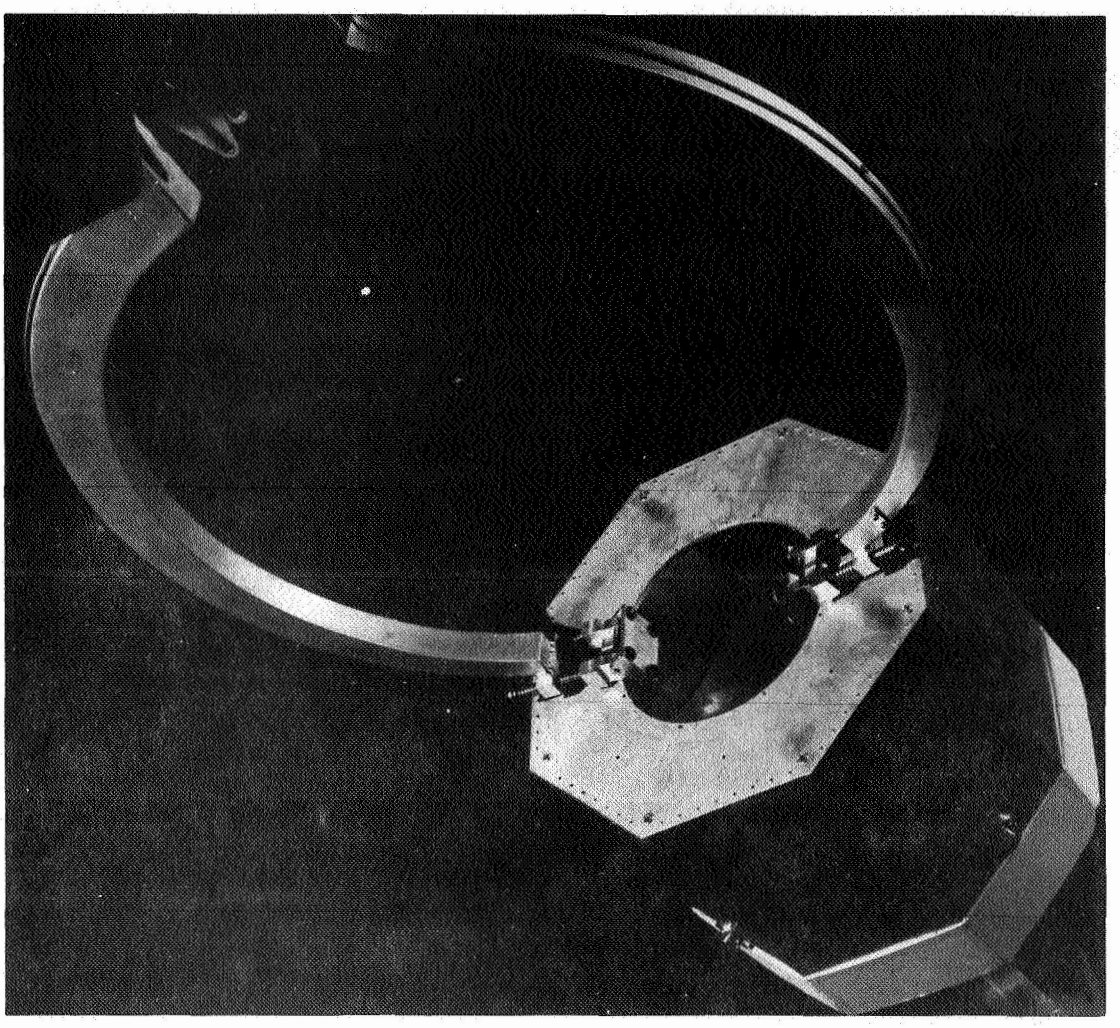

Figure 38 Octagonal Target Flange Attachment Mode

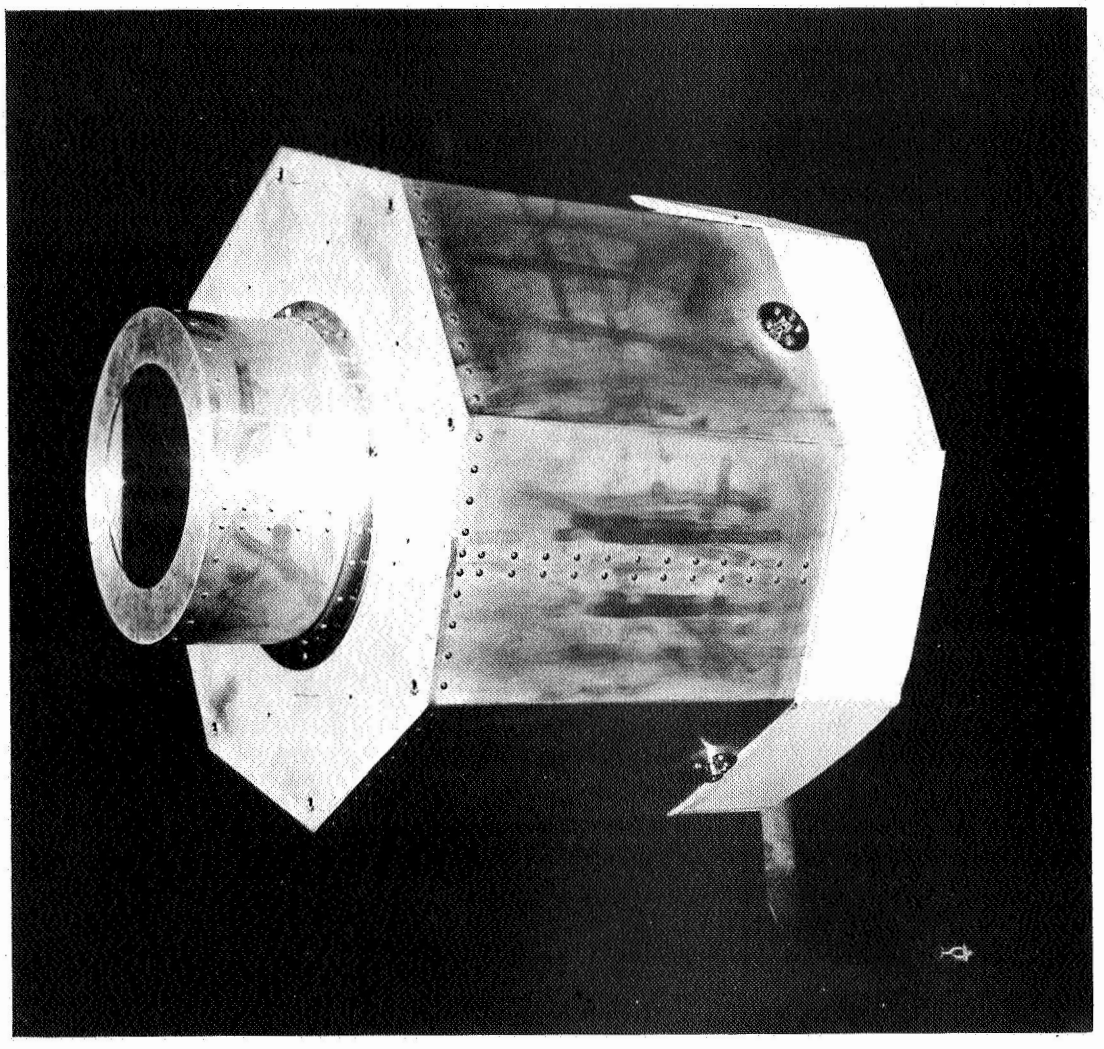

Figure 39 Cylindrical Target

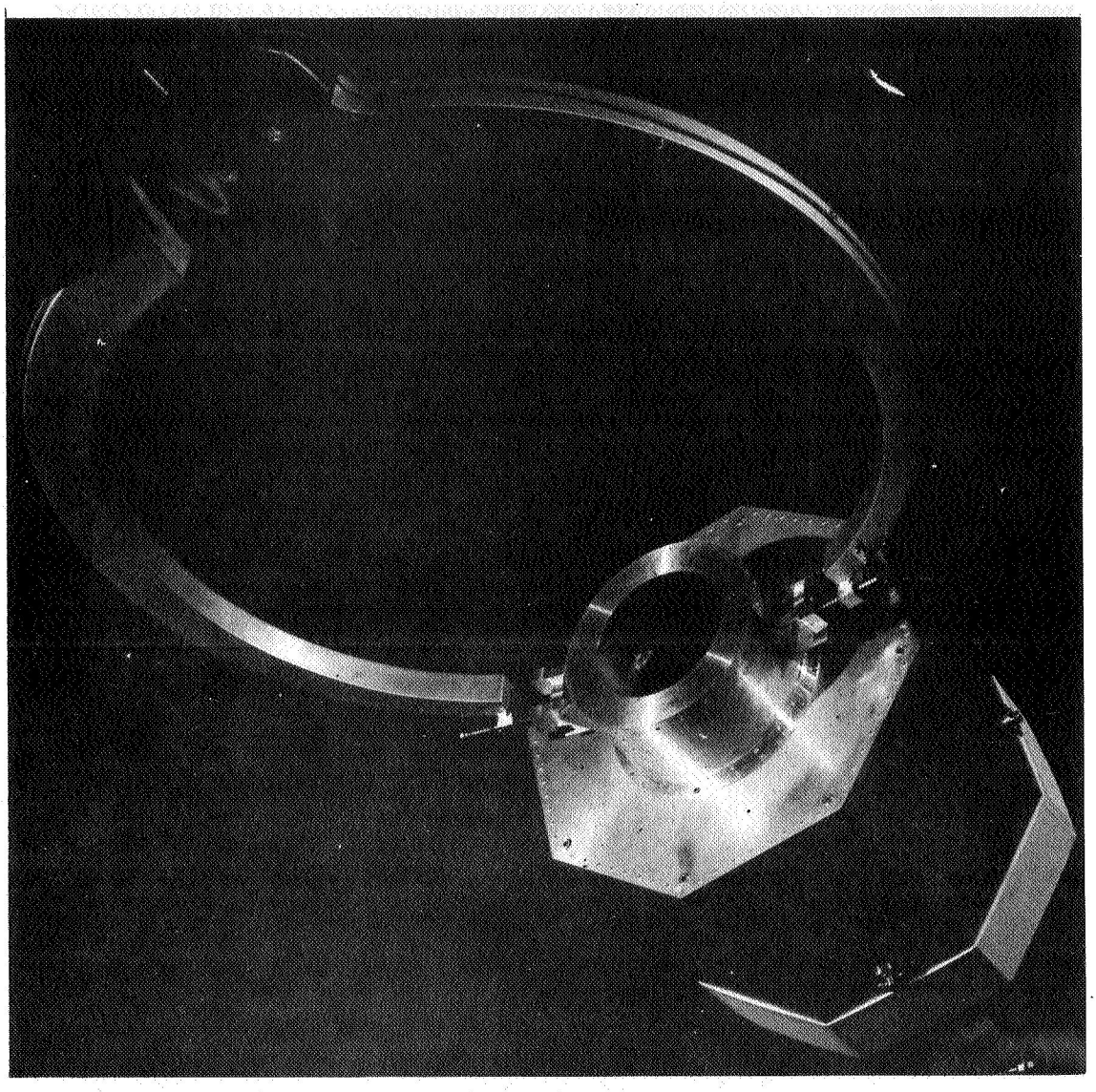

Figure 40 Cylindrical Target Surface Attachment Mode

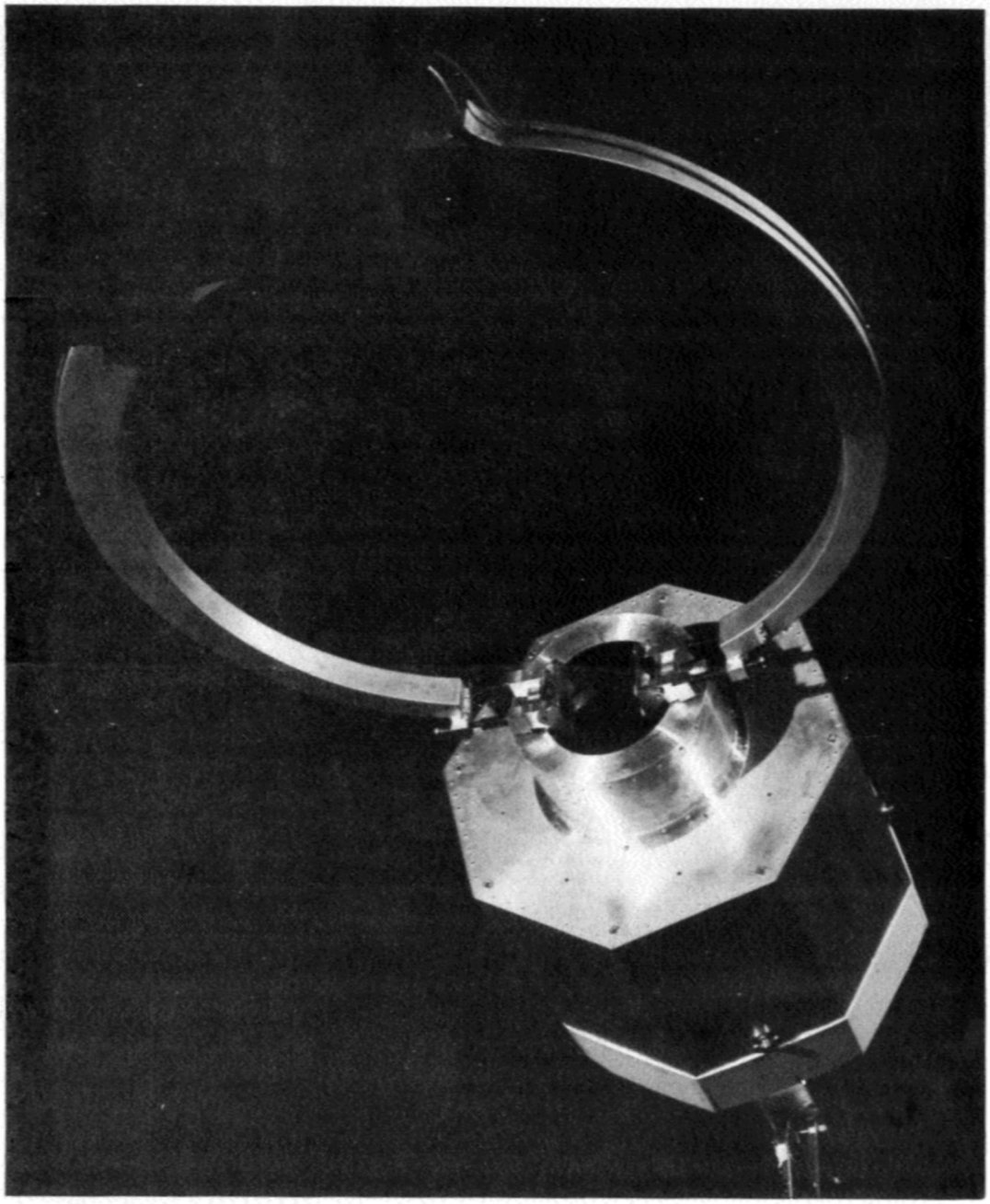

Figure 41 Cylindrical Target Flange Attachment Mode

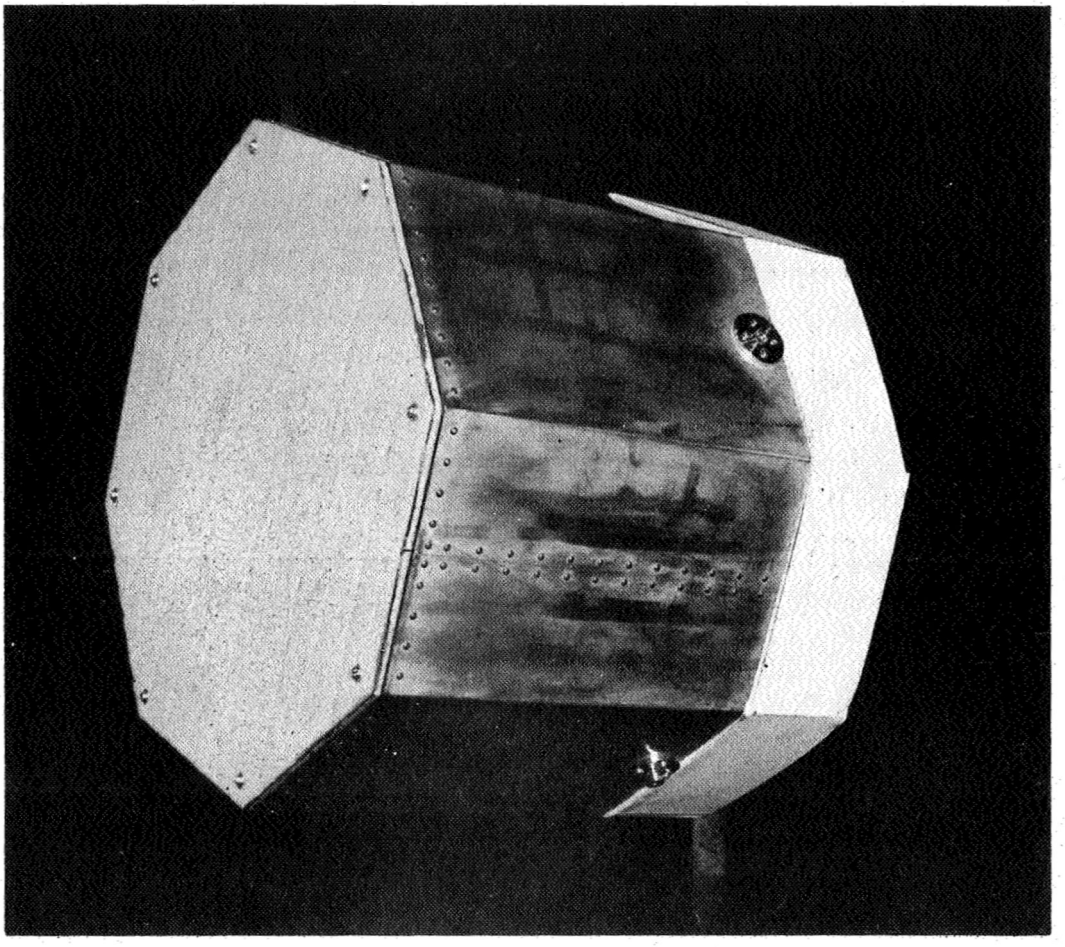

Figure 42 Octagonal Target Configured with Velcro Attachment Surface

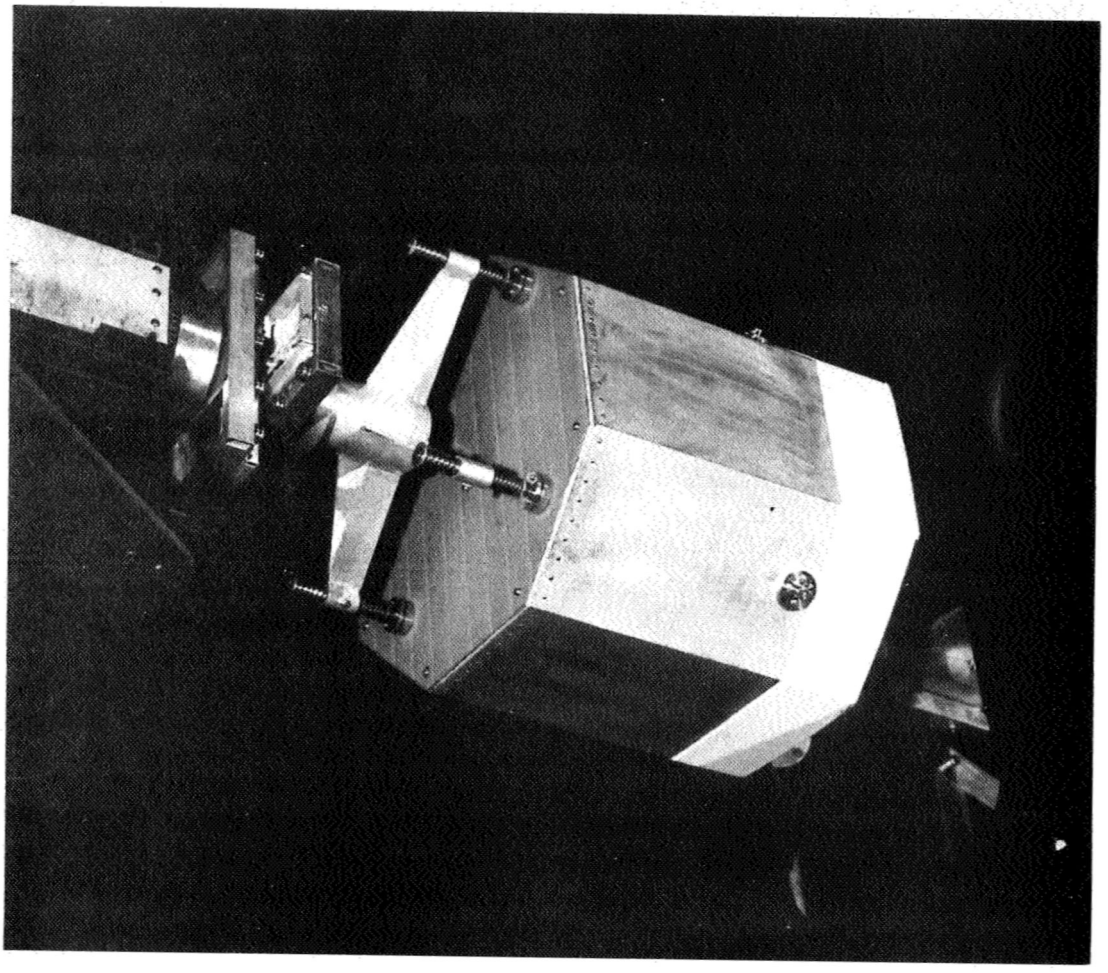

Figure 43 Simulated-Adhesive Attachment Mode

SECTION IV

PROOF TEST PROCEDURE AND RESULTS

1. Approved EMHD and Target Proof Test Procedure

   a. EMHD Proof Test - The EMHD contains two motor-driven parts; 1) the spinning interface and, 2) the grappling arms. The spinning interface is driven by a pair of 28 VDC motors through a chain drive and gear box. This drive has two functional requirements that must be verified. The requirements and proof tests are as follows:

      i. Requirement: The EMHD must be capable of rotating its attachment head at up to 36 revolutions per minute in either direction.

         Test Procedure: Using a variable voltage power supply having -28 VDC to +28 VDC capability, apply voltage to the EMHD spin drive motors. Using a stop watch and counting revolutions for a three-minute interval, determine r.p.m. at -28, -20, -10, 0, +10, +20, and +28 volts (unless 36 rpm is reached at less than 28 volts).

         The test result will be termed satisfactory if the spinning interface achieves 36 rpm at or below 28 volts in each direction. Test documentation will include a description of the test and a plot of rpm versus applied voltage on the spin drive motors.

      ii. Requirement: The spinning interface shall be capable of delivering up to fifteen foot-pounds of torque (about the EMHD longitudinal axis) to an object attached to the EMHD attachment head.

         Test Procedure: With the EMHD longitudinal axis mounted horizontally, attach a cross-bar to the attachment-head side of the spinning interface such that the bar is at a right angle to the EMHD axis. With the bar in a horizontal position, suspend a calibrated ($\pm$ 2% or better) load from

the bar such that the product of the load times the moment arm (suspension point to EMHD axis) equals fifteen foot pounds. Apply power (up to 28 VDC) to the spin drive motors until the spinning interface supports and raises the load.

The test results will be termed satisfactory if the spinning interface supports or rotates against this load (in both directions) with an applied voltage of 28 volts or less. Test documentation will include a description of the test and the voltage (in each direction) at which the EMHD met the torque requirement.

The EMHD contains a 28 VDC linear actuator for opening and closing the curved attachment arms. The two requirements and tests for the arm/drive combination are as follows:

iii. Requirement: The arms must be driven from full closed to full open position (at least 80^{o} rotation of each arm) in ten seconds or less and full open to full closed in ten seconds or less.

Test Procedure: Using a variable voltage $\pm$28 VDC power supply, determine open and close cycle times at 0, $\pm$14, and $\pm$28 VDC.

The test results will be termed satisfactory if the cycle time for open and close is ten seconds or less (for the individual cycles) with an applied voltage of 28 VDC or less. Test documentation will include a description of the test and a plot of open/close cycle times versus applied voltage.

iv. Requirement: The actuator drive plus the mechanical characteristics of the arms and drive links must provide at least ten pounds of force between the arm end pads for both clamping and expansion grappling when the pads are one foot apart.

Test Procedure: Using calibrated (5% or better) spring balances or an equivalent device, determine the inter-pad force required to

stall the open/close arm motion as a function of pad separation (measured between the faces of the gripping pads). The test results will be termed satisfactory if the inter-pad force required to stall the open and close motions equals or exceeds ten pounds at one foot pad separation. Test documentation will include a description of the test and a plot of inter-pad stalling force for the open and close operations from full closed to a pad separation of at least three feet.

All other functions in the EMHD, such as spring motion on the arm end pads, are design features whose suitability will be determined during the EMHD evaluation simulation. In this context, there are no Proof Test criteria that can be applied to such functions. However, following assembly, all EMHD functions will be subjected to dynamic and visual checks to ensure that there are no interferences or binding that will prevent proper operation.

b. Target Proof Test - The Target is driven by a servo-motor through a chain drive and gear box. This system has two functional requirements that must be verified. The requirements and associated tests are as follows:

i. Requirement: The Target must be capable of rotating at up to 36 rpm in either direction.

Test Procedure: Using a variable voltage power supply, apply DC voltage to the Target spin drive motor. Using a stop watch and counting revolutions for a three-minute interval, determine rpm at 0, $\pm 1/3$, $\pm 2/3$, and $\pm$ maximum drive voltage (unless 36 rpm is reached at less than maximum voltage).

The test results will be termed satisfactory if the Target achieves 36 rpm at or below maximum drive voltage in each direction. Test documentation will include a description of the test and a plot of rpm versus applied voltage on the Target spin drive motor.

ii. Requirement: The Target drive shall be capable of delivering up to fifteen foot-pounds of

torque to the Target about the spin axis of the Target.

ii. Test Procedure: Using a torque drag device, apply at least fifteen foot-pounds of torque to the Target support structure where it attaches to the Target cylinder's structure. Verify, for a minimum of three minutes, that the Target drive can maintain 0, $\pm$18, and $\pm$36 rpm while operating against the torque load.

The test results will be termed satisfactory if the drive maintains these rpm levels while combating the applied torque load. Test documentation will include a description of the test and a plot of the voltage required at the given rpm levels to operate under the specified torque load.

2. Proof Test Results

a. EMHD Spin Drive - Requirement Number i - Using the EMHD spin drive control mounted in the CSM mockup, power was applied to the spin drive motors with the EMHD mounted in the SOS in the two-arm (closed) configuration. Twenty-eight volts was applied continuously to the fields of the drive motors. Armature voltage was measured with a Simpson 260 multimeter connected across the armature input leads at the terminal block on the EMHD boom. Figure 44 indicates the applied armature voltage (both motors had equal armature voltage) versus the spin rate. A plus rotation is clockwise as viewed from the cockpit. Each spin rate was measured for three minutes. Figure 44 also presents the total amperage drawn by the spin drive system.

This test proved the capability to achieve 36 rpm at 28 volts or less in both rotation directions.

b. EMHD Spin Drive, Requirement Number ii - The de-spin/spin-up torque capability of the EMHD was proved with the two-arm configuration mounted in the simulator. With the arms closed and the plane of the arms parallel to the floor, power was applied to the spin drive until the arms started rotating with no load other than the arm load on the head support bearing. The armature voltage (measured at the armature input leads) and total spin drive amperage requirements for this operation are listed in Table III under the zero (0) load category.

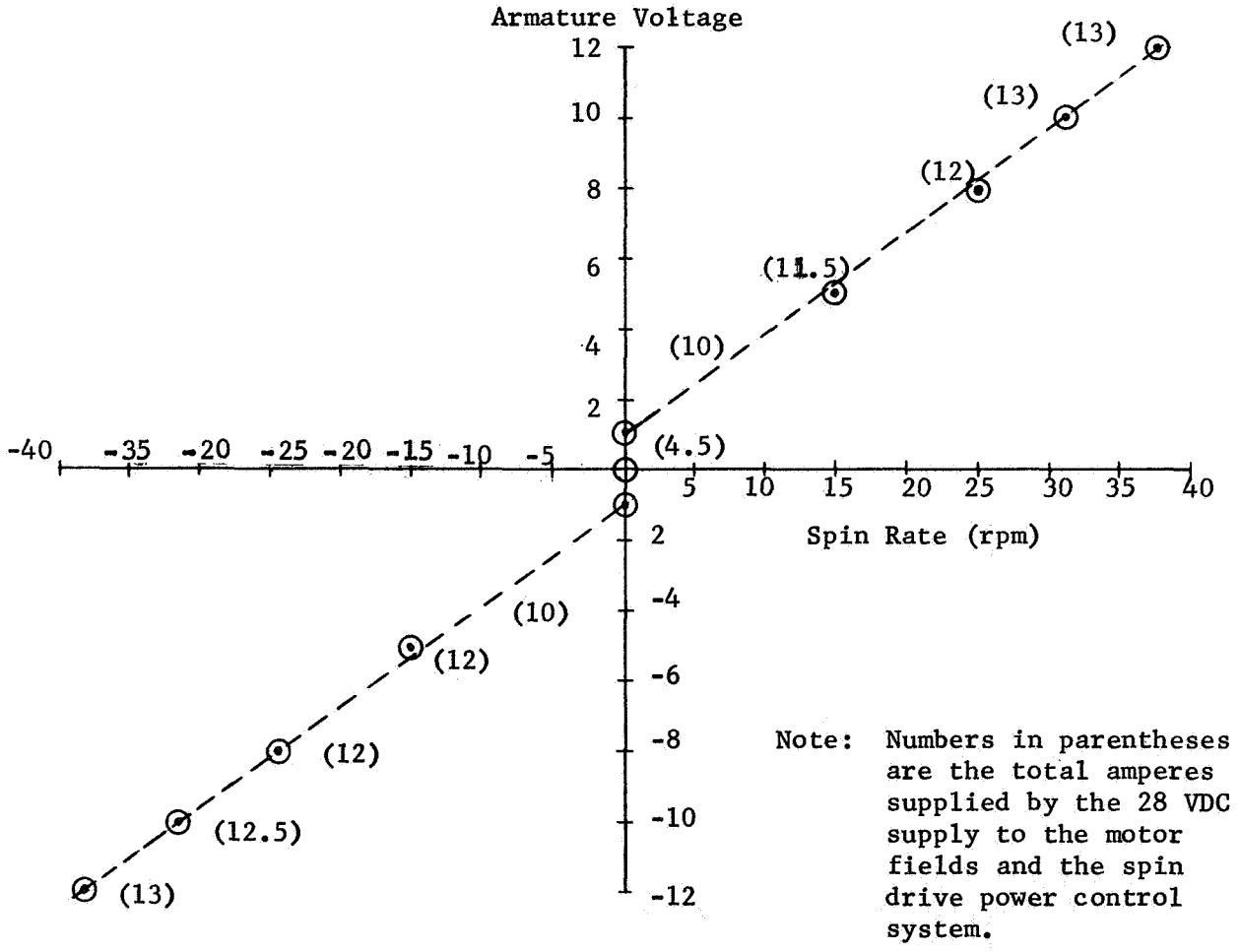

Figure 44 EMHD Proof Test, Armature Voltage verses Spin Rate

With the same starting position, a ten pound weight was suspended from the mid-point of one of the arms. The suspension point was located one and one-half feet to the side (horizontally) of the EMHD axis. This weight and moment arm produced a static fifteen foot pound torque load on the spin drive and spinning interface. Power was applied gradually to the spin drive motor armatures until the head started rotating against this torque load. Voltage and system current were measured at this time. The test was repeated with the weight suspended from the other arm and the direction of rotation reversed. The results of these tests are included in Table III.

These results satisfied the requirement that the EMHD spin drive be able to supply at least fifteen foot pounds of torque with a motor voltage of 28V or less.

Table III Spin Drive Torque Test Results

Load (ft-lb)	Rotation	Armature Voltage	System Amps
0	+	0.9	10
0	-	0.8	10
15	+	1.5	20
15	-	1.4	20

c. EMHD Arm Actuator - Requirement Number iii - With the arm plane in a horizontal position, power was applied to the linear actuator using the EMHD control box and a 28VDC supply. A Simpson 260 multimeter was used to measure the voltage across the input leads to the series-wound actuator motor. With an applied voltage of fourteen (14) volts, the arms could make a complete, 90 degree, open or close cycle in six (6) seconds. Increasing the voltage to twenty-five volts, a complete open or close motion was made in three and one-half (3.5) seconds. These tests met the requirement to open or close the arms completely (90 degree rotation on each arm) in ten seconds or less with an applied voltage of 28VDC or less.

d. EMHD Arm Actuator - Requirement Number iv - With the EMHD mounted in the simulator, clamping force between the pads was determined at one-foot intervals from pad contact to four feet pad separation. A spring scale was attached to one of the pads and pulled in a direction tending to open the arms. The force, F, was applied along a line passing through both pads as shown in Figure 45.

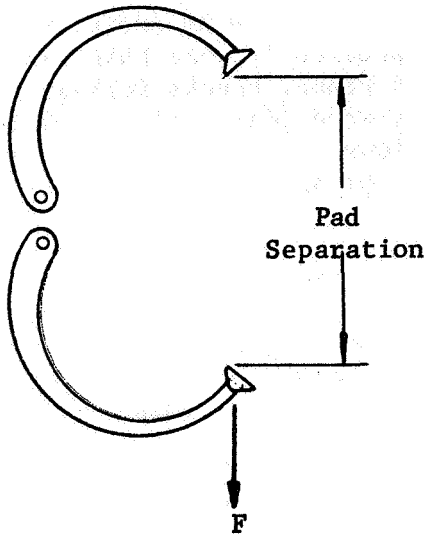

Figure 45 Pad Separation

The test technique consisted of actuating arm closure with 25V applied to the linear actuator. F was increased and the arms stalled at the various pad separations. F was decreased at these points until the arms started closing again. This gives information on both stall and restart force capability at the calibration point. Note that if F/2 was applied to each pad (pulling outward on each pad), the actuator would stall or start in the same manner. Therefore F/2 is the clamping force. The stall force represents the individual pad clamping force that would be exerted if the arms were closed on a target having a resilient surface with characteristics like the spring scale. A more rigid target would be clamped harder.

The test results, which satisfy the requirement to produce ten pounds of clamping force at one-foot pad separation, are presented in Table IV.

Table IV Clamping Force Test Results

Pad Separation (ft)	Stall Force,F/2 (lb)	Restart Force,F/2 (lb)
0	20	10
1	19	10
2	15	10
3	14	10
4	14	9

e. Overall EMHD Checks - In addition to the quantitative tests described previously, the EMHD was subjected to an overall dynamic and visual checks following assembly. No interferences, binding, or other deleterious features were identified. All spring motions, rollers, tracks, bearings, bushings, and electrical contacts performed as desired.

f. Target Spin Drive - Requirements number i and ii - The composite tests were performed with a Westamp A575 SCR amplifier (400 cps) driving the Diehl FD84 motor through an RC buffer network. The system was operated in the rate control mode. Voltage and current measurements were made with Simpson 260 multimeters. The circuit is shown in Figure 46. The AC tach had an output of ±21.5 rpm (at load). The DC tach had an output of +37.0 and -37.3 volts for ±21.5 rpm. The load was 15 ft. lbs. applied on a 6 inch diameter pulley. Test results are given in Table V.

Following these tests, a load of 15 ft. lbs. was applied and pulley was rotated at 40 rpm for a period of 6 minutes. No excessive motor heating was observed. An opinion was formed that the motor could maintain this power output for at least 20 minutes without exceeding rated temperature limits. (Diehl rates the motor at 0.2 hp for 35 minutes without damage).

These tests proved the capability to rotate the Target in excess of 36 rpm (requirement i) and to supply fifteen foot-pounds of torque throughout this range (requirement ii).

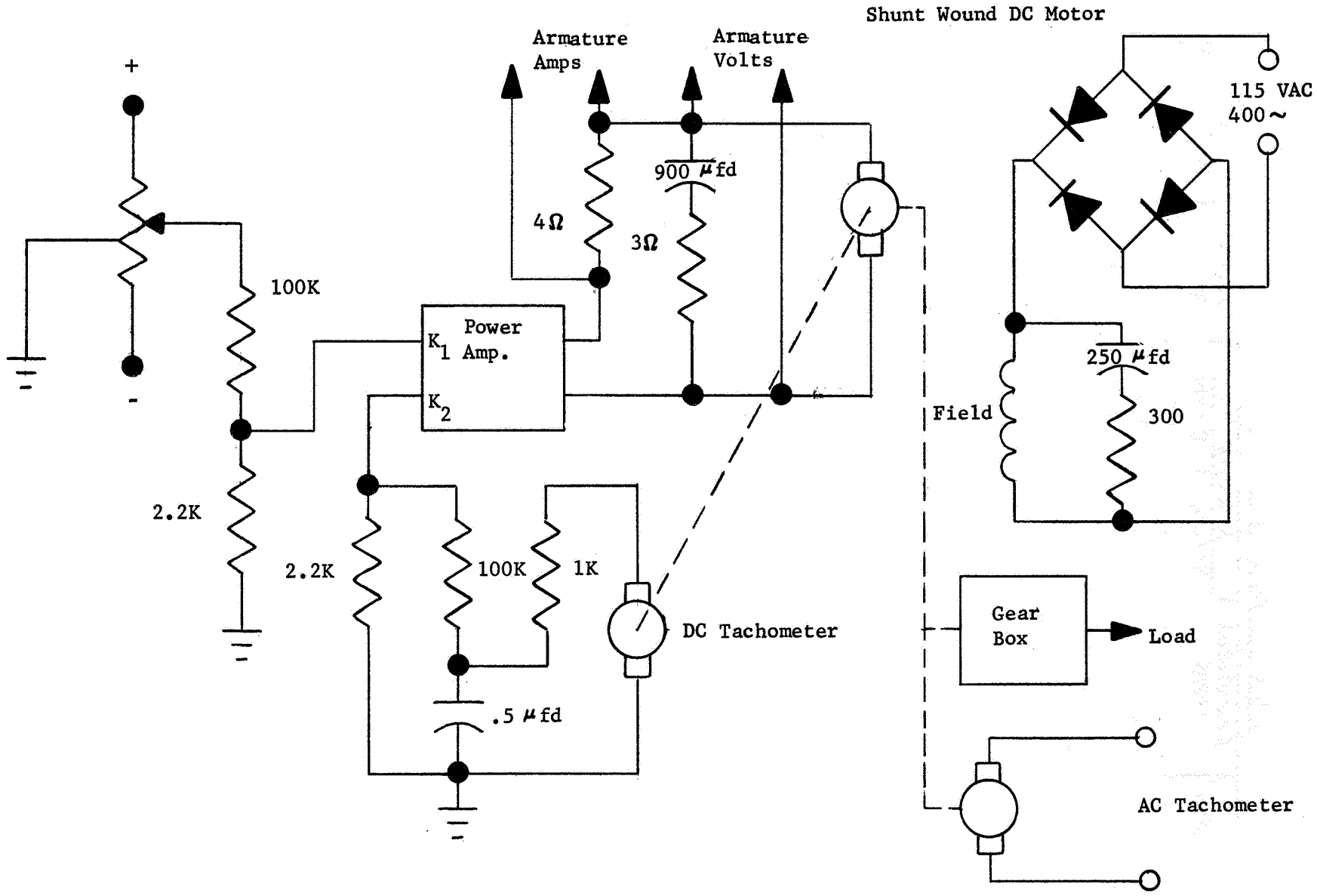

Figure 46 Target Drive Circuit

Table V Target Drive Proof Test

AC Tach Volts	Calculated RPM*	Armature		Load Torque	RPM (full load)
		Voltage	Current (amps)		
+12	10.7	20.5	0.49	No Load	
+24	21.5	37	0.68		
+36	32.2	50	0.80		
+48	43.0	63	0.85		
-12	10.7	20.5	0.48		
-24	21.5	37	0.55		
-36	32.2	53	0.68		
-48	43.0	68	0.75		
+12	10.7	34	2.2	Full Load 15 ft. lbs.	0.9
+24	21.5	50	2.2		0.7
+36	32.2	65	2.3		1.1
+48	43.0	80	2.4		1.1
-12	10.7	34.5	2.2		0.9
-24	21.5	50	2.2		0.7
-36	32.2	68	2.2		0.9
-48	43.0	83	2.2		1.1

*Three minutes at each level

SECTION V

EXPERIMENT DESIGN FOR EMHD EVALUATION

1. Simulation Philosophy and Ground Rules

It was not felt necessary to incorporate total CSM/EMHD/Target system dynamics into the simulation to determine EMHD operational characteristics that would enable development of an Advanced Material Handling Device (AMHD). The complexity of a total dynamic representation led to the decision not to simulate, for example, cross-coupling in the CSM dynamics, fuel slosh disturbances, and the eight (8) degree thrust misalignment about the CSM pitch (θ) and yaw (ψ) axes. The vehicle simulated, therefore, is of the CSM class rather than the CSM explicitly.

The simulation features felt necessary to insure a realistic evaluation of the EMHD were: 1) required CSM/EMHD/Target dynamic representation, 2) Correct Pilot and EMHD Operator position in the CSM mockup relative to the docking windows and the resulting field of view, 3) minimum non-realistic visual cues and 4) proper target lighting.

Two ground rules were applicable to the CSM Pilot and EMHD Operator. They were: 1) subjects could use whichever CSM attitude control mode they preferred and 2) any unintentional bumping of the target constituted a collision and an unsuccessful attempt at target attachment.

2. Simulation Hardware

A flow diagram showing the simulation logic process is illustrated in Figure 47. The chart also implies the supplementary hardware necessary to enable EMHD evaluation. For the purposes of this report this hardware can be grouped and discussed in the following order: a) CSM Mockup, b) Load Cell Array, c) SOS six-degree-of-freedom simulator, d) Analog computer and data systems and e) Simulation lighting.

a. CSM Mockup - The CSM mockup was built to full scale dimensions. The left hand couch was occupied by the CSM Pilot and the right hand couch by the EMHD Operator. The couch position and orientation corresponded to that in the actual CSM with couches in the docking position. The docking windows were built to duplicate the required field of view shown in Figure 33 by placing a grid at the correct distance forward of the Pilot and EMHD Operator eye positions and sizing the windows as required. Shoulder harnesses were used in conjunction with the couches to ensure that the Pilot and EMHD Operators' eyes remained in the correct position. Figures 48, 49 and 50 illustrate the CSM Pilot and EMHD Operator fields of view.

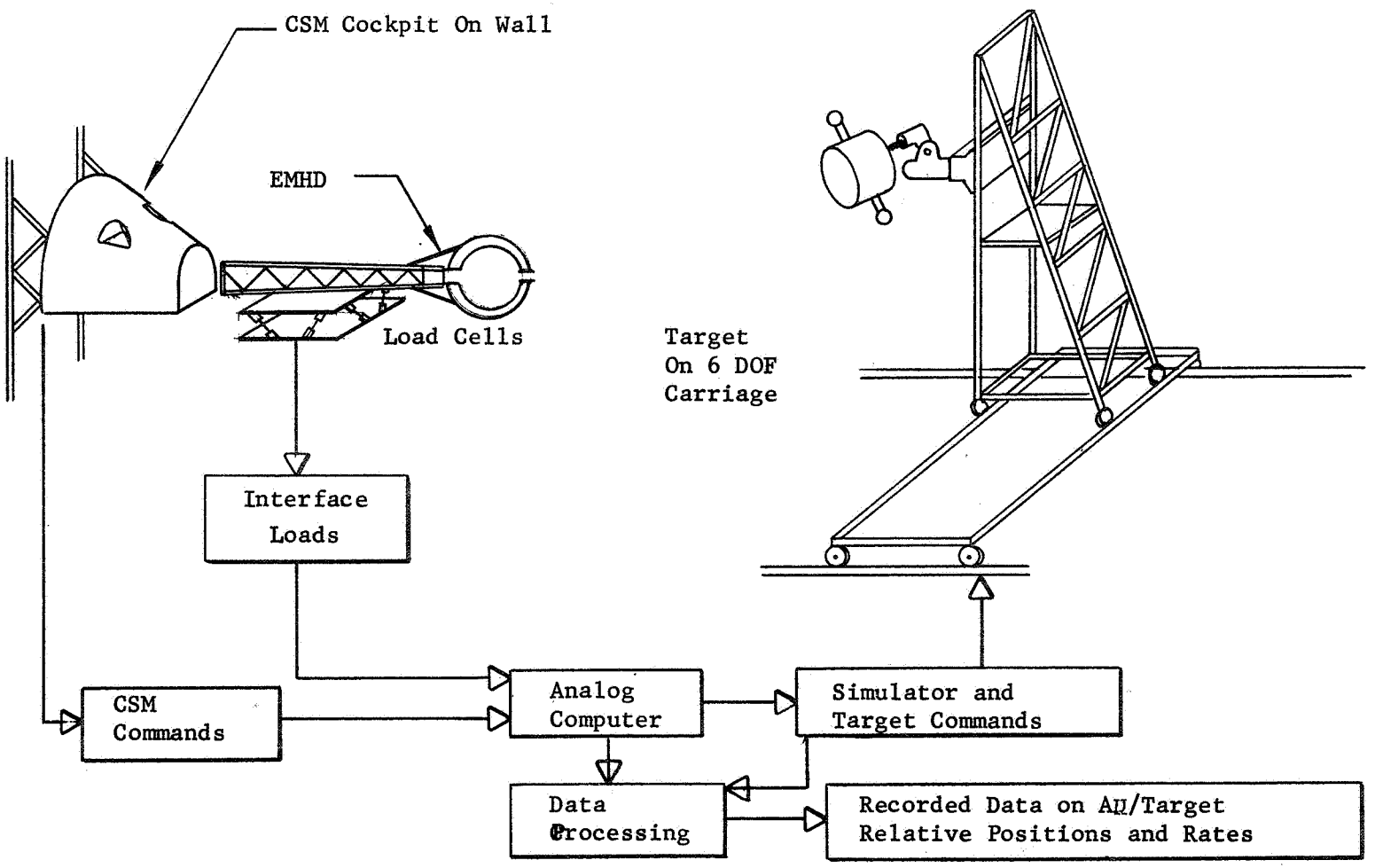

Figure 47 Simulation Flow Chart

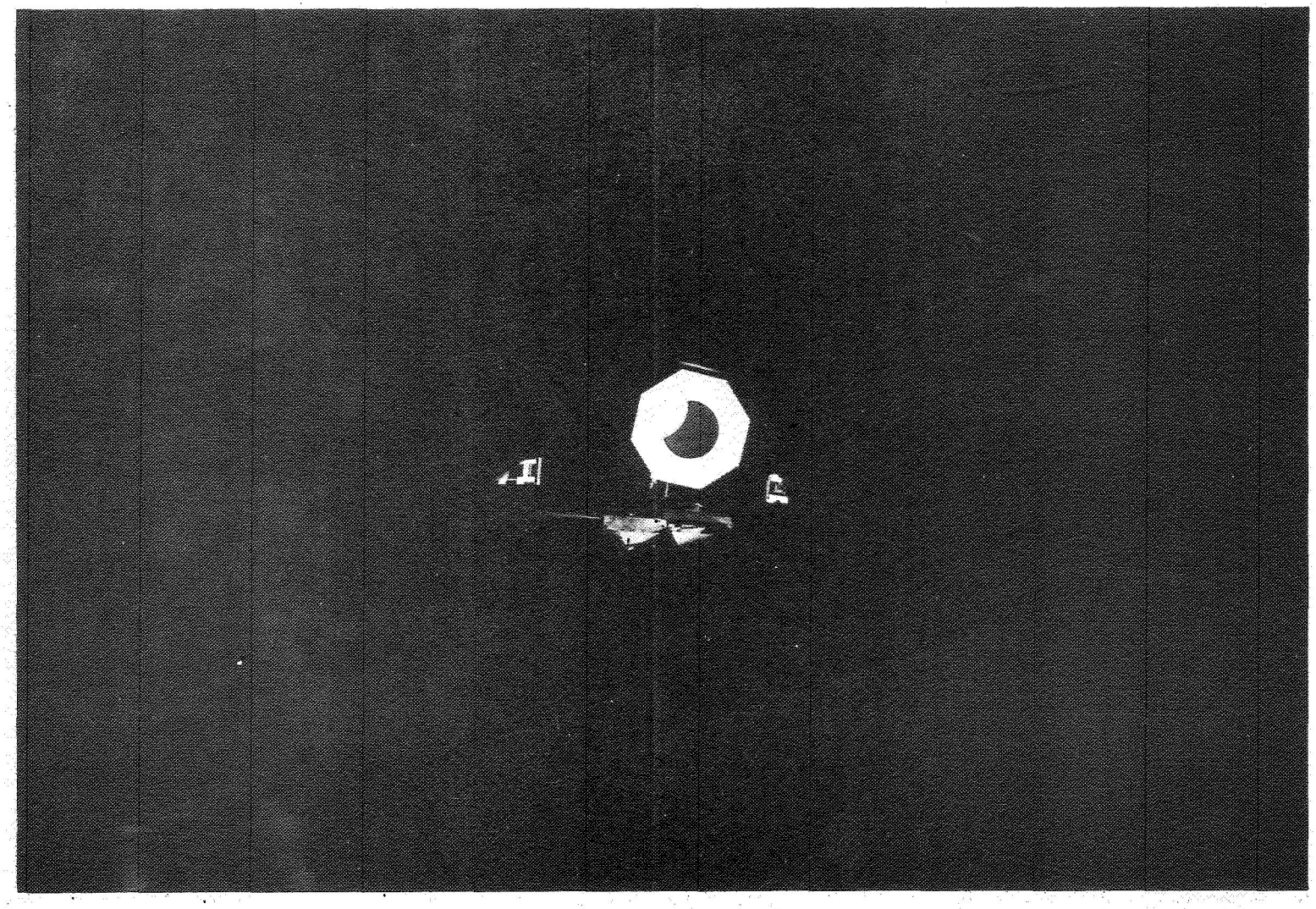

Figure 48 CSM Pilot Field of View with EMHD Configured As a Mechanical Grappler

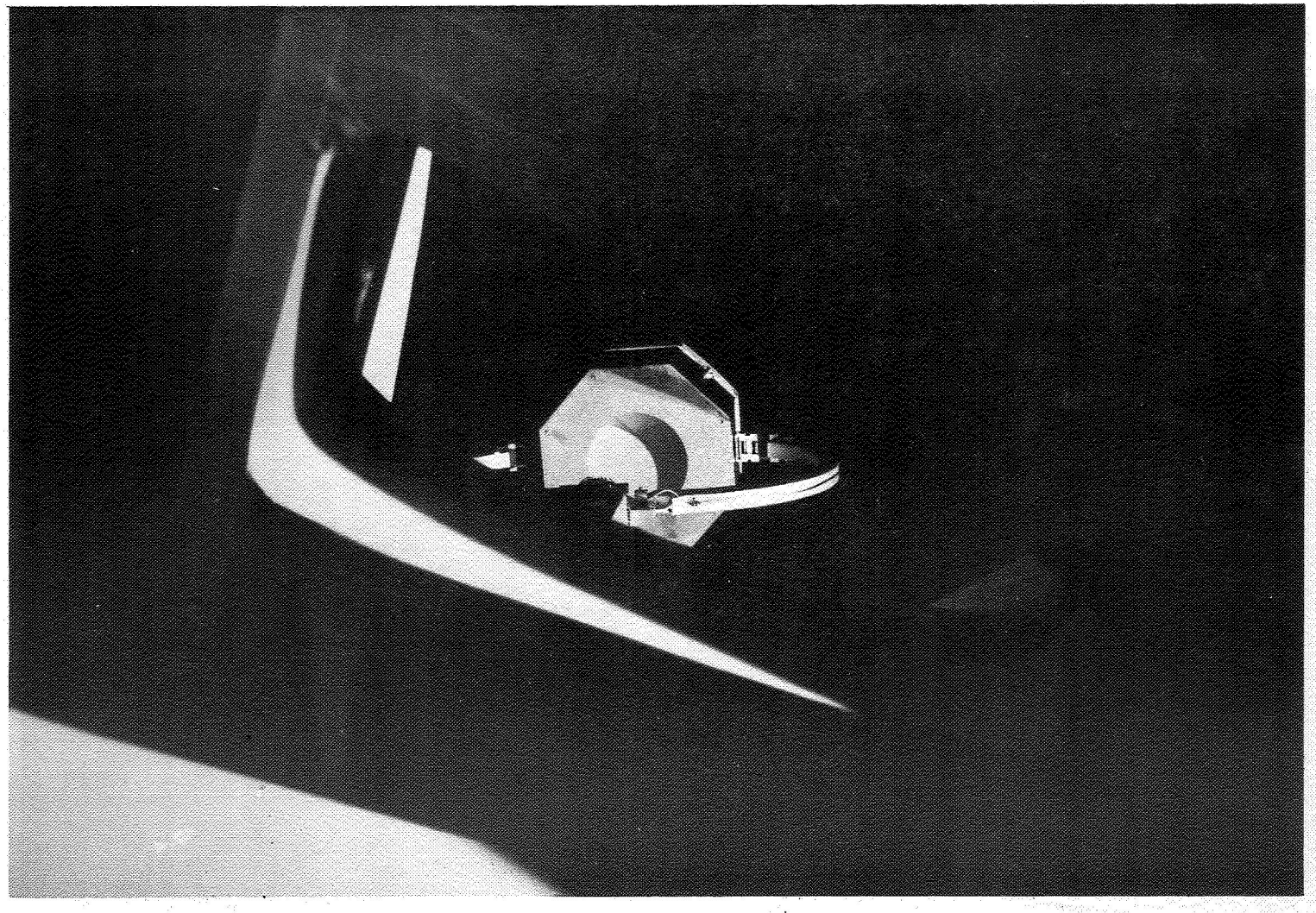

Figure 49 EMHD Operator Field of View with EMHD Configured as a Mechanical Grappler

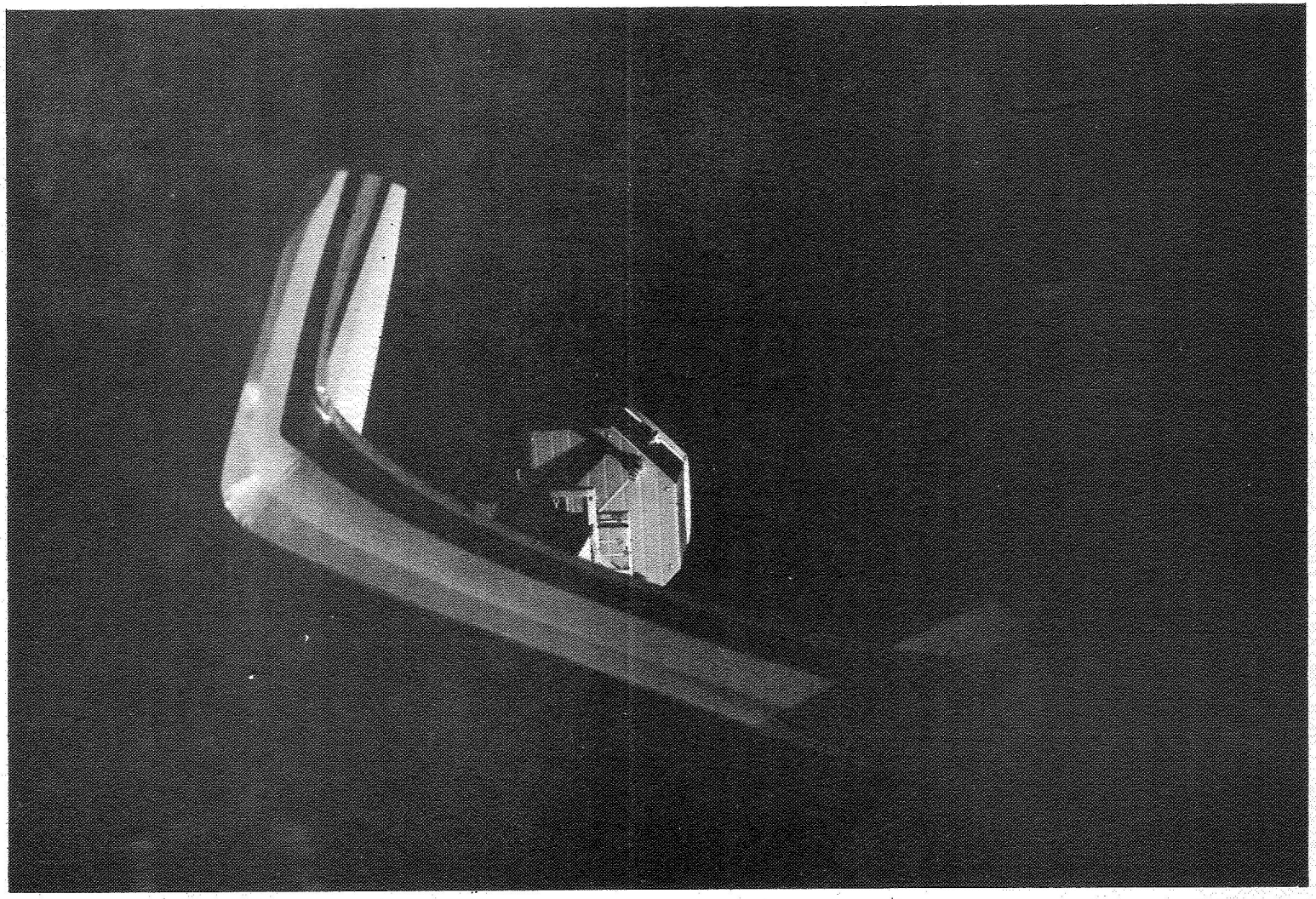

Figure 50 EMHD Operator Field of View with EMHD Configured as a Simulated-Adhesive Grappler

The CSM Pilot's control functions consist of manipulating two control sticks. The Pilot's left hand operates the translation control which functions in the direct (acceleration) mode only. His right hand operates the CSM Attitude Control System (ACS) which can function in three modes. These modes are designated as pulse, rate or direct. The CSM Rate Control System (RCS) thrusters were the only thrusters used in the simulation, i.e., the CSM main engine was not used. Section V.3 contains a detailed discussion of the available CSM control functions. Figure 51 shows the CSM Pilot and EMHD Operator cockpit stations and control hardware.

b. Load Cell Array - The EMHD was installed on a load cell array to obtain forces and moments generated due to EMHD/Target contact.

The array is composed of six load cells, each of which is designated as a type USG1 made by BLH Electronics, a division of Baldwin-Lima-Hamilton Corporation of Waltham, Mass. The array geometry is shown in Figure 52. Force and moment resolution equations are:

$$F_{XL} = \sin45^{\circ}(\sin60^{\circ})(F_3 - F_4 - F_5 + F_6)$$

$$F_{YL} = \sin45^{\circ}\left[F_1 - F_2 + \sin30^{\circ}(-F_3 + F_4 - F_5 + F_6)\right]$$

$$F_{ZL} = \sin45^{\circ}\,(F_1 + F_2 + F_3 + F_4 + F_5 + F_6)$$

$$M_{XL} = \sin45^{\circ}(K_3)(K_3 + F_5 - F_5 - F_6)$$

$$M_{YL} = \sin45^{\circ}(K_1)\left[F_1 + F_2 - \sin30^{\circ}(F_3 + F_4 + F_5 + F_6)\right]$$

$$M_{ZL} = \sin45^{\circ}(K_1)(-F_1 + F_2 - F_3 + F_4 - F_5 + F_6)$$

These equations are used to generate the target and CSM interaction forces and moments as presented in Section V.3 and the resultant dynamics are incorporated into the target motion. Load cell force and moment output was calibrated in both directions for all axes. It was found that the array would resolve each calibration force to: within two (2) degrees of its correct direction and within three (3) percent of its correct magnitude. Figures 53 and 54 illustrate typical data obtained while calibrating $+F_{ZL}$. The method of calibration was to load the array through its geometric center (Figure 52) in the desired direction with calibrated weights. Figure 53 shows the array indicated load as a function of the applied calibration load. Figure 54 shows the method of obtaining the mechanical interactions. Since the interactions were small, the decision was made to accept three (3) percent force and moment errors. During the simulation, three check loads were applied to the array on a daily basis in order to maintain a continual check on its calibration. Figure 55 shows the EMHD mounted on the load cell array.

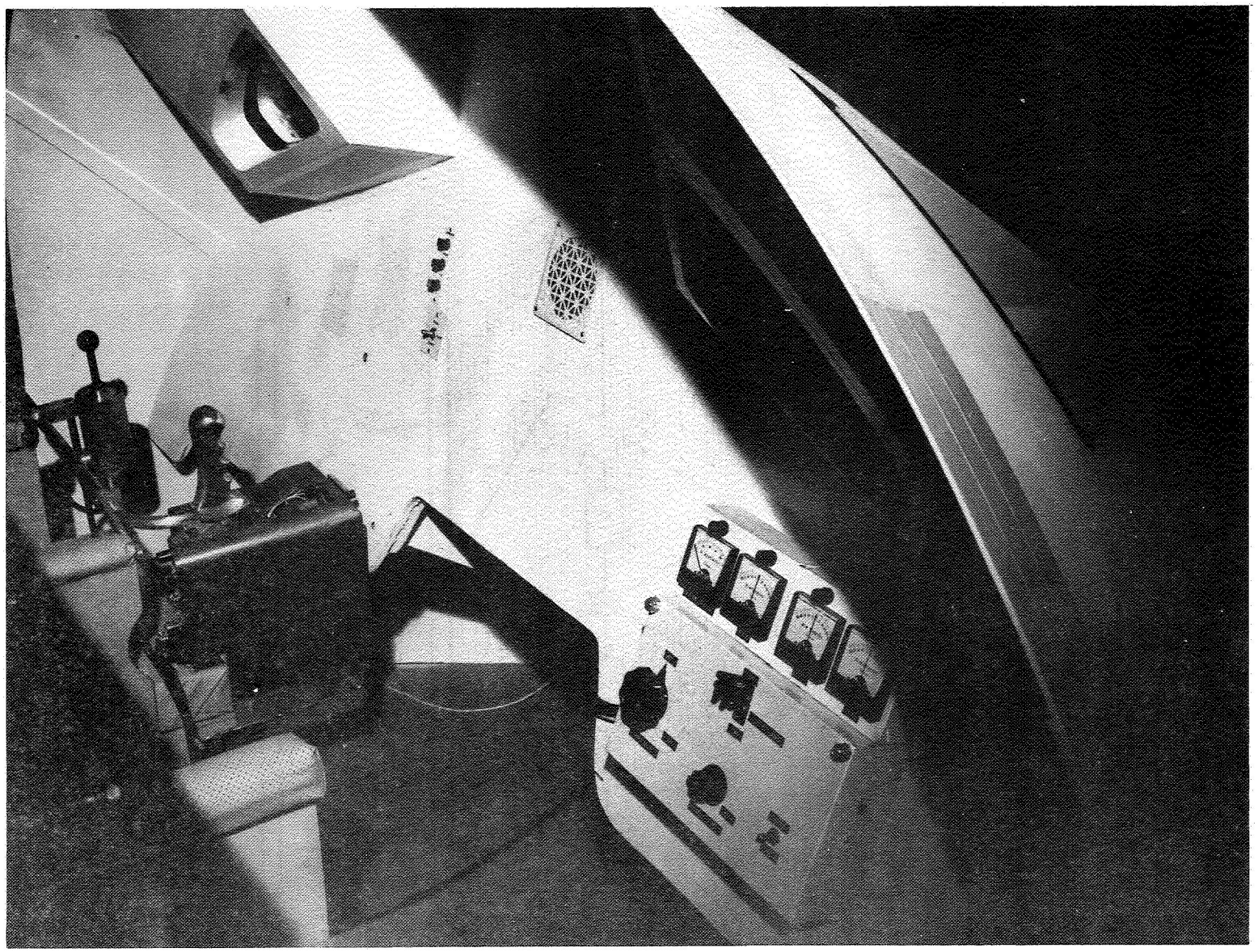

Figure 51 CSM Pilot and EMHD Operator Cockpit Stations and Control Hardware

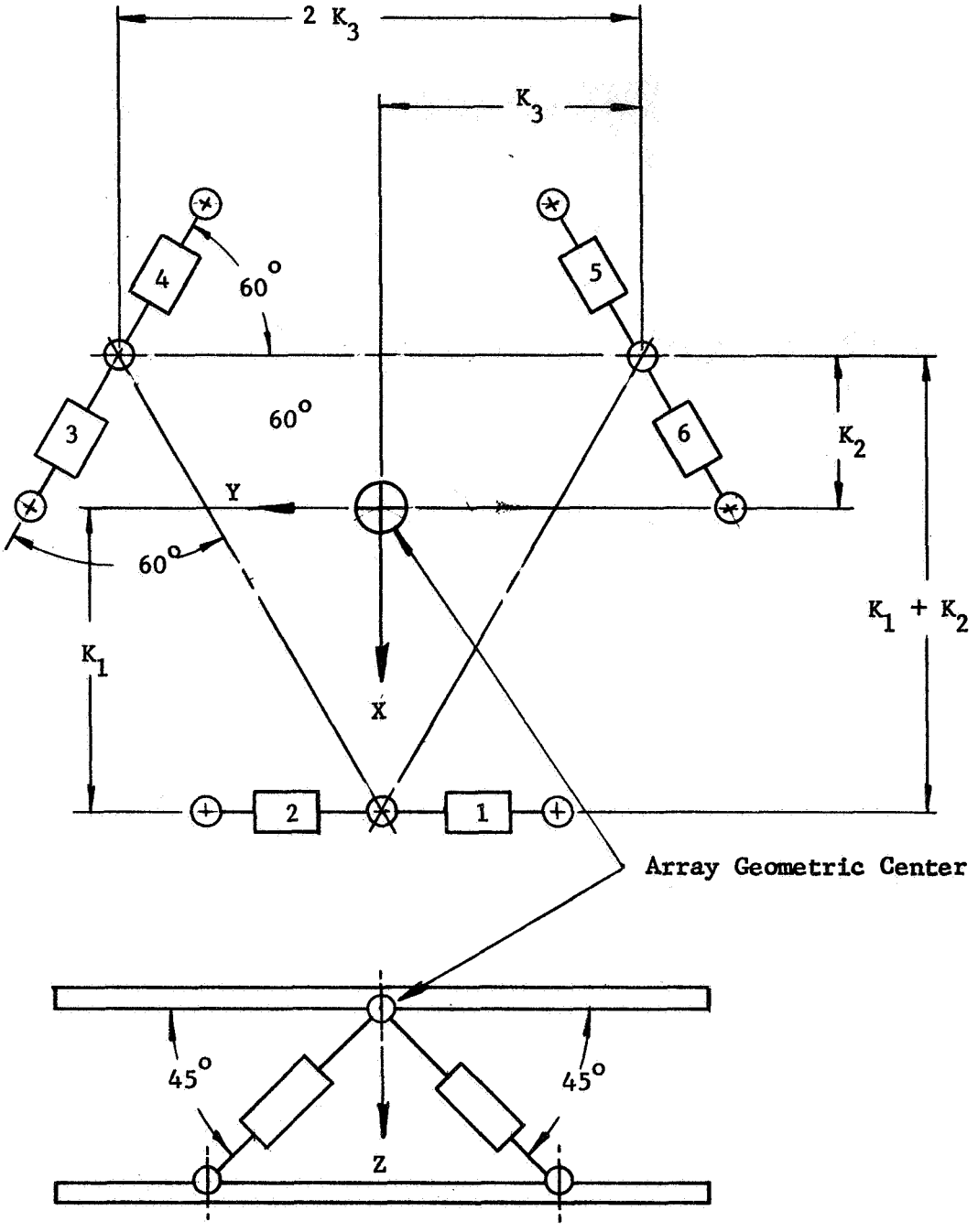

K_1 = 1.50 ft.

K_2 = .75 Ft.

K_3 = 1.30 Ft.

Figure 52 Load Cell Array Geometry

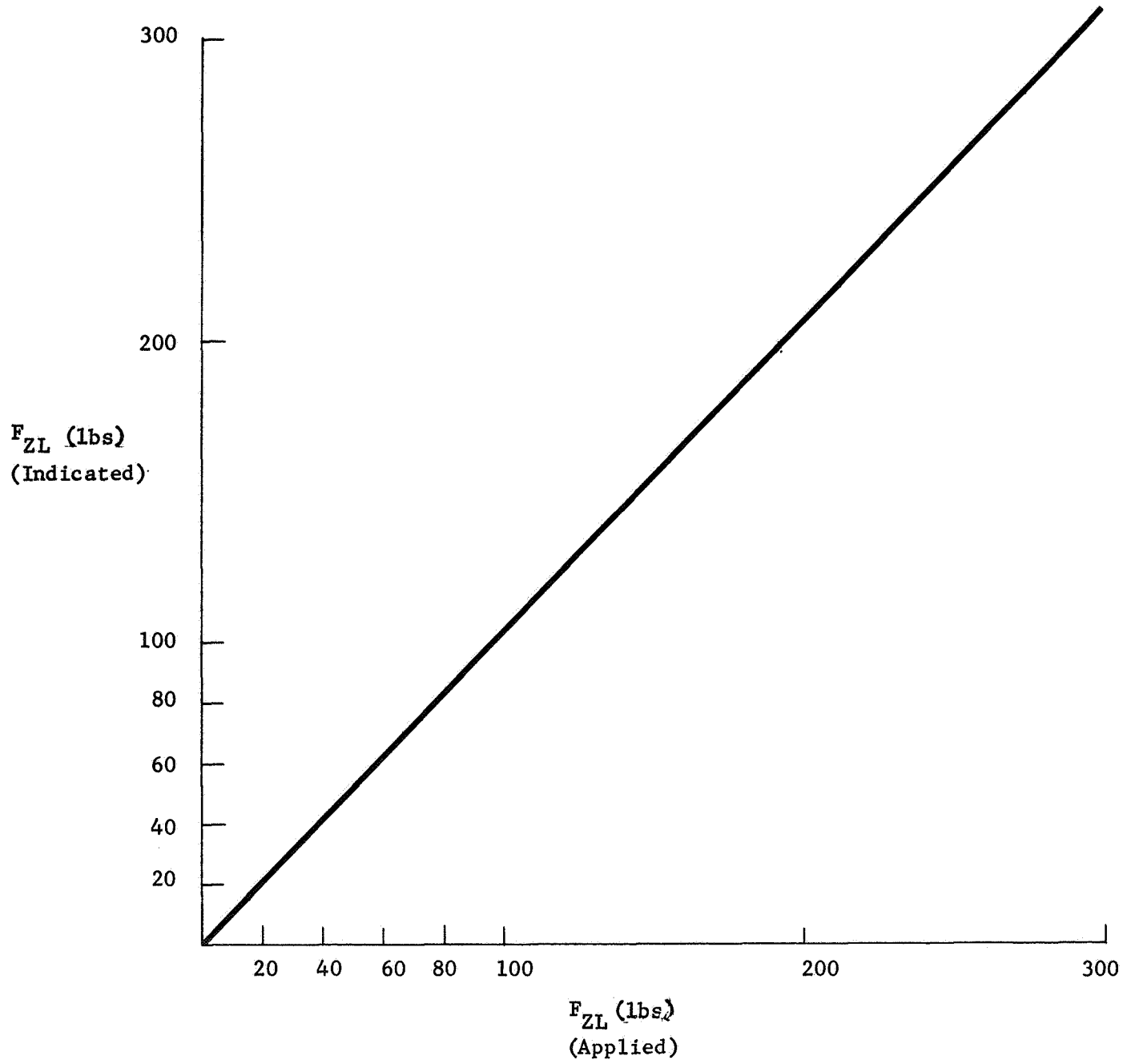

Figure 53 Calibration Load verses Load Cell Array Output

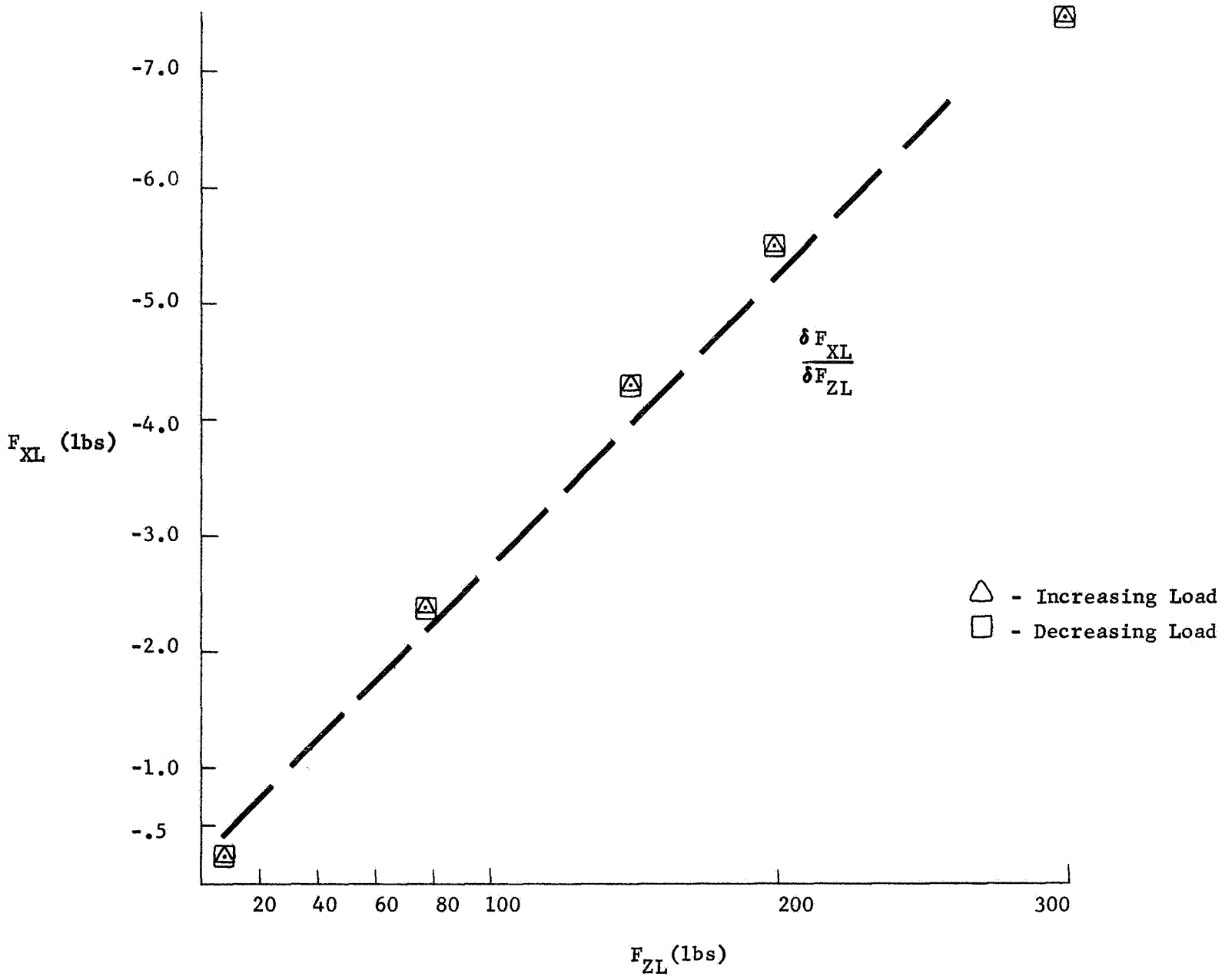

a. Interaction of F_{XL} with a Pure F_{ZL}

Figure 54 Typical Load Cell Array Mechanical Interactions

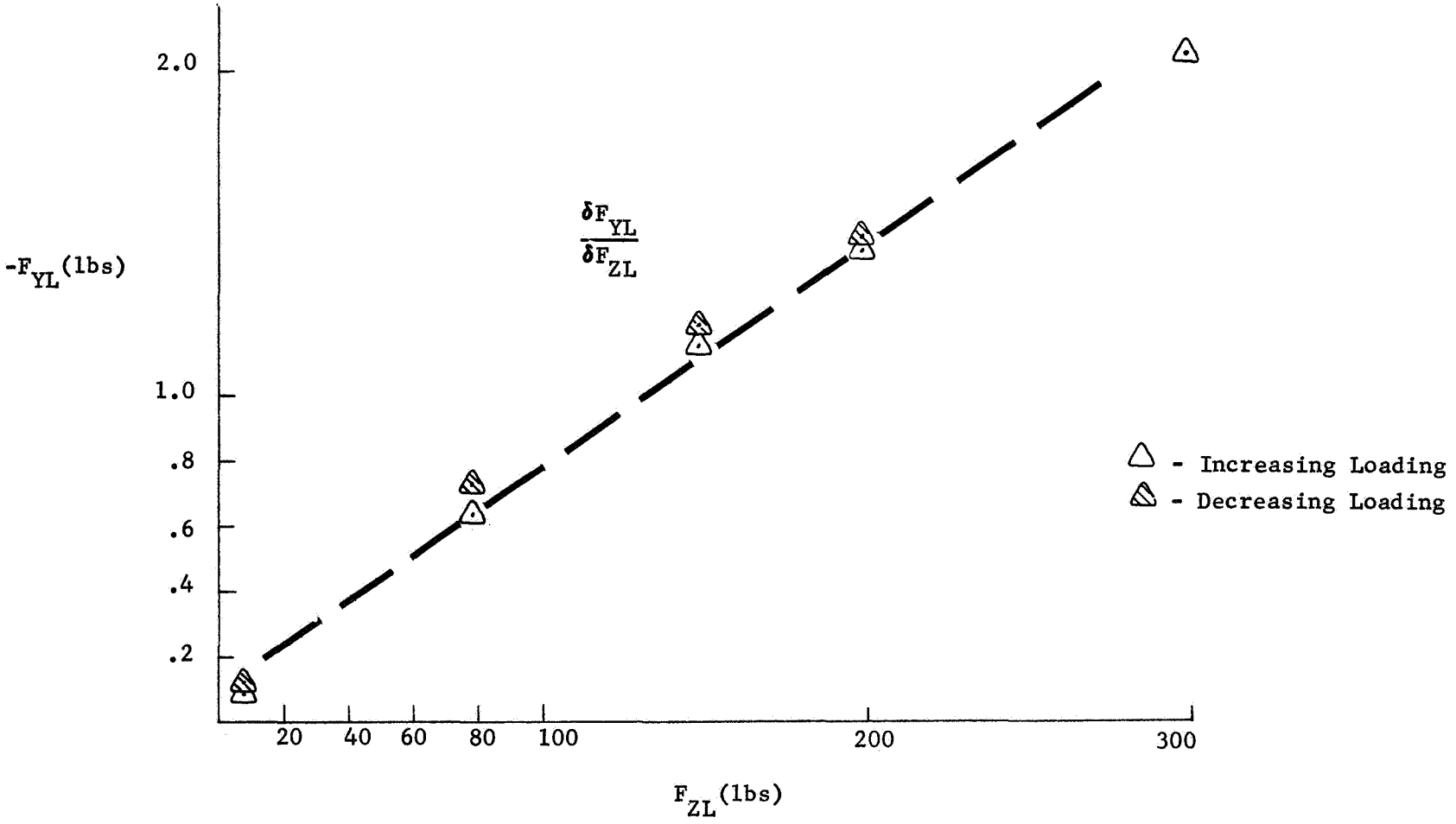

b. Interaction of F_{YL} with a Pure F_{ZL}

Figure 54 Typical Load Cell Array Mechanical Interactions

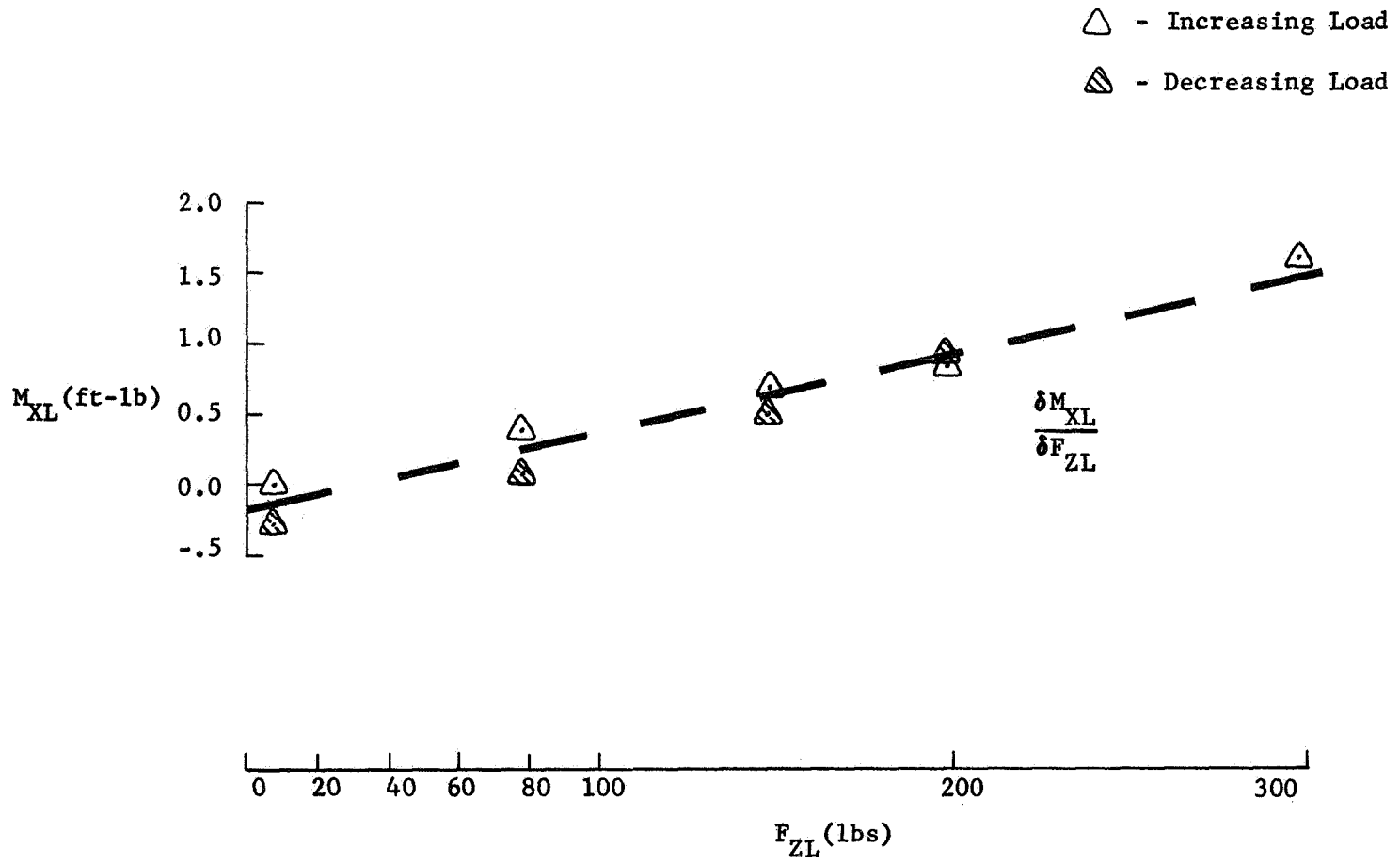

c. Interaction of M_{XL} with a Pure F_{ZL}

Figure 54 Typical Load Cell Array Mechanical Interactions

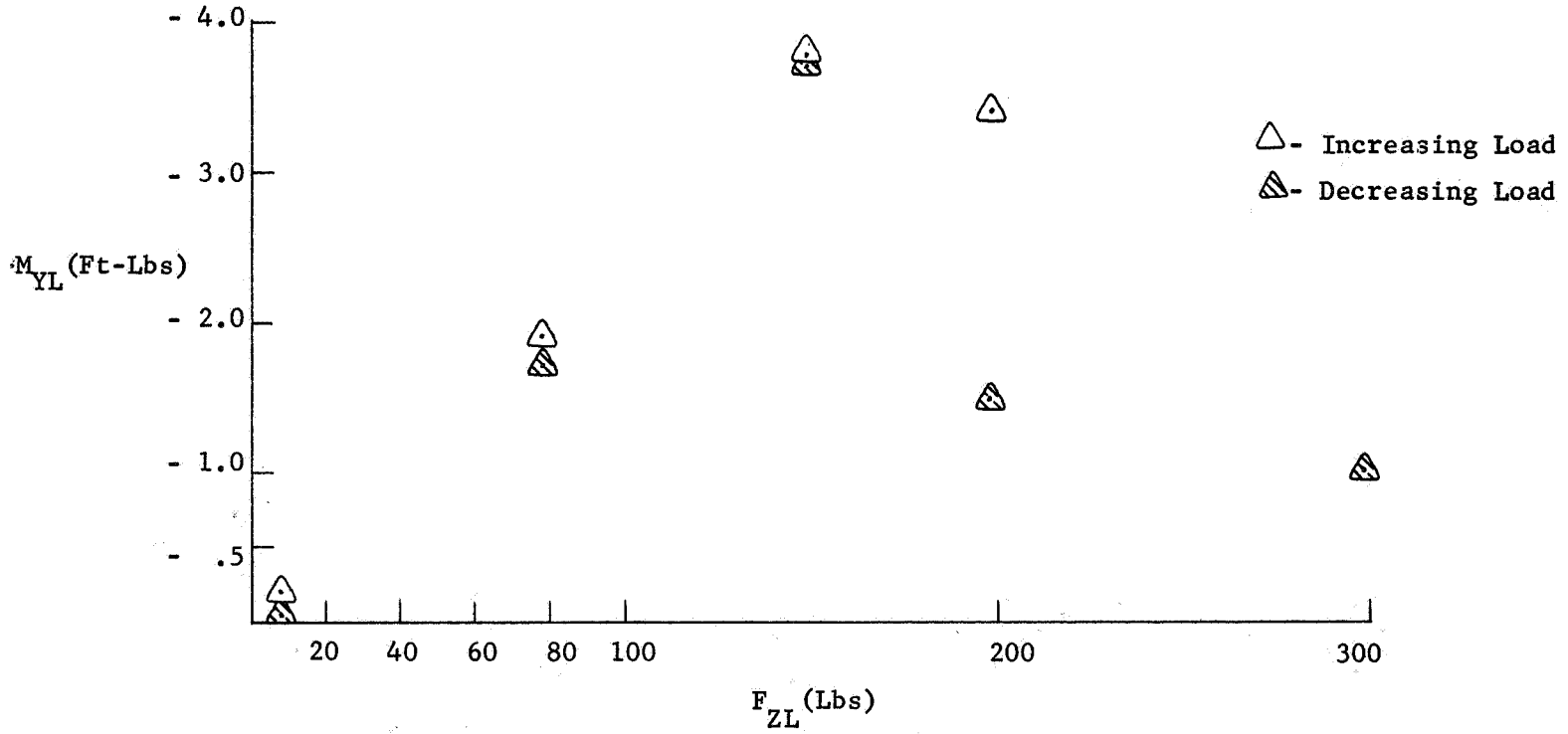

d. Interaction of M_{YL} with Pure F_{ZL}

Figure 54 Typical Load Cell Array Mechanical Interactions

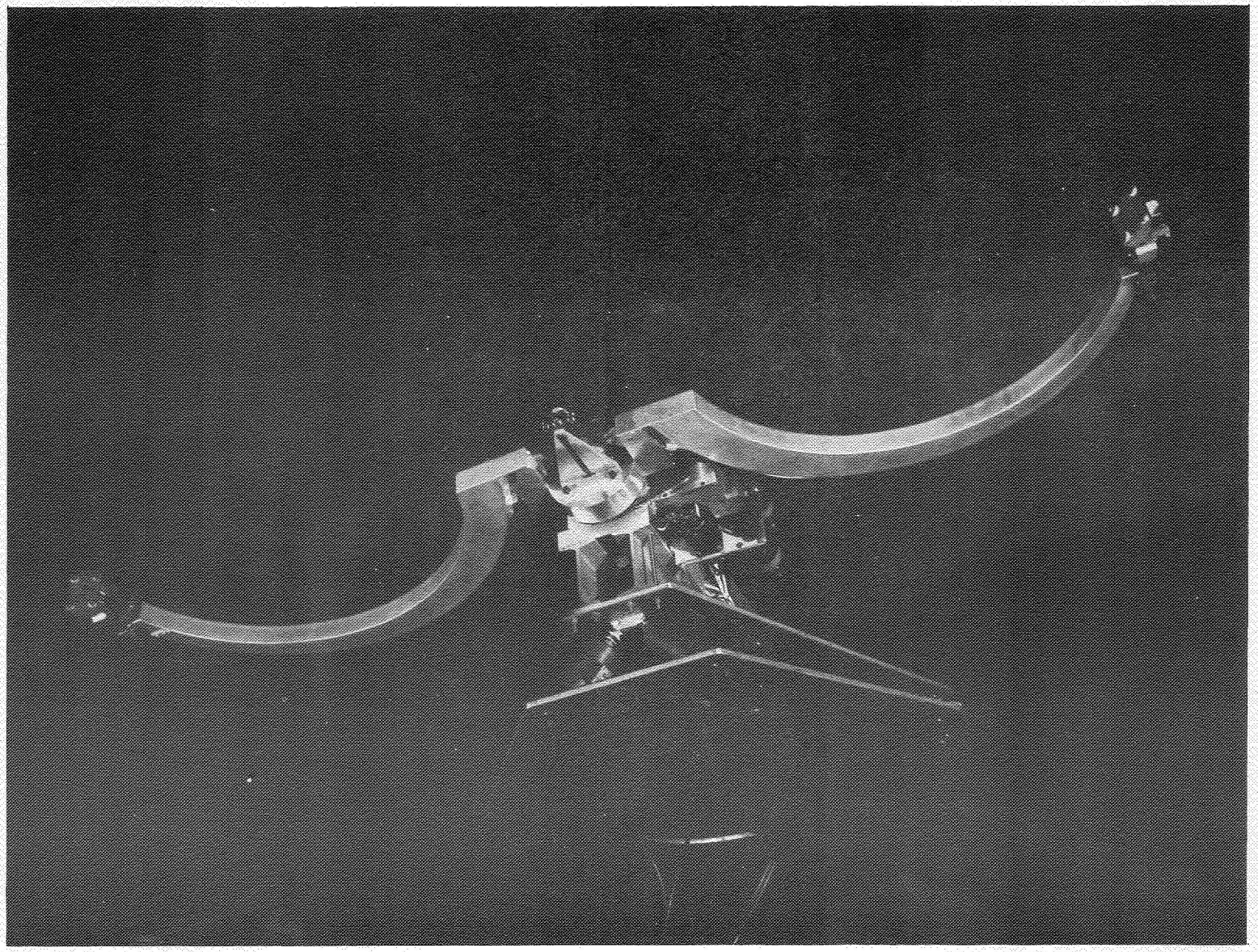

Figure 55 EMHD Mounted on Load Cell Array

c. SOS Six-degree-of-freedom simulator - The Martin Marietta Space Operations Simulator utilizes the "powered" simulation approach rather than the "free-motion" approach. A 90 by 32 by 24 foot room, providing an 8640 cubic foot maneuvering volume, houses the SOS which is servo-driven in three translational and three rotational axes. The base of the carriage translates the length of the room on three rails, as shown in Figure 47, and is driven by four, one horsepower AC motors which engage two gear tracks mounted on the floor. The vertical pedestal translates on rollers and rails laterally on the base structure and is driven by two, one horsepower AC servo-motors. For the EMHD simulation, the target was mounted in the gimbaled head which is located on the front of the pedestal and is supported by a set of negator springs. This system effectively counterbalances the combined weight of the gimbaled head and the target. Two, one-quarter horsepower DC motors, which engage two vertical gear tracks on the front of the pedestal, provide servo-power for vertical translation. The gimbaled head was designed to provide maximum target freedom of motion and enable the target to be commanded in roll rate ($\dot{\phi}$) rather than roll position (ϕ). Motors and gear drives are enclosed in the gimbal structure. Each gimble is driven by a one-quarter horsepower DC motor. Simulator performance is shown in Table VI.

TABLE VI SOS PERFORMANCE CHARACTERISTICS

	Longitudinal	Lateral	Vertical
Travel (ft)	±30	±6	±6
Velocity (fps)	±3.0	±3.0	±3.0
Acceleration (fps)	±6.0	±6.0	±3.0
	Roll	Pitch	Yaw
Travel (rad)	∞	±.8	±.8
Velocity (rad/sec)	±6.0	±2.0	±2.0
Acceleration (rad/sec^2)	±8.0	±8.0	±8.0

The SOS responds to position, rate and acceleration commands with, approximately, 95% accuracy on or about all axes.below the limits specified in Table VI. The longitudinal position command (X_c) was scaled to 3V/ft with the lateral and vertical position commands (Y_c and Z_c, respectively) scaled to 10V/ft. Gimbal pitch and yaw commands (θ_c and ψ_c, respectively) were scaled to 1V/deg and the gimbal roll rate command (Φ) scaled to 1V/3^o per sec.

During the pre-simulation checkout, the stability of the closed-loop simulation was investigated and appropriate compensation networks were added to handle the dynamic ranges expected during the EMHD tests. The problem was approached as described in the following material.

Given a dynamic situation in space where two passive bodies are coupled together and an initial disturbance is generated within the system, a transient condition of damped oscillatory motion will occur for each of the bodies. The behavior of this system is analogous to the closed loop response of a simple servo system where stability is always achieved because the gain of any loop is unity or less at the critical frequencies. In a simulation involving the simulator and two passively interacting bodies, system stability is no longer promised. An additional series of elements (load cells, computational facilities, power servos, etc.) are incorporated into the system and a relatively complicated multi-loop configuration is obtained. This resultant system has numerous non-linearities, cross coupling effects, response time lags, etc., which degrade ideal performance and generate loop instabilities that are difficult to correct.

A complete description of the simulator system maneuvering a target vehicle and making physical contact with an approach vehicle through a grappling device would show target inertia, target moment of inertia diadic, forces and moments in six axes, and a six by six coupling matrix for the six degree-of-freedom displacements. To promote simplicity we will limit our discussion to translation on one axis only; but we will remember that in reality the system must be expanded to include six-degrees-of-motional-freedom and the moment of inertia diadic. The simplified block diagram is shown below in Figure 56.

F_{IN} represents that force due to initial conditions, or vehicle excitation, applied to the load cells and target vehicle through the grappling device which acts as a mutual coupling element. The +F and -F indicate that forces on the load cells and target vehicle are equal and opposite. The SOS is basically a critically damped second order lag, but it also contains significant higher order lags, mechanical resonances, and numerous non-linearities. The SOS frequency response is approximately 1.0 to 4.0 cps, depending upon the axis being considered. X_1 is the displacement of the target vehicle due to the summation of forces (F_T) acting on it. X_2 is the displacement of the SOS due to forces acting on the load cell array. X_3 is the difference between X_1 and X_2. It represents a deviation from ideal which must be minimized for increased realism.

It is apparent from the diagram that the $F_{IN} \rightarrow +F \rightarrow F_T \rightarrow X_1 \rightarrow F_R$ loop represents a passive body and is the natural response of the target vehicle which the SOS attempts to simulate. This means F_S and X_3 must be minimized and X_2 must approach X_1. Failing this, it becomes necessary to modify the $-F \rightarrow X_2 \rightarrow X_3 \rightarrow F_S \rightarrow F_T \rightarrow X_1 \rightarrow F_R$ loop to achieve stability with a minimum degradation of the SOS response. Our approach to stability was two-fold: (1) we added a series second order lead-

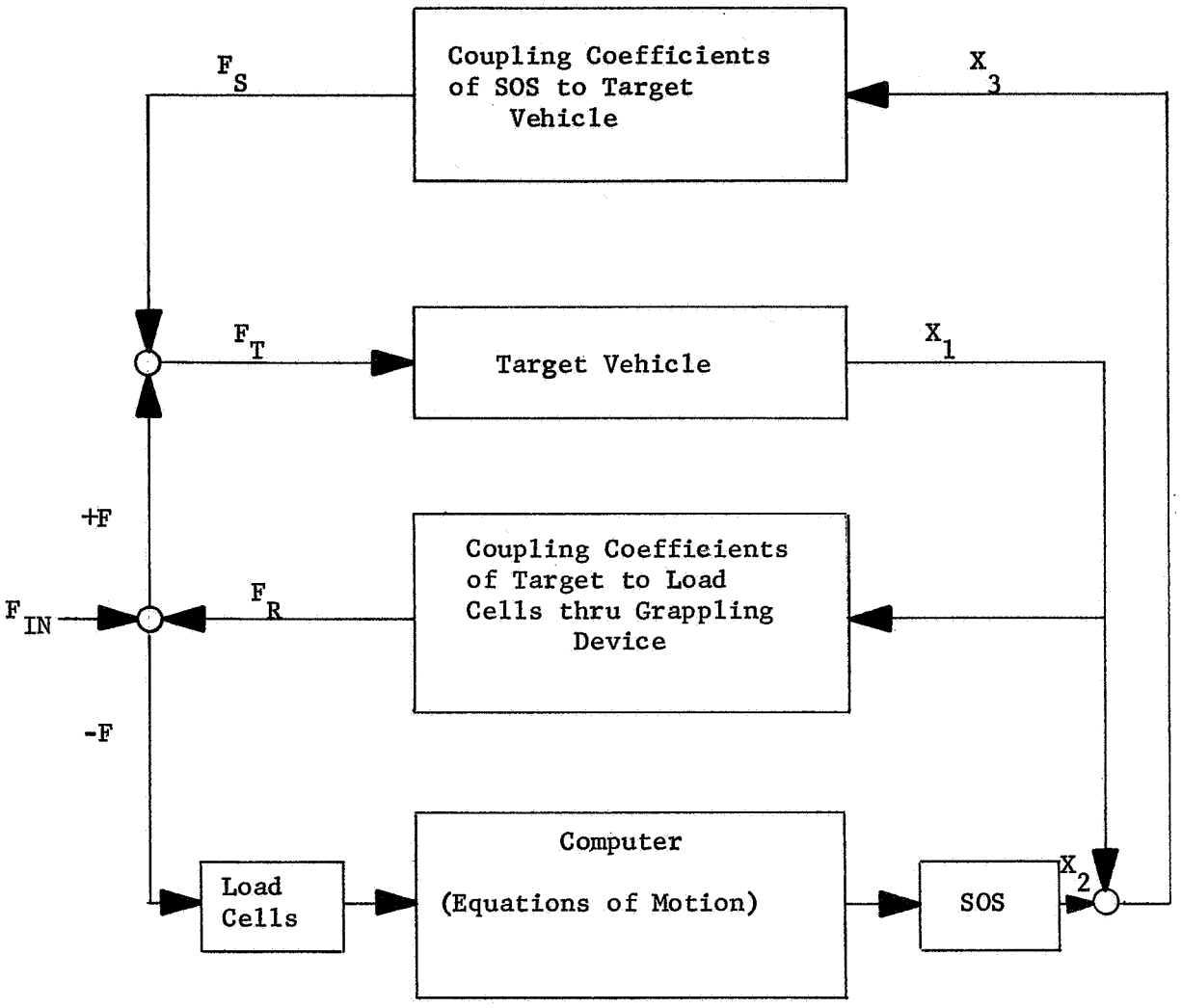

Figure 56 Simulation Stability Block Diagram

lag correction network to each SOS command as it left the computer to decrease its lag, and (2) we added an auxiliary or damping lead-lag network at the same location in the loop to achieve stabilizing phase lead at the frequency where instability occurred.

The second order lead-lag correction network has the two lead break points at the frequencies where that particular SOS axis starts its two lags. The lag points are increased in frequency by a factor of five. This amount of correction appears beneficial in every axis, but is not sufficient to correct gross instabilities that occur during grappling. The networks are tailored to each axis and are not peculiar to the exercise being performed. Additional high frequency roll-off

is used to protect the SCR power amplifiers on the SOS from stray electrical pickup and transients which are enhanced by the lead-lag networks.

The damping lead-lag network was tailored to supply phase lead to the system at the frequency where loop instability occurred during grappling. This frequency is determined by hardware characteristics and problem dynamics and tends to be indefinite. It was necessary to empirically derive both the number and location of the frequency break points that gave optimum performance. Some axes required second order lead-lag damping networks, others behaved well with single order filters.

The correction filter and the damping filter for each axis were both mechanized in the same manner. Each filter network required a single amplifier in the computer (with appropriate RC components) and the two were connected in series at the computer output. Each SOS axis did not require the same amount of correction and damping; the reason for this was not readily apparent and no investigation was performed. The fundamental circuit for either type of filter is shown in Figure 57. A chart showing frequency break points for each axis is also shown.

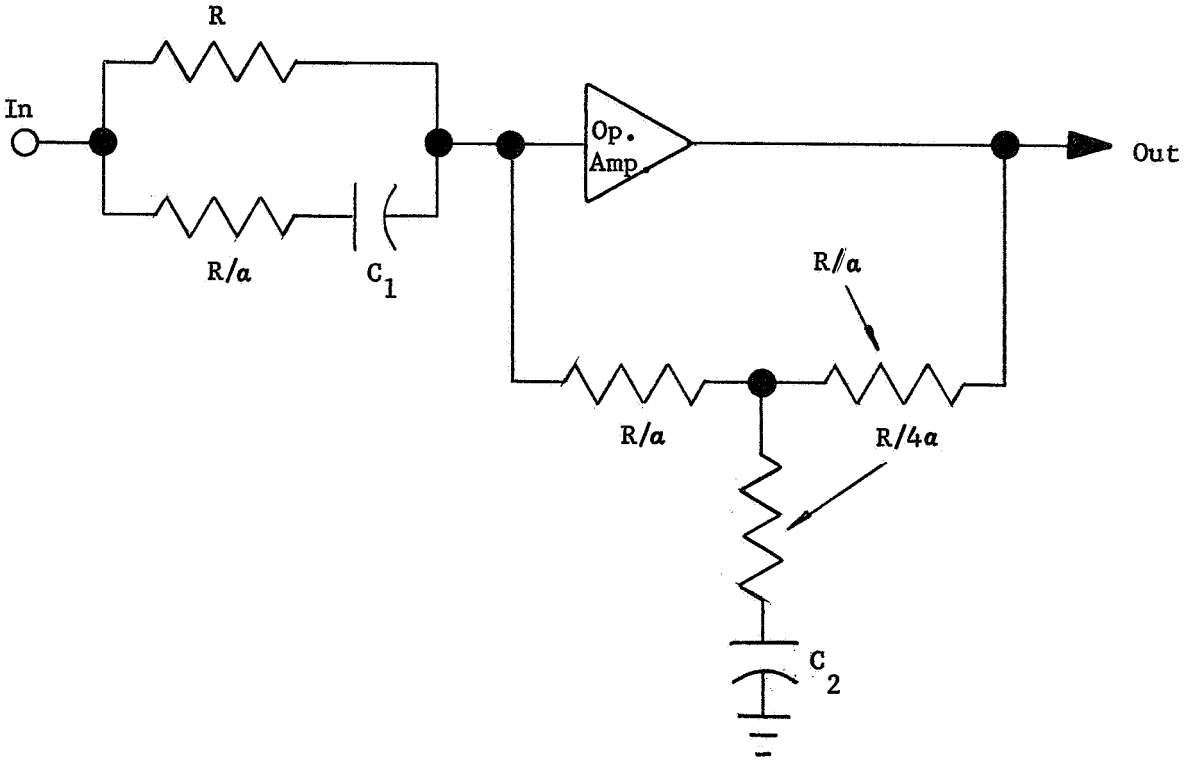

Figure 57 SOS Filter Network

Table VII Frequency Breakpoint for SOS Axes*

Axis	Filter Network			
	Correction		Damping	
	Lead	Lag	Lead	Lag
Longitudinal	1.0 cps (2)	5.0 cps (2)	1.35 cps (2)	8.0 cps (2)
Lateral	1.3 (2)	6.5 (2)	0.6 (2)	2.4 (1)
Vertical	1.3 (2)	6.5 (2)	0.6 (1)	2.4 (1)
Pitch	None	None	0.4 (1)	1.6 (1)
Yaw	None	None	0.2 (1)	0.4 (1)

*Numbers in parenthesis indicate number of break points.

R, C_1, and C_2 are selected to establish the lead breakpoint. The value of α established the lag breakpoint.

Optimum stabilization filters did not, in all cases, give acceptable performance. In most axes SOS deadbands and hysteresis gave rise to small amplitude limit cycling during grappling. This undesirable effect was amelioriated by incorporating amplitude limited rate damping into the computer for each axis needing attention. Impact damping (subtracting an increment of velocity whenever velocity reverses direction) was also tried, but it did not give acceptable results.

d. Analog Computing and Data Systems - The CSM/EMHD/Target system dynamics were programmed into two slaved EAI 231-R analog computers such that the system dynamics were represented in the target motion. The coordinate frames used in equation generation are defined in the Simulation Test Plan, Section V.3, as are the SOS command equations.

To adjust for load cell array thermal drift and resulting SOS command drift, computed forces and moments were nulled and integrators using these forces and moments in SOS command generation were grounded until just prior to an EMHD/Target attachment attempt. Figure 58 shows a typical force and moment nulling circuit. These circuits were controlled by a switch operated by the Test Conductor.

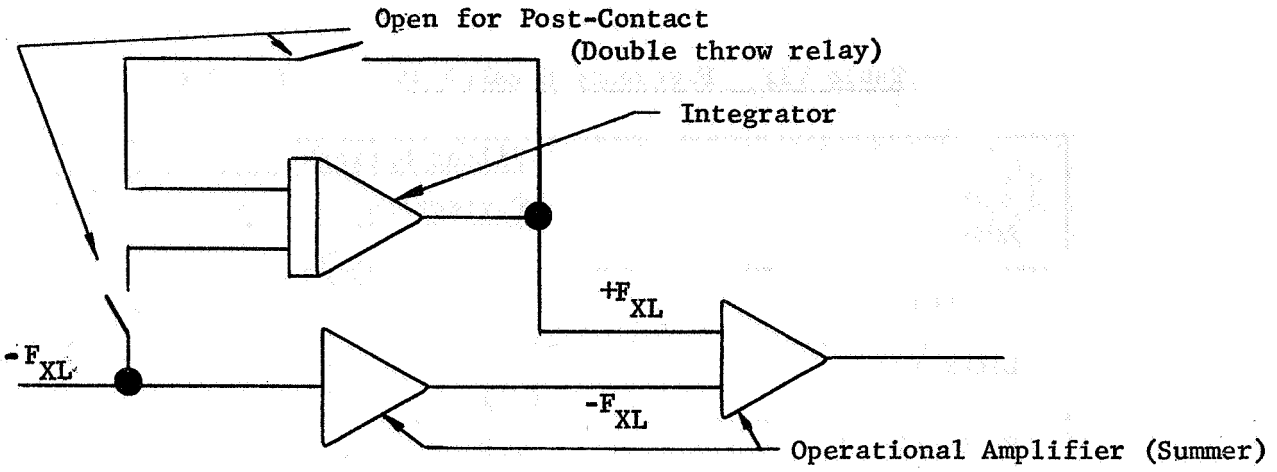

Figure 58 Force and Moment Nulling Circuit

Rate damping networks were utilized around selected load cell force integrators to enhance SOS post-contact stability. The networks contributed a maximum amount of equivalent damping (g) equal to 0.1. This value is representative of mechanical systems similar to the EMHD. Figure 59 illustrates a typical rate damping circuit.

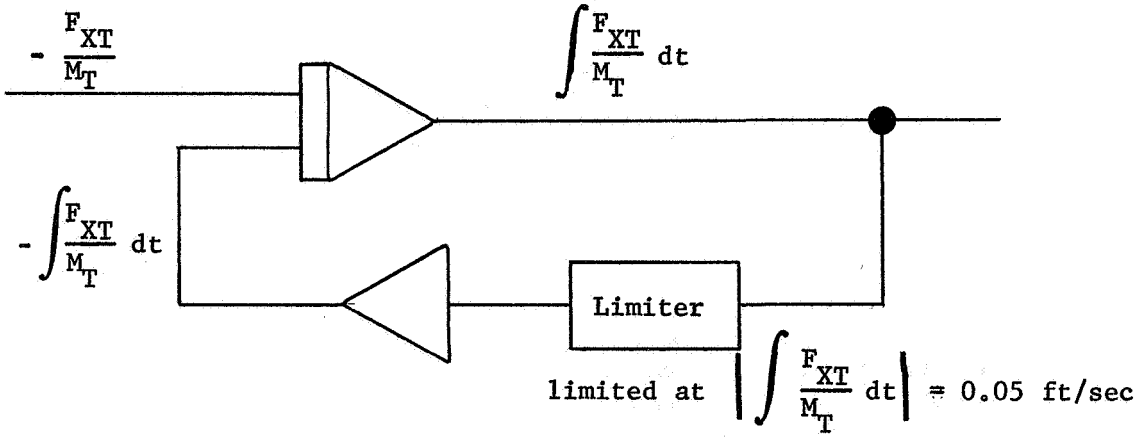

Figure 59 Typical Rate Damping Network

e. Simulation Lighting - Target illumination was obtained with a spotlight simulating a sun angle in the space environment of ten(10) degrees ofset from the subjects' line of sight. The spotlight was located to the left of the CSM mockup and this was the only lighting used in the simulation. Similar target illumination from the right side is shown in Figure 60.

Figure 60 Simulation Target Lighting

3. Simulation Test Plan - Following the completion of Task B, Martin Marietta Corporation was required to submit and obtain approval from MSFC of a Simulation Test Plan (Task C). The following is a complete version of that document in the approved form.

SIMULATION TEST PLAN

The Experimental Material Handling Device (EMHD) simulation for Contract No. NAS8-30069 will be conducted in the Martin Marietta Corporation's Space Operations Simulator (SOS). The EMHD will be mounted on load cells in front of a CSM mockup and the Target will be mounted on the SOS moving base. All relative motions, except for EMHD spin, between the CSM/EMHD and the Target will be implemented with the moving base.

The left-hand test subject will control the CSM and the right-hand subject will operate the EMHD. The test subjects will 1) close with the target starting at ranges up to approximately fifty feet with attitude misalignments up to forty-five degrees, 2) position the EMHD as close as possible to a prescribed position relative to the target, 3) match the EMHD spin rate to the Target's spin rate (if necessary), 4) attach to the Target, and 5) despin the Target (if required). The test subjects will also be required to perform these steps in reverse order.

Simulated Target masses will cover a ten-to-one range with the largest mass being 140 slugs (weight = 4480 lb). Moments of inertia will be varied over a corresponding range and Target spin rates will be varied between 0 and 36 revolutions per minute.

Three basically different attachment modes will be investigated. In the first, the EMHD operator will close the mechanical arms to grip the Target between the arm end pads. Target configurations for this task will be a twelve-inch diameter cylinder and a twenty-four inch diameter octagonal drum. For the second mode, the operator will insert the EMHD arm end hooks into a flange opening and grip the Target by spreading the hooks apart. Eight-inch and twelve-inch inside diameter flanges will be used. In the third mode, Velcro pads on the EMHD will be pressed against a flat, mating Velcro surface on the Target.

All CSM maneuvering will be carried out with simulated RCS quads. Direct quad control will be used for CSM translation and pulse, rate, and direct (acceleration) modes will be available for attitude control.

Data gathered from strip charts and digital printouts will include contact velocities, alignment errors, EMHD spin rate errors, post-contact attachment forces and torques and determination of typical RCS thruster total impulse and fuel consumption profiles.

Formal data gathering will take place during a two-week (ten working days) period. This will give approximately sixty flying hours (based on six hours of running during each of the ten days). Test subjects will be allowed to practice during this time.

The first week of data gathering will be used to explore the overall problem including closure, alignment, attachment, and despinning using the previously-mentioned Target characteristics, attachment modes, and CSM control modes. The second week will be used to examine, in detail, those tasks or portions of tasks that appear to present the most difficult EMHD-utilization problems as determined from the first week of simulation runs.

The following pages contain the information used to program the analog computer for the simulation.

a. Definition of Terms -Figure 61 illustrates the simulator configuration that will be used. The positive axes of the various coordinate systems used in the program are shown. The following is a list of the terms used in the computer program and data recording (scale factors and/or limits are given where applicable):

X_c = carriage longitudinal position command, 3V/Ft, $\pm$ 30 Ft.

Y_c = carriage lateral position command, 10V/Ft, $\pm$ 6 Ft.

Z_c = carriage vertical position command, 10V/Ft, $\pm$ 6 Ft

ψ_c = gimbal yaw position command, 1V/Deg, $\pm 45^o$

θ_c = gimbal pitch position command, 1V/Deg, $\pm 45^o$

$\dot{\phi}_c$ = gimbal roll rate command, $1V/3^o$ per sec, $\pm 240^o$/sec

X_I = carriage longitudinal position readout, 3V/Ft, $\pm$ 30 Ft

Y_I = carriage lateral position readout, 10V/Ft, $\pm$ 6 Ft

Z_I = carriage vertical position readout, 10V/Ft, $\pm$ 6 Ft

ψ_I = gimbal yaw position readout, 1V/Deg, $\pm 45^o$

θ_I = gimbal pitch position readout, 1V/Deg, $\pm 45^o$

$\dot{\phi}_I$ = gimbal roll rate readout, $1V/3^o$ per sec, $\pm 240^o$/sec

X_v = CSM c.g. longitudinal position in room (constant) (approx. - 50')

Y_v = CSM c.g. lateral position in room (constant) (approx. 0')

Z_v = CSM c.g. vertical position in room (constant) (approx. 0')

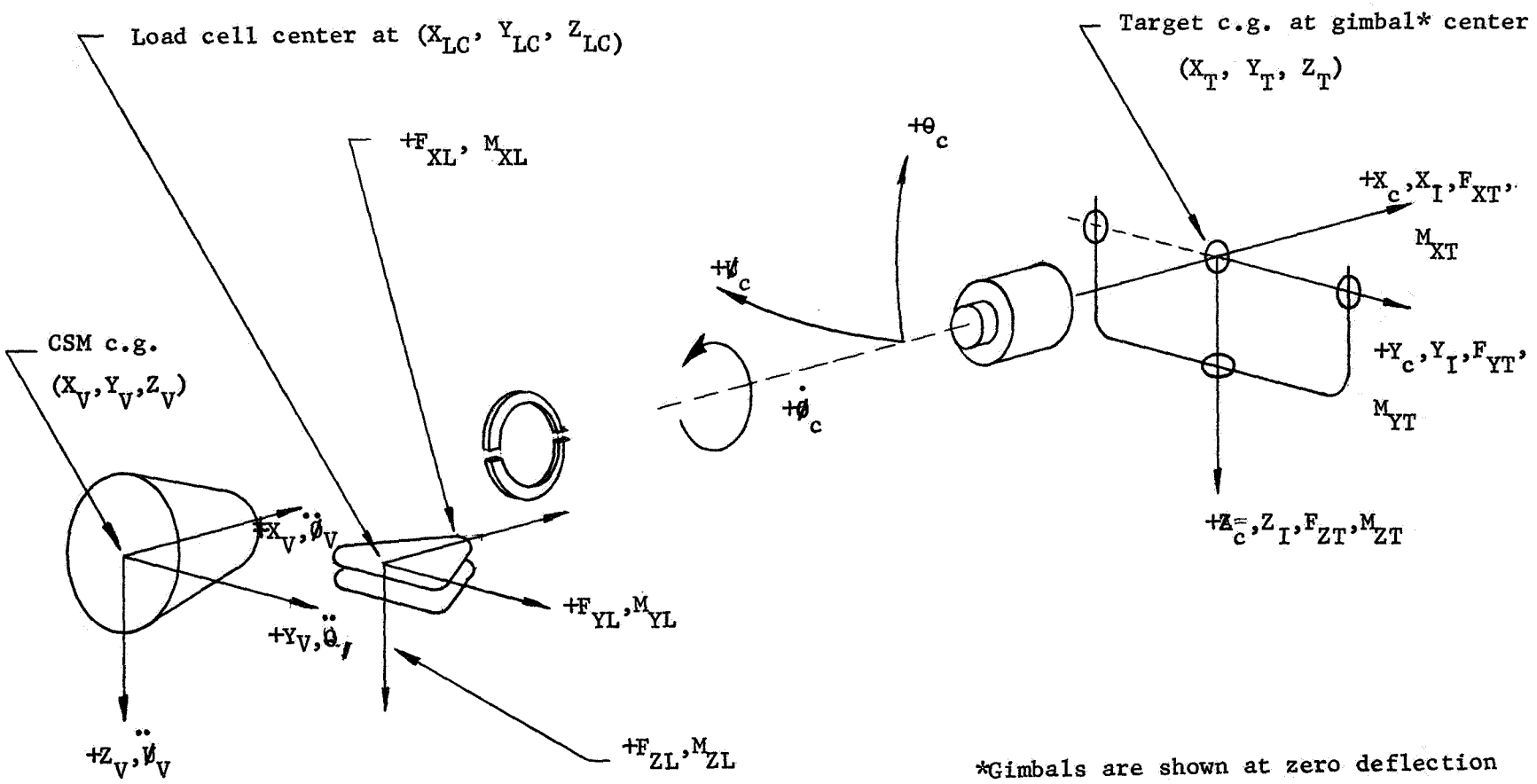

Figure 61 EMHD Simulation Configuration

$X_T = X_I$ = target c.g. longitudinal position in room, $\pm$ 30'

$Y_T = Y_I$ = target c.g. lateral position in room, $\pm$ 6'

$Z_T = Z_I$ = target c.g. vertical position in room, $\pm$ 6'

X_{LC} = load cell center longitudinal position in room (constant)(approx. -30')

Y_{LC} = load cell center lateral position in room (constant)(approx. 0')

Z_{LC} = load cell center vertical position in room (constant)(approx. $+\frac{1}{2}$')

M_{XL} = moment about load cell array X axis ($\pm$ 200 Ft Lb)

M_{YL} = moment about load cell array Y axis ($\pm$ 800 Ft Lb)

M_{ZL} = moment about load cell array Z axis ($\pm$ 800 Ft Lb)

F_{XL} = force along load cell array X axis ($\pm$ 200 Lb)

F_{YL} = force along load cell array Y axis ($\pm$ 200 Lb)

F_{ZL} = force along load cell array Z axis ($\pm$ 200 Lb)

M_{XT} = moment on target c.g. parallel to room X axis ($\pm$ 200 Ft Lb)

M_{YT} = moment on target c.g. parallel to room Y axis ($\pm$ 200 Ft Lb)

M_{ZT} = moment on target c.g. parallel to room Z axis ($\pm$ 200 Ft Lb)

$F_{XT} = -F_{XL}$ = force on target parallel to room X ($\pm$ 200 Lb)

$F_{YT} = -F_{YL}$ = force on target parallel to room Y ($\pm$ 200 Lb)

$F_{ZT} = -F_{ZL}$ = force on target parallel to room Z ($\pm$ 200 Lb)

I_T = moment of inertia of inertially symmetric target, 3 to 3000 slug ft^2

M_T = target mass, 5 to 140 slugs

I_{xx} = CSM roll moment of inertia = 19,000 slug ft^2

I_{yy} = CSM pitch moment of inertia = 50,000 slug ft^2

I_{zz} = CSM yaw moment of inertia = 46,000 slug ft^2

M_c = CSM mass = 1000 slugs

$\ddot{X}_v$ = thrusted acceleration along CSM X axis, $\pm$ 0.4'/sec^2

$\ddot{Y}_v$ = thrusted acceleration along CSM Y axis, $\pm$ 0.2'/sec^2

$\ddot{Z}_v$ = thrusted acceleration along CSM Z axis, $\pm$ 0.2'/sec^2

$\ddot{\psi}_v$ = thrusted CSM yaw acceleration, $\pm$ 1.6^o/sec^2

$\ddot{\theta}_v$ = thrusted CSM pitch acceleration, $\pm$ 1.5^o/sec^2

$\ddot{\phi}_v$ = thrusted CSM roll acceleration, $\pm$ 3.9^o/sec^2

TX = CSM X thrust hand controller command

TY = CSM Y thrust hand controller command

TZ = CSM Z thrust hand controller command

Tψ = CSM yaw thrust hand controller command

Tθ = CSM pitch thrust hand controller command

Tϕ = CSM roll thrust hand controller command

MS: thrust mode select signal (pulse, rate, accel.)

X_o = target initial longitudinal position, $\pm$ 30'

Y_o = target initial lateral position, $\pm$ 6'

Z_o = target initial vertical position, $\pm$ 6'

ψ_o = target initial yaw position, $\pm$ 45^o

θ_o = target initial pitch position, $\pm$ 45^o

$\dot{\phi}_o$ = target initial roll rate, $\pm$ 240^o/sec

α = EMHD arm open angle

ω = EMHD spin rate

f_1 = EMHD No. 1 pad force

f_2 = EMHD No. 2 pad force

$S_1 \longrightarrow S_4$ = Miscellaneous EMHD sensor readouts

$X_{vT} = X_I - X_v$ = Target/CSM c.g. X separation (25' to 80')

$Y_{vT} = Y_I - Y_v$ = Target/CSM c.g. Y separation (-6' to +6')

$Z_{vT} = Z_I - Z_v$ = Target/CSM c.g. Z separation (-6' to +6')

$X_{LT} = X_I - X_{LC}$ = Load cell/Target c.g. X separation (6' to 60')

$Z_{LT} = Z_I - Z_{LC}$ = Load cell/Target c.g. Z separation (-7' to +6')

* The simulator information flow is shown in Figure 62.

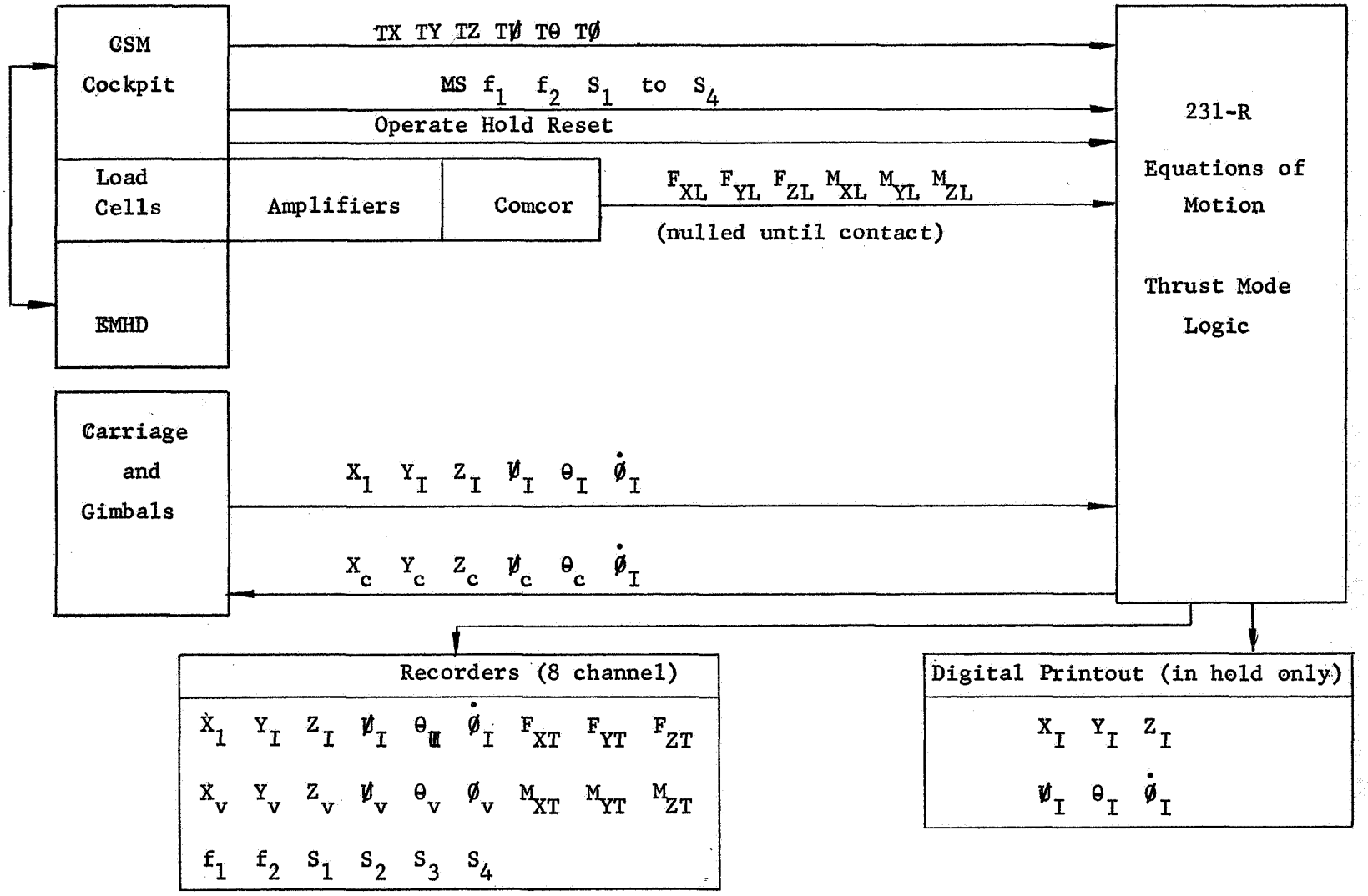

Figure 62 Information Flow Diagram

b. Thrust Logic - The CSM will have translation and rotation control capability. The cockpit mockup will contain the attitude and translation hand controllers built by Department 1640.

The translation controller is a three-axis device with microswitches on each axis. When deflected out of null (zero volts) on an axis, a switch is closed sending either + or - 100V to the computer. These signals will be used to develop the CSM translational accelerations in the computer according to Table VIII.

Table VIII CSM Translation Accelerations

Signal	Voltage to Computer	CSM Acceleration (Ft/Sec^2)		
		$\ddot{X}_V$	$\ddot{Y}_V$	$\ddot{Z}_V$
TX	0 +100 -100	0 +0.4 -0.4	-	-
TY	0 +100 -100	-	0 +0.2 -0.2	-
TZ	0 +100 -100	-	-	0 +0.2 -0.2

The attitude hand controller is a three axis device with potentiometers on each axis. Full deflection on an axis produces either + or - 20 volts depending on the direction of stick motion. Between these limits, the voltage output is proportional to stick deflection with the exception that the zero stick position leaves up to $\pm$ 0.7 volts output on the axes due to mechanical hysterisis in the stick linkage.

Three CSM attitude control modes will be used in the program: pulse, rate, and direct (acceleration). The cockpit will have a mode select (MS) switch that will send the MS signal to the computer as shown in Table IX.

Table IX Attitude Mode Control

MS Switch Position	MS Signal to Computer
Pulse	+100V
Rate	0V
Direct	-100V

It may be advisable to set the relay trigger voltages at some value under 100V to insure positive operation.

The general characteristics of the three modes are as follows:

Pulse: Each time the stick is displaced out of null and passes out through the 4V (+ or -) position, a thrust pulse lasting 0.10 to 0.25 second (this duration should be readily variable on the computer) is generated on that axis. Another pulse may not be generated on that axis until the stick is returned to the null position on that axis. All axes act independently.

The Pulse mode is shown in circuit form in Figure 63

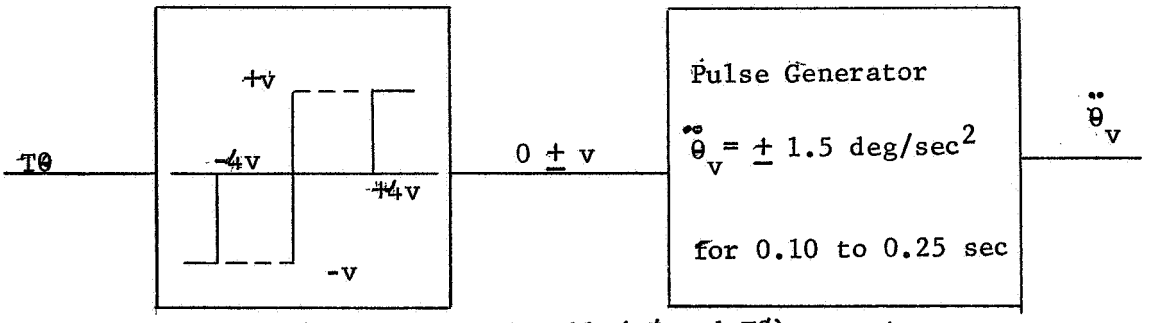

(Same implementation for yaw and roll (TΨ and TΦ) except

$\ddot{\Psi} = \pm 1.6$ deg/sec^2 and

$\ddot{\Phi} = \pm 3.9$ deg/sec^2 and

pulse interval equal on all axes.)

Figure 63 CSM Attitude Control, Pulse Mode Schematic

Rate: In this mode, the CSM accelerates at its fixed levels;

$\ddot{\Psi}_v = \pm 1.6$ deg/sec^2

$\ddot{\theta}_v = \pm 1.5$ deg/sec^2 and

$\ddot{\Phi}_v = \pm 3.9$ deg/sec^2

until the CSM body attitude rates ($\dot{\Psi}_v$, $\dot{\theta}_v$, $\dot{\Phi}_v$) reach a level proportional to the stick displacement (voltage) in excess of one volt on each axis (latter feature due to the zero hysterisis described previously), as shown in Figure 64

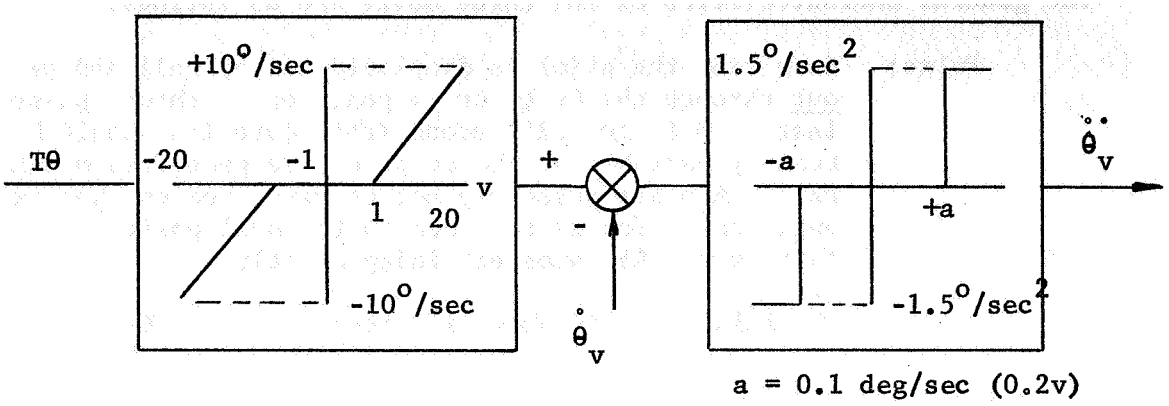

(same implementation for yaw and roll except for the different, fixed output acceleration levels).

Figure 64 CSM Attitude Control, Rate Mode Schematic

Direct: In this mode, the CSM accelerates continuously in yaw, pitch, or roll whenever the stick is deflected past the 3 volt (+ or -) position on the corresponding axis as shown in Figure 65. The acceleration levels are fixed at the same levels given in the rate mode description

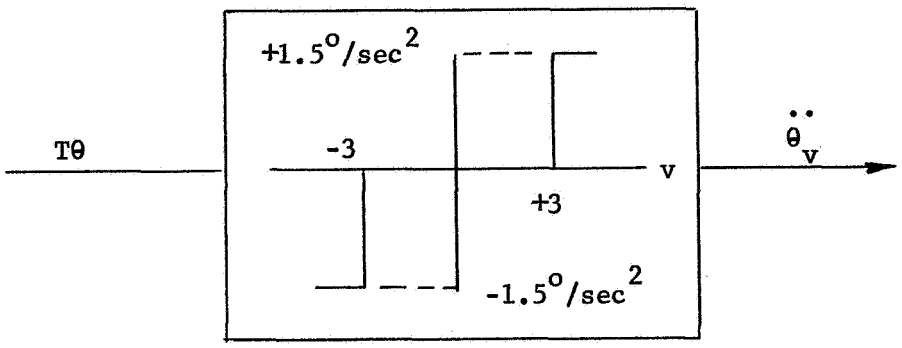

(same implementation for TØ and TØ except for the acceleration levels; $\ddot{\phi}_v = \pm 1.6$ deg/sec^2, $\ddot{\phi}_v = \pm 3.9$ deg/sec^2).

Figure 65 CSM Attitude Control, Direct Mode Schematic

These values of $\ddot{\phi}_v$, $\ddot{\theta}_v$, $\ddot{\phi}_v$, will feed into the equations of motion given in the next section.

c. Equations of Motion - In the simulation, all of the relative motions between the CSM and the Target are generated by moving the Target with the gimbals and carriage. Therefore, the Target will move to: 1) provide the reverse of the CSM's motion in space (caused by thrusting and post-contact forces and torques according to its own mass, inertia, and angular momentum parameters. The Target may be spinning prior to contact (pot setting: $\dot{\phi}_o = 0$ to $\pm 250^o$/sec). If it is, one goal of the test run will be to align the EMHD (CSM) X axis to this spin axis before contact. Off-axis contact torques on the Target will induce yaw and pitch precession in the Target's motion and this effect is included in the equations (see $\dot{\phi}_N$ and $\dot{\theta}_N$).

However, yaw and pitch cross-coupling into roll are not included since any significant, unchecked (not counteracted by EMHD grappling torques) yaw and pitch rates will stop the test when the gimbal limits are reached (yaw and/or pitch = $\pm 45^o$) or the induced precession cone angle exceeds 10^o - 20^o.

The specific command equations that must be implemented are as follows (see DEFINITION OF TERMS and the INFORMATION FLOW DIAGRAM for limits, scale factors, and signal sources):

$$X_c = X_o - \iint \ddot{X}_v dtdt + \iint \frac{F_{XT}}{M_T} dtdt + \int \frac{\dot{\psi}_v Y_{vT}}{57.3} dt - \int \frac{\dot{\theta}_v Z_{vT}}{57.3} dt$$

Note: $\dot{\psi}_v = \int \ddot{\psi}_v dt - \int \frac{1432\ F_{YT}}{46,000}\ dt.$

These integrals may be obtained after the first integration of these terms in the ψ_c logic.

$$\dot{\theta}_v = \int \ddot{\theta}_v dt + \int \frac{1432\ F_{ZT}}{50,000}\ dt$$

These integrals are available in the θ_c logic.

$$Y_c = Y_o - \iint \ddot{Y}_v dtdt + \iint \frac{F_{YT}}{M_T}\ dtdt - \int \frac{\dot{\psi}_v X_{vT}}{57.3}\ dt + \int \frac{\dot{\phi}_v Z_{vT}}{57.3}\ dt$$

Note: $\dot{\phi}_v = \int \ddot{\phi}_v dt$

$$Z_c = Z_o - \iint \ddot{Z}_v dtdt + \iint \frac{F_{ZT}}{M_T}\ dtdt + \int \frac{\dot{\theta}_v X_{vT}}{57.3}\ dt - \int \frac{\dot{\phi}_v Y_{vT}}{57.3}\ dt$$

Note: In the following equations; $S\psi$, $C\psi$, $S\theta$ are the sines and cosines of ψ_I and θ_I.

$$\psi_c = \psi_o - \iint \ddot{\psi}_v dtdt + \int \dot{\psi}_N dt + \iint \frac{1432\ F_{YT}}{46,000}\ dtdt$$

$$+ \int \dot{\phi}_v \frac{C\psi S\theta}{C\theta}\ dt - \int \dot{\theta}_v \frac{S\theta S\psi}{C\theta}\ dt$$

Note: The $\dot{\psi}_N$ equation is given later in this section.

$$\theta_c = \theta_o + \int\left(\int \ddot{\theta}_v dt + \int \frac{1432\ F_{ZT}}{50{,}000}\ dt\right) C\psi dt + \int \dot{\theta}_N dt - \int \dot{\phi}_v S\psi dt$$

Note: The $\dot{\theta}_N$ equation is given later in this section.

$\dot{\phi}_c$ (Note that this is a rate command)

$$\dot{\phi}_c = \dot{\phi}_o + (\dot{\phi}_v - \int 57.3\ \frac{M_{XT}}{I_T}\ dt)\ \frac{C\psi}{C\theta} + (\dot{\theta}_v - \int 57.3\ \frac{M_{YT}}{I_T}\ dt)\ \frac{S\psi}{C\theta}$$

Note: In the following equations;

$$\dot{\phi}_T = \dot{\phi}_I - \dot{\phi}_v$$

$$\dot{\theta}_N = \int (\frac{\dot{\phi}_T \psi_N}{57.3})dt - C\psi \int 57.3\ \frac{M_{YT}}{I_T}\ dt + S\psi \int 57.3\ \frac{M_{XT}}{I_T}\ dt$$

$$\dot{\psi}_N = \int (\frac{\dot{\phi}_T \dot{\theta}_N}{57.3})dt + \int 57.3\ \frac{M_{ZT}}{I_T}\ dt - \frac{S\theta C\psi}{C\theta} \int 57.3 \frac{M_{XT}}{I_T}\ dt$$

$$- \frac{S\theta S\psi}{C\theta} \int 57.3\ \frac{M_{YT}}{I_T}\ dt$$

The moments on the target due to moments and forces on the load cells are given by:

$$M_{XT} = - M_{XL} + F_{ZL} Y_{LT} - F_{YL} Z_{LT}$$
$$M_{YT} = - M_{YL} + F_{XL} Z_{LT} - F_{ZL} X_{LT}$$
$$M_{ZT} = - M_{ZL} + F_{YL} X_{LT} - F_{XL} Y_{LT}$$

SECTION VI

EMHD TEST RESULTS

1. Tabulated Quantitative Data

Data were obtained using strip-chart recorders monitoring computer output. Twenty-four parameters were recorded in real time. Figure 66 shows typical data obtained during a run.

Twenty-seven (27) different runs were assigned to the test subjects. Table X presents the run profile. Three test subjects participated in the simulation. One was an experienced military Test Pilot with five additional years experience flying CSM rendezvous and docking simulators. The two other test subjects were Martin Marietta engineers, one of whom has a Commercial Pilot license rated for instrument flight and the second has seven years experience with Martin Marietta simulator operation. These subjects made one-hundred and fourteen (114) data runs covering the twenty-seven tasks. Subjects took turns flying the CSM and controlling the EMHD. However, the most experienced subject (Mr. W. T. Armstrong) controlled the CSM for just over one-half of the data runs. Table XI presents the test subject groups and the data runs they made.

Tables XII through XVI present the data obtained grouped according to the attachment mode being used. Generally, each run was made three times for each group of subjects.

Tables XVII through XXI present the same data discussed above with the exception that the subject group attempts at each run are averaged. Table XXII presents these data averaged over the four test subject groups.

In Tables XVII through XXII the time colume indicates the average flying time required before contact was made with the Target. Position errors (X, Y, Z, θ and $\not\emptyset$) are the average contact conditions with the signs of the errors included. Translation rate errors (X, Y and Z) are the averages of the absolute values of the individual rate errors. Force (F) and moment (M) data are averaged by absolute value. The axes (X, Y, Z, $\emptyset$, θ and $\not\emptyset$) refer to the axes in the room and in the Target that are parallel to the CSM's longitudinal, lateral, vertical, roll, pitch and yaw axes respectively. Average de-spin times take only successful attempts into account.

In addition to the tabulated runs, the test subjects made six (6) attempts to clamp the octagonal box with a Target mass of two-hundred and five kilograms (fourteen slugs) and a spin rate ($\emptyset$) of two-hundred

and sixteen (216) degrees per second. They were unsuccessful in all six, inducing large nutation at the moment of contact.

For all tests, the Target center-of-gravity (c.g.) was located at the gimbal center. This places the c.g. seven-tenths (0.7) of a meter (2.3 feet) behind the front surface of the octagonal box. The X position given in Table XXII is the X position relative to the center of the sides of the octagonal box. Therefore, the X numbers vary with the grappling mode used. Plus X is toward the rear of the box. Plus Y and Z mean, respectively, grappling the target to the right and below the EMHD axis. Plus θ and ψ represent target front pitched up and yawed to its right, respectively.

Data was also taken to evaluate the forces (F) and moments (M) generated on the target during transport operations. This was accomplished by placing the target in the EMHD grip, activating the available CSM control functions and recording resulting target forces and moments. The results were consistent with those predicted in Section II. Following these tests, the Target was spun-up to seventy-two (72) degrees per second and released without inducing measurable nutation. Target mass for this test was five-hundred and eighty-four (584) kilograms (forty slugs).

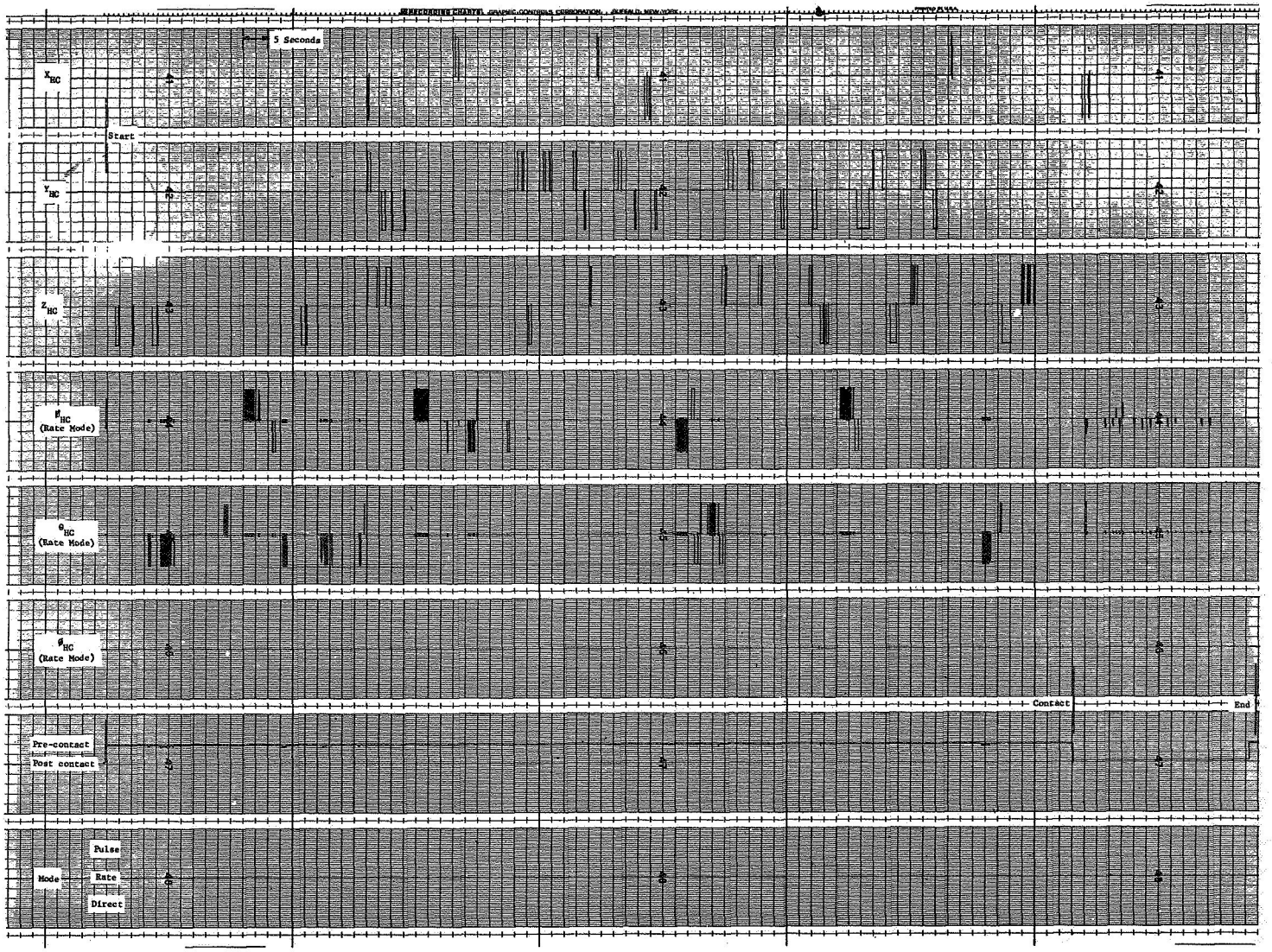

Figure 66a Typical Recorded Data, Run 12

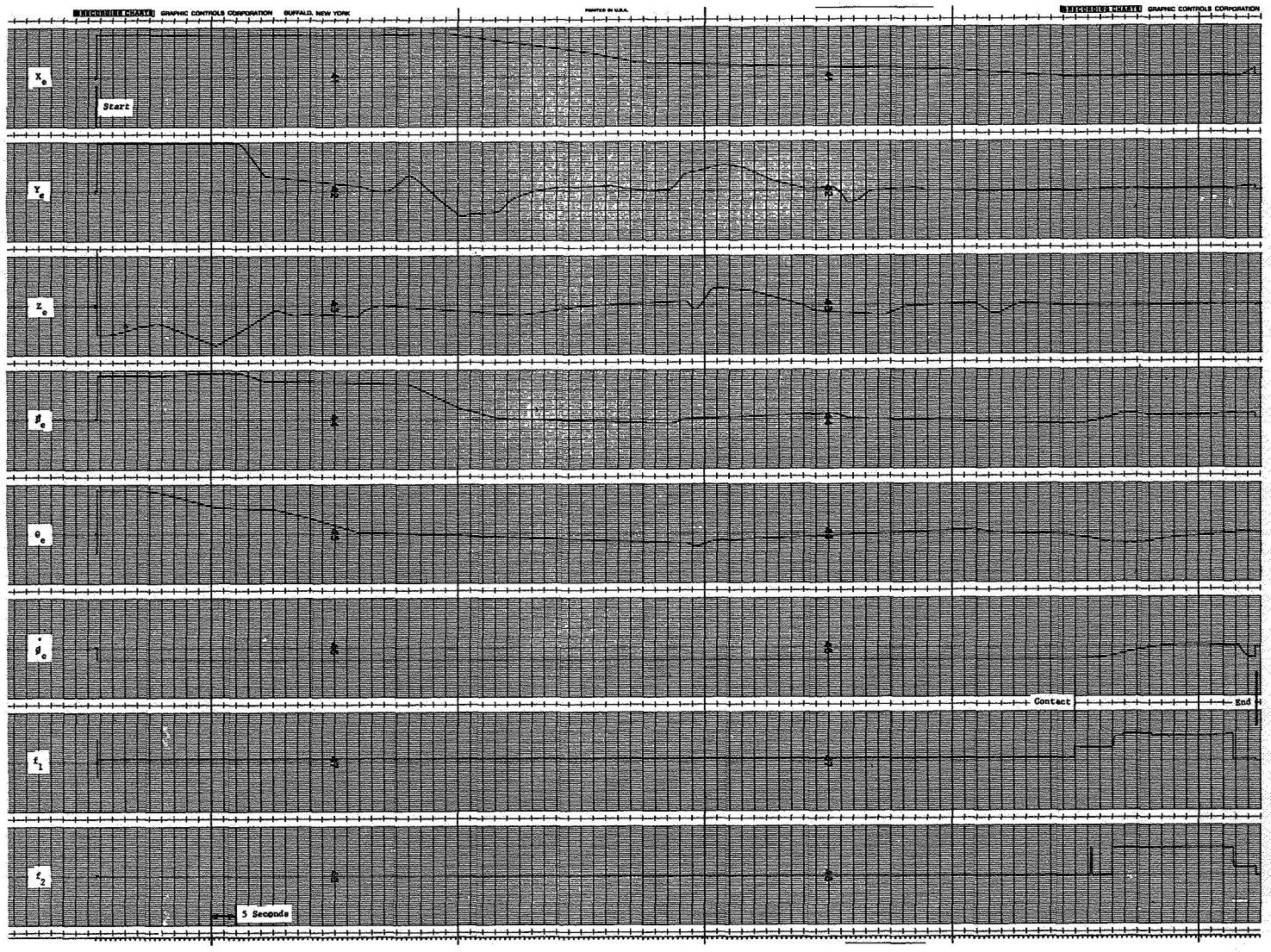

Figure 66b Typical Recorded Data, Run 12

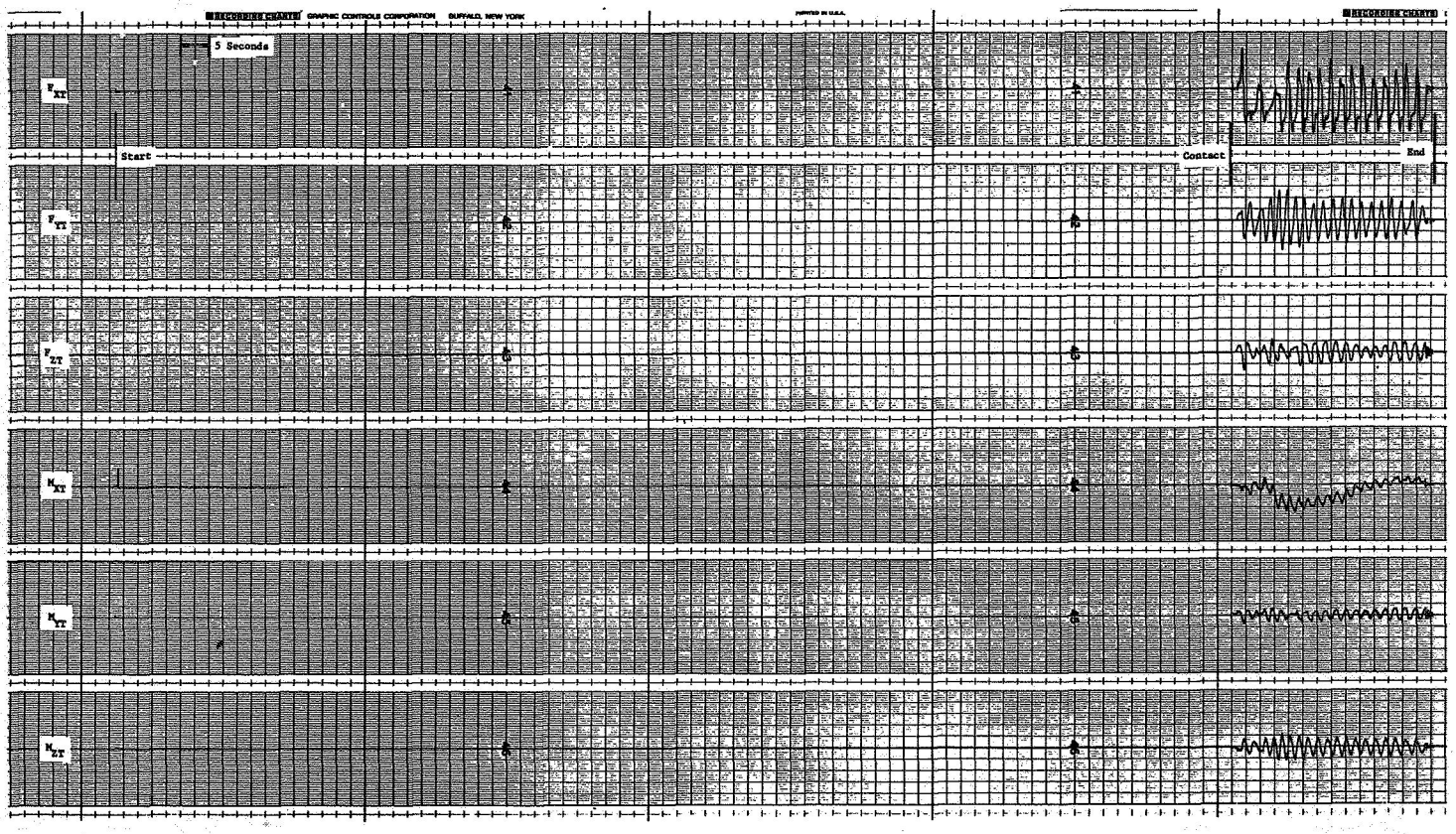

Figure 66c Typical Recorded Data, Run 12

Table X - Simulation Run Schedule

Run No.	Target Configuration	M_T kg(Slug)	I_T $kg\,m^2$ ($Slug\,ft^2$)	X_o m (ft)	Y_o m (ft)	Z_o m (ft)	$\dot{\phi}$ deg/sec	θ deg	ψ deg	Attachment Mode
1	Octagonal	2045(140)	4914(3000)	9.1(30)	0	0	0	0	0	Clamp Octagonal Box
2	Octagonal	2045(140)	4914(3000)	9.1(30)	1.5(5)	-0.9(-3)	0	0	0	Clamp Octagonal Box
3	Octagonal	2045(140)	4914(3000)	9.1(30)	-0.6(-2)	1.5(5)	0	22.5	0	Clamp Octagonal Box
4	Octagonal	2045(140)	4914(3000)	9.1(30)	0	0	0	22.5	22.5	Clamp Octagonal Box
5	Octagonal	2045(140)	4914(3000)	9.1(30)	1.5(5)	-0.9(-3)	18	22.5	22.5	Clamp Octagonal Box
6	Octagonal	2045(140)	4914(3000)	4.6(15)	-0.6(-2)	1.5(5)	0	0	45	Clamp Octagonal Box
7	Octagonal	2045(140)	4914(3000)	4.6(15)	-0.6(-2)	1.5(5)	0	22.5	22.5	Hook twelve (12)" Flg.
8	Cylindrical	2045(140)	4914(3000)	4.6(15)	1.5(5)	-0.9(-3)	-18	22.5	22.5	Clamp Cylinder
9	Cylindrical	2045(140)	4914(3000)	4.6(15)	1.5(5)	-0.9(-3)	18	22.5	22.5	Hook Eight (8)" Flg.
10	Cylindrical	584 (40)	491 (300)	4.6(15)	-0.6(-2)	1.5(5)	18	22.5	0	Clamp Cylinder
11	Cylindrical	584 (40)	491 (300)	4.6(15)	-0.6(-2)	1.5(5)	18	22.5	22.5	Hook Eight (8)" Flg.
12	Cylindrical	584 (40)	491 (300)	4.6(15)	1.5(5)	-0.9(-3)	18	22.5	22.5	Clamp Octagonal Box
13	Octagonal	584 (40)	491 (300)	4.6(15)	1.5(5)	-0.9(-3)	72	22.5	22.5	Clamp Octagonal Box
14	Octagonal	584 (40)	491 (300)	4.6(15)	-0.6(-2)	1.5(5)	0	0	45	Hook Twelve (12)" Flg.
15	Octagonal	205 (14)	49 (30)	4.6(15)	-0.6(-2)	1.5(5)	0	22.5	0	Clamp Octagonal Box
16	Octagonal	205 (14)	49 (30)	4.6(15)	1.5(5)	-0.9(-3)	-72	0	45	Clamp Octagonal Box
17	Cylindrical	205 (14)	49 (30)	4.6(15)	1.5(5)	-0.9(-3)	-18	22.5	0	Clamp Cylinder
18	Octagonal	205 (14)	49 (30)	4.6(15)	-0.6(-2)	1.5(5)	0	0	45	Velcro
19	Octagonal	205 (14)	49 (30)	4.6(15)	1.5(5)	-0.9(-3)	-18	0	45	Velcro
20	Octagonal	205 (14)	49 (30)	4.6(15)	1.5(5)	-0.9(-3)	-72	22.5	22.5	Velcro
21	Octagonal	584 (40)	491 (300)	4.6(15)	-0.6(-2)	1.5(5)	18	22.5	22.5	Velcro
22	Octagonal	584 (40)	491 (300)	4.6(15)	1.5(5)	-0.9(-3)	-72	0	45	Velcro
23	Octagonal	584 (40)	491 (300)	4.6(15)	1.5(5)	-0.9(-3)	-216	22.5	0	Velcro
24	Octagonal	2045 (140)	4914 (3000)	4.6(15)	-0.6(-2)	1.5(5)	0	0	45	Velcro
25	Octagonal	2045 (140)	4914 (3000)	4.6(15)	-0.6(-2)	1.5(5)	0	22.5	22.5	Velcro
26	Octagonal	2045 (140)	4914 (3000)	4.6(15)	1.5(5)	-0.9(-3)	18	22.5	0	Velcro
27	Octagonal	2045 (140)	4914 (3000)	4.6(15)	1.5(5)	-0.9(-3)	72	0	45	Velcro

Table XI Runs Flown by Test Subject Groups

		Runs Flown																										
Group	Personnel	1	2	3	4	5	6	7	8	9	10	11	12	13	14	15	16	17	18	19	20	21	22	23	24	25	26	27
A	CSM Pilot W. T. Armstrong	X	X	X	X	X	X	X	X	X	X	X	X	X	X	X		X	X			X		X			X	X
	EMHD Operator R. T. French																											
B	CSM Pilot W. T. Armstrong																X			X	X		X					
	EMHD Operator A. W. Schlaht																											
C	CSM Pilot R. T. French		X		X		X		X		X									X					X			
	EMHD Operator A. W. Schlaht																											
D	CSM Pilot A. W. Schlaht	X		X		X		X				X														X		
	EMHD Operator R. T. French																											

Table XII - Simulation Data, Attachment Mode - Clamping to Outer Octagonal Target Surface

Position & Rate Conditions at Target Contact																			
Run No.	Test Group	Time* Sec	Translational						Rotational			Target De-Spin Time Sec	Maximum Contact Forces & Moments						Comments
			m (ft)			m/sec (ft/sec)			deg/sec	deg			nt (lbs)			nt-m (ft-lbs)			
			X	Y	Z	$\dot{X}$	$\dot{Y}$	$\dot{Z}$	$\dot{\Phi}$	θ	Ψ		F_{XT}	F_{YT}	F_{ZT}	M_{XT}	M_{YT}	M_{ZT}	
1-1	A	70	-0.1 (-0.3)	-.16 (-.52)	.08 (.25)	-.01 (.03)	.00	.00	0	5.2	0.0	--	102 (23)	76 (17)	18 (4)	-5 (-4)	14 (10)	27 (20)	One arm contacted target first but still good attachment
1-2	A	125	0.0	-.05 (-.17	.18 (.59)	0.0	.00	.00	0	11.0	0.0	--	-134 (-30)	134 (30)	-13 (-3)	18 (13)	41 (30)	-75 (-55)	Deliberate pitch error at contact. Good attachment
1-3	A	60	0.0	-.12 (-.38)	-.05 (-.17)	0.0	.00	.00	0	0.6	0.0	--	-134 (-30)	45 (10)	18 (4)	3 (2)	18 (13)	33 (24)	Target caught on octagonal points. Z and θ drifted post-contact.
1-1	D	75	0.1 (0.3)	.07 (.24)	.01 (.02)	.01 (.03)	.00	.00	0	3.0	0.8	--	-58 (-13)	125 (28)	-27 (-6)	3 (2)	-41 (-30)	-48 (-35)	Good Attachment
1-2	D	70	0.1 (0.2)	.06 (.21)	.01 (.02)	-.01 (-.03)	.00	.00	0	1.4	1.0	--	-71 (-16)	89 (20)	18 (4)	-4 (-3)	34 (25)	-48 (-35)	Good Attachment
1-3	D	60	0.1 (0.2)	.04 (.12)	.00	.03 (.10)	.00	.00	0	1.2	-0.6	--	134 (30)	62 (14)	22 (5)	10 (7)	-41 (-30)	24 (18)	Good Attachment
2-1	A	100	-0.1 (-0.3)	-.04 (-.12)	-.05 (-.17)	.01 (.03)	.01	.00	0	0.0	1.0	--	-174 (-39)	36 (8)	9 (2)	1 (1)	11 (8)	30 (22)	Good Attachment but pads low on target
2-2	A	90	-0.1 (-0.2)	-.01 (-.04)	-.02 (-.06)	.00	.01 (.04)	.00	0	1.2	1.2	--	-89 (-20)	-36 (-8)	9 (2)	1 (1)	15 (11)	24 (18)	Good Attachment but low on target
2-3	A	95	0.0	.06 (.20)	.08 (.25)	.02 (.07)	.00	.01 (.02)	0	3.0	4.2	--	-107 (-24)	-31 (-7)	-9 (-2)	-3 (-2)	18 (13)	-24 (-18)	Target slipped axially in EMHD grip post-contact
2-1	C	385	-0.2 (-0.7)	.09 (.30)	-.07 (-.22)	.00	.01 (.04)	.00	0	-0.2	7.0	--	-107 (-24)	-76 (-17)	-36 (-8)	26 (19)	22 (16)	-14 (-10)	θ and Ψ developed rate post-contact
2-2	C	160	-0.1 (-0.4)	-.02 (-.06)	-.08 (-.28)	-.02 (-.07)	.00	.00	0	-0.2	-0.6	--	18 (4)	18 (4)	-22 (-5)	5 (4)	5 (4)	-4 (-3)	Good attachment
2-3	C	95	-0.2 (-0.6)	.00	-.08 (-.25)	.00	.00	.00	0	0.8	-1.0	--	116 (26)	-36 ((-8)	18 (4)	5 (4)	-14 (-10)	7 (5)	Good Attachment
3-1	A	60	0.0	.03 (.10)	.05 (.16)	.03 (.10)	.00	.01 (.02)	0	4.8	3.0	--	-200 (-45)	-22 (-5	-18 (-4)	3 (2)	18 (13)	-27 (-20)	Good attachment
3-2	A	115	-0.1 (-0.2)	-.02 (-.05)	.03 (.08)	.00	.00	.00	0	4.6	2.8	--	85 (19)	134 (30)	13 (3)	5 (4)	19 (14)	-57 (-42)	Target yawed post-contact but pilot flew it out
3-3	A	115	-0.1 (-0.2)	-.01 (-.02)	.04 (.12)	.00	.00	.00	0	3.6	2.0	--	53 (12)	40 (9)	13 (3)	-3 (-2)	20 (15)	31 (23)	Good attachment
3-1	D	200	0.0	.01 (.02)	-.06 (-.02)	.00	.01 (.02)	.00	0	-2.0	-0.8	--	134 (30)	-53 (-12)	13 (3)	5 (4)	-54 (-40)	-20 (-15)	Good attachment
3-2	D	190	0.0	-.06 (-.20)	.06 (.20)	.00	.00	.00	0	4.4	-3.0	--	-76 (-17)	53 (12)	13 (3)	15 (11)	14 (10)	-12 (-9)	Good attachment
*Flying time between initiating run and target contact																			

Table XII - Simulation Data, Attachment Mode - Clamping to Outer Octagonal Target Surface Continued

Run No.	Test Group	Time* Sec	Position & Rate Conditions at Target Contact: Translational m (ft) X	Y	Z	Translational m/sec (ft/sec) $\dot{X}$	$\dot{Y}$	$\dot{Z}$	Rotational deg/sec $\dot{\phi}$	deg θ	Ψ	Target De-Spin Time Sec	Maximum Contact Forces & Moments nt (lbs) F_{XT}	F_{YT}	F_{ZT}	nt-m (ft-lbs) M_{XT}	M_{YT}	M_{ZT}	Comments
3-3	D	150	-0.2 (-0.5)	-.03 (-.10)	-.02 (-.05)	.06 (.20)	.00	.00	0	1.0	-0.6	--	196 (44)	134 (30)	-27 (-6)	-7 (-5)	-24 (-18)	-23 (-17)	Target yawed post-contact
4-1	A	105	-0.2 (-0.6)	-.04 (-.12)	-.02 (-.05)	.00	.01 (.02)	.00	0	2.4	2.0	--	89 (20)	62 (14)	36 (8)	-7 (-5)	24 (18)	41 (30)	Target pushed away
4-2	A	115	-0.2 (-0.5)	-.02 (-.05)	.08 (.28)	.02 (.05)	.00	.01 (.04)	0	4.6	3.8	--	-178 (-40)	40 (9)	-27 (-6)	8 (6)	54 (40)	33 (24)	Z and θ coupled and pulled target out of grip
4-3	A	105	-0.1 (-0.3)	.00	-.03 (-.10)	.00	.02 (.05)	.00	0	2.6	3.2	--	80 (18)	-58 (-13)	18 (4)	-3 (-2)	23 (17)	38 (28)	Low on target but otherwise good
4-1	C	260	-0.2 (-0.5)	-.08 (-.25)	.03 (.10)	-.01 (-.03)	-.01 (-.03)	.00	0	3.0	-2.0	--	134 (30)	125 (28)	18 (4)	-3 (-2)	-54 (-40)	34 (25)	Good attachment
4-2	C	395	0.0	-.06 (-.20)	.05 (.17)	-.01 (-.02)	.02 (.05)	.00	0	3.0	-4.0	--	-125 (-28)	22 (5)	-13 (-3)	-3 (-2)	41 (30)	23 (17)	Target knocked away (θ)
4-3	C	345	0.0	-.04 (-.12)	.02 (.05)	.00	.00	.01 (.02)	0	3.0	-0.2	--	-89 (-20)	-22 (-5)	-4 (-1)	4 (3)	34 (25)	20 (15)	Good attachment
5-1	A	255	0.0	.08 (.24)	.10 (.32)	.02 (.05)	.01 (.04)	.01 (.03)	+18	4.4	3.4	--	-107 (-24)	-53 (-12)	27 (6)	26 (19)	35 (26)	50 (37)	Target nutated. De-spin not accomplished
5-2	A	200	-0.1 (-0.3)	-.11 (-.38)	.05 (.18)	.00	.00	.00	+18	2.6	3.4	--	-165 (-37)	53 (12)	49 (11)	28 (21)	76 (56)	-46 (-34)	One pad contacted target which caused nutation
5-3	A	160	-0.1 (-0.2)	-.02 (-.05)	.06 (.18)	.02 (.07)	.01 (.02)	.00	+18	3.8	0.8	52	-169 (-38)	107 (24)	45 (10)	30 (22)	22 (16)	-60 (-44)	Good attachment and de-spin
5-1	D	1245	0.0	-.09 (-.30)	.07 (.22)	-.02 (-.08)	.00	.01 (.04)	+18	2.8	-2.6	--	129 (29)	86 (19)	-93 (-21)	11 (8)	-31 (-23)	-11 (-8)	One pad contacted target which caused nutation
5-2	D	360	0.0	-.01 (-.04)	.01 (.04)	.00	.00	.01 (.02)	+18	2.4	1.0	60	45 (10)	62 (14)	36 (8)	28 (21)	7 (5)	-14 (-10)	Good attachment and de-spin
5-3	D	160	0.0	.01 (.02)	.03 (.10)	.00	.00	.00	+18	1.0	0.2	72	84 (19)	-31 (-7)	-58 (-13)	-28 (-21)	-16 (-12)	-14 (-10)	θ and Ψ oscillated during de-spin
6-1	A	130	0.0	-.04 (-.12)	.07 (.24)	.00	-.01 (-.03)	.01 (.03)	0	4.6	1.4	--	-98 (-22)	89 (20)	-9 (-2)	4 (3)	24 (18)	49 (36)	Good attachment but Z and θ developed rates post-contact
6-2	A	105	-0.1 (-0.2)	-.08 (-.25)	.02 (.07)	.04 (.12)	.00	.01 (.04)	0	3.4	0.4	--	-187 (-42)	98 (22)	13 (3)	7 (5)	28 (21)	81 (60)	Good attachment but Z and θ developed rates post-contact
6-3	A	120	0.0	-.04 (-.12)	.02 (.05)	.00	.00	.01 (.03)	0	3.0	2.4	--	125 (28)	134 (30)	-13 (-3)	4 (3)	-24 (-18)	-71 (-52)	Good attachment but Z and θ developed rates post-contact
6-1	C	270	0.1 (0.2)	-.02 (-.08)	.05 (.18)	.00	-.01 (-.03)	.00	0	6.2	-1.8	--	-49 (-11)	-18 (-4)	80 (18)	4 (3)	75 (55)	16 (12)	Good attachment but Z and θ developed rates post-contact

*Flying time between initiating run and target contact

Table XII - Simulation Data, Attachment Mode-
Clamping to Outer Octagonal Target Surface Concluded

Position & Rate Conditions at Target Contact																			
Run No.	Test Group	Time* Sec	Translational						Rotational			Target De-Spin time sec	Maximum Contact Forces & Moments						Comments
			m (ft)			m/sec (ft/sec)			deg/sec	deg			nt (lbs)			nt-m (ft-lbs)			
			X	Y	Z	$\dot{X}$	$\dot{Y}$	$\dot{Z}$	$\dot{\Phi}$	Θ	Ψ		F_{XT}	F_{YT}	F_{ZT}	M_{XT}	M_{YT}	M_{ZT}	
6-2	C	190	0.3 (1.1)	-.03 (-.10)	.10 (.34)	.00	-.01 (-.02)	.01 (.02)	0	3.4	1.8		-58 (-13)	-76 (-17)	-45 (-10)	14 (10)	-27 (-20)	87 (64)	Good attachment but target pitched out of grip
6-3	C	200	-0.1 (-0.3)	-.04 (-.14)	.13 (.44)	.03 (.10)	-.01 (-.02)	.01 (.04)	0	7.6	-0.4	--	-107 (-24)	134 (30)	-22 (-5)	10 (7)	49 (36)	-68 (-50)	One pad slipped off target
12-1	A	195	0.0	.01 (.04)	.06 (.20)	.00	.00	.00	-18	1.8	3.2	17	-62 (-14)	-49 (-11)	-45 (-10)	-14 (-10)	-35 (-26)	32 (24)	Good attachment and de-spin
12-2	A	115	0.1 (0.2)	-.01 (-.03)	.15 (.50)	-.02 (-.07)	-.01 (-.02)	.01 (.04)	-18	5.0	2.8	22	-67 (-15)	76 (17)	-40 (- 9)	-14 (-10)	-35 (-26)	-52 (-38)	Good attachment and de-spin
12-3	A	110	0.1 (0.3)	-.02 (-.07)	.06 (.20)	.00	.00	-.03 (-.11)	-18	4.4	1.0	9	-89 (-20)	67 (15)	36 (8)	-19 (-14)	41 (30)	60 (44)	Target nutated slightly but was de-spun successfully
12-4	A	85	-0.1 (-0.4)	.03 (.10)	.12 (.39)	-.01 (-.02)	-.01 (-.03)	.00	-18	3.6	2.0	--	-94 (-21)	107 (24)	-40 (-9)	-16 (-12)	27 (20)	-68 (-50)	Target nutated away
12-5	A	90	-0.1 (-0.2)	-.01 (-.02)	.05 (.17)	.02 (.07)	.02 (.05)	.01 (.02)	-18	2.6	1.4	44	-76 (-17)	129 (29)	76 (17)	-15 (-11)	56 (41)	68 (50)	Good attachment. Target nutated slightly throughout despin
12-6	A	120	0.1 (0.2)	.02 (.07)	.06 (.20)	-.04 (-.13)	.00	.00	-18	2.4	2.2	38	45 (10)	-36 (-8)	18 (4)	-15 (-11)	22 (16)	-30 (-22)	Good attachment and de-spin
13-1	A	135	0.0	-.02 (-.06)	.04 (.12)	.00	.00	.00	+72	1.0	1.0	--	-120 (-27)	116 (26)	49 (11)	41 (30)	68 (50)	90 (66)	Target nutated and got away
13-2	A	115	0.1 (0.2)	-.01 (-.02)	-.01 (-.04)	-.02 (-.08)	-.01 (-.03)	.00	+72	2.2	2.0	--	36 (8)	-71 (-16)	67 (15)	-20 (-15)	57 (42)	-43 (-32)	Target nutated and got away
13-3	A	95	0.2 (0.6)	.06 (.19)	.02 (.05)	-.03 (-.10)	.00	.00	+72	3.4	2.8	--	-62 (-14)	53 (12)	-40 (-9)	24 (18)	49 (36)	39 (29)	Attached on octagonal points, target nutated and got away
15-1	A	160	-0.1 (-0.3)	.03 (.09)	.06 (.20)	-.01 (-.03)	.00	.00	0	5.4	1.4	--	-53 (-12)	-116 (-26)	-18 (-4)	-14 (-10)	34 (25)	170 (125)	Good attachment
15-2	A	145	0.1 (0.3)	.07 (.24)	.09 (.29)	.00	.00	-.01 (-.02)	0	3.0	3.8	--	-31 (-7)	-116 (-26)	22 (5)	-5 (-4)	22 (16)	117 (86)	Good attachment
15-3	A	90	0.0	.03 (.11)	.04 (.14)	.00	.00	.00	0	2.6	1.2	--	-18 (-4)	-53 (-12)	-13 (-3)	-3 (-2)	-11 (-8)	53 (39)	Good attachment
16-1	A	175	0.0	.08 (.24)	-.01 (-.02)	.02 (.05)	.01 (.02)	.00	-72	-3.6	2.2	--	85 (19)	49 (11)	80 (18)	-31 (-23)	104 (77)	57 (42)	Target nutated and had to be released
16-2	A	140	0.6 (2.0)	.15 (.48)	.02 (.05)	-.04 (-.13)	-.01 (-.02)	.00	-72	0.0	1.4	--	27 (6)	-40 (-9)	-53 (-12)	-12 (-9)	-34 (-25)	27 (20)	One pad contact - Target nutated away
16-3	A	100	-0.2 (-0.8)	-.08 (-.28)	-.04 (-.14)	.00	.00	-.01 (-.02)	-72	-0.2	-0.2	--	-22 (-5)	49 (11)	-67 (-15)	-12 (-9)	-39 (-29)	-24 (-18)	One pad contact - Target nutated away
*Flying time between initiating run and target contact																			

TABLE XIII - Simulation Data, Attachment Mode - Clamping to Outer Cylindrical Target Surface

Run No.	Test Group	Time* Sec	Position & Rate Conditions at Target Contact: Translational: m (ft) X	Y	Z	m/sec (ft/sec) $\dot{X}$	$\dot{Y}$	$\dot{Z}$	Rotational: deg/sec $\dot{\Phi}$	deg Θ	Ψ	Target De-Spin Time Sec	Maximum Contact Forces & Moments: nt (lbs) F_{YT}	F_{YT}	F_{ZT}	nt-m (ft-lbs) M_{XT}	M_{YT}	M_{ZT}	Comments
8-1	A	240	0.3 (1.0)	.04 (.14)	.04 (-.06)	-.02	.00	.01 (.02)	-18	1.4	1.6	--	67 (15)	111 (25)	36 (8)	-39 (-29)	46 (34)	81 (60)	Good attachment but target nutated when tried to de-spin
8-2	A	130	0.3 (1.0)	.03 (.10)	.13 (.42)	.00	.01 (.03)	.01 (.02)	-18	5.4	1.2	63	85 (19)	-40 (- 9)	40 (9)	-23 (-17)	49 (36)	34 (25)	Good attachment and de-spin
8-3	A	115	0.2 (0.8)	.01 (.04)	.01 (.02)	.00	.00	.00	-18	4.8	2.0	58	125 (28)	62 (14)	49 (11)	-23 (-17)	54 (40)	-56 (-41)	Good attachment and de-spin
8-1	C	300	0.3 (1.0)	-.03 (-.11)	-.07 (-.22)	.00	.02 (.06)	.00	-18	-2.6	2.0	--	53 (12)	-18 (- 4)	-31 (-7)	16 (12)	-33 (-24)	20 (15)	EMHD arms not spinning at contact. Target nutated.
8-2	C	405	0.2 (0.7)	.05 (.16)	-.08 (-.26)	-.01 (-.03)	.00	-.01 (-.02)	-18	-1.4	2.6	--	200 (45)	-36 (- 8)	18 (4)	7 (4)	-62 (-46)	35 (26)	EMHD arms hit front of octagonal target. Target nutated
8-3	C	225	0.1 (0.2)	-.04 (-.14)	.17 (.56)	.02 (.05)	.01 (.02)	.01 (.03)	-18	7.0	-0.2	56	134 (30)	-27 (-6)	62 (14)	27 (20)	60 (44)	-42 (-31)	Target nutated but was successfully de-spun.
10-1	A	180	0.4 (1.3)	-.02 (-.08)	.09 (.29)	-.03 (-.10)	.02 (.06)	.01 (.02)	+18	3.4	-0.6	9	223 (50)	45 (10)	-31 (-7)	20 (15)	-32 (-24)	-48 (-35)	Good attachment and de-spin
10-2	A	265	0.3 (0.9)	.02 (.08)	.06 (.21)	.00	-.01 (-.02)	-.01 (-.04)	+18	1.8	1.0	9	-53 (-12)	-13 (-3)	-36 (-8)	19 (14)	-37 (-27)	14 (10)	Good attachment and de-spin
10-3	A	120	0.2 (0.8)	-.01 (-.02)	.02 (.05)	-.01 (-.03)	-.01 (-.03)	.00	+18	4.0	0.8	8	134 (30)	22 (5)	-27 (-6)	23 (17)	32 (24)	28 (21)	Good attachment and de-spin
10-1	C	340	0.2 (0.7)	-.01 (-.02)	.15 (.50)	.00	.00	-.01 (-.04)	+18	5.6	3.0	--	4 (1)	-36 (-8)	31 (7)	-8 (-6)	61 (45)	41 (30)	Target nutated. De-spin not accomplished.
10-2	C	395	0.3 (0.9)	-.10 (-.34)	.04 (.13)	-.02 (-.07)	-.01 (-.02)	.01 (.02)	+18	2.2	-2.4	19	169 (38)	-62 (-14)	49 (11)	10 (7)	-54 (-40)	65 (48)	Good attachment and de-spin
17-1	A	135	0.2 (0.8)	-.02 (-.07)	.13 (.44)	-.03 (-.10)	-.02 (-.05)	-.02 (-.08)	-18	3.4	0.0	--	76 (17)	134 (30)	107 (24)	24 (18)	92 (68)	-204 (-150)	Target nutated and had to be released
17-2	A	150	0.3 (1.0)	-.02 (-.05)	.12 (.38)	-.01 (-.04)	-.01 (-.03)	.00	-18	2.6	1.4	--	-58 (-13)	13 (3)	-53 (-12)	-19 (-14)	65 (48)	22 (16)	Target nutated and had to be released
17-3	A	185	0.3 (1.0)	.04 (.12)	-.02 (-.08)	.00	.00	-.01 (-.04)	-18	0.4	3.2	11	36 (8)	-102 (-23)	80 (18)	-14 (-10)	102 (75)	122 (90)	Good attachment and de-spin

* Flying time between initiating run and target contact.

Table XIV Simulation Data, Attachment Mode - Twelve (12) Inch Flange Attachment

Position & Rate Conditions at Target Contact																			
Run No.	Test Group	Time* Sec	Translational						Rotational			Target De-spin Time Sec	Maximum Contact Forces & Moments						Comments
									deg/sec	deg			nt (lbs)			nt-m (ft-lbs)			
			X	Y	Z	$\dot{X}$	$\dot{Y}$	$\dot{Z}$	$\dot{\phi}$	θ	ψ		F_{XT}	F_{YT}	F_{ZT}	M_{XT}	M_{YT}	M_{ZT}	
7-1	A	205	0.2 (0.5)	.09 (.29)	-.06 (-.19)	.00	.00	.00	0	-3.4	4.8	--	116 (26)	-22 (-5)	-85 (-19)	19 (14)	-136 (-100)	24 (18)	Good attachment.
7-2	A	210	0.2 (0.5)	-.03 (-.11)	-.01 (-.02)	.00	.00	.00	0	-0.6	-2.5	--	-258 (-58)	67 (15)	36 (8)	10 (7)	42 (31)	-92 (-68)	Good attachment.
7-3	A	200	0.2 (0.6)	-.02 (-.05)	-.02 (-.05)	-.01 (-.03)	-.01 (-.02)	.00	0	-1.4	0.4	--	134 (30)	36 (8)	62 (14)	-4 (-3)	62 (46)	54 (40)	Good attachment.
7-1	D	210	0.2 (0.7)	.04 (.13)	.08 (.26)	-.01 (-.03)	.00	.00	0	4.2	1.4	--	134 (30)	-22 (-5)	40 (9)	-7 (-5)	-34 (-25)	35 (26)	Good attachment.
7-2	D	240	0.2 (0.5)	-.06 (-.19)	.15 (.48)	.00	.01 (.04)	-.01 (-.02)	0	5.0	-1.6	--	107 (24)	45 (10)	62 (14)	8 (6)	-44 (-32)	48 (35)	Hooked loosely on top of hook blocks.
7-3	D	360	0.2 (0.6)	-.04 (-.15)	.10 (.34)	.00	.00	.04 (.12)	0	8.0	-1.2	--	267 (60)	40 (9)	89 (20)	10 (7)	-128 (-94)	34 (25)	Good attachment.
14-1	A	120	0.2 (0.7)	.00	.03 (.10)	.00	-.02 (-.05)	.00	0	1.2	0.4	--	49 (11)	-27 (-6)	36 (8)	-3 (-2)	-38 (-28)	30 (22)	Good attachment on third try. First two did not contact target.
14-2	A	80	0.2 (0.7)	.04 (.12)	.03 (.11)	-.01 (-.03)	-.01 (-.02)	.00	0	2.0	1.8	--	-53 (-12)	-27 (-6)	27 (6)	-4 (-3)	35 (26)	43 (32)	Good attachment.
14-3	A	115	0.2 (0.7)	.02 (.06)	.02 (.05)	.00	.00	.00	0	2.0	2.0	--	134 (30)	-45 (-10)	-53 (-12)	4 (3)	-73 (-54)	41 (30)	Good attachment.

* Flying time between initiating run and target contact.

Table XV Simulation Data, Attachment Mode - Eight (8) Inch Flange Attachment

Position & Rate Conditions at Target Contact																			
Run No.	Test Group	Time* Sec	Translational						Rotational			Target De-spin Time Sec	Maximum Contact Forces & Moments						Comments
			m (ft)			m/sec (ft/sec)			deg/sec	deg			nt (lbs)			nt-m (ft-lbs)			
			X	Y	Z	$\dot{X}$	$\dot{Y}$	$\dot{Z}$	$\dot{\Phi}$	Θ	Ψ		F_{XT}	F_{YT}	F_{ZT}	M_{XT}	M_{YT}	M_{ZT}	
9-1	A	160	0.4 (1.3)	.07 (.22)	.12 (.41)	.00	.00	-.02 (-.05)	-18	4.4	4.2	--	214 (48)	-36 (-8)	40 (9)	-11 (-8)	35 (26)	-46 (-34)	Only one pad hooked target and it nutated away.
9-2	A	210	0.5 (1.6)	.06 (.21)	.16 (.52)	.04 (.12)	-.01 (-.02)	-.01 (-.03)	-18	4.4	2.6	41	303 (68)	62 (14)	107 (24)	-39 (-29)	149 (110)	81 (60)	Good attachment on third try. First two did not contact target.
9-3	A	145	0.3 (1.1)	.02 (.08)	.09 (.30)	-.02 (-.05)	.00	.00	-18	4.2	1.8	47	312 (70)	-36 (-8)	49 (11)	-23 (-17)	69 (51)	33 (24)	Good attachment and de-spin.
11-1	A	165	0.4 (1.2)	.02 (.07)	.10 (.33)	-.03 (-.08)	-.01 (-.02)	.00	0	5.0	1.4	--	160 (36)	-13 (-3)	-22 (-5)	1 (1)	19 (14)	20 (15)	Excellent attachment.
11-2	A	60	0.4 (1.2)	.02 (.06)	.13 (.42)	.00	.00	.00	0	6.4	0.8	--	267 (60)	49 (11)	-67 (-15)	7 (5)	-170 (-125)	-83 (-61)	Excellent attachment.
11-3	A	165	0.4 (1.2)	.05 (.15)	.11 (.37)	.00	.00	.00	0	5.4	2.8	--	116 (26)	-36 (-8)	13 (3)	-3 (-2)	16 (12)	-34 (-25)	Good attachment on third try. First two did not contact target.
11-1	D	140	0.4 (1.2)	-.02 (-.05)	-.02 (-.08)	-.02 (-.07)	-.01 (-.02)	.00	0	-1.4	0.8	--	267 (60)	98 (22)	134 (30)	41 (30)	27 (20)	20 (15)	Excellent attachment.

* Flying time between initiating run and target contact.

Table XVI Simulation Data, Attachment Mode - Simulated-Adhesive (Velcro)

Run No.	Test Group	Time* Sec	Position & Rate Conditions at Target Contact: Translational m (ft) X	Y	Z	Translational m/sec (ft/sec) $\dot{X}$	$\dot{Y}$	$\dot{Z}$	Rotational deg/sec $\dot{\Phi}$	deg Θ	Ψ	Target de-Spin time sec	Maximum Contact Forces & Moments: nt (lbs) F_{XT}	F_{YT}	F_{ZT}	nt-m (ft-lbs) M_{XT}	M_{YT}	M_{ZT}	Comments
18-1	A	75	-0.4 (-1.4)	-.02 (-.06)	.02 (.05)	-.07 (-.23)	.00	.00	0	2.0	2.0	--	116 (26)	53 (12)	-116 (-26)	22 (16)	-122 (-90)	-86 (-63)	Target nutated away at contact
18-2	A	155	-0.4 (-1.4)	.02 (.07)	-.07 (-.22)	-.01 (-.03)	.00	.00	0	-2.4	1.0	--	31 (7)	-9 (-2)	-31 (-7)	-3 (-2)	-38 (-28)	14 (10)	Target nutated away at contact
18-3	A	200	-0.4 (-1.4)	-.02 (-.08)	-.02 (-.06)	.00	-.01 (-.03)	.00	0	-1.2	-1.0	--	-67 (-15)	58 (13)	-31 (-7)	-16 (-12)	39 (29)	-57 (-42)	Good attachment
19-1	B	175	-0.4 (-1.4)	.02 (.06)	-.01 (-.02)	.01 (.02)	.00	.00	-18	0.0	0.0	--	85 (19)	53 (12)	22 (5)	-5 (-4)	28 (21)	75 (55)	Target developed large nutation and got away
19-2	B	150	-0.4 (-1.4)	-.02 (-.05)	.08 (.25)	.00	.00	.00	-18	3.4	0.0	--	67 (15)	36 (8)	-53 (-12)	-8 (-6)	-54 (-40)	-42 (-31)	Target developed large nutation and got away
19-3	B	140	-0.4 (-1.4)	.02 (.08)	-.02 (-.05)	-.02 (-.05)	.00	-.01 (-.02)	-18	-0.2	1.8	--	-62 (-14)	36 (8)	40 (9)	5 (4)	52 (38)	-43 (-32)	Target developed large nutation and got away
19-1 ,	C	360	-0.4 (-1.4)	-.04 (-.12)	-.01 (-.04)	-.05 (-.17)	.01 (.04)	.01 (.04)	-18	0.4	-3.4	--	89 (20)	40 (9)	22 (5)	1 (1)	24 (18)	38 (28)	Target nutated away
19-2	C	150	-0.4 (-1.4)	-.02 (-.05)	.00	-.05 (-.17)	.00	.00	-18	-0.2	-0.6	--	89 (20)	-45 (-10)	36 (8)	3 (2)	-44 (-32)	42 (31)	Good try but slipped away when M_{xt} applied
19-3	C	215	-0.4 (-1.4)	-.04 (-.15)	.03 (.10)	-.01 (-.03)	.00	.00	-18	-0.8	0.2	--	31 (7)	-9 (-2)	-13 (-3)	-1 (-1)	-19 (-14)	14 (10)	Target nutated away at contact
20-1	B	200	-0.4 (-1.4)	.00	.04 (.14)	.00	.01 (.02)	.00	-72	3.0	0.4	--	102 (23)	36 (8)	-45 (-10)	5 (4)	-45 (-33)	46 (34)	Target nutated away at contact
20-2	B	235	-0.4 (-1.4)	.01 (.02)	.11 (.36)	.00	-.01 (-.03)	.00	-72	4.4	2.2	--	85 (19)	-18 (-4)	-45 (-10)	-4 (-3)	41 (30)	24 (18)	Target nutated away at contact
20-3	B	230	-0.4 (-1.4)	-.03 (-.10)	.06 (.21)	.00	.00	.00	-72	3.0	-0.2	-	71 (16)	-45 (-10)	-40 (-9)	-5 (-4)	-38 (-28)	43 (32)	Target nutated away at contact
21-1	A	240	-0.4 (-1.4)	.03 (.10)	.11 (.36)	-.05 (-.17)	.01 (.02)	.00	+18	3.6	3.6	--	312 (70)	27 (6)	40 (9)	14 (10)	42 (31)	-32 (-24)	Target nutated away at contract
21-2	A	195	-0.4 (-1.4)	-.03 (-.11)	.03 (.12)	-.03 (-.08)	.02 (.06)	.00	+18	0.2	-0.2	26	-	-	-	-	-	-	Good attachment and de-spin (Force and moment recorder failed)
21-3	A	135	-0.4 (-1.4)	-.02 (-.05)	.04 (.12)	-.06 (-.20)	.00	-.01 (-.04)	+18	2.0	0.4	21	250 (56)	-18 (-4)	36 (8)	12 (9)	-37 (-27)	24 (18)	Good attachment and de-spin
22-1	B	105	-0.4 (-1.4)	.03 (.11)	.02 (.08)	-.05 (-.15)	.01 (.03)	-.01 (-.03)	-72	2.6	0.4	--	187 (42)	-45 (-10)	-45 (-10)	-20 (-15)	-56 (-41)	35 (26)	Good attachment but de-spin torque caused target to nutate out of control

* Flying time between initiating run and target contact.

Table XVI Simulation Data, Attachment Mode - Simulated-Adhesive (Velcro) Continued

Position & Rate Conditions at Target Contact																			
Run No.	Test Group	Time* Sec	Translational						Rotational			Target de-spin time sec	Maximum Contact Forces & Moments						Comments
			m (ft)			m/sec (ft/sec)			deg sec	deg			nt (lbs)			nt-m (ft-lbs)			
			X	Y	Z	$\dot{X}$	$\dot{Y}$	$\dot{Z}$	$\dot{\Phi}$	Θ	Ψ		F_{XT}	F_{YT}	F_{ZT}	M_{XT}	M_{YT}	M_{ZT}	
22-2	B	125	-0.4 (-1.4)	.08 (.24)	.06 (.18)	-.04 (-.12)	.00	.00	-72	3.4	2.0	--	267 (60)	-45 (-10)	-53 (-12)	--	65 (48)	-54 (-40)	Good attachment but de-spin torque caused target to nutate out of control
22-3	B	150	-0.4 (-1.4)	.00	-.01 (-.03)	-.04 (-.14)	.00	.01 (.02)	-72	0.2	1.6	--	312 (70)	98 (22)	58 (13)	--	56 (41)	-98 (-72)	Good attachment but de-spin torque caused target to nutate out of control
23-1	A	95	-0.4 (-1.4)	.07 (.24)	.06 (.21)	-.04 (-.13)	.01 (.04)	.01 (.04)	-216	1.8	1.8	--	214 (48)	-111 (-25)	-107 (-24)	10 (7)	-128 (-94)	102 (75)	Target nutated away
23-2	A	120	-0.4 (-1.4)	.08 (.25)	.04 (.15)	-.05 (-.15)	.01 (.04)	.00	-216	2.8	1.2	--	290 (65)	-111 (-25)	-125 (-28)	-14 (-10)	-160 (-118)	87 (64)	Target nutated away
23-3	A	135	-0.4 (-1.4)	.03 (.10)	.02 (.06)	-.03 (-.10)	.00	.01 (.02)	-216	1.4	0.4	--	263 (59)	-102 (-23)	165 (37)	-31 (-23)	183 (135)	109 (80)	Target nutated away
24-1	C	160	-0.4 (-1.4)	-.02 (-.08)	.01 (.04)	-.07 (-.23)	.01 (.02)	-.01 (-.03)	0	0.0	-0.2	--	285 (64)	-40 (-9)	18 (4)	5 (4)	.35 (26)	30 (22)	Good attachment
24-2	C	125	-0.4 (-1.4)	-.05 (-.18)	-.03 (-.11)	-.04 (-.15)	.00	-.01 (-.03)	0	-0.2	-2.0	--	320 (72)	18 (4)	67 (15)	-4 (-3)	82 (60)	24 (18)	Good attachment but low on target
24-3	C	145	-0.4 (-1.4)	-.07 (-.22)	.01 (.02)	-.03 (-.11)	-.01 (-.04)	.00	0	-0.2	-3.0	--	316 (71)	40 (9)	22 (5)	-4 (-3)	33 (24)	41 (30)	Loose attachment
25-1	C	230	-0.4 (-1.2)	-.09 (-.30)	.11 (.36)	-.03 (-.11)	.00	.00	0	0.8	-3.2	--	356 (80)	-18 (-4)	45 (10)	4 (3)	73 (54)	22 (16)	Only two pads attached to target
25-2	C	190	-0.3 (-1.0)	-.05 (-.16)	.04 (.14)	-.02 (-.05)	.00	-.01 (-.02)	0	2.6	-1.0	--	289 (65)	-18 (-4)	31 (7)	4 (3)	68 (50)	18 (13)	Three pads attached to target
25-3	C	250	-0.4 (-1.3)	-.04 (-.14)	.05 (.16)	-.03 (-.10)	.01 (.02)	.01 (.02)	0	0.4	-2.4	--	343 (77)	18 (4)	62 (14)	7 (5)	95 (70)	26 (9)	Good attachment. All four pads contacted
26-1	A	135	-0.4 (-1.5)	-.04 (-.14)	.05 (.16)	-.07 (-.23)	.00	-.01 (-.02)	+18	1.6	-1.0	--	303 (68)	-22 (-5)	40 (9)	19 (14)	41 (30)	28 (21)	Good attachment but target nutated away during de-spin.
26-2	A	140	-0.4 (-1.5)	-.04 (-.12)	.11 (.36)	-.08 (-.27)	.01 (.04)	.00	+18	3.0	-0.4	--	535 (120)	-27 (-6)	27 (6)	19 (14)	41 (30)	42 (31)	Good attachment but target nutated away during de-spin.
26-3	A	85	-0.4 (-1.5)	.00	.07 (.22)	-.09 (-.30)	-.02 (-.08)	-.03 (-.09)	+18	3.0	1.0	--	552 (124)	27 (6)	85 (19)	23 (17)	81 (60)	46 (34)	Good attachment but target nutated away during de-spin.

* Flying time between initiating run and target contact.

Table XVI Simulation Data, Attachment Mode - Simulated-Adhesive (Velcro) Concluded

Run No.	Test Group	Time* Sec	Position & Rate Conditions at Target Contact: Translational: m (ft) X	Y	Z	Translational: m/sec (ft/sec) $\dot{X}$	$\dot{Y}$	$\dot{Z}$	Rotational: deg/sec $\dot{\Phi}$	deg Θ	Ψ	Target de-spin time sec	Maximum Contact Forces & Moments: nt (lbs) F_{XT}	F_{YT}	F_{ZT}	nt-m (ft-lbs) M_{XT}	M_{YT}	M_{ZT}	Comments
27-1	A	110	-0.4 (-1.4)	-.02 (-.06)	.06 (.21)	-.02 (-.05)	.01 (.02)	.00	+72	0.0	1.4	--	187 (42)	-116 (-26)	-125 (-28)	26 (19)	81 (60)	109 (80)	Off center attachment. Target nutated away during de-spin.
27-2	A	200	-0.4 (-1.4)	.00	.03 (.09)	-.02 (-.08)	.02 (.08)	-.01 (-.04)	+72	1.2	4.0	--	290 (65)	214 (48)	98 (22)	-41 (-30)	-204 (-150)	-204 (-150)	Target nutated away during de-spin.
27-3	A	105	-0.4 (-1.4)	-.06 (-.19)	.01 (.02)	-.05 (-.15)	.00	-.01 (-.02)	+72	-0.2	1.2	--	321 (72)	-147 (-33)	-160 (-36)	-41 (-30)	-102 (-75)	-189 (-139)	Off center attachment. Target nutated away during de-spin.

* Flying time between initiating run and Target contact

Table XVII Average Simulation Data, Attachment Mode - Clamping to Outer Octagonal Target Surface

Position & Rate Conditions at Target Contact																				
Run No.	Test Group	Time* Sec	Translational						Rotational			Target De-spin Time Sec	Maximum Contact Forces & Moments						Comments
			m (ft)			m/sec (ft/sec)			deg/sec	deg			nt (lbs)			nt-m (ft-lbs)			
			X	Y	Z	$\dot{X}$	$\dot{Y}$	$\dot{Z}$	$\dot{\phi}$	θ	ψ		F_{XT}	F_{YT}	F_{ZT}	M_{XT}	M_{YT}	M_{ZT}	
1	A	85	0.0	-.11 (-.36)	.07 (.22)	.00	.00	.00	0	5.6	0.0	--	123 (28)	85 (19)	16 (4)	9 (6)	24 (18)	45 (33)	Three attempts - Three successful attachments.
1	D	70	0.1 (0.2)	.06 (.19)	.01 (.02)	.02 (.05)	.00	.00	0	1.9	0.4	--	88 (20)	92 (21)	22 (5)	6 (4)	39 (28)	40 (29)	Three attempts - Three successful attachments.
2	A	95	-0.1 (-0.2)	.00	.00	.01 (.03)	.00	.00	0	1.4	2.1	--	123 (28)	34 (8)	9 (2)	2 (1)	15 (11)	26 (19)	Three attempts - Three successful attachments.
2	C	215	-0.2 (-0.6)	.02 (.08)	-.08 (-.25)	.01 (.02)	.00	.00	0	0.1	1.8	--	80 (18)	43 (10)	25 (6)	12 (9)	14 (10)	8 (6)	Three attempts - Two successful attachments.
3	A	95	-0.1 (-0.2)	.00	.04 (.12)	.01 (.03)	.00	.00	0	4.3	2.6	--	113 (25)	65 (15)	15 (3)	4 (3)	19 (14)	38 (28)	Three attempts - Three successful attachments.
3	D	180	-.01 (-.02)	-.03 (-.09)	-.01 (-.02)	.02 (.07)	.00	.00	0	1.1	-1.5	--	135 (30)	80 (18)	18 (4)	9 (7)	31 (23)	18 (14)	Three attempts - Three successful attachments.
4	A	110	-0.2 (-0.5)	-.02 (-.06)	.01 (.04)	.01 (.02)	.01 (.02)	.00	0	3.2	3.0	--	116 (26)	53 (12)	27 (6)	6 (4)	34 (25)	37 (29)	Three attempts - One successful attachment.
4	C	335	-0.1 (-0.2)	-.06 (-.19)	.03 (.11)	.01 (.02)	.01 (.03)	.00	0	3.0	-2.1	--	116 (26)	56 (13)	12 (3)	3 (2)	43 (32)	26 (19)	Three attempts - Two successful attachments.
5	A	205	-0.1 (-0.2)	-.02 (-.06)	.07 (.23)	.01 (.04)	.01 (.02)	.00	18	3.6	2.8	52	147 (33)	71 (16)	40 (9)	25 (21)	44 (33)	52 (38)	Three attempts - One successful attachment and de-spin.
5	D	590	0.0	-.03 (-.11)	.04 (.12)	.01 (.03)	.00	.01 (.02)	18	2.1	-0.5	66	86 (19)	60 (13)	62 (14)	22 (17)	18 (13)	13 (9)	Three attempts - Two successful attachments and de-spins.
6	A	120	0.0	-.05 (-.16)	.04 (.12)	.01 (.04)	.00	.01 (.03)	0	3.7	1.4	--	137 (31)	107 (24)	12 (3)	5 (4)	25 (19)	67 (49)	Three attempts - Three successful attachments.
6	C	220	0.1 (0.3)	-.03 (-.11)	.09 (.32)	.01 (.03)	.01 (.02)	.01 (.02)	0	5.7	-0.1	--	71 (16)	76 (17)	49 (11)	9 (7)	50 (37)	57 (42)	Three attempts - One successful attachment.
12	A	135	0.0	.00	.08 (.26)	.02 (.05)	.01 (.02)	.01 (.03)	-18	3.3	2.1	26	72 (16)	77 (17)	42 (10)	16 (11)	36 (26)	52 (38)	Six attempts - Five successful attachments and de-spins.
13	A	115	0.1 (0.3)	.01 (.04)	.02 (.04)	.02 (.06)	.00	.00	72	2.5	1.9	--	73 (16)	80 (18)	52 (12)	28 (21)	58 (43)	57 (42)	Three attempts - No successful attachments.
15	A	130	0.0	.04 (.15)	.06 (.21)	.00	.00	.00	0	3.7	2.1	--	34 (8)	95 (21)	18 (4)	7 (5)	22 (16)	113 (83)	Three attempts - Three successful attachments.
16	A	140	0.1 (0.4)	.05 (.15)	-.01 (-.04)	.02 (.06)	.01 (.01)	.00	-72	-1.3	1.1	--	45 (10)	46 (10)	67 (15)	18 (14)	59 (44)	36 (27)	Three attempts - No successful attachments.

* Flying time between initiating run and target contact.

TABLE XVIII - Average Simulation Data, Attachment Mode -
Clamping to Outer Cylindrical Target Surface

Run No.	Test Group	Time* Sec	Position & Rate Conditions at Target Contact: Translational m (ft) X	Y	Z	Translational m/sec (ft/sec) $\dot{X}$	$\dot{Y}$	$\dot{Z}$	Rotational deg/sec $\dot{\Phi}$	deg Θ	Ψ	Target De-Spin Time Sec	Maximum Contact Forces & Moments: nt (lbs) F_{XT}	F_{YT}	F_{ZT}	nt-m (ft-lbs) M_{XT}	M_{YT}	M_{ZT}	Comments
8	A	160	0.3 (0.9)	.03 (.09)	.06 (.19)	.01 (.02)	.00	.01 (.01)	-18	3.9	1.6	60	92 (21)	71 (16)	42 (9)	28 (21)	50 (37)	60 (42)	Three attempts - Two successful attachments and de-spins
8	C	310	0.2 (0.6)	-.01 (-.03)	.01 (.03)	.01 (.03)	.01 (.03)	.01 (.02)	-18	1.0	1.5	56	129 (29)	27 (6)	37 (8)	17 (12)	52 (38)	32 (24)	Three attempts - One successful attachment and de-spin
10	A	190	0.3 (1.0)	.00	.06 (.18)	.01 (.04)	.01 (.04)	.01 (.02)	18	3.1	0.4	9	137 (31)	27 (6)	31 (7)	21 (15)	34 (25)	30 (22)	Three attempts - Three successful attachments and de-spins
10	C	365	0.2 (0.8)	-.06 (-.18)	.10 (.32)	-.01 (-.02)	.00	.01 (.03)	18	3.9	0.3	19	86 (18)	49 (11)	40 (9)	9 (6)	58 (42)	53 (39)	Two attempts - One successful attachment and de-spin
17	A	155	0.3 (0.9)	.00	.08 (.25)	.01 (.05)	.01 (.03)	.01 (.04)	-18	2.1	1.5	11	56 (13)	83 (19)	80 (18)	19 (14)	86 (64)	116 (85)	Three attempts - One successful attachment and de-spin

*Flying time between initiating run and target contact

TABLE XIX - Average Simulation Data, Attachment Mode -
Twelve (12) Inch Flange Attachment

Position & Rate Conditions at Target Contact																			
Run No.	Test Group	Time* Sec	Translational						Rotational			Target De-Spin Time Sec	Maximum Contact			Forces and Moments			Comments
			m (ft)			m/sec (ft/sec)			deg/sec	deg			nt (lbs)			nt-m (ft-lbs)			
			X	Y	Z	X	Y	Z					F_{XT}	F_{YT}	F_{ZT}	M_{XT}	M_{YT}	M_{ZT}	
7	A	205	0.2 (0.5)	.01 (.04)	-.03 (-.09)	.00	.00	.00	0	-1.8	0.9	--	169 (38)	42 (9)	61 (14)	11 (8)	80 (59)	57 (42)	Three attempts - Three Successful attachments.
7	D	270	0.2 (0.6)	-.02 (-.07)	.11 (.36)	.00	.00	.01 (.03)	0	5.7	-0.5	--	169 (38)	36 (8)	64 (14)	8 (6)	72 (50)	42 (29)	Three attempts - Three successful attachments.
14	A	100	0.2 (0.7)	.02 (.06)	.02 (.05)	.00	.01 (.02)	.00	0	1.7	1.4	--	79 (18)	33 (7)	39 (9)	4 (3)	49 (36)	38 (28)	Three attempts - Three successful attachments.

*Flying time between initiating run and target contact

TABLE XX - Average Simulation Data, Attachment Mode - Eight (8) Inch Flange Attachment

Position & Rate Conditions at Target Contact																			
Run No.	Test Group	Time* Sec	Translational						Rotational			Target De-Spin Time Sec	Maximum Contact Forces and Moments						Comments
			m (ft)			m/sec (ft/sec)			deg/sec	deg			nt (lbs)			nt-m (ft-lbs)			
			X	Y	Z	X	Y	Z					F_{XT}	F_{YT}	F_{ZT}	M_{XT}	M_{YT}	M_{ZT}	
9	A	170	0.4 (1.3)	.05 (.17)	.12 (.41)	.02 (.06)	.00	.01 (.03)	-18	4.3	2.9	44	276 (62)	45 (10)	65 (15)	24 (18)	84 (62)	53 (39)	Three attempts - Two successful attachments and de-spins
11	A	130	0.4 (1.2)	.03 (.09)	.11 (.37)	.01 (.02)	.00	.00	0	5.6	1.7	--	181 (41)	33 (7)	34 (8)	4 (3)	68 (50)	46 (34)	Three attempts - Three successful attachments
11	D	140	0.4 (1.2)	-.02 (-.05)	-.02 (-.08)	.02 (.07)	.01 (.02)	.00	0	-1.4	0.8	--	267 (60)	98 (22)	134 (30)	41 (30)	27 (20)	20 (15)	One attempt - One successful attachment

* Flying time between initiating run and target contact

Table XXI Average Simulation Data, Attachment Mode - Simulated-Adhesive (Velcro)

Run No.	Test Group	Time* Sec	Position & Rate Conditions at Target Contact: Translational m (ft) X	Y	Z	Translational m/sec (ft/sec) $\dot{X}$	$\dot{Y}$	$\dot{Z}$	Rotational deg/sec $\dot{\Phi}$	deg Θ	Ψ	Target De-Spin Time Sec	Maximum Contact Forces & Moments: nt (lbs) F_{XT}	F_{YT}	F_{ZT}	nt-m (ft-lbs) M_{XT}	M_{YT}	M_{ZT}	Comments
18	A	145	-0.4 (-1.4)	-.01 (-.02)	-.02 (-.08)	-.03 (-.09)	.00	.00	0	-0.5	0.7	--	71 (16)	40 (9)	59 (13)	14 (10)	66 (49)	52 (38)	Three attempts - One successful attachment.
19	B	155	-0.4 (-1.4)	.01 (.03)	.02 (.06)	.01 (.02)	.00	.00	-18	1.1	0.6	--	71 (16)	42 (9)	38 (9)	6 (5)	45 (33)	53 (39)	Three attempts - No successful attachments.
19	C	240	-0.4 (-1.4)	-.03 (-.11)	.01 (.02)	-.04 (-.12)	.00	.00	-18	-0.2	-1.3	--	70 (16)	31 (7)	24 (5)	2 (1)	29 (21)	31 (23)	Three attempts - No successful attachments.
20	B	220	-0.4 (-1.4)	-.01 (-.02)	.07 (.24)	.00	.00	.00	-72	3.5	0.8	--	86 (19)	33 (7)	43 (10)	5 (4)	41 (30)	38 (28)	Three attempts - No successful attachments.
21	A	190	-0.4 (-1.4)	-.01 (-.02)	.06 (.20)	-.05 (-.15)	.01 (.03)	.00	+18	1.9	1.3	24	281 (63)	23 (5)	38 (8)	13 (10)	40 (29)	28 (21)	Three attempts - Two successful attachments and de-spins.
22	B	120	-0.4 (-1.4)	.04 (.12)	.02 (.08)	-.04 (-.14)	.00	.00	-72	3.1	1.3	--	255 (57)	63 (14)	52 (12)	20 (15)	59 (43)	62 (46)	Three attempts - Three successful attachments but no de-spins.
23	A	115	-0.4 (-1.4)	.06 (.20)	.04 (.14)	.04 (.13)	.01 (.03)	.01 (.02)	-216	2.0	1.1	--	256 (57)	108 (24)	132 (30)	18 (13)	157 (127)	99 (73)	Three attempts - No successful attachments or de-spins.
24	C	145	-0.4 (-1.4)	-.05 (-.16)	.00	.05 (.16)	.01 (.02)	.01 (.02)	0	-0.1	-1.7	--	307 (69)	33 (7)	36 (8)	4 (3)	50 (37)	32 (23)	Three attempts - Three successful attachments.
25	C	225	-0.4 (-1.2)	-.06 (-.20)	.07 (.22)	.03 (.09)	.00	.01 (.01)	0	1.3	-2.2	--	329 (74)	18 (4)	46 (10)	5 (4)	79 (58)	22 (13)	Three attempts - One successful attachment.
26	A	120	-0.4 (-1.5)	-.03 (-.09)	.08 (.25)	.08 (.27)	.01 (.04)	.01 (.04)	18	2.5	-0.1	--	463 (104)	25 (6)	51 (11)	20 (15)	54 (40)	39 (29)	Three attempts - Three successful attachments but no de-spins.
27	A	140	-0.4 (-1.4)	-.03 (-.08)	.03 (.11)	.03 (.09)	.01 (.03)	.01 (.02)	72	0.3	2.2	--	266 (60)	159 (36)	128 (29)	36 (26)	129 (95)	167 (123)	Three attempts - Three successful attachments but no de-spins.

* Flying time between initiating run and target contact.

Table XXII Averaged EMHD Test Results

Position & Rate Conditions at Target Contact																		
Run No.	Time* Sec	Translational						Rotational			Target De-spin Time Sec	Maximum Contact Forces & Moments						Comments
		m (ft)			m/sec (ft/sec)			deg/sec	deg			nt (lbs)			nt-m (ft-lbs)			
		X	Y	Z	$\dot{X}$	$\dot{Y}$	$\dot{Z}$	$\dot{\Phi}$	Θ	Ψ		F_{XT}	F_{YT}	F_{ZT}	M_{XT}	M_{YT}	M_{ZT}	
1	77	.01 (.02)	-.03 (-.08)	.04 (.12)	.01 (.02)	.00 (.00)	.00 (.00)	0	3.8	0.2	--	106 (24)	88 (20)	19 (4)	7 (5)	31 (23)	42 (31)	Six attempts Six successful
2	155	.01 (.02)	.01 (.04)	-.04 (-.12)	.01 (.03)	.00 (.00)	.00 (.00)	0	0.8	2.0	--	102 (23)	38 (9)	17 (4)	7 (5)	14 (10)	17 (12)	Six attempts Five successful
3	137	.02 (.05)	-.02 (-.04)	.01 (.05)	.02 (.05)	.00 (.00)	.00 (.00)	0	2.7	0.6	--	124 (27)	72 (16)	16 (4)	6 (5)	25 (18)	28 (21)	Six attempts Six successful
4	222	.01 (.02)	-.04 (-.12)	.02 (.07)	.01 (.02)	.01 (.02)	.00 (.00)	0	3.1	0.4	--	116 (26)	54 (12)	20 (5)	4 (3)	38 (28)	31 (24)	Six attempts Three successful
5	398	.01 (.03)	-.03 (-.08)	.05 (.17)	.01 (.03)	.00 (.01)	.00 (.01)	18	2.8	1.2	59	117 (26)	66 (15)	51 (12)	24 (19)	31 (23)	32 (24)	Six attempts Three successful de-spins
6	170	.01 (.04)	-.04 (-.13)	.06 (.22)	.01 (.03)	.00 (.01)	.01 (.02)	0	4.7	0.6	--	104 (24)	92 (20)	30 (7)	7 (6)	38 (28)	62 (46)	Six attempts Four successful de-spins
7	238	0.2 (0.5)	-.01 (-.02)	.04 (.13)	.00 (.00)	.00 (.00)	.00 (.01)	0	2.0	0.2	--	169 (38)	39 (9)	62 (14)	10 (7)	76 (54)	50 (36)	Six attempts Six successful de-spins
8	235	0.2 (0.7)	.01 (.03)	.04 (.11)	.01 (.02)	.01 (.02)	.01 (.02)	-18	2.4	1.6	58	110 (25)	49 (11)	40 (8)	22 (16)	51 (38)	46 (33)	Six attempts Three successful de-spins
9	170	0.4 (1.3)	.05 (.17)	.12 (.41)	.02 (.06)	.00 (.00)	.01 (.03)	-18	4.3	2.9	44	276 (62)	45 (10)	65 (15)	24 (18)	84 (62)	53 (39)	Three attempts Two successful de-spins
10	278	0.3 (0.9)	-.03 (-.09)	.08 (.25)	.00 (.01)	.01 (.02)	.01 (.03)	18	3.5	0.4	14	112 (24)	38 (8)	36 (8)	15 (10)	46 (34)	42 (30)	Five attempts Four successful de-spins
11	135	0.4 (1.2)	.00 (.02)	.04 (.14)	.02 (.04)	.00 (.01)	.00 (.00)	0	2.1	1.2	--	224 (50)	66 (14)	84 (19)	22 (16)	48 (35)	33 (24)	Four attempts Four successful de-spins
12	135	0.0 (0.0)	0.0 (0.0)	.08 (.26)	.02 (.05)	.01 (.02)	.01 (.03)	-18	3.3	2.1	26	72 (16)	77 (17)	42 (10)	16 (11)	36 (26)	52 (38)	Six attempts Five successful de-spins
13	115	0.1 (0.3)	.01 (.04)	.02 (.04)	.02 (.06)	.00 (.00)	.00 (.00)	72	2.5	1.9	--	73 (16)	80 (18)	52 (12)	28 (21)	58 (43)	57 (42)	Three attempts No successful de-spins
14	100	0.2 (0.7)	.02 (.06)	.02 (.05)	.00 (.00)	.01 (.02)	.00 (.00)	0	1.7	1.4	--	79 (18)	33 (7)	39 (9)	4 (3)	49 (36)	38 (28)	Three attempts Three successful de-spins
15	130	0.0 (0.0)	.04 (.15)	.06 (.21)	.00 (.00)	.00 (.00)	.00 (.00)	0	3.7	2.1	--	34 (8)	95 (21)	18 (4)	7 (5)	22 (16)	113 (83)	Three attempts Three successful de-spins
16	140	0.1 (0.4)	.05 (.15)	-.01 (-.04)	.02 (.06)	.01 (.01)	.00 (.00)	-72	-1.3	1.1	--	45 (10)	46 (10)	67 (15)	18 (14)	59 (44)	36 (27)	Three attempts No successful de-spins
* Flying time between initiating run and target contact.																		

Table XXII Averaged EMHD Test Results Concluded

Position & Rate Conditions at Target Contact																		
Run No.	Time* Sec	Translational						Rotational			Target De-spin Time Sec	Maximum Contact Forces & Moments						Comments
		m (ft)			m/sec (ft/sec)			deg/sec	deg			nt (lbs)			nt-m (ft-lbs)			
		X	Y	Z	$\dot{X}$	$\dot{Y}$	$\dot{Z}$	$\dot{\Phi}$	Θ	Ψ		F_{XT}	F_{YT}	F_{ZT}	M_{XT}	M_{YT}	M_{ZT}	
17	155	0.3 (0.9)	.00 (.00)	.08 (.25)	.01 (.05)	.01 (.03)	.01 (.04)	-18	2.1	1.5	11	56 (13)	83 (19)	80 (18)	19 (14)	86 (64)	116 (85)	Three attempts One successful de-spin
18	145	-0.4 (-1.4)	-.01 (-.02)	-.02 (-.08)	-.03 (-.09)	.00 (.00)	.00 (.00)	0	-0.5	0.7	--	71 (16)	40 (9)	59 (13)	14 (10)	66 (49)	52 (38)	Three attempts One successful de-spin
19	198	-0.4 (-1.4)	-.01 (-.04)	.02 (.04)	-.02 (-.05)	.00 (.00)	.00 (.00)	-18	0.4	-0.4	--	70 (16)	36 (8)	31 (7)	4 (3)	37 (37)	42 (31)	Six attempts No successful de-spins
20	220	-0.4 (-1.4)	-.01 (-.02)	.07 (.24)	.00 (.00)	.00 (.00)	.00 (.00)	-72	3.5	0.8	--	86 (19)	33 (7)	43 (10)	5 (4)	41 (30)	38 (28)	Three attempts No successful de-spins
21	190	-0.4 (-1.4)	-.01 (-.02)	.06 (.20)	-.05 (-.15)	.01 (.03)	.00 (.00)	+18	1.9	1.3	24	281 (63)	23 (5)	38 (8)	13 (10)	40 (29)	28 (21)	Three attempts Two successful de-spins
22	120	-0.4 (-1.4)	.04 (.12)	.02 (.08)	-.04 (-.14)	.00 (.00)	.00 (.00)	-72	3.1	1.3	--	255 (57)	63 (14)	52 (12)	20 (15)	59 (43)	62 (46)	Three attempts No successful de-spins
23	115	-0.4 (-1.4)	.06 (.20)	.04 (.14)	.04 (.13)	.01 (.03)	.01 (.02)	-216	2.0	1.1	--	256 (57)	108 (24)	132 (30)	18 (13)	157 (127)	99 (73)	Three attempts No successful de-spins
24	145	-0.4 (-1.4)	-.05 (-.16)	.00 (.00)	.05 (.16)	.01 (.02)	.01 (.02)	0	-0.1	-1.7	--	307 (69)	33 (7)	36 (8)	4 (3)	50 (37)	32 (23)	Three attempts Three successful de-spins
25	225	-0.4 (-1.2)	-.06 (-.20)	.07 (.22)	.03 (.09)	.00 (.00)	.01 (.01)	0	1.3	-2.2	--	329 (74)	18 (4)	46 (10)	5 (4)	79 (58)	22 (13)	Three attempts One successful de-spin
26	120	-0.4 (-1.5)	-.03 (-.09)	.08 (.25)	.08 (.27)	.01 (.04)	.01 (.04)	18	2.5	-0.1	--	463 (104)	25 (6)	51 (11)	20 (15)	54 (40)	39 (29)	Three attempts No successful de-spin
27	140	-0.4 (-1.4)	-.03 (-.08)	.03 (.11)	.03 (.09)	.01 (.03)	.01 (.02)	72	0.3	2.2	--	266 (60)	159 (36)	128 (29)	36 (26)	129 (95)	167 (123)	Three attempts No successful de-spins

* Flying time between initiating run and target contact.

2. Subjective Data

Subjective data concerning CSM and EMHD performance was obtained from all test subjects and is reflected in Section VIII, Conclusions. One subject possessed a large amount of CSM Simulator and Test Pilot experience. The following is that subject's Pilot Report in its entirety.

PILOT REPORT

(W. T. Armstrong, Jr.)

Introduction - During the period of the contract, one Martin Marietta research pilot participated in a six-degree-of-freedom space simulation program at the Martin Denver facility. The purpose of this simulation was to conduct a limited evaluation of the feasibility of a proposed space-hardware retrieval and transportation systems with adaptive capability to typical manned space vehicles such as the Apollo Command/ Service Module. This report presents the qualitative results of that simulation based on pilot evaluation.

The primary flight-oriented objectives of this simulation were:

a) To evaluate the suitability of an Apollo-type flight control system in performing the rendezvous, station keeping, and docking maneuvers required to capture typical space hardware that was either inertial or spin stabilized.

b) To determine the relative flight control and alignment problems associated with various capture mechanisms.

c) To assess the natural visual environment and determine requirements for special alignment aids.

Description of Equipment - The simulation program was conducted as a "pilot-in-the-loop" study which utilized analog computing techniques, the six-degree-of-freedom transport rig, and a fixed-base crew compartment simulator.

The crew compartment was an Apollo Command Module mockup with representative docking windows. Two crew couches were installed so as to provide a realistic field of view through the windows. The left couch was the flight-control station and included an attitude and translation controller mounted on the right and left couch arm rests, respectively. The right couch was the EMHD control station and included the controls and displays required for EMHD operation.

The EMHD, consisting of a fixed boom and rotatable adaptive-head, was mounted on the nose of the Command Module with the boom extending along the +X axis. The adaptive-head was controllable in rotation about the X-X axis of the vehicle with the speed of rotation infinitely variable from zero to maximum available rate.

Two capture devices, a two-arm, symmetrical "C" clamp and a cruciform, four-pad compression-adhesive device were evaluated. The clamp was capable of grasping a target vehicle on the exterior using a compression force or from the inside of an oriface or flange using an expansion force. The cruciform pads required a direct compression force in combination with an adhesive material to effect attachment. For the purpose of this study, Velcro was used as the adhesive material.

The target vehicle was mounted on the six-degree-of-freedom transport rig and was configured as an eight sided, symmetrical shape to represent typical unmanned space hardware. The configuration of the docking face was varied throughout the simulation to include either the female portion of the Velcro adhesive, a grasping flange, or a clean face, depending upon the attachment method under investigation.

Flight dynamics were provided by the moving base and analog computers. The Command Module was fixed-base with the attitude phase-plane and translation vectors superimposed on the transport rig. The Rate Command, Pulse, and Acceleration flight control modes of the Apollo CSM were provided. The attitude rate deadbands were mechanized at 0.1 deg/sec. about the X-X axis.

Simulation Program - There were three basic tasks associated with the simulation program: To approach and stabilize in a station-keeping position relative to the target vehicle; to attach the flight module to the target vehicles; and to despin the target vehicle without inducing divergent nutations.

The three basic tasks were further divided into sub-tasks with 27 different sets of conditions. These sub-tasks involved varying the mass, moments of inertia, and spin rate of the target; method of attachment; and the relative attitudes and position between the two vehicles. Due to limiting transport rig geometry, the maximum separation distance investigated was approximately 45 feet.

Pilot Comments and Recommendations -

a) General - The simulator used for this investigation was an excellent device with which to analyze the concept of capturing space vehicles. The flight characteristics of the Apollo CSM were well represented and very little imagination was required to achieve realism. Although the flight module was fixed-base, the out-the-window display was effective to the point of inducing a feeling of actual motion in the pilot.

b) Lighting - Orbital lighting conditions were simulated through the use of a high-intensity flood light and appeared quite realistic at high sun angles. As is typical of artificial illumination, low sun angles did not present the brilliance nor sharply defined shadow effects encountered in exoatmospheric flight.

c) Flight Control - Control of the flight module was representative of the Apollo CSM and was easily accomplished. The lack of an attitude hold feature complicated station-keeping slightly and induced a definite, although acceptable, degradation to alighment accuracy during capture operations. It is recommended that future studies of this nature provide for an attitude hold capability if such capability exists or is expected to exist in the spacecraft being simulated.

d) Alignment - Manual alignment between the two vehicles was generally acceptable but was compromised by the lack of visual aids. During capture of inertially stabilized targets, this lack of aids did not induce significant errors; however, on spinning targets, the rotation of the capture device between the pilot and the target was quite distracting and tended to mask any buildup in angular misalignment that occurred during the time required to match the spin rate and effect capture with the clamp or compression pads. It is recommended that future studies of this nature incorporate a two-body alignment system that utilizes the pilot's line-of-sight as the reference axis.

e) Separation - At times it was difficult to estimate the separation distance between the two vehicles. This was especially true with spinning targets and when attempting inside out attachments. A fixed probe on the end of the boom would have been very useful and it is recommended that future studies incorporate a device of this nature.

f) Target Rotation - In general, target rotation about a single axis did not present unsurmountable capture problems; however, it was not possible to despin low-mass targets without inducing divergent nutations. Due to the two-point attachment system, this problem was anticipated and it is recommended that future studies give consideration to a four-point cruciform configuration for either inside or outside attachment.

g) Attachment - Of the three methods evaluated, the inside-out (flange) attachment was preferred. This preference is primarily based on the improved alignment capability with a closed clamp as opposed to an open clamp where the extended clamp arms create false cues. The four-point adhesive pad concept provided alignment cues that were equally as good as the closed clamp, but the difficulty encountered in maintaining attachment during despin operations induced excessive station-keeping control inputs. Although the inside-out method of attachment was preferred, there was a significant disadvantage to this method in that the tolerance to vehicle separation distance during initial attachment operations was considerably reduced. It is recommended, however, that this method be given further consideration as it is compatible with the instinctive reactions of a trained pilot and it is felt that any disadvantages could be eliminated through a better attachment pad design.

h) Post-Contact Dynamics - During the evaluation of low-mass targets, several attempts were made to "fly-out" induced nutations. In

general, these attempts were unsuccessful for two reasons: The low torque-to-inertia values of the CSM control system prevented matching the nutation rates prior to the onset of inertia coupling, and transport rig dynamic feedback that would not have been present had the flight vehicle been moving rather than fixed-base. It is concluded that pilot control of post-contact dynamics is feasible but probably not advisable in the general case due to the potential variance between flight vehicle control power and target mass/moment of gyration characteristics.

i) Attachment Technique - Three methods for effective attachment to spinning targets were evaluated. The first consisted of an approach to the target with the attachment device rotating at the proper rate. The second method was to approach the target with a stationary attachment device, then match target spin rate during the final two to three feet of closure. The third was to place the attachment device in the proper attachment position through vehicle maneuvering, then match the spin rate of the target. Although all three methods were successful, the third method was preferred due to improved alignment cues.

j) Capture Operations - Although not included as a part of the pilot evaluation, it was apparent that significant difficulty was encountered by the boom operator when trying to effect attachment at the higher spin rates. This was due to the difficulty in establishing a spin rate for the capture device that was equal to the spin rate of the target. In some cases, blinking the eyes rapidly to create a strobe effect enabled satisfactory capture. This technique was not always effective, however. It is recommended that future studies provide a visual cue for this task. From the limited results of this evaluation, it appeared that a controllable-rate strobe light would be highly effective. Also, a strobe could serve an additional purpose of allowing detailed still photography or visual inspection of a rotating body.

Conclusion - The concept of capturing and transporting space hardware with a properly equipped manned spacecraft appears feasible and should be a subject for additional investigation. There are many practical applications for such a capability in connection with the assembly, servicing, and resupply of future hardware configurations. In particular, the simplicity of this concept plus the potential for reducing the extent of extra-vehicular crew activity render it especially attractive. Such a capability must evolve if man's role in space is to be fully exploited.

SECTION VII

ANALYSIS OF TEST RESULTS

1. Quantitative Data

Table XXIII presents the percentage of completely successful runs for the individual clamping modes and for all modes combined. Columns are given for non-spinning and spinning Targets, also. A successful run is defined as one where the target was brought to a halt (including de-spin if required) and firmly gripped by the EMHD.

Table XXIII Percentages of Successful Runs

Attachment Mode	Percent Successful	Percent Successful	
		No Target Spin	Target Spinning
clamp	66	82	50
hook	94	100	67
adhesive*	21	55	8
all	58	82	34

* Velcro

Times required for the closure maneuvers prior to contact were almost always between two and five minutes. The longer times were generally associated with alignment to a spinning target.

Position errors at contact averaged less than five (5) centimeters (0.17 foot) on each axis. Figures 67 and 68 indicate the distribution of lateral (Y) and vertical (Z) position errors at Target contact for all data runs.

Contact velocities were on the order of two (2) centimeters per second (0.06 feet per second) or less on all axes except during the Velcro runs. During these, a positive closure velocity along the X axis was required to seat the Velcro pads on the Target. Velocities averaging four (4) centimeters per second (0.13 feet per second) were used to do this.

On the average, the Target was pitched nose-up three (3) degrees and yawed right one (1) degree at contact. Deviations of five degrees

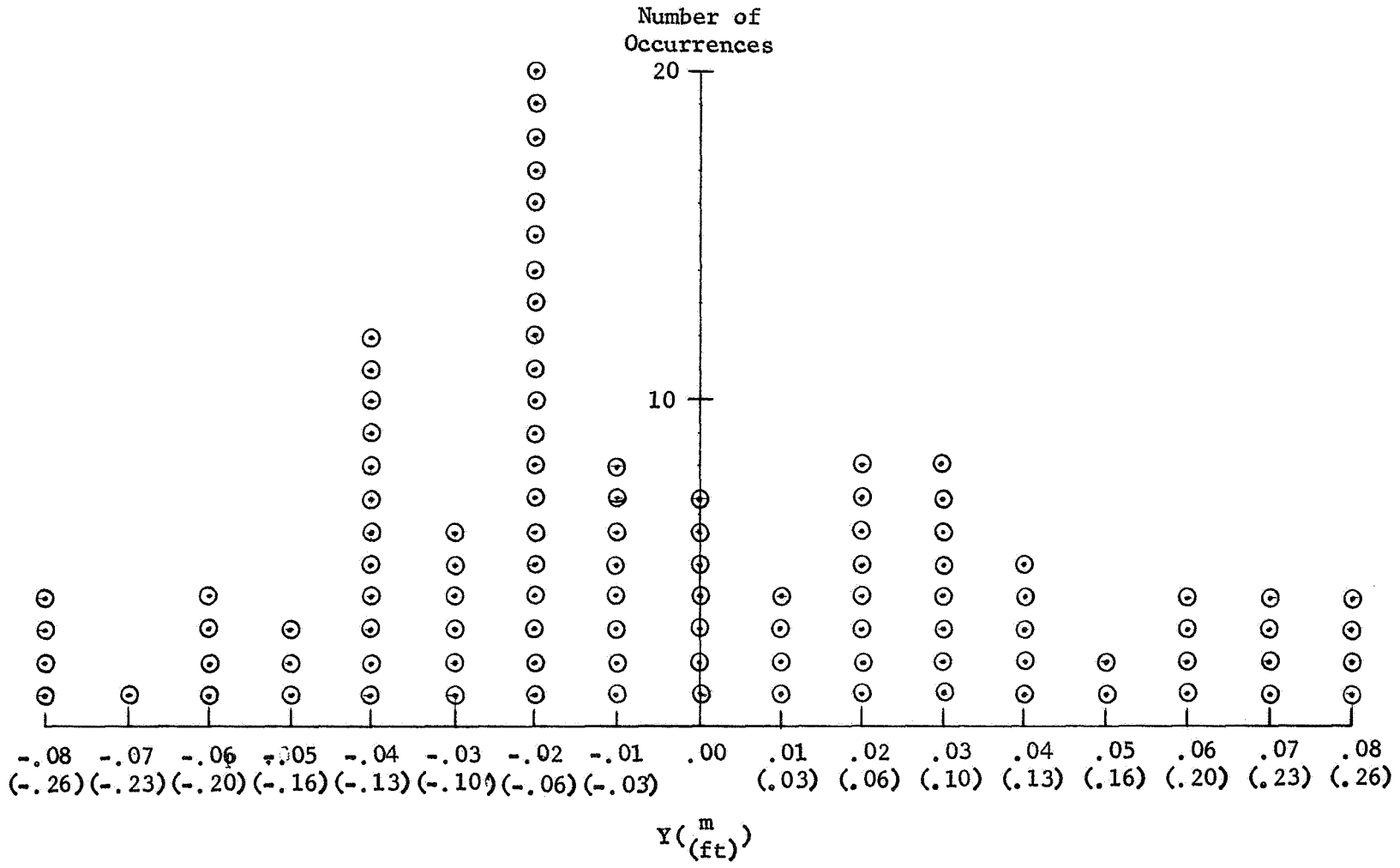

Figure 67 Lateral (Y) Position Error Distribution at Contact

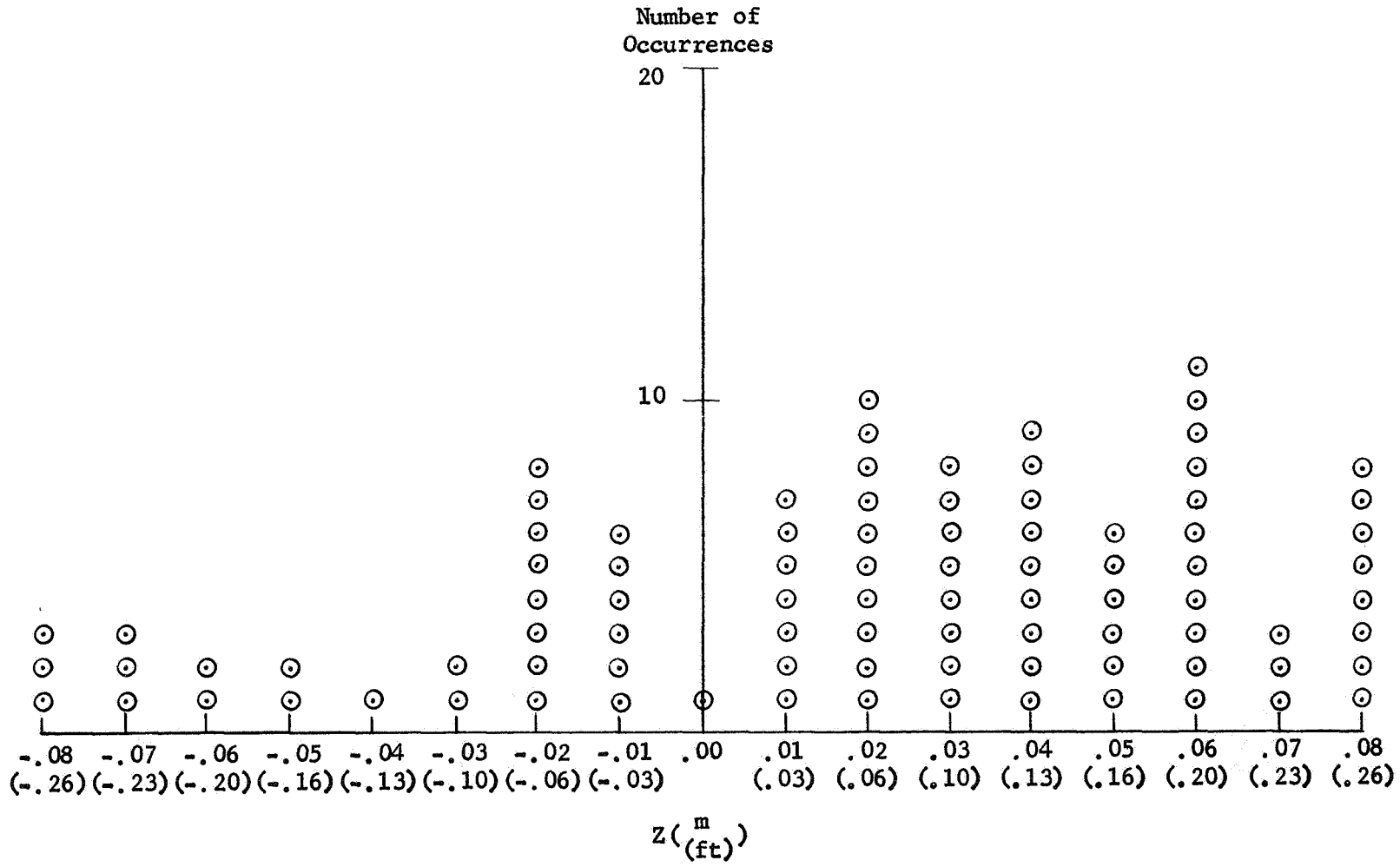

Figure 68 Vertical (Z) Position Error Distribution at Contact

from these positions were easily observable and were reduced prior to contact. Figures 69 and 70 show the distribution of pitch (θ) and yaw (ψ) errors at Target contact irrespective of attachment mode.

All completely successful de-spin operations occurred with a spin rate of eighteen (18) degrees per second. Several nearly successful de-spins were accomplished at seventy-two (72) degrees per second with the arms clamping the octagonal box. The two-hundred and sixteen (216) degree per second rate was virtually impossible to handle.

Maximum forces on the Target averaged under 100 newtons (22 pounds) on the Y and Z axes. On the X axis, maximum forces were approximately twice as large due to the contact velocity along the line connecting the CSM and Target centers.

Maximum moments on the Target averaged less than sixty (60) newton meters (44 foot pounds).

CSM thrusters were on for approximately twenty percent of the closure maneuvering time. For an average run of two-hundred (200) seconds, this would give forty (40) seconds of thrust, almost all of which utilized two-hundred (200) pounds of thrust for Y, Z, pitch, and yaw acceleration. This represents a fuel impulse consumption of eight thousand (8000) pound-seconds. No attempt was made to conserve fuel during any of the data runs.

Transport, spin-up, and release functions were examined following completion of the data runs. The five-hundred and eighty-four (584) kilogram (40 slugs) target was accurately positioned initially with the two arms clamping the octagonal box. CSM thrusters were fired for each of the translation and attitude axes. The forces and moments on the Target were consistent with those predicted in the Feasibility Study (Task A). Following this, the Target was spun-up to seventy-two (72) degrees per second and released and the CSM was backed away. No measurable nutation was induced at release.

2. Subjective Data

The subjects generally felt that the EMHD was an excellent device to examine the problems associated with material handling with a simple, manually controlled device. All subjects felt that the flight dynamics were adequately represented and that little imagination was necessary in the CSM to achieve a sense of realism. The CSM Pilot an EMHD Operator work load was generally moderate but increased with Target spin rate. The faster spin rates were difficult to handle with the two-arm head primarily because the Target's center of gravity could not be placed in the attachment plane and the attachment link could not be rigidized adequately to prevent rotations about the axis connecting the two clamping pads.

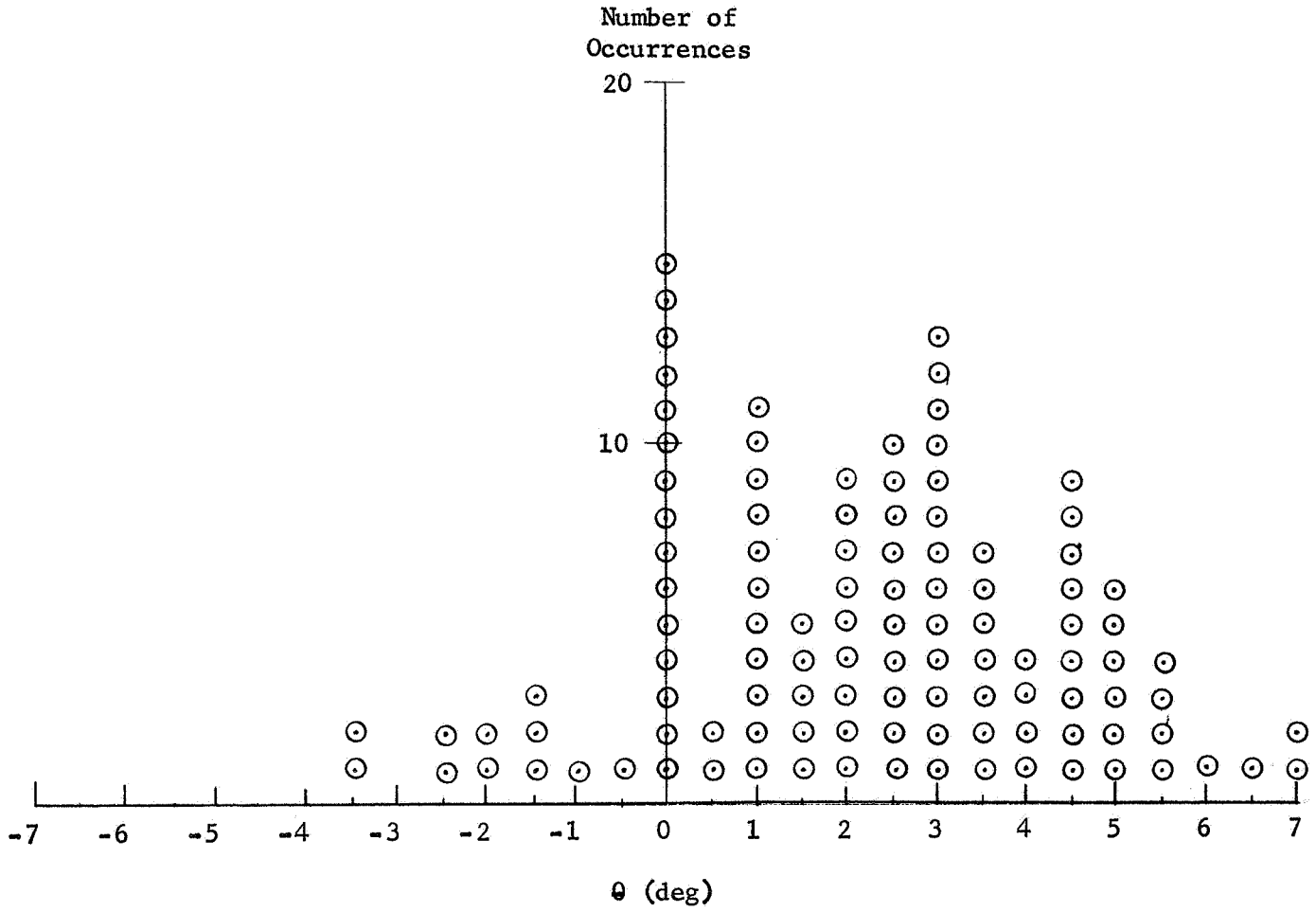

Figure 69 Pitch (θ) Position Error Distribution at Contact

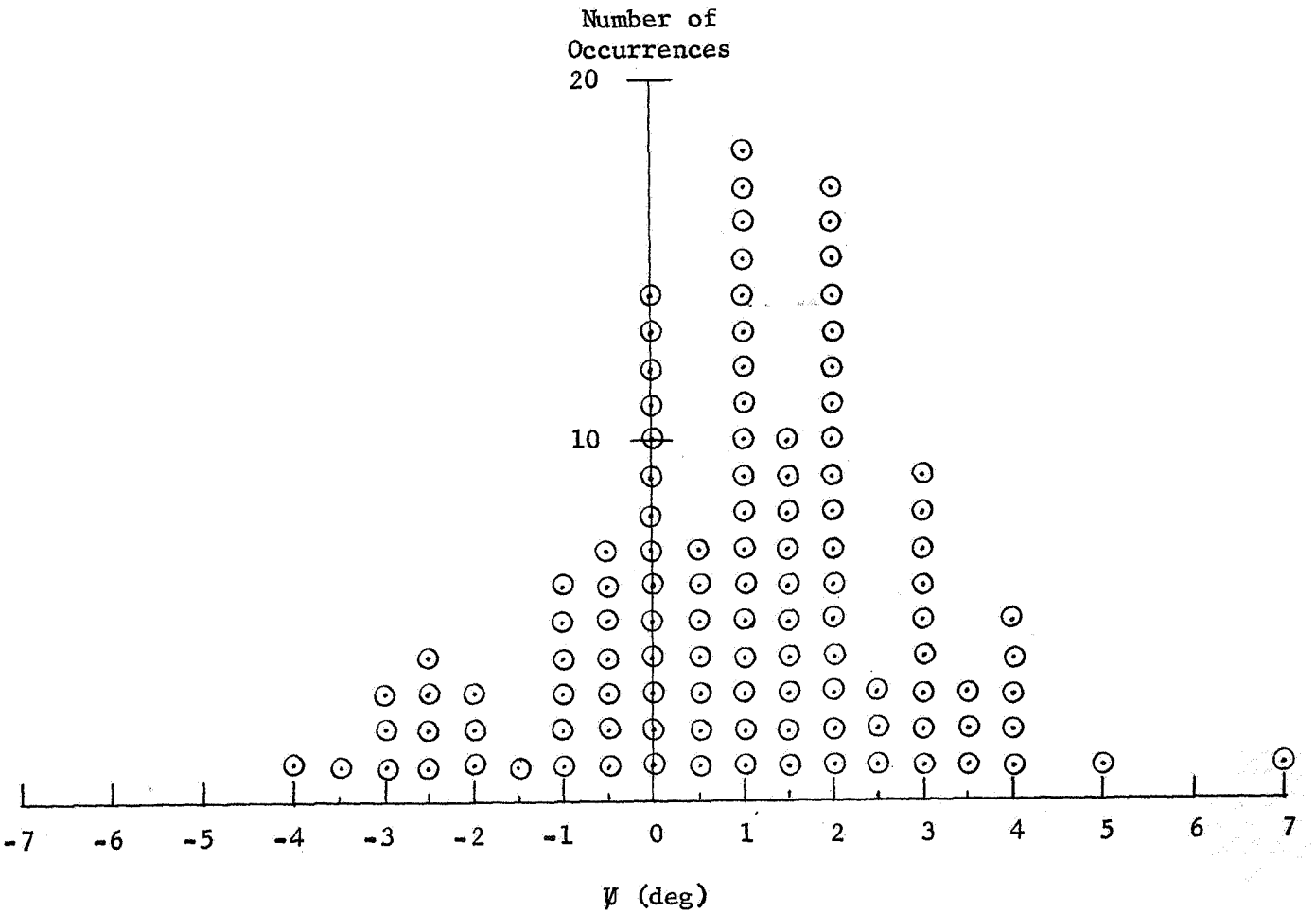

Figure 70 Yaw (Ψ) Position Error Distribution at Contact

Preference for the flange/hook mode was expressed because it presented a better EMHD/Target relative position reference. In addition, it provided the most rigid attachment link.

The Velcro head was easy to position but required extremely close control of longitudinal axis velocities to seat the Target on the pads and keep it there. In the successful runs, CSM X thrust pulses were used after contact to seat the pads better. However, these pulses must be timed accurately to prevent build-up of oscillations in the pad-support springs.

During clamping operations on spinning Targets, subjects preferred keeping the arms stationary in the horizontal (X, Y) plane until just prior to contact. This preserved their position reference as long as possible with the arms open. Because of this, precise spin rate matching was not achieved. Subjects generally were adjusting the phase of the rotating arms up until the moment of contact in order to clamp on the centers of the Target's flat sides.

One of the deliberate departures from true CSM conditions was the absence of an attitude position hold loop in the rate command mode. Because of this, the subjects had to adjust for errors created by up to one-tenth (0.1) degree per second attitude drift rates. The subject with the CSM simulator experience indicated that the tasks would be easier if the attitude position hold loop is included in the control system of a material handling vehicle.

SECTION VIII

CONCLUSIONS

The Feasibility Study (Task A) indicated that a Man Rated Flight Material Handling Device could be built and used with a vehicle such as the Apollo CSM. No significant advances in the state-of-the-art of space hardware would be required to build such a device.

Following approval of the Feasibility Study results, the EMHD was fabricated and tested. These tests, of which fifty-eight (58) percent were completely successful, confirmed that even with this simple, manually-controlled device, a variety of targets could be grappled and stabilized with the clamp, hook, and adhesive attachment modes. This verified the MRFMHD concept. The data gathered during these tests will make possible the design and testing of a more advanced device that will significantly increase the percentage of successful attachment tasks.

Among the recommended design improvements resulting from these EMHD tests are: 1) a collapsible probe such as a deHaviland Boom extending forward along the EMHD axis to provide an axial position reference at all times, 2) increased pad area on the two-arm head to increase its torque capability about the axis connecting the pads, 3) lower force springs on the adhesive pads to allow them to follow the Target motion more easily, 4) dampers on these springs, 5) wider and longer capture spans on the flange-attachment hooks to increase their visibility from the cockpit and to decrease the control precision required on the vehicle's longitudinal axis, and 6) visual aids or equipment to assist in matching head and target spin rates.

The next-generation device should also include packaging and materials that will progress toward prototype flight hardware characteristics.

The tests also indicated that the controllability of a vehicle such as the CSM would satisfy the requirements for material handling operations.

SECTION IX

RECOMMENDATIONS FOR FUTURE STUDIES

The next study phase should carry the Material Handling Device (MHD) through the preliminary flight hardware prototype design. The elements of this phase should include:

a. design (based on EMHD data), fabrication, and test, under the same simulation conditions used for the EMHD tests, an improved EMHD to test and verify arm-end pad design, flange hook design, adhesive pad spring and damper characteristics, alignment aids, and spin rate matching aids;

b. analysis of the integration and use of manipulators and/or additional arms to enhance post-attachment stability;

c. detailed analysis, including costs, of the launch modes available for an MHD;

d. analysis to determine the optimum vehicle to support the MHD;

e. analysis of the MHD modifications necessary to adapt it to a large, space shuttle vehicle;

f. design and fabrication of an advanced MHD incorporating packaging and materials progressing toward flight hardware;

g. testing the advanced MHD in a simulation that is similar to the EMHD simulation, but more comprehensive in terms of dynamic accuracy, lighting, range and configuration of targets, etc.;

h. analysis of these test results;

i. design of a prototype, flight hardware MHD with documentation to support the functional aspects, material and packaging choices, and an integration plan including cost estimates for an experiment or direct operational use of the eventual flight hardware.

REFERENCES

1. Emerson Electric Co., "Design and Engineering Analysis for Mechanical Rendezvous Attachment Mechanisms", Report No. 1972 AFFDL, RTD ASC, WPAFB, Dayton, Ohio, September 1965, Unclassified.

2. Ball Brothers Research Corp., "Experiments for Satellite and Material Recovery from Orbit - ESMRO", Vol. II Technical Report, Contract No. NAS8-18119, March 1967, Unclassified.

3. Chrysler Corp., Space Division, "Application Study of Electro-Adhesive Devices", submitted under NAS1-7307, Langley Research Center, Hampton, Va., Unclassified.

4. Chrysler Corp., Space Division, "Application Study of Electro-Adhesive Devices", Monthly Report submitted under Contract F33615-68-C-1186, New Orleans, Louisiana, May 6, 1968, Unclassified.

5. Feher, S., "Design, Development, and Fabrication of a Functional Adhesive Bonding Repair Experiment to be Performed During Space Flight", Contract No. NAS8-20677, Whittaker Corp., Narmco Research & Development Division, San Diego, Calif., June 1968, Unclassified.

6. Holmes, A. E., "Space Tool Kit Survey, Development and Evaluation Program", ER13942 Final Report, NAS9-3161, Martin Co., Baltimore, Maryland, Unclassified.

7. Skeist, I., Handbook of Adhesives, Skeist Laboratories, Inc., Newark, New Jersey, 1962, Unclassified.

8. Peters,G. H., Shaefer, R. J., and Hanny, J. F., "Extravehicular Capsular Adhesive Systems", National Cash Register Co., presented at National Conference on Space Maintenance and EVA, March 1966, Unclassified.

9. I. C. I./Organics/Inc., "Alloprene", Technical Bulletin 707, I. C. I./Organics/Inc., Stamford, Conn., Unclassified.

10. American Society for Testing and Materials, Adhesion, presented at the Sixty-Sixth Annual Meeting of American Society for Testing and Materials, Atlantic City, N. J., June 1963, Unclassified.

11. Kolb, D. J., "Designing Plastic Parts for Ultrasonic Assembly", Machine Design, Vol. 39, March 16, 1967, Unclassified.

12. Test and Evaluation Division, "Data Book for Environmental Testing and Spacecraft Evaluation", GSFC Greenbelt, Maryland, August, 1967, Unclassified.

13. USM, "Harmonic Drive", Mechanical Power Transmission Systems, United Shoe Machinery Corporation, Beverly, Mass., Unclassified.

14. Kidde/Rotax, "Development of a Successful and Unique Recirculating Ball Screw", Walter Kidde & Co., Inc., Belleville, N. J., Unclassified.

15. Ball Brothers Research Corporation, "Vac Kote, Long Life Lubricants", B. B. R. C., January 1968, Unclassified.

16. Fafnir Bearing Co., "Fafnir Ball Bearings, Catalog 68", New Britain, Connecticut, 1967, Unclassified.

17. Poly-Scientific Division of Litton Precision Products, "Application Manual for Capsule Type Slip Ring Assemblies", Annex to Final Report, NASA Contract No. NAS8-5091, May 1966, Unclassified.

18. "Proceedings of the Symposium on Precision Sliding Contact Devices", sponsored by Poly-Scientific Division of Litton Precision Products, Roanoke, Virginia, November 1965, Unclassified.

19. Harris, L. A., "Apollo Systems Engineering Manual Structural Dynamics", NAS9-150 North American Aviation, Inc., Space and Information Systems Division, Revised 10 July 1966, Unclassified.

20. Carmean, W. D., "CM Window Visibility and Viewfinder Study", Contract No. NAS8-21004, Martin Marietta Corporation, Denver, Colorado, September 1967, Unclassified.

21. Guerster, R. L., "Stacer Prestressed Spiral Tube Design Data", Hunter Spring Division of AMETEK, Inc., Hatfield, Pennsylvania, November 1967, Unclassified.

22. Hughes Aircraft Company, "Surveyor Spacecraft A-21A Model Description", NASA Contract Report No. CR84186, Space Systems Division, September 1964, Unclassified.

23. Tewell, J. R., Tobey, W. H., "Gemini GT-5 Orbital Tracking Study", Final Report, Martin Co., Denver, Colorado, June 1965, Unclassified.

24. General Electric, "Application of Remote Manipulation to Satellite Maintenance", Midterm Briefing on Contract NAS2-5072, General Electric, Missile and Space Division, Philadelphia, Pa., November 22, 1968, Unclassified.

BIBLIOGRAPHY

AC Electronics, Division of General Motors, "Apollo Guidance and Navigation System", NAS9-947 General Motors, Milwaukee, Wisconsin, November 1966, Unclassified.

Adams, J. J., "Measurements of Human Transfer Function with Various Model Forms", NASA TND-2394, August 1964, Unclassified.

Aerospace Industries Association, "Standard Method for 3 Minute Maximum, 600-1500°F Tests of Structural Adhesive Bonds", Los Angeles, California, 7 November 1960, Unclassified.

All American Engineering Co., "Ferry Vehicle Docking System for MOL/ Gemini B Vehicles", S.O. 9748-2 Q-354, All American Engineering Co., Wilmington, Delaware, April 1964, Unclassified.

Alner, D. J., Aspects of Adhesion, Proceedings of the Conference at Northampton College of Advanced Technology, EC1, University of London Press, March 1963, Unclassified.

Bellman, R., Kagiwada, H., Kalbo, R., "Orbit Determination as a Multipoint Boundary Value Problem and Quasilinearization", Memo RM-3129-PR, ASTIA 275933, Rand Co., Santa Monica, California, May 1962, Unclassified.

Benediht, E. T., "Electromagnetic Docking Operations in Space", Preprint 61-90, AAS, San Francisco, California, August 1961, Unclassified.

Bennie, B. B., "Post-Impact Dynamics During the Docking of a Logistics Vehicle to a Space Station", AIAA Third Manned Space Flight Meeting Paper, Houston, Texas, November 1964, Unclassified.

Benton, W. G., "Gravity Gradient Rod Thermal Bending Test Report", G E Doc. No. 64SD4368, NAS2-1946, October 1964, Unclassified.

Bikerman, J. J., The Science of Adhesive Joints, MIT, Cambridge, Mass., 1961, Unclassified.

Blackmer, R. H., Interian, A., Clodfelter, R. G., "The Role of Space Manipulator Systems for Extravehicular Tasks", Second National Conference on Space Maintenance and EVA, Las Vegas, Nevada, August 1968, Unclassified.

Born, D. C., "Control Criteria for Manual Orbital Rendezvous", Engr. Paper No. 1617 EAFB, California, September 1963, Unclassified.

Bouerschub, J. P., "A Lightweight Folding Boom for Accurately Placing Scientific Experiments up to 25 feet from Large Spacecraft", NASA TMX-941, January 1964, Unclassified.

Brissenden, R. F., "A Study of Human Pilot's Ability to Detect Angular Motion with Application to Control of Space Rendezvous", NASA TN-D-1498, Langley Research Center, Va., December 1962, Unclassified.

Bullock, "The Applications Technology Satellite", Program Summary, Goddard Space Flight Center, Greenbelt, Maryland, Revised April, 1968, Unclassified.

Burmeister, G. J., "Gemini Docking Simulation", D2-22213, Boeing, Seattle, Wash., November 1962, Unclassified.

Buzzard, W. C., "Methodology for Evaluating and Validating Mechanical Rendezvous Subsystems", RTD-TDR-63-4292, WPAFB, Ohio, February 1964, Unclassified.

Callahan, J. A., "The Development of the Gemini Docking System", McDonnell Paper 857E SAE-ASME, May 1964, Unclassified.

Cannon, R. H. Jr., Eppler, W. G. Jr., "The Vector Reticle and Control Action Display in Manual Control of Space Vehicle Attitude", AIAA/NASA Third Manned Space Flight Meeting, November 1964, Unclassified.

Carlson, J. A., Sapetta, L. P., "Stresses in Assemblies Bonded with Thermosetting Adhesives", Adhesives Age, p. 26, December 1967 issue, Unclassified.

Central Research Laboratories Inc., "Installation, Operation and Maintenance Manual for the Model 8 Master-Slave Manipulator", Central Research Lab, Red Wing, Minnesota, 1966, Unclassified.

Cloutier, G. J., "Dynamics of Deployment of Extendible Booms from Spinning Space Vehicles", Journal of Spacecraft and Rockets, Vol. 5 Number 5, May 1968, Unclassified.

Cohen, C. J., Hubbard, E. C., "A Nonsingular Set of Orbital Elements", NWL Report No. 1756 AD267155, Dahlgren, Virginia, July 1961, Unclassified.

Coover, H. W. Jr., "Advances in Polymer Chemistry Provide Key to New Adhesives", Adhesives Age, p. 20, February 1968 issue, Unclassified.

Dalkeg, N. C., "Man's Role in Space", ARS-P-2669, November 1962, Unclassified.

Dean, D. K., "Six-Degree-of-Freedom Flight-Path Study Generalized Computer Program", TR-60-781, WPAFB, Ohio, October 1962, Unclassified.

deRuiter, E., Oth, J. F. M., Sandor, V., and Tschamber, "Research and Development on Advanced Graphite Materials", Supp. to Vol. XI-Characterization of Binders Used in the Fabrication of Graphite Bodies, WADD-TR-61-72, AF33(616)-6915, Union Carbide European Research Assoc., 1964, Unclassified.

Dow Corning, "Selected Guide to Dow Corning Aerospace Sealants and Coatings-Silicone, Fluorosilicone Rubber", Engineering Products Division, Dow Corning Corp., Midland, Mich., Unclassified.

Dryden, H. L., "Aeronautical Research in the Sixties", SAE National Aeronautic Meeting, April 6, 1961, New York, Unclassified.

Ellis, G. A., Diana, A. C., "The Use of Earth-Moon Libration, Points as Terminals for Space Stations", RADC-TDR-62-1, AD272027, Griffiss AFB, N. Y., January 1962, Unclassified.

Emerson Electric Co., "Pegasus-C Coupon Retrieval Procedures and Techniques - Final Report", Report No. 2106, NAS8-18122, October 1966, Unclassified.

Epstein, G., Adhesive Bonding of Metals, North American Aviation Inc., Downey, Cal., Reinhold Publishing Corp., 1954, Unclassified.

Flight Refueling, Inc., "Space Catch", Technical Report TR61-2, Flight Refueling, Inc., Aeronca Aerospace Division, Unclassified.

Fox, J. C., "Six Degree-of-Freedom Simulation of a Manned Orbital Docking System", Space Technology Laboratories, Inc., Rodondo Beach, Cal., April 1962, Unclassified.

Gedeon, G. S., "Orbital Segment Mechanics", TM NSL62-13, February 1962, Unclassified.

Gellman, N., Burns, A. B., "Exploratory Investigation of Extendible Tubular Boom", AF33(657)11627, American Machine & Foundry Co., Stamford, Conn., August 1963, Unclassified.

Goddard SFC, "Satellites and Sounding Rockets", GSFC/NASA, August 1959-December 1967, Unclassified.

Goldstein, H. Ph.D., Classical Mechanics, Addison-Wesley Publishing Co., Mass., 1959, Unclassified.

Grasshoff, L. H., "An Onboard, Closed-Loop Nutation Control System for a Spin-Stablized Spacecraft", Journal of Spacecraft and Rockets, Vol. 5, Number 5, May 1968, Unclassified.

Gray, W. E., Mosher, R. S., "Manipulators for Astronauts", General Electric Research and Development Center, Schenectady, New York, 1967, Unclassified.

Green, W. L., "Apollo Docking Test Device Design Study", GDA-DDB64-036, NASA Contract NAS9-3716, December 1964, Unclassified.

GSFC Operations Control Center, "Satellite Situation Report", Vol. 8, No. 10, May 1968, Unclassified.

Hamilton, R. S., "Gemini Translation on Docking Trainer Detail Specification", McDonnell Report 9114 submitted under NAS9-170, Unclassified.

Herman, R. A., "Rendezvous Between an Astronaut and a Spacecraft", Hamilton Standard E. R. 3023, August 1964, Unclassified.

James, M. E., "Extendible Boom", Boeing Co., D2-23133, February 1964, Unclassified.

Joos, G., Freeman, I. M., Theoretical Physics, Hafner Publishing Co., New York, 1950, Unclassified.

Jones, J. C., "Preliminary Design of Ring and Cone Docking Mechanism", MSC Internal Note No. 64-ET-35, July 1964, Unclassified.

Kasten, D. F., "Human Performance in a Simulated Short Orbital Transfer", AMRL-TDR-62-138, WPAFB, Ohio, December 1962, Unclassified.

Kearns, J. H., "A Study of Selected Control-Display Problems for Manned Aerospace Vehicles", ASD-TDR-63-170, WPAFB, Ohio, March 1963, Unclassified.

Kober, C. L., "Rendezvous Mate (Mechanism and Technique Evaluation)", P-62-51A (Vol. II) Martin Co., Denver, Colo., October 1962, Unclassified.

Koh, S. L., Eringan, A. C., "On the Foundations of Non-Linear Thermo-Viscoelasticity", Contract NONl-1100(02), Purdue University, Lafayette, Indiana, June 1962, Unclassified.

Lineberry, E. C., Brissender, R. F., Kurbijun, M. C., "Analytical and Preliminary Simulation Study of a Pilot's Ability to Control the Terminal Phase of a Rendezvous with Simple Optical Devices", NASA TND-965, Langley Research Center, Va., October 1961, Unclassified.

MacNaughton, J. D., "Unfurlable Metal Structures for Spacecraft", The DeHavilland Aircraft of Canada Limited, Downsview, Ontario, March 1963, Unclassified.

Meissinger, H. F., Belsky, F. J., "Visual Display Simulation of Lunar Handling under Remote Control by a Human Operator", P-63-135, Edwards AFB, Cal., August 1963, Unclassified.

Menk, M. A., Nash, R. C., "A Study of the Orbital Requirements for a Global Surveillance Satellite", Tech. Memo 61-1, ASRMDF-21, March 1961, Unclassified.

Midolo, L. L., "Design of a Three Degree-of-Freedom Simulator for Validation of Rendezvous Mechanisms", T. M. FDFM 64-42, WPAFB, Ohio, November 1964, Unclassified.

Montgomery, J. E., "Manned Control of Space Vehicle Docking", American Astronautical Society Vol. 16, Part 1, Edwards AFB, September 1963, Unclassified.

Musiolinio, C. J., "Orbital Attachment and Grappling Technique, Phases I, II, Report", Contract No. AF33(657)-7567 (AMF proj. No. B132-0-00) BPSN2(1-1369) 13529, American Machine and Foundry Co., Stamford, Conn., August 1962, Unclassified.

Musiolinio, C. J., "Space Vehicle Attachment and Connection", ASD-TDR-62-950 WPAFB, Ohio, November 1962, Unclassified.

NASA, "Apollo Operations Handbook", Block II Spacecraft, Vol. 1 Spacecraft Description NAS9-150, Revised March 1968, Unclassified.

National Space Science Data Center, "Data Catalog-Satellite and Locket Experiments", NASA, Goddard Space Flight Center, July 1968, Unclassified.

Nyland, F. S., "The Synergetic Plane Change for Orbiting Spacecraft", RM-3231-PR, Rand Corp., Santa Monica, Cal., August 1962, Unclassified.

Perry, H. A., Adhesive Bonding of Reinforced Plastics, McGraw-Hill Book Co. Inc., Naval Ordnance Laboratory, White Oak, Maryland, 1959, Unclassified.

Peters, R. A., "Single-Axis Attitude Regulation of Extra-Atmospheric Vehicles", ASD-TR-61-129, ASTIA 277221, WPAFB, Ohio, February 1962, Unclassified.

Pierce, D. A., "Direct Ascent Rendezvous After a Delayed Launch", TM-NSL62-72 Northrop Space Lab., Hawthorne, Cal., May 1962, Unclassified.

Pringle, R. Jr., "On the Capture Stability and Passive Damping of Artificial Satellites", NASA CR-139 Stanford University, Stanford, Calif., December 1964, Unclassified.

Puri, N. N., Lambert, A. I., Gido, J. F., "Unmanned Rendezvous, Station-Keeping and Docking for Extravehicular Space Activities", Second National Conference on Space Maintenance and EVA, Las Vegas, Nev., August 1968, Unclassified.

Rennie, B. B., "Summary of Space Docking Studies Conducted a Boeing in 1963", D2-20260-1, December 1963, Unclassified.

Riley, D. R., "A Fixed-Base Visual-Simulator Study of Pilot Control of Orbital Docking of Attitude Stabilized Vehicles", NASA TND-2036, January 1964, Unclassified.

Rogers, P. C., "Space Rendezvous, Rescue, and Recovery", AD410085, DDC, Alexandria, Virginia, August 1963, Unclassified.

Sando, R. M., "Some Docking Techniques for Satellite Rendezvous", AIR ARM Report 2211, May 1961, Unclassified.

Schecter, H. B., "A Brief Survey of Trajectory, Guidance, and Propulsion Aspects of Orbital Rendezvous", RM-3275-PR, ASTIA-414106, Rand Corp., Santa Monica, Cal., May 1963, Unclassified.

Schwartz, L., "Control Requirements for Space Vehicles", WADD Tech. Report 60-840 AD264844, January 1961, Unclassified.

Siracuse, R. J., "Orbital Grappling and Attachments", ASNCC Internal Memo 63-3, January 1963, Unclassified.

Snogen, R. C., "Adhesives Bonded Heat Sinks to Printed Circuit Boards", Adhesive Age, p. 21, June 1968 issue, Unclassified.

Solavski, A. H., Tuner, R., Doerr, F., "Dynamics of Separating Bodies, Volume I - Theoretical Analysis", AFOSR-109, AD271998, Holloman AFB, New Mexico, March 1961, Unclassified.

Summers, L. G., Shea, R. A., Fiedman, K., "Unaided Visual Detection of Target Satellites", AIAA/NASA Third Manned Space Flight Meeting November 1964, Unclassified.

Tachis, J., "A Study of an Orbital Maintenance and Material Transfer Shuttle", RTD-TDR-63-4057, WPAFB, Ohio, September 1963, Unclassified.

Technical Information Center, "Non-Destructive Testing of Adhesive Bonded Joints: A Partially Annotated Bibliography", North American Aviation, Inc., Space and Information Systems Division, January 1962, Unclassified.

Thomson, W. T., Introduction to Space Dynamics, John Wiley & Sons, Inc., New York, August 1963, Unclassified.

Traenkle, C. A., "Layout of Satellite Ferry Operation", ARLTR 60-313 AD249382, October 1960, Unclassified.

TRW Space Log, "Spacecraft Details", TRW Systems, Redondo Beach, Calif., 1966-1968, Unclassified.

Van Schaik, P. N., "Feasibility of a Self-Maneuvering Unit for Orbital Maintenance Workers", S.M.U. ASD-TDR-62-728, WPAFB, Ohio, August 1962, Unclassified.

Waterman, L. T., "Orbital Docking Studies and Model Tests, Model DSV-4B", Douglas Report SM-41901, Douglas Aircraft Co., Inc., Santa Monica, Cal., May 1962, Unclassified.

Wolowicz, C. H., "Simulator Investigation of Controls and Display Required for Terminal Phase of Coplanar Orbital Rendezvous", NASA TND-511, AD244288, FRS, Edwards, Cal., October 1960, Unclassified.

Worthington, D. T., "Passive Satellite System", RADC-TN-61-65, ASTIA 272296, Griffiss AFB, N. Y., April 1961, Unclassified.